ISBN 978-82-471-3167-1 (printed ver.)
ISBN 978-82-471-3168-8 (electronic ver.)
ISSN 1503-8181

Doctoral theses at NTNU, 2011:297

Sindre Sandbakk

Fibre Reinforced Concrete

Evaluation of test methods and material development

Sindre Sandbakk

Doctoral Thesis

NTNU
Norwegian University of
Science and Technology

NTNU
Norwegian University of
Science and Technology
Thesis for the degree of
philosophiae doctor
Faculty of Engineering Science and Technology
Department of Structural Engineering

Doctoral theses at NTNU, 2011:297

NTNU

NTNU
Norwegian University of
Science and Technology

Sindre Sandbakk

Fibre Reinforced Concrete

Evaluation of test methods and material development

Thesis for the degree of philosophiae doctor

Trondheim, November 2011

Norwegian University of
Science and Technology
Faculty of Engineering Science and Technology
Department of Structural Engineering

NTNU
Norwegian University of
Science and Technology

NTNU
Norwegian University of Science and Technology

Thesis for the degree of philosophiae doctor

Faculty of Engineering Science and Technology
Department of Structural Engineering

ISBN 978-82-471-3167-1 (printed ver.)
ISBN 978-82-471-3168-8 (electronic ver.)
ISSN 1503-8181

Doctoral Theses at NTNU, 2011:297

Printed by Tapir Uttrykk

Acknowledgement

First of all I would like to express my gratitude to my supervisor Professor Terje Kanstad for all support during the last four years. His professional support and knowledge, permanent enthusiasm and encouragement are highly appreciated, and cannot be overrated.

Several hours have been spent in the laboratory to carry out the experiments of this thesis. These experiments could not have been performed without the help of the laboratory personnel, in particular: Ove, Steinar, Gøran and Paal at NTNU and Knut, Stig, Erik, Chris and Roger at SINTEF. The work in the lab would have been much more complicated and frustrating without their expertise and not least nice sense of humour.

All my concrete colleagues at SINTEF and NTNU have contributed one way or another, thank you for making my time at Gløshaugen a pleasant one.

The research in this thesis has been carried out at SINTEF Building and Infrastructure in cooperation with the Department of Structural Engineering at the Norwegian University of Technology in Trondheim. The present work has been performed within the Concrete Innovation Centre (COIN), a centre for research based innovation, funded by the Norwegian Research Council and several industrial partners (www.coinweb.no). COIN is greatly acknowledged for the financial support and for facilitating the interaction between experts, students and industry. There are several people, employed by the industrial partners within COIN, who have contributed to the work in this thesis. In fear of forgetting someone, I simply say: Thank you!

Finally, I would like to thank my wife Katrine for her support and patience, especially the last couple of months.

Abstract

Concrete is a structural material with excellent properties when subjected to compression, but the abilities to resist tensile stresses are rather poor. The concrete's tensile zone is normally reinforced with large continuous steel bars, a combination which ensures an excellent construction material. Placing the re-bars generates many man-hours, which means that the reinforcement work accounts for a considerable part of the total concrete cost. An alternative to the conventional re-bars is fibre reinforced concrete.

Fibre reinforced concrete is concrete reinforced with small randomly distributed discontinuous fibres instead of large unidirectional continuous steel bars. In cases where the strength and ductility of fibre reinforced concrete is sufficient with regard to the actions, fibre reinforced concrete can be an adequate and cheaper alternative to conventionally reinforced concrete. If fibres are used together with conventional re-bars, both the total load carrying capacity and the stiffness of the structure will increase, and the crack widths will decrease.

One working hypothesis in the present thesis has been that the behaviour of fibre reinforced concrete can be uniquely described by the fibre slip, and an objective has been to investigate whether this hypothesis is correct or not. Due to the fact that the maximum fibre stress achieved during pull-out test is considerably less than the fracture stress for most fibre types, it is reasonable to assume that the fibres' pull-out length in a real structure is identical with the crack width, because the fibres will simply loosen at the weakest side of a crack. Based on a large number of experiments, and some simplified models which relate the experimental results to crack openings, it seems like the working hypothesis is correct.

A theoretical relation between the results from energy absorption test found by two different test codes is established. This relation is based on the above mentioned working hypothesis, and it is shown that the theoretical relation corresponds well to an empirical relation found in the literature.

A second objective has been to show that fibre reinforcement actually has sufficient strength and ductility to be used as a replacement to conventional re-bars in some types of concrete structures. A concrete called ductile high tensile strength all round concrete is developed, and this concrete shows promising properties with regard to both shear strength, bending strength and ductility.

The last few pages of the present thesis deals with some paradoxes from some of the material models used to describe fibre reinforced concrete from the literature. The experiences from the experimental work, and the analyses of the results, indicate that the fibre efficiency is increased by increasing crack widths until the crack widths reaches a certain level, while most of the models suggest that fibres are most effective at smaller crack widths.

Table of Content

Symbols and abbreviations

1. Roman letters

A_c	Cross sectional area of the concrete	[mm^2]
$A_{c,c}$	Cross sectional area of the concrete in the compressive zone	[mm^2]
$A_{c,t}$	Cross sectional area of the concrete in the tensile zone	[mm^2]
A_f	Cross sectional area of a fibre	[mm^2]
$A_{s,min}$	Minimum cross sectional area of reinforcement according to EC 2	[mm^2]
b	Width of a cross section	[mm]
d	Effective depth of a cross section; Diameter of a panel	[mm]
d_f	Fibre diameter	[mm]
d_{max}	Maximum particle size	[mm]
E_c	Modulus of elasticity	[MPa]
E_{ext}	External energy, the work done by moving loads	[J]
E_{int}	Internal energy, the work done by rotating yield lines	[J]
f_{ccm}	Mean value of concrete cube compressive strength	[MPa]
f_{ck}	Characteristic compressive cylinder strength of concrete at 28 days	[MPa]
f_{cm}	Mean value of concrete cylinder compressive strength	[MPa]
f_{ct}	Tensile strength of concrete	[MPa]
$f_{ct,fl}$	Flexural tensile strength of concrete	[MPa]
f_{ctm}	Mean value of axial tensile strength of concrete	[MPa]
f_{yk}	Characteristic yield strength of reinforcement	[MPa]
F	Load	[N]
F_c	Force resultant in the compressive zone	[N]
F_{crack}	Cracking load	[N]
F_f	Fibre load; Force resultant	[N]
$f_{ft,res}$	Residual tensile strength (or stress)	[MPa]
$f_{ft,res,2.5}$	Residual tensile strength at 2.5 mm deflection	[MPa]
f_{Fts}	Ultimate residual strength, MC 2010	[MPa]
f_{Ftu}	Serviceability residual strength, MC 2010	[MPa]
f_{fu}	Fibre fracture strength	[MPa]
f_R	Residual flexural tensile strength (or stress)	[MPa]
f_{yk}	Characteristic yield strength of re-bars	[MPa]
h	Height of a specimen	[mm]
h_{sp}	Effective height of a notched beam	[mm]
$h_{tensile}$	Height of the tensile zone	[mm]
K	Fibre overlap factor; Factor	[-]

l	Length; Span length; Length of a yield line projected to the axis of rotation	[mm]
l_b	Embedment length of a fibre	[mm]
l_{crit}	Critical embedment length with regard to fibre rupture	[mm]
l_f	Fibre length	[mm]
M_{cap}	Calculated bending moment capacity	[kNm]
M_{crack}	Bending moment at cracking	[kNm]
M_E	Applied bending moment	[kNm]
M_{Ed}	Design value of the applied internal bending moment	[kNm]
M_R	Bending moment capacity	[kNm]
M_{Rd}	Bending moment capacity of the compressive zone of the concrete	[kNm]
m_l	Moment capacity per unit length of a yield line	[kNm/m]
n_f	Total number of fibres per volume of concrete	[-]
$n_{f,layer}$	Number of fibres in each layer	[-]
$n_{f,tensile}$	Number of fibres in the tensile zone	[-]
O	Surface area	[mm^2]
R	Radius of a concrete panel	[mm]
r	Radius; Radius of the support configuration in panel tests	[mm]
r_r	Distance from the axes of rotation to the external load	[mm]
V_c	Volume of concrete	[mm^3]
V_E	Applied shear force	[kN]
V_{Ed}	Design value of applied shear force	[kN]
V_f	Total fibre volume	[mm^3]
$V_{R,c}$	Shear resistance of member without shear reinforcement (=$V_{R,ct}$ + $V_{R,cf}$)	[kN]
$V_{R,ct}$	Shear resistance of member without shear reinforcement due to concrete	[kN]
$V_{R,cf}$	Shear resistance of member without shear reinforcement due to fibres	[kN]
$V_{l,f}$	Volume of one fibre	[mm^3]
v_f	Volume fraction of fibres (V_f/V_c), normally given in percent	[-]
X	Height of the compressive zone	[mm]
y	Distance from the compressive surface	[mm]
y_t	Distance from the neutral axis to F_c	[mm]
Z	Internal moment arm, the distance between F_s and F_c	[mm]

2. Greek letters

Δ	Distance: Enlargement (Increment)	[mm]
Δc_f	Average distance between fibre centres	[mm]
ε_{c2}	Concrete strain at reaching the maximum strength	[-]
$\varepsilon_{ct,crack}$	Concrete tensile strain at cracking	[-]
ε_{cu2}	Ultimate concrete compressive strain according to table 3.1 in EC 2	[-]
ε_{yk}	Characteristic strain in re-bars at reaching f_{yk}	[-]
η_0	Capacity factor for fibres	[-]
σ	Stress	[MPa]
σ_c	Concrete compressive stress	[MPa]
σ_{ct}	Concrete tensile stress	[MPa]
$\sigma_{ct,f}$	Post cracking concrete stress due to fibres	[MPa]
σ_f	Fibre stress	[MPa]
$\sigma_{f,0}$	Fibre stress anchored by the end hook	[MPa]
$\sigma_{f,max}$	Maximum fibre stress	[MPa]
$\sigma_{f,max,1}$	Maximum fibre stress due to fibre rupture	[MPa]
$\sigma_{f,max,2}$	Maximum fibre stress due to fibre slippage	[MPa]
$\sigma_{f,max,3}$	Maximum fibre stress due to cone shaped concrete failure	[MPa]
$\sigma_{f,mean}$	Mean fibre stress in all fibres crossing a crack	[MPa]
τ_b	Bond stress between fibre and concrete	[MPa]

3. Abbreviations

1D	One dimensional
2D	Two dimensional
3D	Three dimensional
ASTM	The American Society for Testing and Materials
CMOD	Crack mouth opening displacement
EABS	Energy absorption capacity
FRC	Fibre reinforced concrete
NS-EN	European standard with the Norwegian Annex
LVDT	Linear Variable Differential Transformers
MC 2010	CEB-FIB Model Code 2010
RILEM	The International Union of Testing and Research Laboratories for Materials and Structures

1 Introduction

1.1 Background

Concrete is a structural material with excellent properties when subjected to compression, but the ability to resist tensile stresses are rather poor. Concrete cracks at relatively small tensile strains; leading to a rapid decrease in capacity, which means that concrete is a brittle material. To be able to resist tensile stresses, steel reinforcement is normally placed in the tensile zone. Reinforced concrete is an excellent construction material, and used in large scale. Because concrete is a plastic material in the fresh phase, there is virtually no limit to the architectural design for a concrete structure. Another advantage with concrete is that if it is used properly, concrete is a durable material.

There are some structural elements where reinforcement is not necessary with regard to the static calculation. This is typically structural elements subjected to compression, or when the tensile stresses due to shear or bending is less than the concrete's tensile stress capacity. The European Code for design of concrete structures, EC 2, requires that a minimum steel reinforcement ratio is used also for these kinds of structures to ensure that the ductility is satisfactory. The philosophy of the minimum required reinforcement area is that the capacity after cracking shall be at least as large as the capacity prior to cracking. The use of reinforcing bars may therefore roughly be divided into two groups:

1. To increase the ductility of a structural member.
2. To increase the strength of a structural member.

Fibre reinforced concrete is concrete reinforced with small randomly distributed discontinuous fibres instead of large unidirectional continuous steel bars. Fibre reinforcement may to a certain extent increase the strength of a structural member, but usually not sufficient to be an alternative to concrete reinforced with conventional re-bars. The use of fibre reinforcement will normally not affect the strain at cracking either, but the fibres are capable to transfer stresses across cracks, leading to a significant improvement of the residual strength. With sufficient amount of fibres, the residual strength may be larger than the cracking strength.

Löfgren has found that for a concrete building about 36 % of the total cost of the superstructure is related to labour costs, and about 22 % of the labour cost is related to the reinforcement work [Löfgren 2005]. Because EC 2 requires that also concrete members that do not need reinforcement based on the static calculation shall have a minimum reinforcement ratio, fibre reinforcement may be a cost effective alternative, even though the material cost is somewhat larger.

Fibre reinforcement may also increase the capacity of conventional reinforced concrete. In structural members reinforced with both re-bars and fibres, this makes it possibility to reduce the amount of re-bars. Alternatively, the amount of re-bars may be kept constant, resulting in reduced crack widths and increased stiffness.

Early age concrete is a continuously changing material that changes from being plastic to solid during the hardening. During cement hydration, the total volume of cement and water is reduced, leading in chemical shrinkage. In addition to chemical reaction, several other types of shrinkage can take place. If the volume change is restrained, stresses will be built up in the concrete, independent by the reason of the volume change. If the stress due to restrained

volume reduction is larger than the tensile strength of the concrete, the concrete will crack without being subjected to external loads. This occurs typically on slabs on ground. To control this kind of cracking it is common practice to place re-bars in two directions. To get the desired effect of this so-called "shrinkage-reinforcement" (which by the way cannot prevent shrinkage, just control the shrinkage cracking), the reinforcement should be placed in the upper third of the height of the slab. This may be hard to control. With use of fibre reinforcement, the fibres will be more or less randomly distributed across the cross section and in all directions, and thereby fibres may be more effective regarding crack limitation.

Fibre reinforced concrete is also used for rock support, for instance in tunnels. In such cases long bolts are used to prevent large stones from falling down, while fibre reinforced sprayed concrete is used to strengthen the tunnel lining between the bolts. Depending by the quality of the rock, the loads from the rock itself may be reduced with increasing deformation, which means that it is important that the fibre reinforced concrete has sufficient capacity at a certain deformation. Whether the crack widths are large or small is less important, as long as nothing falls down.

1.2 Objective and scope of research

There are several standardized test methods for fibre reinforced concrete. With regard to fibre reinforced sprayed concrete, the European standard NS-EN 14488-5, the Norwegian Concrete Association Publication nr 7, and the American standard ASTM C 1550 describes energy absorption tests on concrete panels [NS-EN 14488-5, NB 7 (2003/2011), ASTM C 1550]. In addition, there is a European standard NS-EN 14488-3 for determination of flexural strengths of fibre reinforced beam specimens in four point bending [NS-EN 14488-3].

For fibre reinforced concrete, the European standard NS-EN 14651 describes three point bending tests on beam specimens to measure the flexural tensile strength [NS-EN 14651]. To determine the flexural strength of non-reinforced concrete, the European standard NS-EN 12390-5 describes four point bending tests on beam specimens similar to NS-EN 14488-3, or alternatively three point bending tests [NS-EN 12390-5]. In Norway, four point bending tests [Thorenfeldt et al. (2006)] similar to the description in NS-EN 14390-5 and NS-EN 14488-3 have been used in fibre reinforced concrete research [Døssland (2008), Gjestemoen (2005), Sandbakk, Lauvålien & Stenvaag (2006), Lauvålien & Sandbakk (2007)].

In general, panel tests are performed to determine the energy absorption capacity, while beam tests are performed to determine the residual tensile strength. It is, however, different deflection limits in the different energy absorption related codes, which makes it difficult, if not impossible, to compare the absorbed energy directly. Further, to compare absorbed energy directly with residual strengths is impossible for the same reason.

Concrete reinforced with conventional re-bars are designed in such a way that the anchorage length is sufficient to prevent pull-out failure. The stress in the re-bars is increasing until it reaches the yield stress, but still the re-bars shall not be pulled out of the concrete, which ensure a ductile behaviour of the material. For fibre reinforced concrete, the ductility is ensured by fibre slippage. It is therefore reasonable to assume that it should be possible to describe the behaviour of fibre reinforced concrete by the pull-out response of single fibres. Further, because the maximum fibre stress during pull-out is considerably less than the fracture stress for most fibre types, it is reasonable to assume that the pull-out length is identical with the crack width, i.e. no yielding of the fibres.

The working hypothesis has been that the behaviour of fibre reinforced concrete can be described by the pull-out response of single fibres, and the main objective has been to prove whether this hypothesis is correct or not. The implication of the working hypothesis is that both beam tests and panel tests investigate the same material property, namely the *capacity vs. fibre slippage*, or the *capacity vs. crack opening*. In the present thesis a method to calculate the *residual flexural tensile stress* from panel tests are introduced, and the results from beam tests and panel tests can then be compared as *residual flexural tensile stress vs. crack opening*. With regard to the working hypothesis, the *residual flexural tensile stress vs. crack opening* should be comparable no matter which test method used to find this relationship.

Another objective is to show that fibre reinforcement actually has sufficient strength and ductility to replace conventional re-bars in some structures. To achieve this objective a considerable number of fibre types and concrete mixes have been included in the test programs.

1.3 Organization of the thesis

The present thesis is organized in 10 chapters.

Chapter 2 summarize the materials that are used in the present study. The different concrete mix designs and the different fibre types are shown and discussed briefly.

In chapter 3, results from pull-out tests on single fibres are reported. In total 232 pull-out tests have been performed, in which 210 is considered successful. Six different fibre types were tested in eight different concrete mixes. Chapter 3.1 gives a description of the test procedure, chapter 3.2 to chapter 3.5 show the results from all successful pull-out tests, chapter 3.6 introduces three different failure mechanisms and in chapter 3.7 these three failure mechanisms are evaluated by use of the results from the experimental work. Finally, a method to predict the fibre reinforced concrete's behaviour in tension and bending based on the results from pull-out tests are shown in chapter 3.8 and chapter 3.9, respectively.

Chapter 4 deals with different methods to perform beam tests. The chapter is divided into one theoretical part and one experimental part. In the theoretical part (chapter 4.1) the two different test methods that have been used are described, and a calculation method to be able to compare results from these test methods are proposed. In the experimental part (chapter 4.2), results from beam test of 30 small beams are reported and evaluated. 9 of the beams were reinforced with synthetic fibres, 15 were reinforced with steel fibres and the remaining 6 beams were reinforced with conventional steel bars. The latter six beams were tested simply to determine the post-cracking capacity of conventionally reinforced beams when tested according to the test methods for fibre reinforced beams.

Chapter 5 deals with different methods to perform panel tests. Similar to chapter 4, chapter 5 is divided into one theoretical part and one experimental part. A calculation model to determine the *flexural tensile stress vs. crack opening* relationship from panel tests is introduced in the theoretical part. By use of this model, it is possible to compare the energy absorption capacity also when the panel dimension and the support condition vary. In the experimental part, results from 60 panel tests are reported and evaluated. 30 panels were reinforced with synthetic fibres and the remaining 30 panels were reinforced with steel fibres. The fibre volume was constant, and the investigated parameters were the panel dimension and

the support condition. Two different support conditions were used in the experimental work, and the consequence of different panel dimensions and support conditions are evaluated.

In chapter 6 the results of beam- and panel tests are compared, and it is shown that if the results from both beam- and panel tests are expressed as *residual flexural tensile stress vs. crack opening*, both methods actually gives comparable results, as predicted by the working hypothesis.

In chapter 7 the theoretical relation between energy absorption capacity determined from panel tests according to ASTM C 1550 and NB 7 (2011) is shown. The assumption that the behaviour can be described by the *stress vs. crack opening* relation is used to find this relation. In addition, the theoretical relation is compared with the empirical relation found by Bernard [Bernard, E. S. (2002)], and it is shown that the theoretical relation is in good agreement with the empirical relation.

In chapter 8 the results from the *ductile high tensile strength all round concrete* project are reported and evaluated. This project involves both small beam testing, and testing of larger beams and slabs. The small beams were tested according to NS-EN 14651, a test method that is described in chapter 4. The small beam tests were performed to range different concrete compositions, and different fibre additions/combinations. The most promising combinations were thereafter tested in larger specimens, and both shear and moment strengths are investigated. In total 57 small beams were cast and tested in the development stage, and six large beams and 2 large panels were made to evaluate whether the results from small beam testing are comparable with the behaviour in larger structures. In addition to the 57 small beams tested in the development stage, three small beams were cast and tested for every concrete batch to control the reproducibility of the concrete.

A short discussion of some paradoxes for the fibre concrete material models are given in chapter 9, while the overall conclusions are summarized in chapter 10.

2 Materials

2.1 Concrete mixes

Because pull-out tests have been performed to map the pull-out response in almost all fibre reinforced concretes used at NTNU the last couple of years, a large number of different mixes have been used. The mix designs for all concretes used to map the pull-out response are shown in Table 2-1.

The mix designs of concrete C and concrete H were developed by Sandbakk, Lauvålien and Stenvaag and used in their project work at NTNU [Sandbakk, Lauvålien & Stenvaag (2006)], and further used in the experimental work of the master thesis of Lauvålien and Sandbakk [Lauvålien & Sandbakk (2007)].

When concrete C was developed, the main objective was to find a mix design that could be used to make a self-consolidating concrete (SCC) in strength class C 35/45. The concrete should be self-consolidating also after adding 0.5 vol% steel fibres or 1 vol% synthetic fibres. In [Sandbakk, Lauvålien and Stenvaag (2006)], the slump flow and compressive cylinder strength were reported to be 450-500 mm and 51 MPa respectively (inclusive fibres), while in [Lauvålien and Sandbakk (2007)] the slump flow and compressive cylinder strength were reported to be 650 mm and 39 MPa (exclusive fibres). The reason why it was a remarkable difference in compressive strength is unknown, but most likely one of the constituents were wrongly weighted. Normally it is considered difficult to make a SCC in the lower strength classes, because the amount of cement is low. To compensate for this a quite high amount of limestone powder was added. The idea was that the limestone powder, which is considered an inert material with respect to the chemical reaction between cement and water, would increase the amount of fines and thereby stabilize the concrete in the fresh phase.

When concrete H was developed, the main objective was to make a high strength concrete which was possible to cast when the steel fibre content was 2 vol%. High amount of silica fume and cement should guarantee for high strength, and a high matrix volume was necessary to make the concrete workable at all. In [Sandbakk, Lauvålien and Stenvaag (2006)], the slump flow and compressive cylinder strength were reported to be 420 mm and 124 MPa respectively (inclusive 2 vol% steel fibres), while in [Lauvålien and Sandbakk (2007)] the slump flow and compressive cylinder strength were reported to be 550 mm and 125 MPa (exclusive fibres).

The mix design of concrete A, E and G was developed by Lauvålien and Sandbakk and used in their master work at NTNU [Lauvålien & Sandbakk (2007)].

The mix design of concrete A and E was developed based on the experience from packing density tests performed as a part of the project work reported in [Sandbakk, Lauvålien & Stenvaag (2006)]. The packing density, ϕ, is simply defined as:

$$\phi = 1 - \varepsilon \tag{2-1}$$

where

ε: is the volume fraction of voids

The results from packing density tests showed that by limiting the maximum particle size, d_{max}, to 8 mm, the reduction in packing density was insignificant for steel fibre content up to 5

vol%. For that reason, d_{max} of concrete A and E was limited to 8 mm. Concrete A was meant to be a SCC in strength class C 25/30, while concrete E was meant to be a SCC in strength class C 45/55. The concretes were used to cast specimens which were tested according to the Norwegian sawn beam test method, and concrete A had a fibre content of either 1 vol% steel fibre or 2 vol% synthetic fibre, while concrete E had a fibre content of either 2 vol% steel fibre or 3 vol% synthetic fibre. The concretes were meant to be SCC before these amounts of fibres were added, but it should still be possible to cast specimens after adding the fibres. The test specimens for pull-out test on single fibres were made of concrete including fibres, but it is assumed that the pull-out resistance not is affected by the fibre amount in the concrete. With regard to the pull-out tests on fibres embedded in concrete A, the steel fibres were pulled out of concrete A including 1 vol% steel fibres, while the synthetic fibres were pulled out of concrete A including 2 vol% synthetic fibres. For concrete E, the steel fibre results are average results from pull-out tests on fibres embedded in concrete E including 0.5, 1.0 and 2.0 vol% steel fibres, while the synthetic fibre results are average results from pull-out tests on fibres embedded in concrete E including 2.0 and 3.0 vol% synthetic fibres.

The slump flow of concrete A was 430 mm and 470 mm for 2 vol% synthetic fibres and 1 vol % steel fibres, respectively. The slump flow of concrete E was in the range 450-650 mm depending on the fibre content. All results from slump flow tests for concrete A and E are reported in [Lauvålien and Sandbakk (2007)].

The mix design of concrete G was made as similar to concrete C as possible. This was done so that the only difference in mix design should be the water to binder ratio. While concrete A, C, E and H have been used to make other test specimens, concrete G has only been used for pull-out tests. The slump flow of concrete G was 700 mm.

The pull-out tests on fibres embedded in concrete A, C, E, G and H were performed as a part of the experimental program in the master thesis of Lauvålien and Sandbakk. Some results from the pull-out tests are reported in [Lauvålien and Sandbakk (2007)], but the present analyses of the results are unique for the present thesis.

More information about the development work and fresh properties of concrete C and H can be found in [Sandbakk, Lauvålien & Stenvaag (2006], while information of concrete A, E and G can be found in [Lauvålien and Sandbakk (2007)].

The mix design of concrete B and F has only been used in the pull-out tests reported in chapter 3. As seen in Table 2-1 concrete B and F had less matrix volume than the other mixes and instead of using limestone powder to reduce the water to powder ratio it was used aggregate with particle size 0-2 mm.

Concrete D has been used in several experimental programs at NTNU the last couple of years, and concrete D is the only concrete that has been used for both pull-out tests, beam tests and panel tests. With regard to the beam- and panel tests reported in chapter 4 and chapter 5, concrete D has been used for all beams and panels. Concrete D has been used because the content of limestone powder and silica fume is in the normal range, the aggregate is quite typical for ordinary concrete and also the compressive strength is quite typical for ordinary concrete.

The mix design of concrete A to H is shown in Table 2-1.

The mix design for the different concretes used in the *ductile high tensile strength all round concrete* project reported in chapter 8 are not included in Table 2-1.

Table 2-1 Overview mix design

	Mix design, concrete:							
	A	B	C	D	E	F	G	H
Cement type	CEM II/A-V 42.5 R					CEM I 52.5 N	CEM II/A-V 42.5 R	CEM I 52.5 N
Cement[1]	284	341	373	368	439	413	426	608
Silica[1]	6 % (17)	5 % (17)	5 % (19)	6 % (22)	6 % (26)	5 % (21)	5% (21)	20 % (122)
Limestone powder[1]	30 % (85)	-	25 % (94)	5 % (18)	-	-	25 % (106)	-
Water[1]	223	199	194	214	197	182	170	168
Aggregate, 0-2mm[1]	-	224	-	-	-	223	-	-
Aggregate, 0-8mm[1]	1701	943	1345	1025	1701	943	1345	1229
Aggregate, 8-16mm[1]	-	631	337	683	-	631	337	308
Super plasticizer type	Glenium Skyflux 550	Sika Eco 20	Glenium Skyflux 550	Glenium 151	Glenium Skyflux 550	Glenium 151	Glenium Skyflux 550	Glenium Skyflux 550
Super plasticizer[2]	0.6	1.0	1.8	1.0	1.2	1.0	1.8	2.0
v/b-ratio[3]	0.7	0.53	0.47	0.52	0.4	0.4	0.36	0.20
v/p-ratio[4]	0.47	0.45	0.35	0.42	0.36	0.35	0.28	<0.2
Matrix volume [l/m^3]	390	355	390	380	390	355	390	450
f_{cm} [MPa]	24	38	39[6]	50	54	68	77	125
f_{ctm} [MPa]	3.1[5]	-	-	3.23	4.4[5]	-	-	-

[1]The numbers are given in percent of cement weight and (kg per m^3 concrete)
[2]The numbers are given in percent of cement weight
[3]w/b-ratio = w/(c+Σkp)
[4]v/p-ratio varies somewhat within the different mixes because of different batches of aggregate. Powder is defines as all particles with particle size less than 125µm [Mørtsell, E. (1996)]
[5]Tested on concrete with 2 vol% synthetic fibres [Lauvålien and Sandbakk(2007)]
[6] f_{cm} = 52 MPa when used first time in [Sandbakk, Lauvålien and Stenvaag (2006)]

The content of the materials are shown as kg per m^3 of concrete, and will be correct when the air content and fibre content is zero. When fibres were added to the concrete, the matrix volume has been kept constant which means that some of the aggregates were removed to make place for the fibres within the 1 m^3 of concrete inclusive fibres.

The other possibility is simply to add the fibres in addition to all other constituents, but then the mix design would not give 1 m^3 of concrete, and the matrix volume per m^3 would have been reduced.

2.2 Fibre types

In total six different fibre types have been used in different experimental tests. The characteristics for all the tested fibre types are shown in Table 2-2, while Figure 2-1 shows photos of them.

Table 2-2 Fibre characteristics, from product data sheets

	Performance class	Fibre length, l_f [mm]	Fibre diameter, d_f [mm]	Aspect ratio [l_f/d_f]	Tensile strength [MPa]	E-modulus [MPa]
HE 8060	80	60	0.75	80	1160	210000
HE 6560	65	60	0.9	66.7		
HE 6535	65	35	0.55	63.6		
FE 1050	-[1]	50	1.0	50	1050	~210000[1,3]
URW 1050						
Synthetic	-[1]	48	0.9[1,2]	53.3[1,2]	550	10000

[1]Not specified from the producer
[2]Assumed to be equal 0.9 mm
[3]Assumed to be as for the HE-fibres

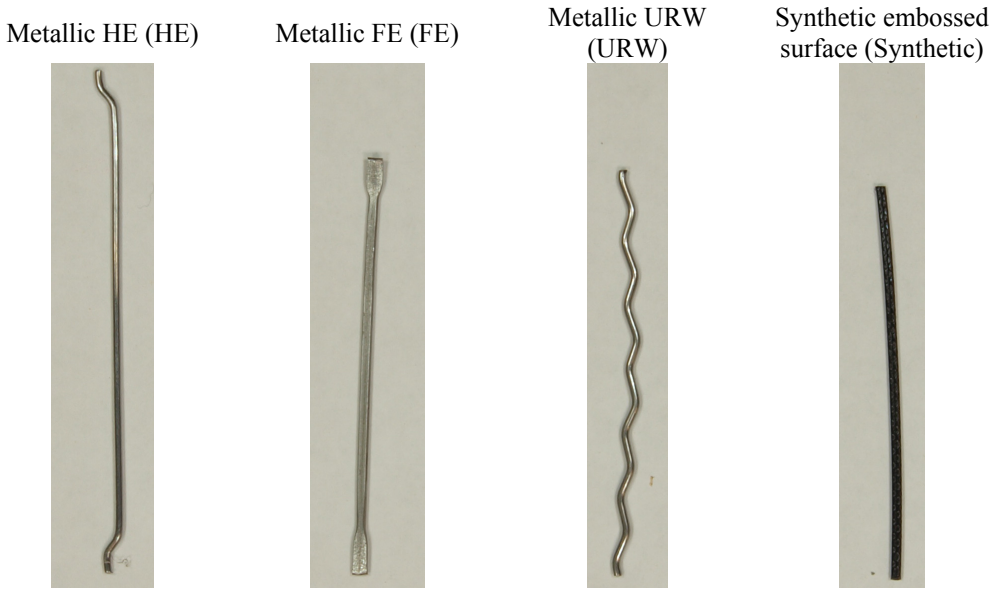

Figure 2-1 Typical shape of the different fibre types

The typical shape of the hooked end fibres (HE) are shown in Figure 2-1. The HE fibres used in the present study are Dramix fibres produced by Bekaert. The brand name is *Dramix RC-XXYY-BN*, where XX is the performance class and YY is the fibre length. A typical misunderstanding regarding the Dramix fibres is that the performance class is equal to the aspect ratio, but as seen in Table 2-2 this is not entirely correct. If the performance class is used to calculate the fibres' cross sectional area, the cross sectional area will be somewhat overestimated for the Dramix 6560 fibres and somewhat underestimated for the Dramix 6535

fibres. From the product data sheet [Bekaert] it is found that these HE fibres are cold drawn steel wire fibres made of low-carbon steel with bright steel surface and glued together. Even though only HE fibres produced by Bekaert is used, it is expected that other fibres that have similar shape and material will show equal behaviour.

The FE and URW fibres used in the present study are Novocon 1050 fibres produced by Propex Concrete Systems. These fibres are cold drawn steel wire fibre as the Dramix fibres, but in contrast to the Dramix fibres, the Novocon fibres are not glued together. The two types of Novocon fibres used in the present investigation are shown in Figure 2-1. There is also a Novocon 1050 hooked end fibre available in the market, but the Novocon hooked end fibres are not included in these studies.

Elasto Plastic Concrete produces the synthetic fibres used in the present studies. The fibres are made of polyolefin, and they have an embossed surface to increase the bond to the concrete. The brand name of these fibres is Barchip Shogun, and a picture of one fibre is shown in Figure 2-1.

Results from pull-out test on single fibres are reported in chapter 3, and the behaviour of five types of steel fibre and one type of synthetic fibre is investigated. All fibre types have been tested with an embedment length $l_b=l_f/2$, and some of them have in addition been tested with embedment length $l_b=l_f/6$. In each series, at least five fibres were tested. The characteristics for all the tested fibre types are shown in Table 2-2.

With regard to the experimental work on beams and panels, only the hooked end steel fibre and the synthetic fibre have been used.

3 Pull-out tests on single fibres

Pull-out tests on single fibres have been performed on a wide range of fibres embedded in various concrete mixes. This reported mapping of fibre-concrete properties has been carried out as part of several comprehensive fibre reinforced concrete projects. Therefore, the range of concrete properties and fibre types is quite broad. The most probable failure mechanism for some of the fibre and concrete combinations is described and evaluated.

In chapter 3.2 to chapter 3.5, the *fibre stress vs. slip* relationship is reported for all fibre and concrete combinations. During the pull-out tests it has been observed that different types of failure mechanisms have occurred, which might explain why an increase in fibre volume not necessarily results in higher load carrying capacity for instance for a beam exposed to bending. A suggestion of three different failure mechanisms is presented in chapter 3.6.

It will be shown that the maximum fibre stress is not only a fibre parameter, but strongly influenced also by the concrete composition. Not only the concrete strength influences the bond between concrete and fibre, but also the content of fine particles as for instance limestone powder.

Pull-out tests on single fibres give valuable information of the stress vs. slip relation for a given fibre embedded in a particular concrete. This relation might be used to foresee the fibre's influence on the hardened concrete's behaviour in tension or bending. In chapter 3.8, it is described in which way results from pull-out tests might be used to predict the tensile behaviour, while in chapter 3.9 prediction of the behaviour in bending is explained. The predicted behaviour is also compared with experimental results.

3.1 Test procedure

The test specimens for pull-out tests on single fibres were made by casting concrete into a formwork made of a plastic tube with diameter and height of 100 mm and 60 mm, respectively. At one end, a plastic plate was glued to the tube to make the formwork watertight, and in the centre of the plate, a hole was drilled for fibre placement. To ensure that the fibre embedment length was as prescribed, the fibres were stuck through the plastic plate and into a layer of expanded polyester, as shown in Figure 3-1.

Figure 3-1 Formwork for a pull-out test specimen

After casting, the test specimens were stored under plastic sheets for approximately 24 hours, before they were placed in water until testing at 28 days.

The pull-out tests was performed according to the procedure described in the Norwegian design rule draft from 2006 [Thorenfeldt et al. (2006)]. The test specimens were fixed to the table with nippers; while the fibre was fastened in a gripping device connected to the test machines load recorder, see Figure 3-2. The synthetic fibres have a tendency to break in the gripping device [Døssland (2008)], and to avoid the problem the synthetic fibres were placed into a thin plastic tube which protects the fibre.

Figure 3-2 Test rig for pull-out tests

The pull-out tests were displacement controlled, and while the Norwegian design rule draft from 2006 prescribes a displacement rate of 0.2 mm/min [Thorenfeldt et al. (2006)], which is very time consuming, Gysel described a similar pull-out test setup with a displacement rate of 1.0 mm/min [Gysel (2000)]. Therefore, in the present pull-out tests a constant rate of 1.0 mm/min was chosen. After approximately 500 seconds, the tests were stopped at a pull-out length of approximately 8 mm. During the tests, corresponding values for load and pull-out displacement were recorded.

In the present thesis, the following terminology is used:

Pull-out resistance:	The fibres total resistance to be pulled out of the concrete.
Anchorage capacity:	The end anchorage's contribution to the total pull-out resistance.
Static friction:	The pull-out resistance before the fibre starts to slide out of the concrete.
Sliding friction:	The pull-out resistance after the fibre has started to slide out of the concrete.
Fibre-concrete bond:	The bond stress between concrete and fibre, due to either static friction or sliding friction dependent by the slip. The anchorage capacity is not included in the fibre-concrete bond.

3.2 Results from pull-out tests on HE fibres

The results from pull-out tests on HE fibres are shown as fibre stress vs. slip curves in Figure 3-3. All HE fibres were tested with two embedment lengths, namely $l_b = l_f/2$ and $l_b = l_f/6$.

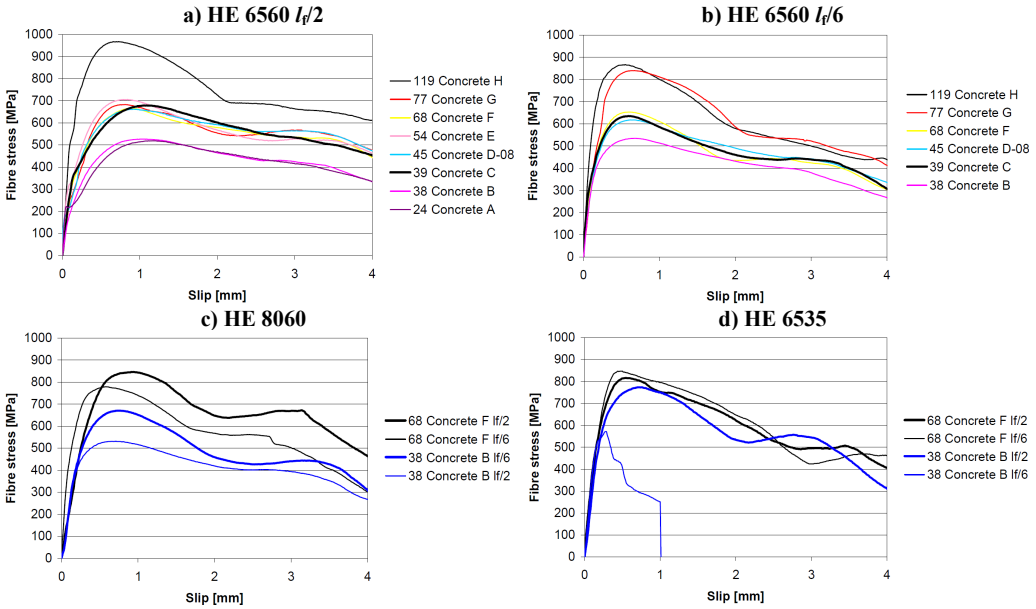

Figure 3-3 Pull-out tests, HE fibre

The behaviour will be discussed in details in the following sub-chapters.

3.2.1 HE 6560

Embedment length $l_b = l_f/2$

As seen from Figure 3-3a), the fibre stress is strongly dependent on the concrete type and quality. The fibres embedded in concrete H, which had a compressive strength of 119 MPa, reached approximately 970 MPa, while the fibres embedded in concrete A and B (compressive strength 24 and 38 MPa) only reached approximately 520 MPa. Concrete C had almost the same compressive strength as concrete B, but still the fibre stress reached approximately 680 MPa. As seen in the mix design, the main difference between concrete B and C is that in concrete B sand with particle size between 0 and 2 mm was used to increase the amount of fines, while in concrete C limestone powder was used. The water to powder ratio was 0.45 and 0.35 in concrete B and C respectively. It is therefore likely to believe that addition of limestone, or other small particles, may increase the fibre-concrete bond.

Fibres embedded in concrete D, E, F and G had almost identical fibre stress vs. slip curves, and the maximum fibre stress was approximately 675 MPa, while the compressive strength varied from 50 to 77 MPa.

Another important result is that the maximum fibre stress occurred at a slip of approximately 1 mm in the concrete A and B, approximately 0.9 mm for concrete D to G, and 0.7 mm for concrete H. Consequently, the slip at maximum stress is decreasing with increasing concrete strength.

Embedment length $l_b = l_f/6$

Figure 3-3b) shows the fibre stress vs. slip curves for all HE 6560 fibres tested with embedment length $l_f/6$. Similar concrete strength dependency was found also when the embedment length was reduced to $l_f/6$. The maximum fibre stress in all HE fibres is listed in Table 3-1. The maximum fibre stresses shown in Table 3-1 are determined as the average of the highest measured fibre stress in all fibres within each series.

Table 3-1 Maximum fibre stress, HE 6560

	Maximum fibre stress [MPa]			Ratio $l_f/6$ / $l_f/2$
	$l_f/2$	$l_f/6$	No hook	
Concrete A	523	-[1]	-[1]	-
Concrete B	536	538	-[1]	1.00
Concrete C	684	641	339	0.94
Concrete D-08	667	619	-[1]	0.93
Concrete E	719	-[1]	-[1]	-
Concrete F	683	656	-[1]	0.96
Concrete G	694	844	301	1.22
Concrete H	971	874	632	0.90
[1]Not tested				

As seen from Table 3-1, approximately 95% of the fibres capacity can be related to the end anchorage, because when the embedment length was reduced from 30 mm to 10 mm, the maximum fibre stress was only reduced by approximately 95 %. If the bond between the steel surface and the concrete is important, the reduction in fibre stress should have been larger when the total bond area is reduced by 67 %. The maximum fibre stress was actually larger in the $l_f/6$- fibres than for the $l_f/2$-fibres in concrete B and G, which is quite surprising. Certain explanation is not found, but one possible explanation may be that if the maximum fibre stress is mainly due to the end anchorage, statistical variation may lead to this phenomena.

The maximum fibre stress occurred at approximately 0.5 mm slip, which is less than for fibres with $l_f/2$ embedment length.

To investigate the effect of the end anchorage further, pull-out tests were performed on fibres where the end hook was cut off. Fibres were cast in concrete C, G and H, and the fibre stress vs. slip curves are shown in Figure 3-4.

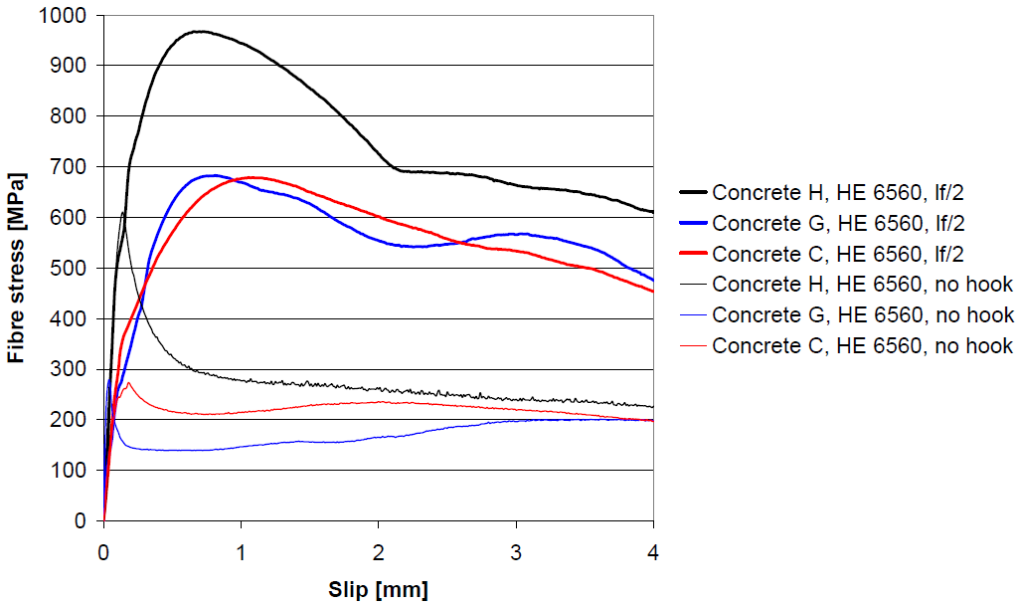

Figure 3-4 End hook effect HE 6560

The fibres without end anchorage embedded in concrete H reached approximately 630 MPa before the fibres started to slide, but once they started to slide, the fibre stress was reduced rapidly until the fibre stress was about 300 MPa. From 1 mm to 4 mm slip, the fibre stress was gradually reduced from about 280 MPa to 220 MPa. The fibres embedded in concrete C and G did not have a similar high fibre stress before they started to slide. At 4 mm slip, the fibre stress in fibres embedded in concrete C, G and H was about the same level, which implies that the sliding friction between fibres and concrete is not significantly affected by the concrete strength, which is in contrast to the total resistance. When the total resistance seems to be affected by the concrete strength, this seems to be better described by the static friction than the sliding friction.

At small slip values (<0.1 mm), the pull-out resistance was more or less the same for fibres with embedment length $l_f/2$ and $l_f/6$, and also for the fibres without end hook. This means that before any deformation in the fibre has occurred, the static friction between a fibre and the concrete is independent of the shape of the fibre, and this friction contributes to around 50% of the maximum pull-out resistance, as seen in Table 3-1. It may be assumed that the first peak for the *no hook* curves in Figure 3-4 is when the fibre end starts sliding out of the concrete. Pompo et al have shown similar relationships between load and slip in a test where they made test specimens with steel fibres with different end anchorages [Pompo et al. (1996)]. At different stages of the tests, Pompo et al. made photos of the fibre's position in the cement matrix and compared the photos with the load vs. slip graph.

At larger slip (but still before maximum load) the pull-out resistance was quite similar for fibres with embedment length $l_f/2$ and $l_f/6$.

3.2.2 HE 8060

Pull-out tests on HE 8060 have been performed in concrete B and F. Fibres with embedment length $l_f/2$ and $l_f/6$ have been tested, and the fibre stress vs. slip curves are shown in Figure 3-3c).

As for the HE 6560 fibres, the fibre stress is dependent by the concrete strength, and the major contribution is from the end hook. The maximum fibre stresses are shown in Table 3-2.

Table 3-2 Maximum fibre stress, HE 8060

	Maximum fibre stress [MPa]		Ratio $l_f/6$ / $l_f/2$
	$l_f/2$	$l_f/6$	
Concrete B	527	648	1.23
Concrete F	851	790	0.93

For concrete B, the maximum fibre stress was higher when the embedment length was $l_f/6$ than for $l_f/2$, which is similar to the results for the HE 6560 fibres in concrete C.

The maximum fibre stress was reached at a slip ranging from 0.8 to 0.9 mm, which also is similar to the results for the HE 6560 fibres.

3.2.3 HE 6535

Pull-out tests on HE 6535 fibres have been performed in concrete F and B. The fibre stress vs. slip curves are shown in Figure 3-3 d), and the maximum fibre stress are summarized in Table 3-3.

Table 3-3 Maximum fibre stress, HE 6535

	Maximum fibre stress [MPa]		Ratio $l_f/6$ / $l_f/2$
	$l_f/2$	$l_f/6$	
Concrete B	777	698	0.90
Concrete F	816	888	1.09

The most interesting finding from the pull-out tests on HE 6535 fibres is that the maximum fibre stress is considerably higher than for HE 6560 fibres embedded in equal concrete, even though the aspect ratio is equal. Reducing the embedment length from $l_f/2$ to $l_f/6$ increased the resistance for the fibres embedded in concrete F (supporting the assumption that the major contribution to the pull-out resistance is from the end hook) while the fibres in concrete B showed a very different fibre stress vs. slip relation. HE 6535 with 5.8 mm embedment length came out of the concrete without straightening out the end hook, and the surrounding concrete was broken. This behaviour may be explained by a *cone-shaped concrete failure mechanism*, which will be further discussed in chapter 3.6. The maximum fibre stress was reached at a slip of approximately 0.5 mm, which is less than for HE 6560 and HE 8060 fibres.

3.2.4 HE summarized

HE fibre's bond to the concrete is mainly due to the end hook. The maximum fibre stress is more or less unaffected if the embedment length is reduced from $l_f/2$ to $l_f/6$, but HE 6535 fibres with $l_f/6$ embedment length may create cone-shaped concrete failure if the concrete strength is insufficient to carry the load from the fibre. In concrete structures, it is impossible to control the embedment length in a random crack, and it seems reasonable that the average

embedment length in all fibres crossing a random crack will be $l_f/4$. This makes it important to be aware of the pull-out resistance also at embedment lengths less than $l_f/2$.

Figure 3-5 shows the fibre stress vs. slip curves for the different HE fibres with embedment length $l_f/2$ in concrete B and F.

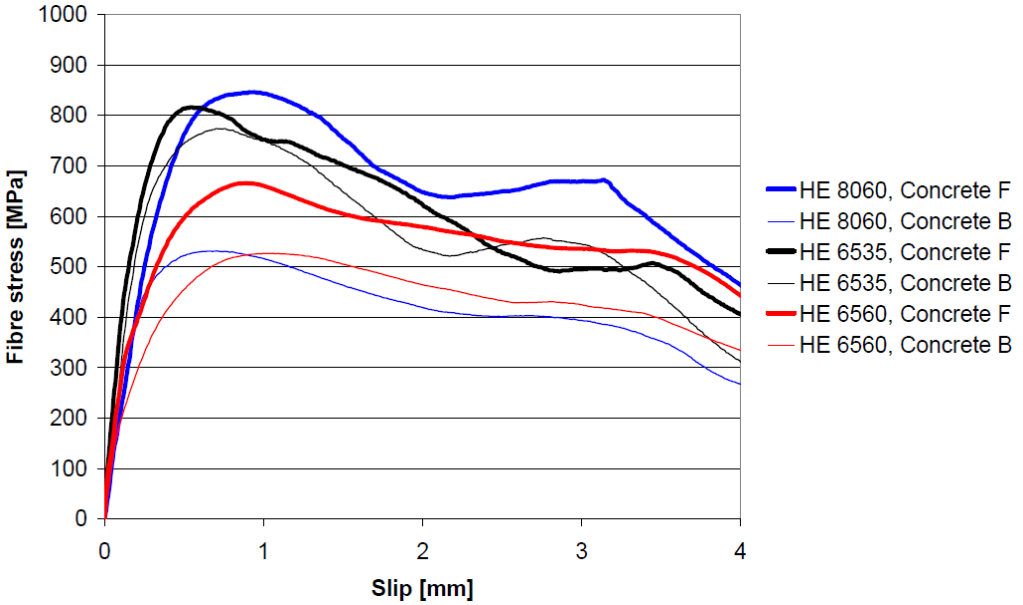

Figure 3-5 HE fibres in concrete B and F, $l_f/2$

From the curves in Figure 3-5 it seems like the HE 8060 fibres would be most effective in concrete F, and HE 6535 in concrete B. But again, because the HE 6535 fibres created a cone-shaped concrete failure at reduced embedment length, it is probable that the concrete strength is insufficient to utilize the fibre potential.

The $(l_f/6)/(l_f/2)$-ratio for maximum fibre stress is shown in Table 3-1 and Table 3-2 for HE 6560 and HE 8060 respectively, and varies from 0.76 to 1.2, which once again indicates that the end anchorage contributes to most of the pull-out resistance.

The shape of the fibre stress vs. slip curves for pull-out tests on HE fibres is in good agreement to similar tests by Weiler and Grosse [Weiler and Grosse (1996)], who made pull-out tests on Dramix fibres embedded in transparent epoxy resin. At different stages during pull-out, they made photographs of the hooked end steel fibre's position in the transparent epoxy resin, and compared those photos with the load vs. slip curve. In this way, they showed that the first load maximum has its reason in a partial straightening of the two angles in the end hook. The second maximum, or the end of partial stable plateau, may also be explained by a straightening of the end hook, and in this case the remaining hook has only one angle (the other is already straightened) and therefore the load is less. The end of the partial stable plateau in the present tests is typical at 3 to 4 mm slip.

3.3 Results from pull-out tests on FE 1050- and URW 1050-fibres

It has been performed pull-out tests on two types of 1050 fibres, FE 1050 and URW 1050. Both fibre types are tested with embedment length $l_f/2$ and $l_f/6$, and the fibre stress vs. slip curves are shown in Figure 3-6.

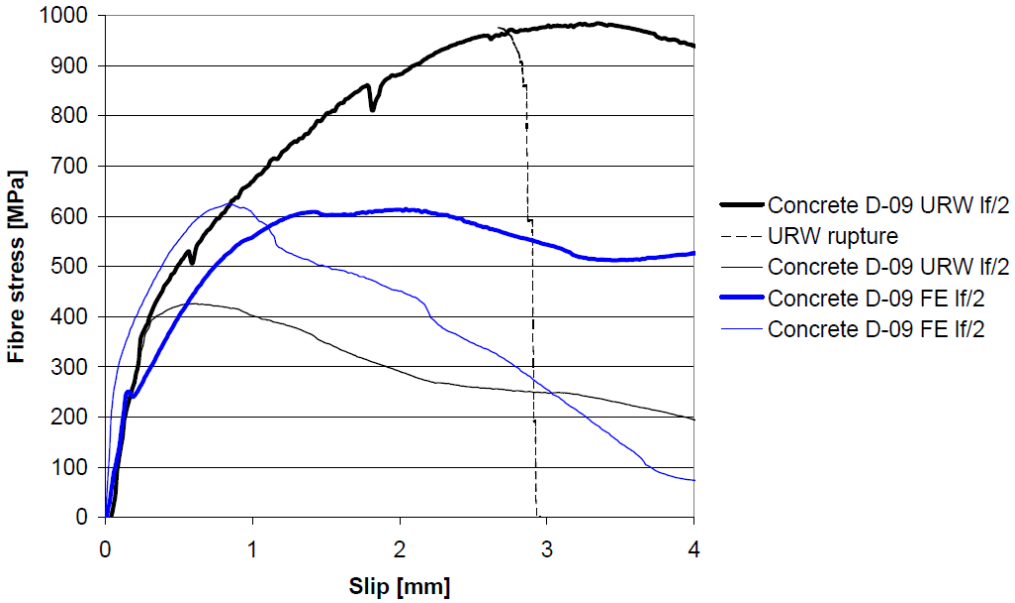

Figure 3-6 Pull-out tests, 1050 fibres

The bond between the concrete and URW fibres was sufficient to create fibre rupture in 4 of 5 fibres, which means that the URW curve shown in Figure 3-6 is not representative for the fibre behaviour in this concrete. Nevertheless, the curve for the only fibre that did not break is shown because it is likely to believe that the curve is representative for this fibre type in a concrete with less strength. The URW fibres came out of the concrete completely straightened out regardless of the embedment length, and while the fibres with $l_f/6$ embedding reached maximum fibre stress at approximately 0.5 mm slip, the fibres with $l_f/2$ embedding showed increasing fibre stress until about 3 mm slip.

The flat end of the FE fibres did not change its geometry during the pull-out tests, unlike the other steel fibres. This is the explanation why the pull-out resistance for embedment length $l_f/2$ is almost constant with increasing slip. The maximum fibre stress for the FE fibres with $l_f/6$ embedding was almost equal to the maximum fibre stress for fibres with $l_f/2$ as shown in Table 3-4, which indicates that also for these fibres the end anchorage contributes to most of the pull-out resistance.

Table 3-4 Maximum fibre stress, 1050 fibres

Concrete D-09	Maximum fibre stress [MPa]		Ratio $l_f/6$ / $l_f/2$
	$l_f/2$	$l_f/6$	
FE 1050	647	668	1.03
URW 1050	981	419	0.43

The URW fibres with $l_f/6$ embedding reached 43 % of the capacity of the fibres with $l_f/2$ embedding at maximum fibre stress. If the sliding friction is proportional with the embedment

length, which seems reasonable if the bond between concrete and fibre is constant, the capacity at sliding should be 33 %. This statement is not possible to analyze further because the pull-out tests were stopped before the slip was large enough to be sure that all the waves of the URW fibre were really straightened out. When the embedment length was reduced from $l_f/2$ to $l_f/6$ the maximum fibre stress was reduced from approximately 980 MPa at 3 mm slip (fibre rupture) to a maximum fibre stress of about 420 MPa at 0.5 mm slip. The curve for the fibres with $l_f/6$ embedding follows the curve for the fibre with $l_f/2$ embedding until the fibre stress reached approximately 380 MPa. At this level, the $l_f/6$ fibres started to slide in the concrete and the pull-out resistance depends on the sliding friction between fibre and concrete.

With increasing slip, the pull-out resistance for the FE fibres with $l_f/2$ embedding remains more or less at the same level. Unlike the HE and URW fibres, these fibres were not straightened when they were pulled out of the concrete. This fact also indicates that the end anchorage for the FE fibres contributes to most of the resistance, because if the friction between concrete and the straight part of the fibres were an important parameter the resistance should be proportional to the embedment length.

The FE fibres with $l_f/6$ embedding showed a considerably reduced resistance with increasing slip, and at 4 mm slip, the resistance was practically zero. The explanation for this is that the surrounding concrete was not able to carry the load from the fibre, resulting in a cone-shaped concrete failure, a mechanism that will be discussed in chapter 3.6.

3.4 Synthetic fibres with embossed surface

The synthetic fibres were only tested with embedment length $l_b=l_f/2$ and the fibre stress vs. slip curves from the pull-out tests are shown in Figure 3-7.

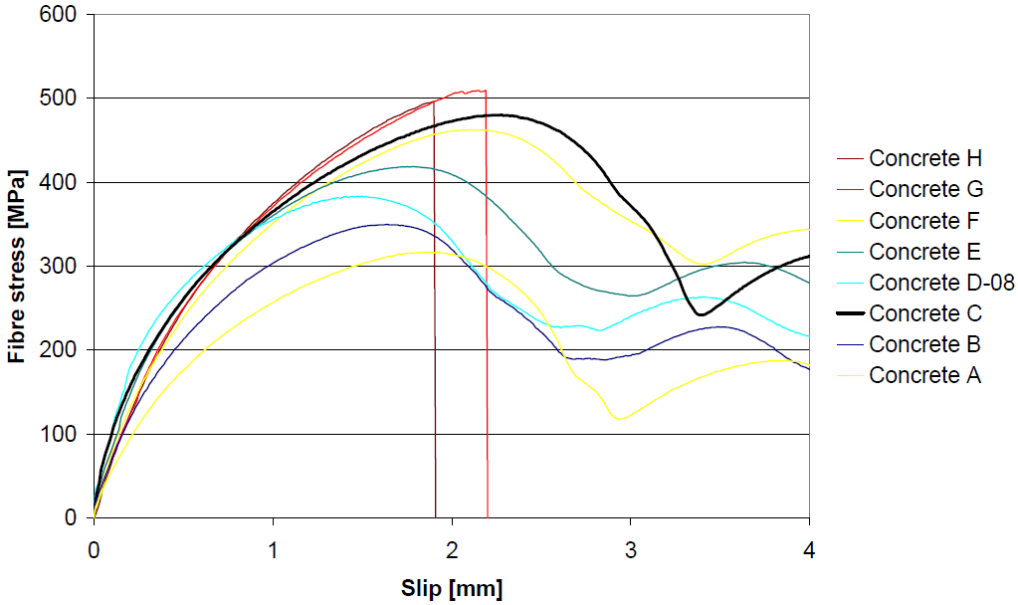

Figure 3-7 Pull-out tests, synthetic fibres

The fracture strength of the synthetic fibres is reported by the producer to be 550 MPa. As for the HE fibres, the fibre stress is increasing with increasing concrete strength. In concrete G and H, the fibres reached almost 500 MPa, and then tensile failure occurred. It was shown in Figure 3-3 that the HE 6560 fibres reached surprisingly high fibre stress with regard to the concrete strength in concrete C, and this is even more pronounced for the synthetic fibres. The maximum fibre stress for the synthetic fibres embedded in concrete C was 480 MPa, and the best explanation for this high fibre stress is that the high limestone powder amount created a really good bond between the fibre and the concrete.

The synthetic fibres reach their maximum fibre stress at a slip of typically 2 mm, which means that it is expected that these fibres need larger crack openings than the HE fibres to achieve their capacity for transferring stresses across cracks.

Even though all fibres reached their fracture stress in concrete G and H, it does not necessarily mean that the fibres are insufficient to use in concrete with compressive strength larger than 77 MPa, simply because a crack opening of 2 mm is larger than expected in a real structure and it is furthermore unlikely that all fibres are placed with half the fibre on each side of the crack.

3.5 Comparison all fibre types

The maximum fibre stress for all fibre types embedded in all concrete mixes is summarized in Table 3-5.

Table 3-5 Maximum fibre stress, all mixes and all fibre types

Fibre type and embedment length			Concrete								
			A	B	C	D 08	D 09	E	F	G	H
HE	6560	$l_f/2$	523	536	684	667	-	719	683	694	971
		$l_f/6$	-	538	641	619	-	-	656	844	874
		No hook	-	-	339	-	-	-	-	301	632
	8060	$l_f/2$	-	527	-	-	-	-	851	-	-
		$l_f/6$	-	648	-	-	-	-	790	-	-
	6535	$l_f/2$	-	777	-	-	-	-	816	-	-
		$l_f/6$	-	698	-	-	-	-	888	-	-
1050	FE	$l_f/2$	-	-	-	-	647	-	-	-	-
		$l_f/6$	-	-	-	-	668	-	-	-	-
	URW	$l_f/2$	-	-	-	-	981	-	-	-	-
		$l_f/6$	-	-	-	-	419	-	-	-	-
Synthetic		$l_f/2$	395	360	485	394	-	440	473	537	528

Unfortunately, not all fibres were tested embedded in the same concrete. The HE 6560 fibre and the synthetic fibre were tested in all concretes, while the FE and URW fibres were only tested embedded in concrete D 09. The HE 8060 and HE 6535 fibres were only tested when embedded in concrete B and F. Based on the results from pull-out tests on HE 6560 fibres shown in Figure 3-3a) and b), it is assumed that the HE 8060 and HE 6535 fibres embedded in concrete D would have had a fibre stress vs. slip curve similar to the average of the curves for these fibres embedded in concrete B and F, respectively. In this way, it is possible to compare the results from pull-out tests by using concrete D as a reference.

Figure 3-8 shows the expected results from pull-out tests on HE 8060 and HE 6535 fibres embedded in concrete D and the real results from pull-out tests on synthetic, FE, URW and HE 6560 fibres embedded in concrete D. All fibres have embedment length $l_f/2$.

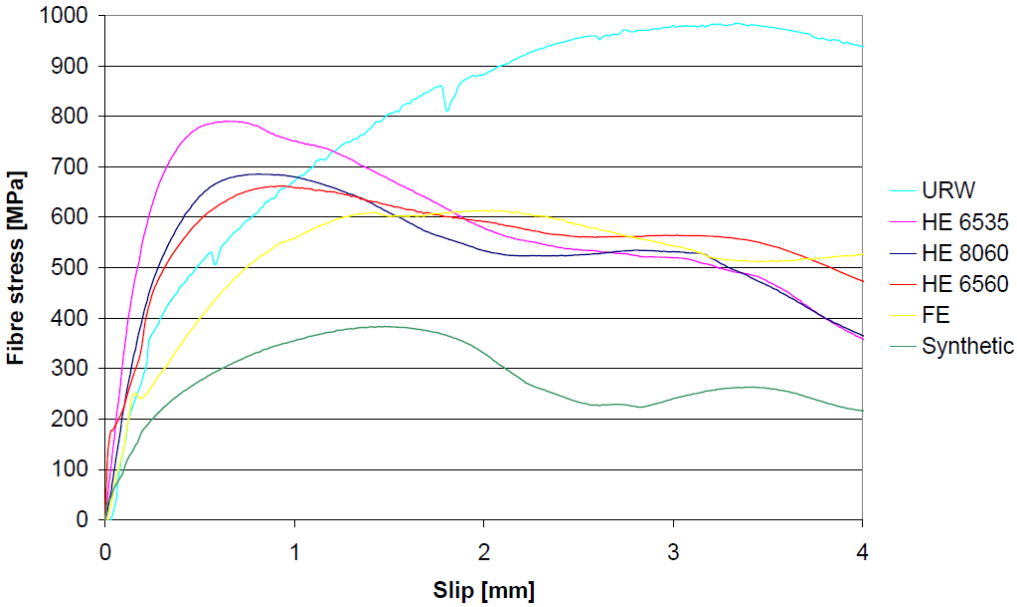

Figure 3-8 Pull-out tests, comparison all fibre types

As seen from the curves in Figure 3-8, the different fibre types have very different behaviour when they are pulled out of the concrete. It should be noted that the different fibre types have different length, which means that the embedment length measured in millimetres is not equal. This fact is probably of minor importance for the fibres with end anchorage because the major contribution to the pull-out resistance is due to the end anchorage. It should also be noted that even if the pull-out resistance for fibres embedded in concrete D does not be the average of the pull-out resistance for fibres embedded in concrete B and F, the differences in behaviour for the different fibre types should be as illustrated in Figure 3-8.

The HE fibres reached their maximum fibre stress at less slip than all other fibres, which may be favourable in order to be effective at small crack widths. The FE fibres had more stable fibre stress after about 1 mm slip than the other fibres, which may result in a constant capacity to transfer stresses across cracks even though the crack widths for some reason increases. The URW fibres seem to have the largest potential, but they may be less effective if small crack widths are important.

The synthetic fibres reached their maximum capacity at larger slip than the HE fibres, but at less slip than the FE and URW fibres.

The different fibre types have considerably different behaviour:

- The FE fibres reached their maximum fibre stress at approximately 2 mm slip, and the fibres stress was roughly constant with increasing slip, at least compared to the other fibre types. Due to the large stiffness of the geometrical shape, the FE fibres were not straightened when they were pulled out of the concrete, i.e. the end anchorage was still effective even at large slip.

- The URW fibres reached their maximum fibre stress at approximately 3 mm slip, and the bond between fibre and concrete was strong enough to cause fibre rupture.
- The HE fibres were straightened when they were pulled out of the concrete, i.e. the end anchorage was straightened out and the effect of the end anchorage was therefore decreasing with increasing slip. The slip at maximum fibre stress was approximately 0.6 mm, 0.8 mm and 1.0 mm for HE 6535, HE 6560 and HE 8060 respectively.
- The synthetic fibres did not break during pull-out tests on fibres embedded in concrete D, which means that their bond to the concrete was not sufficiently strong to cause fibre rupture. This is beneficial due to ductility as will be discussed later.

3.5.1 Effect of end anchorage

Figure 3-3 and Figure 3-6 show the fibre stress vs. slip relation for HE, FE and URW fibres, respectively. These fibre types were tested with two different embedment lengths. From these figures, it is possible to see that for fibres with end anchorage (flat end or hooked end) the pull-out resistance at small slips was approximately equal even though the embedment length was reduced from $l_f/2$ to $l_f/6$. This means that for small slip, which may be related to small crack widths, the main contributor to the pull-out resistance is the end anchorage, thus the embedment length is not important. Pull-out tests on HE 6560 fibres where the end hook were cut off confirm this finding. Figure 3-9 shows the fibre stress in fibres with $l_f/6$ embedding and fibres with cut off end hooks relative to the corresponding fibre stress in fibres with $l_f/2$ embedding.

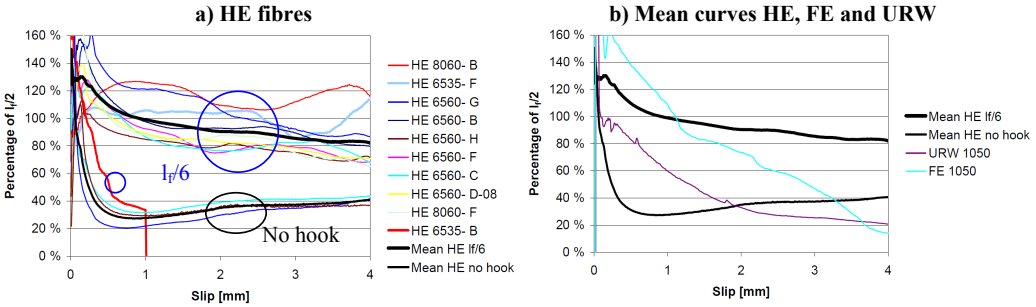

Figure 3-9 Relative effect of $l_f/6$ embedding and cut off end hook

As seen from Figure 3-9, the straight part of the HE fibres contributes to about 30 to 40 % of the total pull-out resistance. The HE fibres with $l_f/6$ embedding had in average higher capacity at less than 1 mm slip than the HE fibres with $l_f/2$ embedding. At larger slip, the HE fibres with $l_f/6$ embedding had gradually reduced capacity, and at 4 mm slip the capacity was about 80 % of the fibres with $l_f/2$ embedding. This is actually an advantage for the HE fibres, because the effectiveness of the fibres is very good also when the anchorage conditions are not optimal, as it typically is in real structures. The HE 6535 fibres with $l_f/6$ embedding in concrete B created a cone shaped concrete failure, and they are therefore not included in the *Mean HE $l_f/6$* curves in Figure 3-9a) and b).

The results are rather different for the FE and URW fibres compared to the HE fibres. With increasing slip, the effectiveness of the fibres with $l_f/6$ was rapidly reduced, and at 4 mm slip the effectiveness was only about 20 % of the maximum fibre capacity.

The fibre stress from the pull-out tests gives only information of the fibre stress in a single fibre. The fibres ability to transfer stresses over a random crack will naturally be dependent by the total cross sectional area of fibres crossing the crack, and how they work together in groups. This matter will be further discussed in the following chapters.

3.6 Failure mechanisms

From the pull-out tests reported in chapter 3.2 to chapter 3.5 it is obvious that the tensile stress capacity is dependent on the fibre type, and while the upper limit of the fibre stress is the fibre fracture stress, the fibre stress does in most cases not reach the fracture stress. Therefore, to be able to estimate the effect of adding fibres to a given concrete, it is necessary to understand how the fibres work when the concrete cracks.

It seems to be three mechanisms, which may limit the maximum fibre, stress ($\sigma_{f,max}$), namely:

- Fibre rupture
- Fibre slippage in the concrete
- Cone-shaped concrete failure

Moreover, the major parameters, which are deciding the mechanism, are:

- The fibre's fracture stress
- The bond between fibre and concrete
- The surrounding concrete's tensile strength

As already mentioned, fibre rupture does normally not occur because the fibre starts sliding in the concrete before the fracture stress is reached. Fibre slippage is extensively discussed in the literature, and the mechanism is normally associated with three bond mechanisms [Robins et al. (2002)], namely:

- Adhesion; the elastic shear bond at the fibre-concrete interface
- Friction; the frictional shear bond at the fibre-concrete interface
- Mechanical anchorage; the end hook effect

Pull-out tests on single fibres are normally performed on fibres that are aligned parallel to the applied load. However, [Robins et al. (2002)], who performed a comprehensive experimental test program regarding pull-out tests on fibres with different inclination angles and lengths, have demonstrated that the pull-out response is greatly influenced by the inclination angle. Furthermore, [Laranjeira et al. (2010)] have made a model to predict the pull-out response of inclined straight steel fibres with a reduced number of input parameters. The limitation of this model is that most steel fibres have some sort of end anchorage, which has great influence on the pull-out response. [Chanvillard (1999)] has developed a micromechanical model that takes into account the mechanism of steel deformation.

Several other researchers have also investigated the fibre-concrete interface bond, but it appears that none of them has included the *cone-shaped concrete failure* mechanism.

In the following three main parameters are investigated

1. Different fibre types
2. Effect of end anchorage
3. Concrete quality

In addition to these parameters, an extra test series was performed with fibres embedded in a light weight aggregate concrete (LWAC) with density around 1050 kg/m^3. This was done as a part of a larger test program regarding development of LWAC, and both different fibre types and the effect of end anchorage were investigated. The results from pull-out tests on fibres embedded in LWAC are reported by Kanstad [Kanstad (2009)] and will not be analyzed in the present thesis.

3.6.1 Fibre rupture

To achieve fibre rupture, the bond between the fibre and the concrete must be sufficiently strong to build up the fibre's fracture stress, f_{fu}, which normally is in the range from 1000 to 1100 MPa for metallic fibres and in the range from 400 to 550 MPa for synthetic fibres. Figure 3-10a) shows a simplified model for the stress build up in a fibre without end hook embedded in concrete.

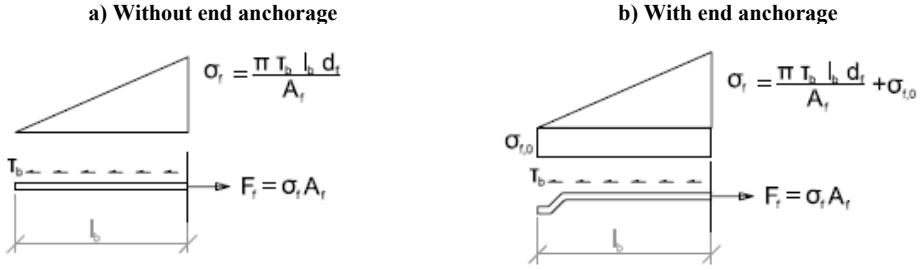

Figure 3-10 Simplified stress build up in an embedded fibre

The following notations are used:

F_f: is the fibre load [N]
σ_f: is the fibre stress [MPa]
τ_b: is the bond stress between fibre and concrete [MPa]

The critical embedment length for the fibre, l_{crit}, which is necessary to achieve fibre rupture may be found by requiring $\sigma_f = f_{fu}$ $l_b > l_{crit}$ will result in fibre rupture. Equation 3-1 below gives the critical embedment length for fibres without end anchorage.

$$l_b = l_{crit} = \frac{f_{fu} A_f}{\tau_b \pi d_f} = \frac{f_{fu} d_f}{4\tau_b} \tag{3-1}$$

where

f_{fu}: is the fibre's fracture stress [MPa]
A_f: is the fibre's cross-sectional area [mm^2]
τ_b: is the bond stress between fibre and concrete [MPa]
d_f: is the fibre diameter [mm]

A similar simple model may be made for fibres with end anchorage, simply by adding an initial stress, $\sigma_{f,0}$, at the fibre end. Figure 3-10b) shows this model.

In this case, the critical embedment length may be found as:

$$l_{crit} = \frac{d_f \left(f_{fu} - \sigma_{f,0} \right)}{4\tau_b} \tag{3-2}$$

In which $\sigma_{f,0}$ is the fibre stress which is anchored by the end hook.

If the embedment length is larger than the critical length, $l_b > l_{crit}$, the fibre's fracture stress will be the limiting factor, and the maximum fibre stress, $\sigma_{f,max,1}$, will be equal to the fibre's fracture stress:

$$\sigma_{f,max,1} = f_{f,u} \tag{3-3}$$

Normally fibre rupture does not occur because most of the fibres are made with fibre length $l_f < 2l_{crit}$, which means that the fibre stress will be less than the fracture stress.

3.6.2 Fibre slippage in the concrete

If the fibre's embedment length is less than the critical fibre length, $l_b < l_{crit}$, the fibre will be pulled out of the concrete with a fibre stress less than the fracture stress. The maximum slippage stress in the fibre, $\sigma_{f,max,2}$, will then depend on the bond between fibre and concrete. The previous calculation model can be used, and for fibre without end anchorage the maximum fibre stress, $\sigma_{f,max,2}$, may be found as:

$$\sigma_{f,max,2} = \frac{F_f}{A_f} = 4\frac{\tau_b l_b}{d_f} \tag{3-4}$$

To take the effect of an end anchorage into account, an initial stress may be added as previously discussed, and the maximum fibre stress, $\sigma_{f,max,2}$, may then be found as:

$$\sigma_{f,max,2} = 4\frac{\tau_b l_b}{d_f} + \sigma_{f,0} \tag{3-5}$$

It should be noted that if τ_b is the sliding friction, equation 3-5 is only valid if the end hook is still active at slips large enough to overcome the static friction, and not for calculation of the maximum fibre stress before the fibres start sliding in the concrete. It has been shown earlier that the maximum fibre stress is mainly due to the end anchorage.

[Laranjeira et. al. (2010)], [Chanvillard (1999)], [Li et al. (1997)] and [Banholzer et al. (2006)] among others, have developed more sophisticated models to describe the bond between the fibre and the concrete. Nevertheless, for the purpose of the present work this simple model seems to describe the behaviour sufficiently accurate.

3.6.3 Cone-shaped concrete failure

If a fibre has sufficient bond to the concrete, the surrounding concrete may not be able to carry the anchorage forces of the fibre. A reasonably accurate calculation model for this failure mechanism is illustrated in Figure 3-11.

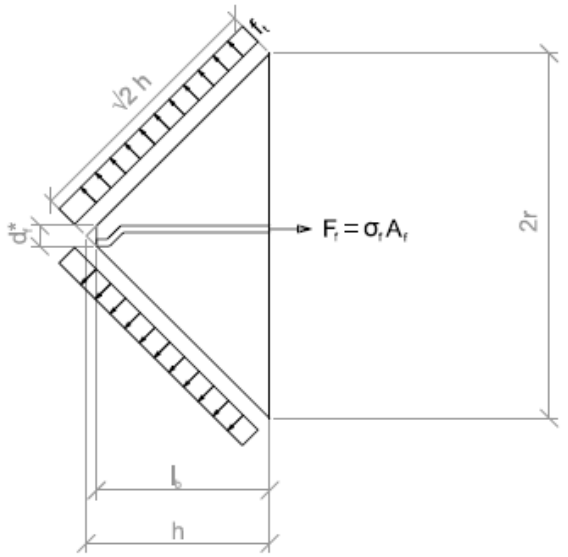

Figure 3-11 Calculation model for cone-shaped concrete failure

In Figure 3-11 the following definitions are used:

l_b: is the embedment length [mm]
r: is the radius of the base of the concrete failure cone [mm]
h: is the height of the concrete cone [mm]
$45°$: is the assumed rupture angle
f_{ct}: is the concretes tensile strength [MPa]
d_f^*: is the diameter of the fibre if the fibre has no end anchorage, if the fibre has an end anchorage d_f^* is shown in Figure 3-11.

In this case, the maximum fibre stress, the cone failure stress $\sigma_{f,max,3}$, is dependent on the surface area of the failure cone, O, and the tensile strength of the concrete, f_{ct}, as:

$$\sigma_{f,max,3} = \frac{1}{2}\sqrt{2} f_{ct} \frac{O}{A_f} \tag{3-6}$$

The surface area of the failure cone, O, may be found as:

$$O = \pi \cdot ra \tag{3-7}$$

where

$$h = r = l_b + \frac{d_f^*}{2}$$

$$a = h\sqrt{2}$$

The failure surface area, O, may then be rewritten as:

$$O = \pi \cdot r^2 \cdot \sqrt{2} \tag{3-8}$$

And the maximum fibre stress may be found as:

$$\sigma_{f,max,3} = \frac{1}{2}\sqrt{2} f_{ct} \frac{O}{A_f} = f_{ct} \frac{\left(2l_b + d_f^*\right)^2}{d_f^2} \tag{3-9}$$

3.7 Possible failure mechanisms for fibres cast in concrete D

3.7.1 General

The maximum fibre stresses $\sigma_{f,max,1}$ and $\sigma_{f,max,3}$ for the different fibres in the present test program are shown together with the maximum measured fibre stress in Table 3-6. $\sigma_{f,max,2}$ cannot be included in the table due to the complicated anchorage mechanism. To calculate $\sigma_{f,max,2}$ both $\sigma_{f,0}$ and τ_b must be known, which they are not.

The fibre fracture stress, $\sigma_{f,max,1}$ in Table 3-6 was found in the product data sheets, while the cone failure stress, $\sigma_{f,max,3}$, was calculated from equation 3-9 considering the conical failure surface with f_{ct} = 3.23 MPa and $d_f^* = d_f$. If the maximum measured fibre stress is larger than $\sigma_{f,max,1}$ and less than $\sigma_{f,max,3}$, then fibre slippage is the failure mechanism, and $\sigma_{f,max,2} = \sigma_{f,max}$ found by pull-out tests on single fibres.

Table 3-6 Calculated maximum fibre stress

Fibre type	$\sigma_{f,max,1}$ [MPa]	Measured $\sigma_{f,max}$ [MPa]		$\sigma_{f,max,3}$ [MPa]	
		$l_b=l_f/2$	$l_b=l_f/6$	$l_b=l_f/2$	$l_b=l_f/6$
HE 6560	1100[1]	667	619	14789	1742
FE 1050	1050[1]	647	668	8401	1008
URW 1050	1050[1]	981	419	8401	1008
Synthetic	550[1]	394	-[2]	9535	1139

[1]From product data sheet
[2]Not tested with $l_b=l_f/6$

By comparing $\sigma_{f,max,1}$ with $\sigma_{f,max,3}$ shown in Table 3-6, none of the fibre types will create a cone-shaped failure in the surrounding concrete if the embedment length is equal to $l_f/2$, because the fracture stress is less than the cone failure fibre stress ($\sigma_{f,max,3} > \sigma_{f,max,1}$). If the effect of the end anchorage ($\sigma_{f,0}$) is sufficiently large (larger than 1008 MPa!), it is possible to reach the cone failure stress, $\sigma_{f,max,3}$, for the FE fibres with embedment length equal to $l_f/6$, because then $\sigma_{f,max,1}$ is larger than $\sigma_{f,max,3}$. Similarly, the URW fibres may create a cone shaped concrete failure if the fibre-concrete bond is sufficiently large. The HE 6560 fibres are limited by fibre slippage ($\sigma_{f,max,2}$), or fibre rupture simply because $\sigma_{f,max,3}$ is too large also when the embedment length is reduced to $l_f/6$.

By comparing $\sigma_{f,max,1}$ and $\sigma_{f,max,3}$ with the maximum measured fibre stress, $\sigma_{f,max}$, shown in Table 3-6, it is quite clear that all fibre types (except the URW fibres which failed in fibre rupture even though the measured fibre stress was less than the fracture stress given by the producer in product data sheet) had a maximum fibre stress that was less than both $\sigma_{f,max,1}$ and $\sigma_{f,max,3}$; hence fibre slippage is the apparent failure mechanism, and that $\sigma_{f,max,2}$ is found for all fibre types embedded in that particular concrete. This seems to contradict the statement from chapter 3.3 that the FE fibres created a cone-shaped concrete failure, but in fact it does not because the numbers in Table 3-6 are only valid for embedment lengths equal to $l_f/2$ and $l_f/6$, and $\sigma_{f,max,3}$ is a function of the embedment length.

From the pull-out tests on fibres with embedment length $l_b=l_f/2$ and $l_b=l_f/6$ the maximum fibre stress was found to be 619-667 MPa and 647-668 MPa for the HE 6560 and the FE fibres respectively, as shown in Table 3-6. This implies that $\sigma_{f,0}$ is rather close to the lower values for the HE 6560 and the FE fibres respectively, because $\sigma_{f,0}$ is considered to be the contribution from the end anchorage in the present calculation model.

If $\sigma_{f,max,2} > \sigma_{f,max,3}$ the cone-shaped concrete failure will be the limiting mechanism, and if equation 3-4 and 3-9 are used, the inequality may be written as:

$$\sigma_{f,max,2} = 4\frac{\tau_b l_b}{d_f} + \sigma_{f,0} > \sigma_{f,max,3} = f_{ct}\frac{\left(2l_b + d_f^*\right)^2}{d_f^{*2}} \quad (3\text{-}10)$$

To simplify this equation, d_f is set equal to d_f*, and with some mathematical rearrangements the corresponding anchorage length, l_b, may be found as:

$$l_b < \frac{-b \pm \sqrt{b^2 - 4ec}}{2e} \Rightarrow \text{Possible cone-shaped concrete failure} \quad (3\text{-}11)$$

where

$$e = -4f_{ct}$$
$$b = 4d_f\left(\tau_b - f_{ct}\right)$$
$$c = d_f^2\left(\sigma_{f,0} - f_{ct}\right)$$

By use of equation 3-4 and the results from pull-out tests on the URW fibres with $l_f/6$ embedding (because these fibres showed the fibre slippage mechanism), the maximum static friction bond between concrete and a URW fibre is calculated to 12.6 MPa.

For fibres without end anchorage, the c-term in equation 3-11 is simplified to:

$$c = -f_{ct}d_f^2$$

For fibres with end anchorage $\sigma_{f,max,2} \approx \sigma_{f,0}$ (because the end anchorage contributes to about 95 % of the total resistance) and with some mathematical rearrangements, the expression for l_b may be simplified to:

$$l_b < \frac{d_f}{2}\left(\sqrt{\frac{\sigma_{f,0}}{f_{ct}}} - 1\right) \quad (3\text{-}12)$$

The mean value of the axial tensile strength, f_{ctm}, of concrete D was found to be 3.23 MPa in a uni-axial tensile strength test. The embedment lengths that would create a cone-shaped concrete failure found by equation 3-11 are shown in Table 3-7, and the tensile strength is then assumed equal to f_{ctm} for concrete D.

Table 3-7 Calculation of l_b to create a cone-shaped concrete failure in concrete D

	f_{ct} [MPa]	d_f [mm]	τ_b [MPa][1]	$\sigma_{f,0}$ [MPa][1]	l_b [mm]
HE 6560	3.23	0.9	-	619	**5.8**
FE 1050		1.0	-	647	**6.6**
URW 1050		1.0	12.6	-	**2.8**
[1]Assumptions based on the calculation from the present test program					

As seen from Table 3-7, if the embedment length is less then 5.8 mm, 6.6 mm and 2.8 mm for the HE 6560, FE and URW fibres, respectively, cone-shaped concrete failure may occur. This may explain the shape of the load-slip curve for the FE fibres with embedment length equal to $l_f/6$ shown in Figure 3-6. The FE and URW fibres are 50 mm long, and with an embedment length of $l_f/6$ only 8.3 mm is embedded in concrete. The maximum fibre stress was reached at a slip in the range 0.7-2.1 mm, which corresponds to a remaining embedment length of 7.6-6.2 mm. From Table 3-7 cone-shaped concrete failure is expected to take place when the remaining embedment length is 6.6 mm, corresponding to a fibre slippage of 1.7 mm, which is within the range where this mechanism actually was observed. The implication of this finding is that if the FE fibres are used to transfer stresses across a given crack in a structure

made of concrete D all fibres with embedment length less than 6.6 mm do not contribute to increase the ductility, because they will create a brittle cone-shaped concrete failure.

When HE 6560 fibres are pulled out, the end hook is straightened out; hence $\sigma_{f,0}$ is reduced, and a cone-shaped concrete failure is not expected unless the embedment length is sufficiently short when a crack occurs. When URW fibres are pulled out, the sinus wave formed fibres is straightened out, resulting in reduced τ_b; hence the cone-shaped concrete failure is not expected for this fibre either, unless the embedment length is very short when the crack occurs.

3.7.2 Results and mechanisms for the synthetic fibres

The embossed surface does not make the bond between the fibre and concrete sufficiently strong to reach fracture stress in the fibre. The fibre is gradually pulled out of the concrete.

The mechanisms for the synthetic fibres in concrete D are summarized in Table 3-8.

Table 3-8 Mechanism for synthetic fibres in concrete D

Fibre type	$l_f/2$	$l_f/6$
Synthetic	Fibre slippage	Fibre slippage

3.7.3 Results and mechanisms for the metallic fibres

FE-fibres
The end-anchorage contributes to most of the pull-out resistance, which is roughly constant until the embedment length is small enough so that a cone-shaped concrete failure is created. At an embedment length equal to $l_f/2$, fibre slippage is the mechanism that describes the pull-out response. At embedment $l_f/6$, fibre slippage still is the mechanism that describes the maximum pull-out resistance, but the fibres are expected to create a cone-shaped concrete failure after 1.5 mm slip. It is likely that also the fibre with embedment length equal to $l_f/2$ will create a cone-shaped concrete failure if the slip is large enough, because the stress level is more or less constant with increasing slip. This is not tested, since the tests were stopped at approximately 8 mm slip, which means that about 17 mm of the fibres were still embedded in the concrete. When the fibres are pulled completely out of the concrete, the shape of the fibres is unchanged.

URW-fibres
The bond between fibre and concrete is sufficiently strong to create fibre rupture if the embedment length is equal to $l_f/2$. When the embedment length is reduced to $l_f/6$, fibre slippage describes the pull-out response, and when these fibres are pulled completely out of the concrete, the sinus wave formed fibres are straightened out.

HE 6560-fibres
The end anchorage contributes to most of the pull-out resistance, but the end anchorage is straightened out which results in a decreasing pull-out resistance with increasing slip. Consequently, the difference in measured fibre stress for different embedment lengths is not as large as for the URW fibres, because the same mechanism decides the pull-out response even though the embedment length is different.

The mechanisms for the non-metallic fibres are summarized in Table 3-9.

Table 3-9 Mechanisms for the metallic fibres in concrete D

Fibre type	$l_f/2$	$l_f/6$
FE 1050	Fibre slippage – possible secondary cone-shaped concrete failure	Fibre slippage – Secondary cone-shaped concrete failure
URW 1050	Fibre rupture	Fibre slippage
HE 6560	Fibre slippage	Fibre slippage

3.8 Prediction of uni-axial tension behaviour from pull-out tests

Concrete D has been used in several experimental tests, including tensile strength tests. The tensile strength test was performed on 6 test specimens with dimensions 100x100x600 mm according to a test description normally used for tensile strength tests of plain concrete at SINTEF Building and Infrastructure. In contrast to the SINTEF description, the specimens were notched to control the location of cracking, and the effective cross section was 80x80 mm. The specimens were clamped at both ends by two pistons driven by hydraulic pressure as shown in Figure 3-12. The two pistons near the ends of the specimens, marked A, was operated to have 1.6 times the pressure relative to the two pistons near the centre of the specimens, marked B, to reduce the unfavourable combination of compressive and tensile stresses near the fastening points, which of course is of larger importance when the specimens are not notched. A calliper was mounted at the middle of the specimens and the displacement were measured by two LVDTs on two opposite sides over a distance l=100 mm, which means that both the tensile strength, the tensile strain at cracking and the E-modulus may be calculated.

The tests were run displacement controlled, with a displacement rate of 0.1 mm/min for three of the specimens and 0.5 mm/min for the remaining three specimens.

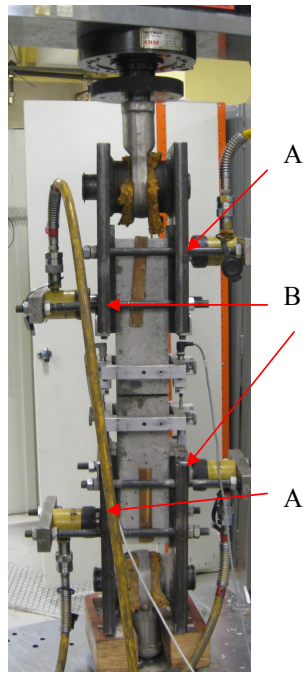

Figure 3-12 Arrangement for tensile strength tests

The tensile strength of concrete D was found to be 3.23 MPa, which corresponds to a tensile load of 32.3 kN for a concrete specimen with cross section 100x100 mm. To have the same capacity to resist a tensile load after concrete cracking, the fibres have to transfer 32 kN over the crack. A theoretical model, based directly on the previous experimental data is established, and with 2D-orientation according to [Thorenfeldt (2003)], all fibres having $l_f/2$ embedding and no negative interaction between neighbouring fibres, the necessary fibre amount to resist a tensile load of 32 kN and corresponding *load vs. CMOD* diagram is shown in Figure 3-13.

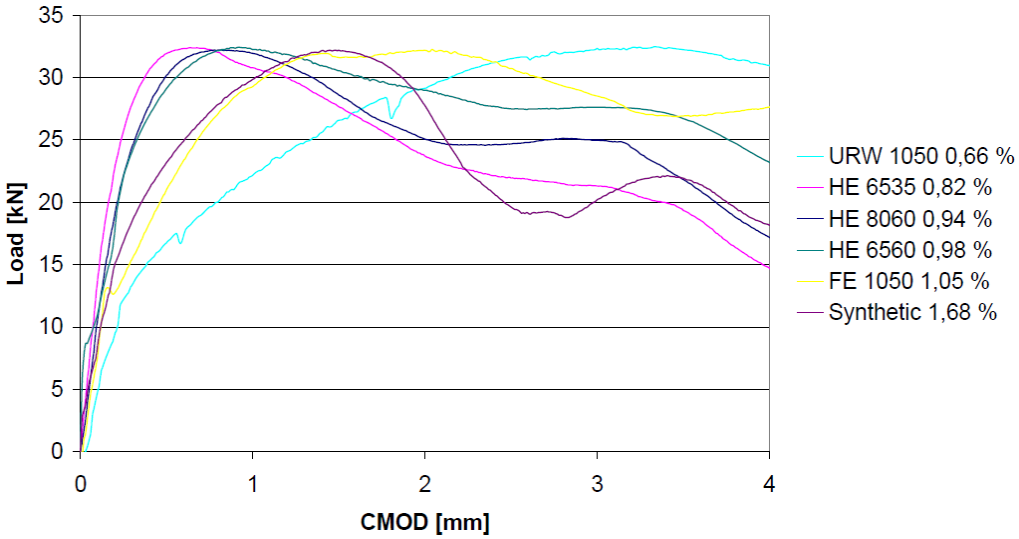

Figure 3-13 Load vs. crack opening curves to reach 32.3 kN uni-axial capacity

The results in Figure 3-13 show that if the fibre reinforcement shall be able to transfer 32 kN over the crack, the necessary fibre amount will of course vary for the different fibre types. What is more important is the large difference in crack opening at 32 kN load capacity. If the crack opening is not considered, it seems like the URW fibres are more effective than all other fibre types, but URW reach 32 kN first when the crack opening reach approximately 3 mm.

Once concrete is cracking, the concrete's tensile stress capacity in the crack is zero, and the fibres have to resist the total load that is released. If the concrete is not restrained the concrete strain will be reduced from the cracking strain, $\varepsilon_{ct,crack}$, to zero, and the opening of the crack will be equal to $\varepsilon_{ct,crack}$ x L, where L is the free length of the specimen. It is important to notice that for a test arrangement as shown in Figure 3-12, the free length L is not equal to the distance l where the LVDTs are measuring the elongation of the specimens. For concrete structures where it is important to limit the crack widths, it is important that the fibres are effective once cracking occurs. For fibre reinforced sprayed concrete used in tunnel linings etc., it is more important with high energy absorption, and then it is favourable with high maximum capacity at large crack opening.

To investigate the different fibre types further, the necessary fibre amount to resist a tensile load of 32 kN from 0.5 mm to 2.0 mm crack opening is calculated, and this is shown graphically in Figure 3-14.

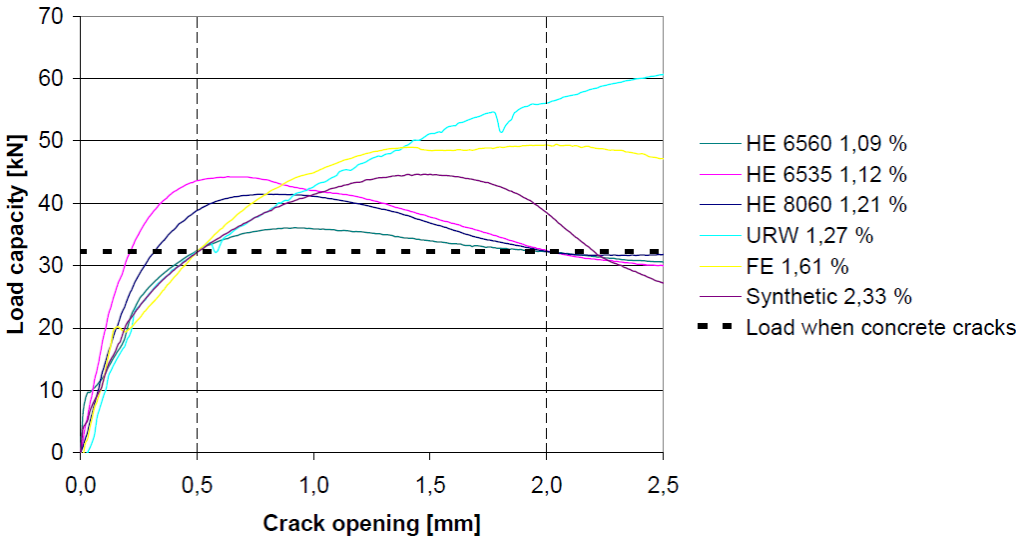

Figure 3-14 Load vs. crack opening and necessary fibre volume to exceed 30 kN from 0.5mm to 2.0 mm crack opening

Figure 3-14 shows the difference in the fibres ability to maintain a given load capacity. To maintain a total capacity of 32 kN in the crack range between 0.5 mm and 2 mm, the necessary fibre volume varies between the different fibre types. Further, the HE fibres have their limitation at 2 mm crack opening, while the other fibre types have their limitation at 0.5 mm crack opening, which means that the maximum capacity of these fibre types is not utilized if small cracks are important. Necessary fibre volume and the corresponding capacity and crack range is summarized in Table 3-10.

Table 3-10 Necessary fibre volume to resist a tensile load of 32 kN from 0.5 mm to 2.0 mm crack opening

	v_f	F_{max} in the range 0.5- 2 mm	σ_f at F_{max}	σ_f at $F = 32.3$ kN	Crack range, $F > 32.3$ kN	$\sigma_{f,max}$ from pull-out tests
	[%]	[kN]	[MPa]	[MPa]	[mm]	[MPa]
HE 6560	1.09	36.1	331	296	0.5-2.0	662
HE 6535	1.12	44.3	395	288	0.22-2.0	790[1]
HE 8060	1.21	41.5	343	267	0.32-2.0	686[1]
URW 1050	1.27	56.1	442	254	0.5-	984
FE 1050	1.61	49.4	307	201	0.5	615
Synthetic	2.33	44.7	192	139	0.5-2.2	383
[1]Average values for fibres in concrete B and F						

An estimate of the fibre reinforced concrete's behaviour in tension, based on the results from pull-out tests, may be calculated as described in the following.

The total number of fibres per litres of concrete, n_f, can easily be calculated when the volume of one fibre, $V_{1,f}$, and the total fibre volume, V_f is known:

$$n_f = \frac{V_f}{v_{1,f}} \tag{3-13}$$

The total fibre volume is easily calculated when the volume ratio, v_f, is known:

$$V_f = v_f \cdot V_c \tag{3-14}$$

If all fibres are placed unidirectional in a cubic pattern as described by the orthogonal fibre orientation model by [Thorenfeldt (2003)] and the centre of each fibres are placed in the corners of these cubic pattern, as shown in Figure 3-15, the average distance between each fibre centre, Δc_f, can be calculated by the average concrete volume per fibre:

$$\Delta c_f = \sqrt[3]{\frac{V_c}{n_f}} \tag{3-15}$$

a) Orthogonal fibre orientation [Thorenfeldt (2003)]

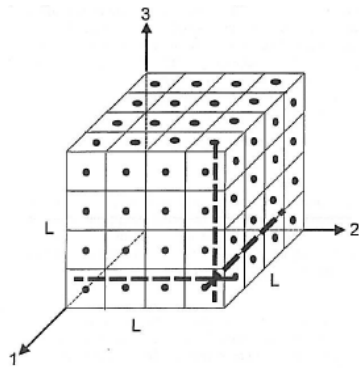

b) Fibre localization in this pattern. The shaded area represents the concrete area (volume) per fibre area (volume)

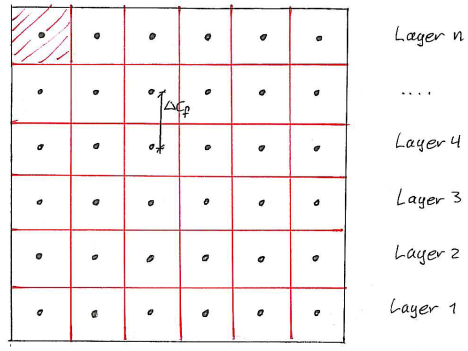

Figure 3-15 Cubic pattern and fibre localization in this pattern

If all fibres are directed the same way and according to the cubic pattern, as shown in Figure 3-16 the distance between each fibre centre, Δc_f, may be less than the fibre length, l_f, which means that the fibres must overlap each other, and the average overlap factor, K, will be:

$$K = \frac{l_f}{\Delta c_f} \tag{3-16}$$

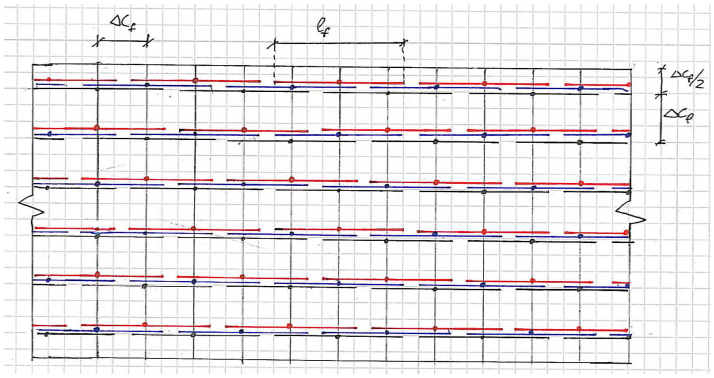

Figure 3-16 Stretching fibres from the centre point to its length, l_f

The number of active fibres, $n_{f,tensile}$, will then be:

$$n_{f,tensile} = \frac{A_{c,t}}{\Delta c_f^2} K \tag{3-17}$$

where

$A_{c,t}$: is the cross section area of the concrete in tension [mm^2]

From the pull-out tests on single fibres, the relationship between tensile stress and slip is found, and when the total number of active fibres in the tensile zone, $n_{f,tensile}$, is found and the cross section area of one fibre is known, it is straight forward to calculate the total tensile capacity as a function of fibre slip.

Before the concrete is cracking, the strain vs. stress relationship follows Hooke's law. If the concrete is considered to be brittle, with no strain softening behaviour, all elongation is transformed to crack opening once the crack strain (or stress) limit is reached. As already shown, the fibres ability to obtain stresses is greatly influenced by the fibre slip, which may be related to the crack opening.

By use of equation 3-15 the average distance between each fibre centre, Δc_f, is found to be approximately 20 mm, which limits radius of the base of the concrete failure cone, r, in Figure 3-11 to 10 mm to avoid negative interactions of neighbouring fibres. The maximum embedment length for cone shaped concrete failure to occur is found to be 5.8 mm (Table 3-7), which means that the average distance between each fibre must be less than 11.6 mm if negative interactions with regard to cone shaped concrete failure is expected.

The number of active fibres according to equation 3-17 is 50.3. It is a rather rough simplifications to assume that all fibres are placed uni-directed and at the same time with an average embedment length, l_b, equal to $l_f/2$. However, a reduced embedment length is found to be of minor influence because the end anchorage is the major contributor to the efficiency of the end hooked fibres. If half the fibres are considered to be effective, the number of active

fibres according to equation 3-17 is adjusted downward to 25. Thorenfeldt has introduced a capacity factor, η_0, which represents the theoretical normal resultant of fibres with known mean stress assuming unchanged direction of fibres crossing a tensile crack. For random 2D-oriented fibres in planes parallel to the tension direction, this factor is 0.5 [Thorenfeldt (2003)].

The cracking strain, $\varepsilon_{ct,crack}$, of concrete D was found to be 0.13 ‰. Because the fibres are able to transfer stresses across cracks, the strain is not reduced to zero, and the CMOD can be calculated as:

$$\text{CMOD} = L\left(\varepsilon_{ct,crack} - \frac{\sigma_{ct,f}}{E_c}\right) \tag{3-18}$$

where

$\sigma_{ct,f}$: is the post cracking concrete stress due to fibres
E_c: is the concrete's E-modulus

By these assumptions, the expected behaviour of 0.5 vol% HE 6560 fibres in concrete D is shown in Figure 3-17.

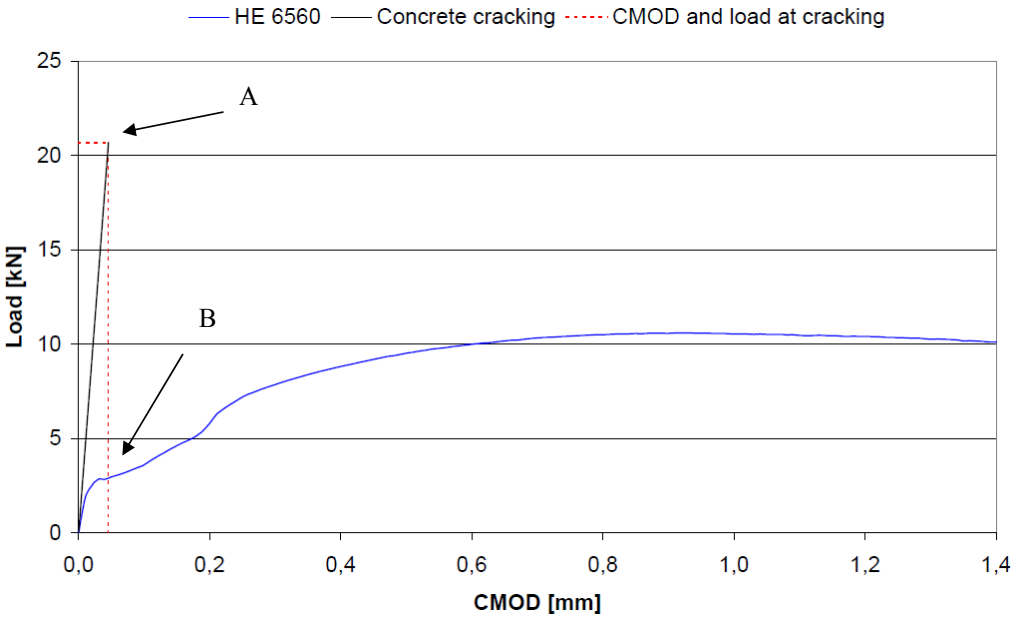

Figure 3-17 Expected load vs. CMOD relation tensile test

To calculate the CMOD in the pre-cracked state is of course a self-contradiction. In Figure 3-17 the apparent CMOD in the pre-cracked state is the total elongation of the test specimen immediately before cracking, which is calculated as $\Delta L = \varepsilon_{ct,crack} L$, where L is set to 350 mm, resulting in a total elongation immediately before cracking equal to 0.046 mm, marked as A in Figure 3-17. With the assumption of no softening behaviour in tension, the capacity of plain concrete is reduced to zero once concrete cracks, while the fibres' capacities are found from pull-out tests at a slip equal to 0.046 mm, marked as B in Figure 3-17. Whether L=350 mm is correct or not is not investigated. Clearly, L is larger than 100 mm, and probably somewhat larger than the free distance between the plates that hold the specimens. It is likely to believe that the concrete strain is constant between the plates, but if the tensile strain is zero

between the pistons marked B in Figure 3-12 and the end of the plates, the idea of having reduced hydraulic pressure to prevent unfavourable combinations of tensile and compressive stresses is not succeeded. If L is reduced (in equation 3-18), the gradient of the *concrete cracking* curve will increase and point A in Figure 3-17 will be located at less CMOD resulting in reduced fibre capacity immediately after cracking. Whether the total elongation at cracking in Figure 3-17 is correct or not has no influence on the calculated load vs. CMOD curve for fibres, but it will influence the calculated capacity immediately after cracking represented by the intersection between the *CMOD and load at cracking* and the *HE 6560* curves. Whether the concrete should be considered to have softening behaviour or not will also only affect the capacity directly after cracking by increasing the CMOD at the intersection point between the *CMOD and load at cracking* and the *HE 6560* curves, meaning that point A will not be affected, but point B will be located at larger CMOD. The last remark to Figure 3-17 is that even though L is correct and the concrete has no softening behaviour, a total elongation of 0.046 mm will not correspond to a CMOD = 0.046 mm because the fibres are able to transfer about 2.5 kN across the crack, which reduces the CMOD as shown in equation 3-18. None of these effects have any influence on the calculated fibre contribution, but they will influence the location of point B, and thereby the calculated capacity immediately after cracking.

As seen from Figure 3-17, once the concrete cracks the predicted load capacity is rapidly decreasing because the crack opening is not large enough for the HE 6560 fibres to be fully effective.

To investigate if pull-out tests actually can be used to predict the behaviour in uni-axial tension, the expected load vs. CMOD relation is compared with results from uni-axial tensile tests shown in Figure 3-18.

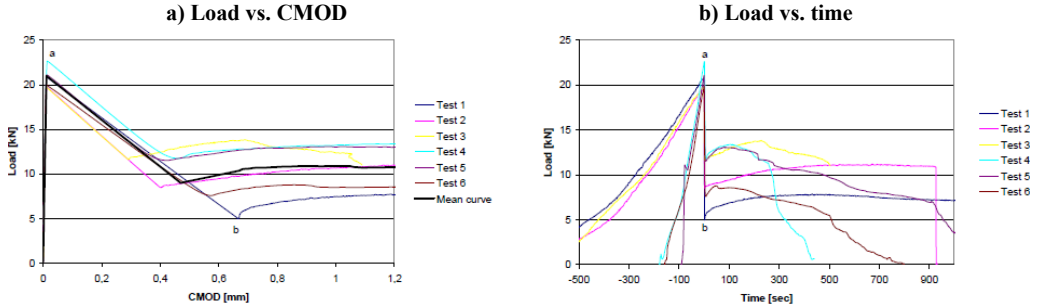

Figure 3-18 Experimental results form uni-axial tensile tests

At first glance, the results in Figure 3-18a) seems to disagree with the prediction from the pull-out tests, but most likely the experimental results from uni-axial testing show that uni-axial testing itself is complicated. First of all it seems like the calculated elongation at cracking is sorely overestimated, but the CMOD in Figure 3-18a) do not give valuable information of the total elongation in the pre-cracked state because the LVDTs measures only the elongation over 100 mm, which is less than the free span. Secondly, it seems like the concrete shows very pronounced softening behaviour. This softening behaviour is not pronounced at all if the *load vs. time* curve is made as shown in Figure 3-18b). In this figure the curves are shifted horizontally so that every beams crack at time equal to zero. From the load vs. time curves, it is obvious that the load capacity is decreasing rapidly once cracking occurs. The time increment from point *a* to point *b* is 2 second in both diagrams. The tests were run displacement controlled, and then the rate of displacement is meant to be constant. It

is quite clear from Figure 3-18a) and b) that the stiffness of the machine was not sufficient to prevent a sudden increase in the displacement rate immediately after cracking.

The tests machine was programmed to have a constant displacement rate. An overview of the displacement rate, logging frequency and belonging displacement per logging point is shown in Table 3-11.

Table 3-11 Displacement rate, logging frequency and displacement per logging point

	Displacement rate [mm/min]	Logging frequency [Hz]	Displacement per logging point [mm]
Specimen 1-3	0.1	0.5	0.003
Specimen 4-5	0.5	2	0.004

Because both time and displacement were recorded during the tests, it is possible to calculate the real displacement rate measured at the test specimen. The real displacement rates are shown in Figure 3-19.

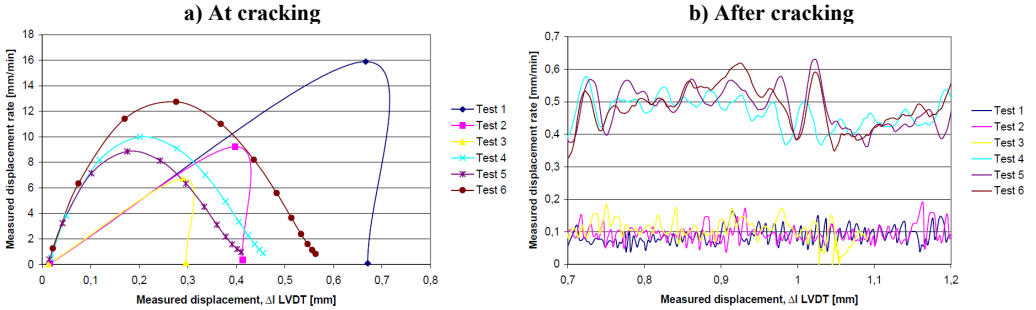

Figure 3-19 Measured displacement rate

As seen in Figure 3-19a), the displacement rate at cracking was dramatically higher than intended. For test specimen 1 to 3, there is only one logging point that gives this high displacement rate, which may lead to the conclusion that the logging frequency should be higher than 0.5 Hz to avoid this big leap in displacement between two readings. However, as seen for test specimen 4 to 6, there are several logging points that show this high displacement rate, which means that the high displacement rate is actually correct. This high displacement rate at cracking is in reality not surprisingly, because all elastic strain in the concrete is released when the concrete cracks, so even if the test machine did not moved at all, the crack will be formed almost immediately. The displacement at the test machine's load cell was also registered, and the *displacement rate vs. displacement* curve can also be made for the displacement at the load cell, which actually shows that the displacement rate of the load cell also increased at concrete cracking, as shown in Figure 3-20.

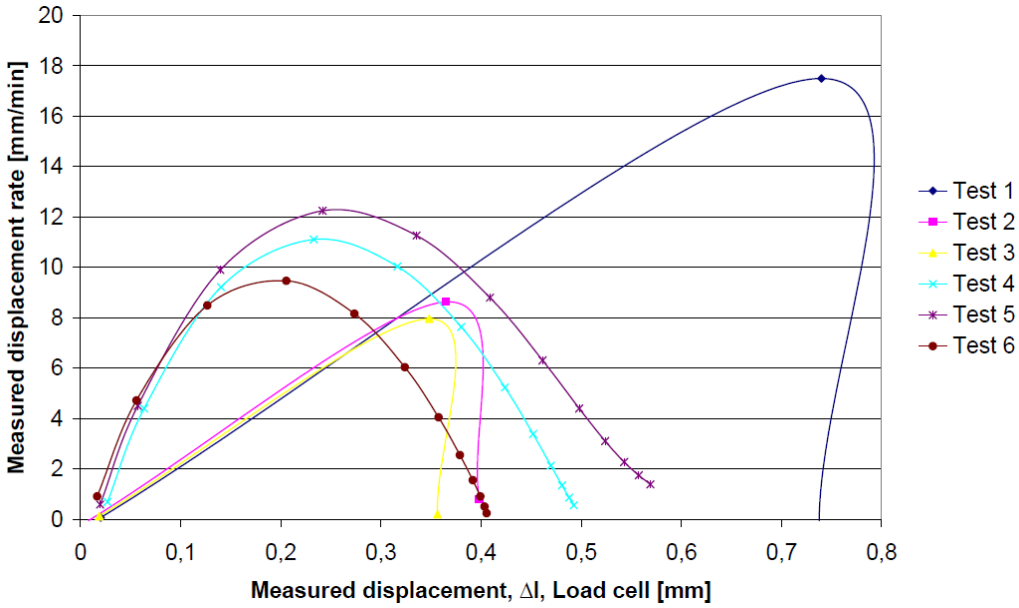

Figure 3-20 Measured displacement rate at cracking, load cell

The implication of this is that the large leap in displacement is real, but the displacement rate was not constant; it was largely increased at cracking and constant and according to the intended rate after cracking. For the test specimen 4 to 6, the load was also registered in the decreasing part of the curve directly after cracking. To attribute this to a strain softening behaviour will most likely be an erroneous conclusion, because even though the load was registered 2 times per second, it is dubiously that the signal from the test machine was correct when the stiffness of the test specimen changes so rapidly.

The author's conviction is that the signal from the test machine is reliable and correct up to cracking, and after cracking when the displacement rate has stabilized again. For the test results shown in Figure 3-18a) this means that the author's conviction is that all CMOD records are correct, but that the registered loads in the decreasing part of the load vs. CMOD curves are simply wrong because the test machine was not able to internally process the signals 2 times per second. With regard to the displacement rate, it is beyond doubt that the test machine was unable to internally process the signals fast enough to keep the displacement rate constant when the concrete cracked and it seems quite reasonable to believe that the load signals may be encumbered with errors as well.

In Figure 3-21 the mean curve from Figure 3-18a) is drawn together with the expected load vs. CMOD curve from Figure 3-17. The CMOD at cracking from the experimental test is multiplied with a factor 3.5 to take into account the total length subjected of tensile stress.

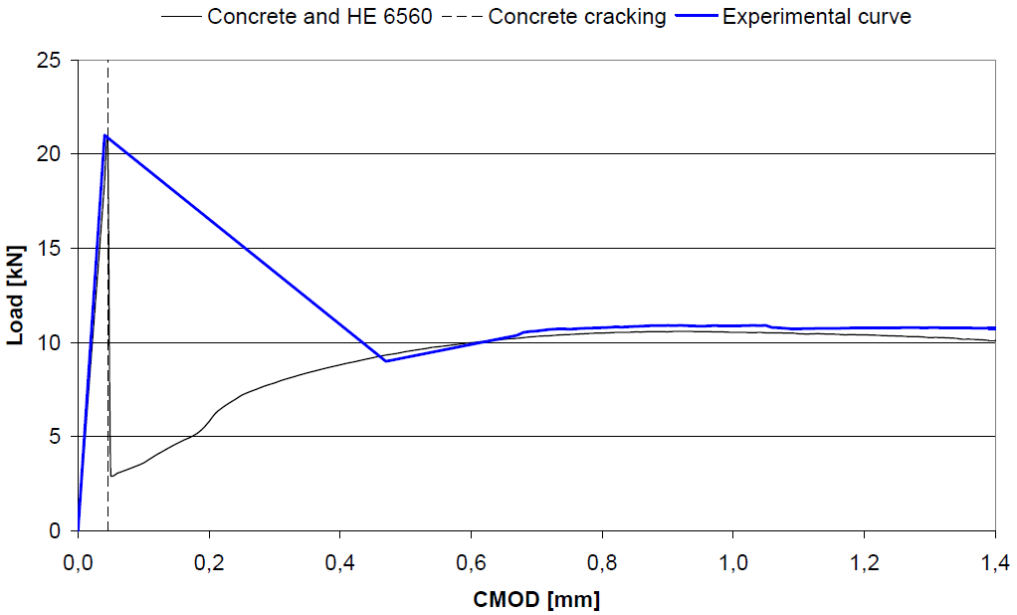

Figure 3-21 Comparison experimental and predicted load vs. CMOD curves, concrete in tension

With the above mentioned adjustments, it seems quite likely that it is actually possible to use pull-out tests on single fibres to predict the behaviour of fibre reinforced concrete in uni-axial tension.

3.9 Prediction of bending behaviour from pull-out tests

Concrete D has also been used to cast and test beams with ordinary reinforcement. This is further discussed in chapter 4.2.6.1. Based on the cracking load from these beam tests the flexural tensile strength was found to be 5.2 MPa, which according to equation 3.23 in EC 2 corresponds to a tensile strength of about 3.5 MPa (and not 3.2 MPa, which was measured in tensile strength tests). In the following calculation, the tensile strength is therefore assumed to be 3.5 MPa, or more precise: the flexural tensile strength is assumed to be 5.2 MPa.

To calculate the bending capacity, equation 3-13 to equation 3-17 from chapter 3.8 are used to calculate the number of active fibres.

In addition to the above mentioned equations, the number of fibre layers over the height of the tensile zone must be calculated. Figure 3-16 may also illustrate the different fibre layers in a beam, and the number of layers can be calculated as:

$$n_{\text{layer}} = \frac{h_{\text{tensile}}}{\Delta c_{\text{f}}} \tag{3-19}$$

where

h_{tensile}: is the height of the tensile zone [mm]

The number of fibres in each fibre layer, $n_{\text{f,layer}}$, will be:

$$n_{\text{f,layer}} = \frac{n_{\text{f,tensile}}}{n_{\text{layer}}} \tag{3-20}$$

From the pull-out tests on single fibres, the relationship between tensile stress and slip is found. By placing fibres in layers with centre distance equal to Δc_f it is possible to use the results from pull-out tests to estimate the bending capacity of a beam reinforced with fibres. To do so, a stress distribution must be assumed to calculate the height and cross section area of the tensile zone. The stress distribution recommended by RILEM [RILEM TC 162-TDF (2003)] shown in Figure 3-22 may be used for CMOD equal to 0.5 mm and 3.5 mm.

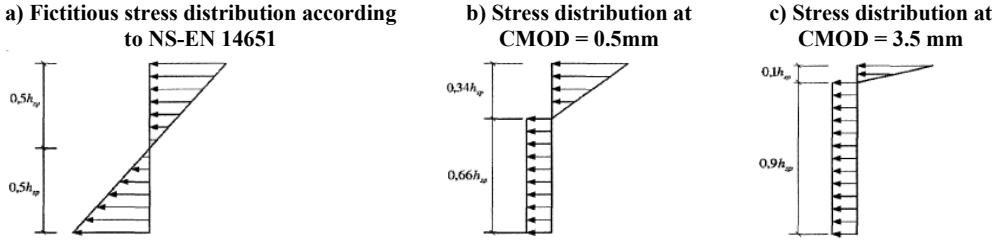

Figure 3-22 Calculation model according to [RILEM TC 162-TDF (2003)]

For intermediate CMODs, a linear interpolation is used, and the relationship between the height of the compressive zone, X, and the CMOD will then be:

$$X = -0{,}08\text{CMOD} + 0{,}38 \tag{3-21}$$

And the height of the tensile zone, h_{tensile}, is:

$$h_{\text{tensile}} = h - X \tag{3-22}$$

where

h: is the effective height of the cross section ($h = h_{sp}$ for notched beams)

As for the calculation of uni-axial tensile capacity, it is assumed that all fibres have optimal embedding, which means that the centres of all fibres are located in the centre of the crack and that 50% of the fibres are effective (or that all fibres are effective with $\eta_0 = 0.5$). In reality, all fibres will not have optimal embedment length, but for fibres with end anchorage, it does not really matter for the calculation, because it is found that approximately 95% of the pull-out capacity is due to the end anchorage.

Because the tensile zone height according to the recommended stress distribution in [RILEM TC 162-TDF (2003)] is increasing with increasing deflection (or CMOD), and the fibre efficiency is a function of the slip, the fibres contribution to the bending capacity must be calculated for different CMODs. For every CMOD the height of the tensile zone can be calculated according to equation 3-22, and the total number of fibre layers, $n_{f,\text{layer}}$, is calculated according to equation 3-20. In the following calculation, the number of fibre layers will be approximated down to the nearest integer, and the fibre layer nearest to the tensile surface of the beam is placed with a distance from the tensile surface equal to $\Delta c_f/2$. The remaining fibre layers are placed with centre distances equal to Δc_f.

A beam tested according to the test method for metallic fibre concrete [NS-EN 14651 (2005)] has a span, height at crack location, and width equal to 500 mm, 125 mm and 150 mm, respectively. (The NS-EN 14651 will be further discussed in chapter 4.)

The cracking load, F_{crack}, for a beam tested as described in NS-EN 14651 can be calculated as:

$$F_{\text{crack}} = 4\frac{M_{\text{crack}}}{l} \tag{3-23}$$

where

$$M_{\text{crack}} = f_{\text{ct,fl}}\frac{bh_{\text{sp}}^2}{6} \tag{3-24}$$

As shown, it is straight forward to estimate the cracking load of a beam, but to estimate the crack opening directly after cracking is actually quite difficult. From the pull-out tests, it is possible to estimate the moment capacity as a function of the crack opening, and an estimate of the crack opening directly after cracking is necessary to find the intersection between the *strength vs. CMOD* curve for the concrete and the *strength vs. CMOD* curve for the fibres.

If the beam cracks when the flexural tensile stress, $f_{\text{ct,fl}}$, reaches the flexural tensile strength, $f_{\text{ctm,fl}}$, the predicted bending moment at cracking can be calculated by use of $f_{\text{ctm,fl}}$ and the tensile strain at cracking is then:

$$\varepsilon_{\text{ct,crack}} = \frac{f_{\text{ctm,fl}}}{E_{\text{c}}} \tag{3-25}$$

If the applied moment is constant over the span, l, and the concrete stress in the un-cracked regions is zero, which means that the beam act as two rigid bodies rotating at the crack, the crack opening immediately after cracking, $\text{CMOD}_{\text{cracking}}$, can be calculated as:

$$\text{CMOD}_{\text{cracking}} = \varepsilon_{\text{ct,crack}} l \tag{3-26}$$

To take into account the tensile stresses transferred over a crack due to the fibres, the non-linear hinge approach may be used. Löfgren has shown that the crack opening can be calculated as [Löfgren (2003)]:

$$\text{CMOD} = \varphi(h - X) - \frac{f_{\text{ct}}}{E_{\text{c}}} s \tag{3-27}$$

where:

- φ: is the angular deformation of the hinge, assumed to be equal to the crack opening angle
- h: is the specimen height
- X: is the depth of the neutral axis, which is equal to the compressive zone height
- f_{ct}: is the tensile strength of the concrete
- E_{c}: is the E-modulus of concrete
- s: is the length of the non-linear hinge, which is set to be the average crack spacing

The first term in equation 3-27 represents the largest possible crack opening due to the rotation in the non-linear hinge, while the latter term reduces the crack opening due to the elastic curvature in the non-cracked regions of the non-linear hinge. (With regard to the expression in [Löfgren (2003)] the expression for crack opening is simplified because it is no external normal forces in the beams considered in the present thesis.)

Equation 3-27 is not suitable to calculate the CMOD at cracking for a beam tested as described in NS-EN 14651 because equation 3-27 is only valid if the applied moment is constant over the length s. First of all, NS-EN 14651 prescribe a three point bending test, which means that the moment varies over the span, and secondly it is always only one crack. The length of the non-linear hinge might be considered equal to the span l, and instead of using the tensile strength of the concrete, an average tensile stress over the span l could be

used. Another possibility is to assume that the non-linear hinge has a length equal to the height of the beam, but then the contribution to the crack opening for the remaining part of the beam must be added to equation 3-27.

To overcome the problem with estimating the CMOD immediately after cracking, results from beam tests on standard small beams made of plain concrete is used. 9 beams without reinforcement was cast and tested according to NS-EN 14651 as a part of the *ductile high tensile strength all round concrete* project, which will be presented in chapter 8. These 9 beams were made of 3 different mixes, and none of them was similar to concrete D. To make them useful for the present purpose, the normalized capacity for every measured CMOD is calculated as $f_{R,n}/f_{ct,fl}$. The normalized capacity vs. CMOD curves are shown in Figure 3-23.

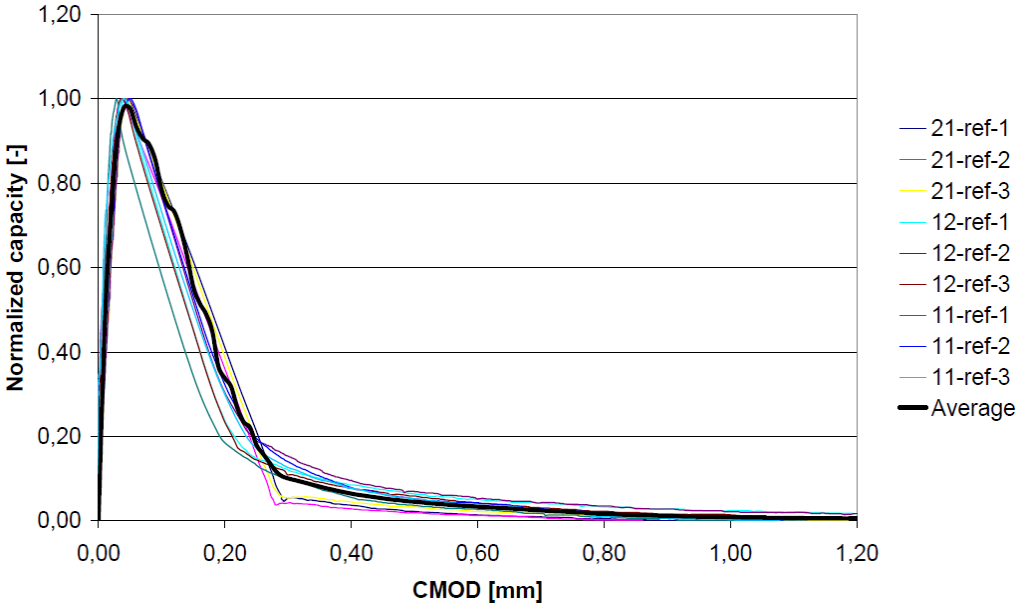

Figure 3-23 Normalized capacity vs. CMOD curves plain concrete

The average CMOD at cracking was 0.04 mm, and used in the following calculations meaning that once the concrete is cracking, the CMOD will be as large as $CMOD_{cracking}$ = 0.04 mm, and the height of the tensile zone can be calculated according to equation 3-22. It should be noted that the deflection vs. CMOD relationship used in the curves in Figure 3-23 is as described in chapter 4.1.3 and not as described in NS-EN 14651.

The moment capacity of beams can be calculated based on the calculation model shown in Figure 3-24.

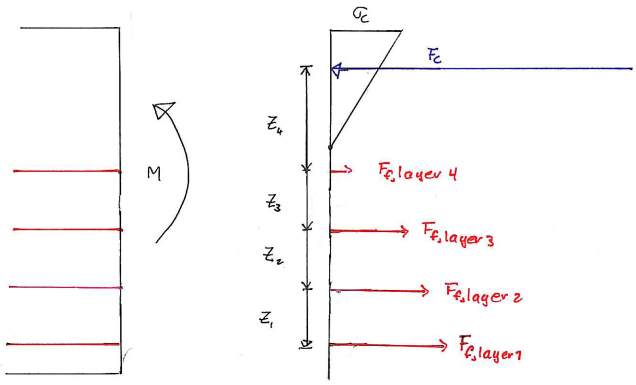

Figure 3-24 Calculation model for moment capacity

With this model, the moment capacity is:

$$M(\text{CMOD}) = \sum_{i=1}^{i=n} F_{\text{f,i}} Z_{\text{i}} \tag{3-28}$$

where

$$F_{\text{f,i}} = A_{\text{f}} n_{\text{f,layer}} \sigma_{\text{f,i}} \tag{3-29}$$

and

$\sigma_{\text{f,i}}$: is the fibre stress found from pull-out tests and dependent by the slip, which means that it will be different for every layer
F_{c}: is the force resultant in the compressive zone
$F_{\text{f,i}}$: is the force resultants in the fibres in layer *i*
Z_{i}: is the distance from F_{c} to the corresponding $F_{\text{f,i}}$

Both $n_{\text{f,layer}}$ and Z_{i} are functions of the CMOD, so equation 3-28 must be solved for every considered CMOD.

To find the moment capacity it is assumed that the crack width is linearly increasing from zero at $y=X$, to CMOD at $y=h$, where y is the distance from the compressive surface. As already mentioned, it is assumed that the embedment length will not influence the fibre stress, and furthermore it is assumed that once a fibre reach its maximum stress it will start to slide at the weakest end, which means that the slip is equal to CMOD.

When the moment capacity for a beam tested according to NS-EN 14651 is calculated at CMOD equal to 0.25, 0.5, 1.0, 1.5, … 4.0, and the corresponding load is calculated based on the static system, the calculated load vs. CMOD curves for the different fibre types is as shown in Figure 3-25.

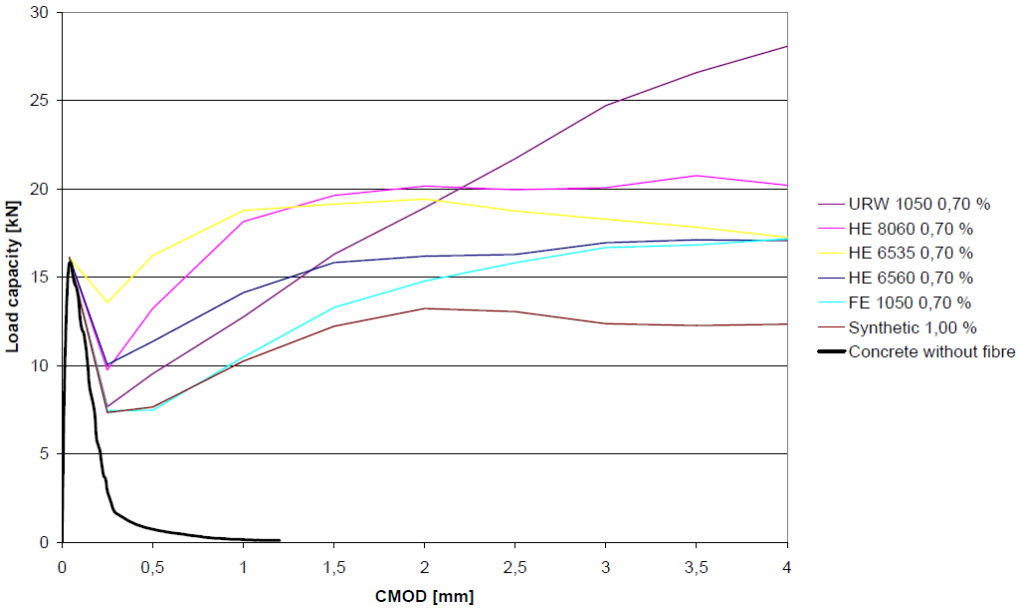

Figure 3-25 Calculated load vs. CMOD for a beam tested according to NS-EN 14651

The input to this calculation is:

- The fibre stress vs. slip curves shown in Figure 3-8.
- The fibre volume is set to 0.7 vol% for the metallic fibre types and 1.0 vol% for the synthetic fibre
- The plain concrete contribution is identical to the average curve in Figure 3-23
- According to the European Standard for specification, performance, production and conformity [NS-EN 206-1], concrete D belongs to strength class C40/50, and the tensile strength, f_{ctm}, according to EC 2 for this concrete is 3.5 MPa. The flexural tensile strength, $f_{ctm.fl}$, according to equation 3.23 in EC 2 is 5.16 MPa.

The heights of the un-notched sections of the beams are 150 mm, which means that the capacity of these parts should be 1.44 times higher than for the cracked section. If the cracking load is 16 kN, the un-notched sections should crack at 23 kN. This is not taken into consideration in this simple calculation, which means that the load capacity for the URW fibres is overestimated at CMOD larger than about 3.4 mm.

The most interesting finding from this calculation is that it indicates that:

- None of the fibre types have sufficient capacity to avoid a drop in load capacity immediately after cracking
- The HE 6535 fibre is more effective than the other fibres at CMOD less than about 1.25 mm
- The HE 8060 should be more effective than the other HE fibres at CMOD larger than about 1.25 mm
- Even though the URW 1050 fibres show the largest pull-out capacity, they are not more effective than the HE fibre before the CMOD is larger than about 2.25 mm.
- The FE 1050, HE 6535 and HE 6560 seems to be equally effective at CMOD equal to 4 mm, but the HE fibres are more effective at less CMODs.

The reason why the calculations are performed with a fibre volume of 0.7 % and 1.0 %, steel fibres and synthetic fibres respectively, is that beam tests according to NS-EN 14651 are performed on beams made of concrete D with this fibre volumes. The results from these beam tests are analyzed in details in chapter 4.2. The average load vs. CMOD curves for the beams cast and tested according to NS-EN 14651 (beam 090210-4 to -6, and beam 160210-4 to -6 in chapter 4.2.3) are shown together with the predicted load vs. CMOD curves in Figure 3-26.

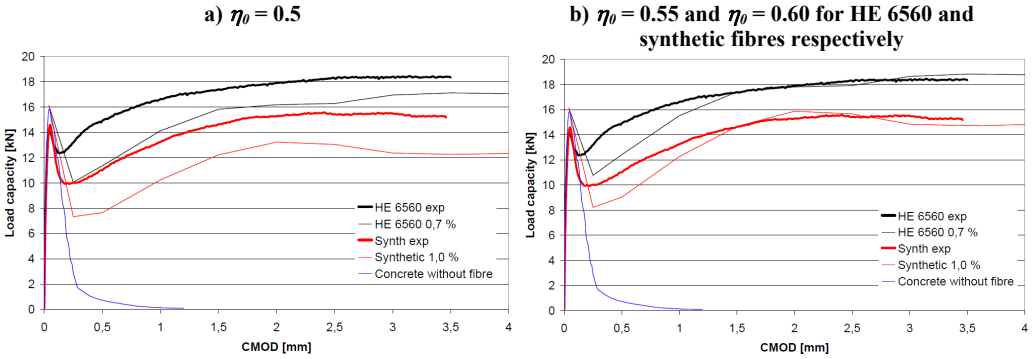

Figure 3-26 Comparison experimental and predicted load vs. CMOD curves, concrete in bending

As seen from Figure 3-26a), there is not a perfect match between the predicted and the experimental curves with a capacity factor η_0 = 0.5. If the capacity factor is set to 0.55 and 0.60 for HE 6560 fibres and synthetic fibres respectively, the predicted curves and the experimental curves coincide quite well. These capacity factors may perfectly well be correct; even though, the present calculations may not be considered to prove neither the size of the capacity factor nor the calculation model itself, because the coefficient of variation is about 25 % for the *HE 6560 exp* curve and about 9 % for the *Synth exp* curve. Nevertheless, the main points are that pull-out tests on single fibres give valuable information also when the behaviour in bending is of interest, and that it is quite likely that the most important parameter with regard to the fibres efficiency is the size of the crack opening.

3.10 Summary of pull-out tests on single fibres

The results from the experimental program show that the various fibre types have different behaviour in pull-out tests. The three suggested failure mechanisms, fibre fracture, fibre slippage and cone-shaped concrete failure describe the different behaviour quite well.

It is shown that the concrete strength will influence the pull-out resistance to a large extent. The reason is most likely that the bond between fibres and concrete increases when the concrete strength increases. This means that the limiting mechanisms described above are not only related to fibre types, but also concrete types. If, for instance, the synthetic fibres are cast in concrete with high strength, it is possible that the bond is large enough to reach fracture stress in the fibres, as shown from pull-out tests in concrete G and H.

To be able to maximize the effect of adding one type of fibre, it is necessary to tailor the *fibre-concrete* composition. Even though the effect of one fibre type is satisfactory in one concrete type, it does not need to be satisfactory if the concrete properties are changed. Further, it is important to be aware of the fact that different fibre types needs different crack openings to be fully effective.

To be able to tailor the fibre-concrete composition, it is important to know whether the limiting factors are, fibre fracture, fibre slippage or cone-shaped concrete failure, or a combination of them. Even though it is shown from pull-out tests on single fibres that the failure mechanism for one fibre type is fibre slippage, it is possible that several fibres together creates a collective cone-shaped concrete failure if the fibre volume is large enough. When the average distance between two fibre centres are equal to the minimum embedment length to avoid cone-shaped concrete failure, it seems reasonable to assume that the critical fibre volume is reached, meaning that a further increase in the fibre volume will most likely not result in increased capacity. Another implication is that even though it is reasonable to assume that it is a linear relationship between the capacity and the fibre volume, this relationship should be less pronounced when the fibre content are approaching the critical fibre volume. This effect can be explained by the increased possibility for two parallel neighbouring fibres to have centre distance less than the minimum embedment length to avoid a cone-shaped concrete failure.

It is also shown that it may be possible to use results from pull-out tests to predict the behaviour in both direct tension and bending, but then the crack opening must be correctly estimated, which off course can be very difficult in practice.

4 Beam test

4.1 Theoretical part

Beam tests can be performed in several ways, and in this PhD-thesis, two different test methods have been used:

- 4-point bending on un-notched beams
- 3-point bending on notched beams

The purpose of both methods is to measure the residual flexural tensile strength of fibre reinforced concrete. In the following both *residual flexural tensile stress* and *residual flexural tensile strength* are used. These two terms are calculated equally, and in general the *stress* notation is used while the *strength* notation is used when a given deflection or crack mouth opening displacement (CMOD) is considered.

In Norway a 4-point bending test on sawn un-notched beams has been used the last years, while the European Standard for testing metallic fibre concrete describes a 3-point bending test on notched beams [NS-EN 14651 (2005)], which is proposed to be used in the current proposal for Norwegian fibre guidelines.

The main differences between the Norwegian sawn beam test (NSBT) [Thorenfeldt et al. (2006)] and NS-EN 14651 are due to:

- The casting procedure and production of test specimens
- The test set-up

The casting procedure

According to the NSBT a panel with dimension 600x600x150 mm is cast, and from one panel three beams with dimension 150x150x600 mm are sawn. The two remaining 75 mm wide beams are not used. The span width is 450 mm, which means that 75 mm of the beams are outside the supports. In this way the wall's ability to affect the orientation of the fibres are reduced to practically zero. The casting procedure is meant to imitate the casting procedure at a construction site. If a slab shall be imitated, a horizontal plate is cast, while a vertical plate may represent a wall, as illustraded in Figure 4-1. In both cases, the sawn beams are tested from the side the expected loads are acting.

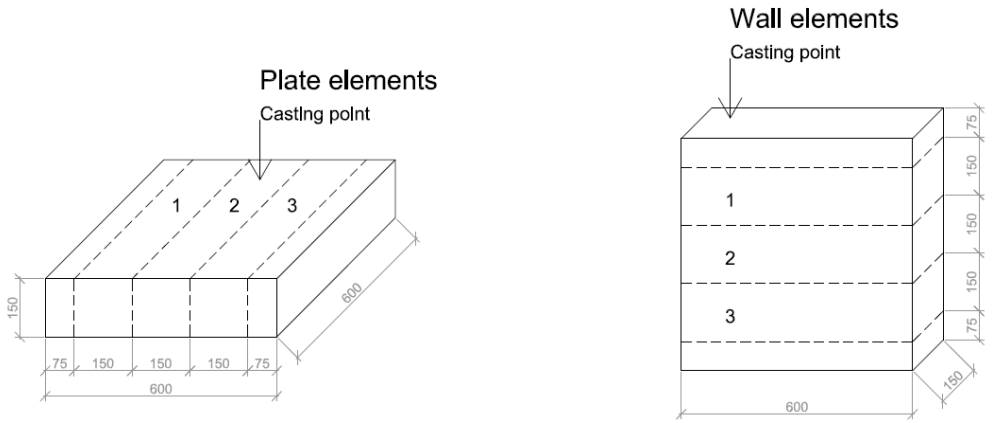

Figure 4-1 Plate and wall elements

When beams are made according to NS-EN 14651 the beams are cast as beams, and the walls in the formwork will influence the orientation of the fibres.

In general, the orientation of the fibres will be more uni-directed when the beams are cast according to NS-EN 14651 than when they are cut according to the NSBT.

The test set-up
The test set-up for the NSBT and NS-EN 14651 are shown in Figure 4-2, and a picture of one beam tested according to the two methods is shown in Figure 4-3.

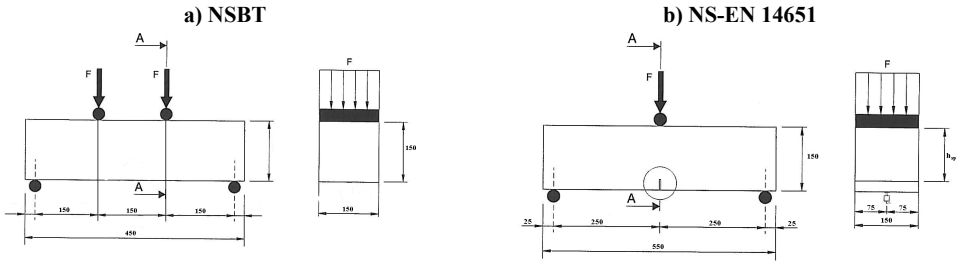

Figure 4-2 Test setup beam tests

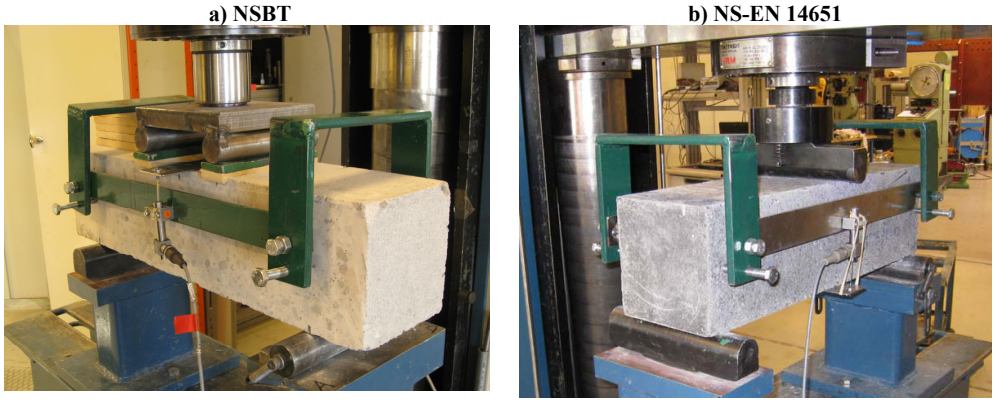

Figure 4-3 Pictures of beams being tested

When a beam is tested according to the NSBT, the concrete will crack somewhere between the two point loads where the concrete stress is equal. The position of the crack is decided by the microstructure of the concrete; the crack occurs in the weakest section where the concrete's strength first is reached.

When a beam is tested according to NS-EN 14651, the crack is always located at the notch, because the concrete stress is highest and the cross section is smallest in the same location. The flexural tensile stress at cracking is therefore expected to be larger when the concrete is tested according to NS-EN 14651 than when it is tested according to the Norwegian sawn beam test.

In general, the main objective to perform beam tests is to measure the concrete's residual flexural tensile strength, which is a main design parameter. In addition, beam tests may be used to range different concrete recipes, for instance if the concrete strength, fibre type or

fibre dosage varies. Beam tests may also be used to compare the effect of different fibre types in the same concrete.

The major advantage of the NSBT is that the casting method is as in real structures, and it is possible to saw beams from a real structure to document the in-situ flexural tensile strength. For instance, for a wall it is possible to cast the whole wall, and then to saw beams from the areas where windows or doors is located. In chapter 4.2.4, the results from the two test methods are compared to establish a relation between the NSBT and NS-EN 14651.

4.1.1 Norwegian sawn beam test (NSBT)

The results from tests performed according to the NSBT are the residual flexural tensile strength at different deflections, and the equivalent flexural tensile strength calculated from the average load between the upper and the lower deflection limits, δ_2 and δ_1. Figure 4-4 shows a typical load-deflection curve, and the different load values used to calculate the various residual flexural tensile strengths.

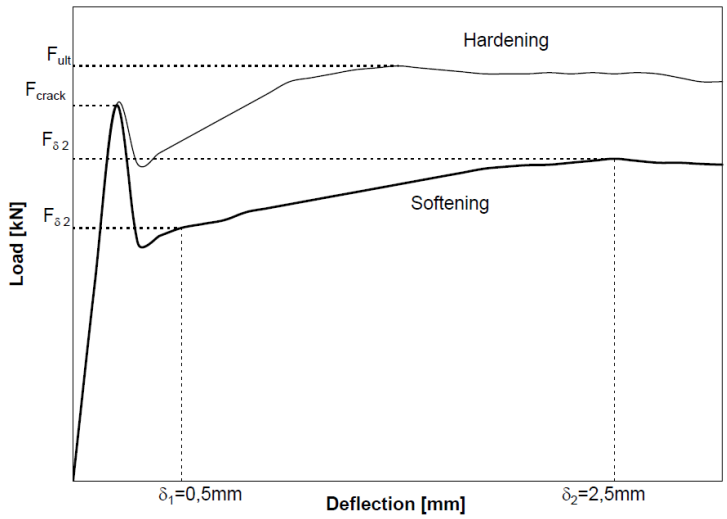

Figure 4-4 Typical load vs. deflection curve, NSBT

The following load values are to be determined:

F_{crack}: Load at cracking [N]
F_{ult}: Ultimate load, if strain hardening [N]
$F_{\delta 1}$: Load at δ_1=0.5 mm [N]
$F_{\delta 2}$: Load at δ_2=2.5 mm [N]
$F_{\delta 12}$: Average load between δ_1 and δ_2 [N]

The average load between δ_1 and δ_2 is simply found by numerical integration:

$$F_{\delta 12} = \sum_{i=\delta 1}^{\delta 2} \left[\left(\delta_{i+1} - \delta_i\right) \frac{F_i + F_{i+1}}{2\left(\delta_2 - \delta_1\right)} \right] \qquad (4\text{-}1)$$

And the belonging residual flexural tensile strengths, f_x, are calculated according to the following equation, based on linear elastic theory:

$$f_x = \frac{6M_x}{bh^2} = \frac{F_x l}{bh^2} \tag{4-2}$$

where

F_x: is the load corresponding to δ_1, δ_2 or δ_{12} [kN]
M_x: is the bending moment corresponding to the load F_x [kNm]
b: is the width of the specimen [mm]
h: is the height of the specimen [mm]
l: is the span length [mm]
f_x: is the residual flexural tensile strength corresponding to δ_1, δ_2 or δ_{12} [MPa]

Because there is a small variation in widths and heights of the test specimens, the fictitious stress at the tensile surface should be calculated according to equation 4-2 using measured dimensions, and plotted versus the related deflection instead of making load vs. deflection plots.

In the present thesis, results from beams tested according to the NSBT are presented as *flexural tensile stress vs. deflection* curves, together with the calculated strengths.

4.1.2 NS-EN 14651

The results from tests performed according to NS-EN 14651 are the residual flexural tensile strength at different CMODs, and the limit of proportionality (LOP).

Figure 4-5 shows a typical load-CMOD curve, and the different load values used to calculate the LOP and the different residual flexural tensile strengths based on the theory of linear elasticity.

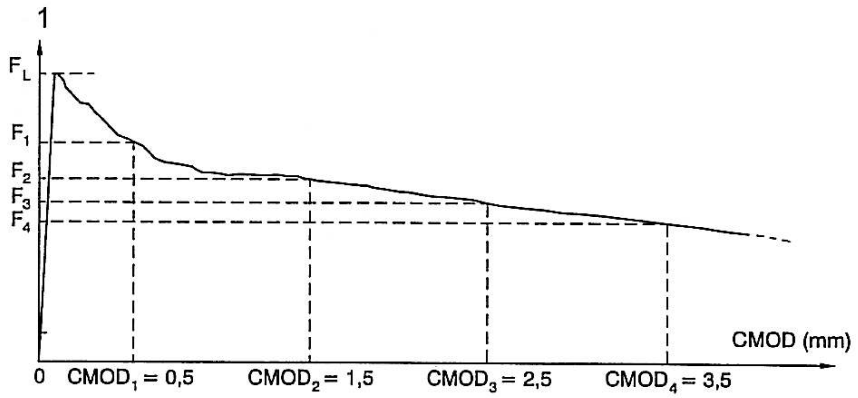

Figure 4-5 Load vs. CMOD diagram [NS-EN 14651]

The LOP, $f^{f}_{ct,L}$, is given by the expression:

$$f^{f}_{ct,L} = \frac{6M_L}{bh^2_{sp}} = \frac{3F_L l}{2bh^2_{sp}} \tag{4-3}$$

And the residual flexural tensile strength, $f_{R,j}$, (j=1, 2, 3, 4) is given by the expression:

$$f_{R,j} = \frac{6M_j}{bh^2_{sp}} = \frac{3F_j l}{2bh^2_{sp}} \tag{4-4}$$

where

F_L: is the load corresponding to the LOP [N]
F_j: is the load corresponding to $CMOD_j$ or δ_j (j=1, 2, 3, 4) [N]
l: is the span length [mm]
M_L: is the bending moment corresponding to the load at LOP [Nmm]
M_j: is the bending moment corresponding to the load F_j (j=1, 2, 3, 4) [Nmm]
b: is the width of the specimen [mm]
h_{sp}: is the distance between the tip of the notch and the top of the specimen in the mid-span section [mm]
$f^f_{ct,L}$: is the LOP [N/mm^2 or MPa]
$f_{R,j}$: is the residual flexural tensile strength corresponding to $CMOD_j$ or δ_j (j=1, 2, 3, 4) [N/mm^2 or MPa]

As for the NSBT-beams, there is a small variation in widths and heights of the test specimens, and the fictitious stress at the tip of the notch is calculated as in equation 4-4 using measured dimensions, and plotted versus the related deflection.

The results from beam tested according to NS-EN 14651 will be presented as *flexural tensile stress vs. CMOD* curves with calculated *f*-values.

4.1.3 Comparison NSBT vs. NS-EN 14651

NS-EN 14651 gives the residual flexural tensile strength, $f_{R,j}$, at different CMODs. The Norwegian sawn beam test gives an average residual flexural tensile strength based on the mean strength from 0.5 mm to 2.5 mm deflection, and the residual flexural tensile strength at 0.5 mm and 2.5 mm deflection. This means that it is rather difficult to compare the results directly. To be able to analyze the difference between the results from these two methods, one possibility is to calculate the residual flexural tensile strengths for the beams tested according to the NSBT procedure at the same CMODs as described in NS-EN 14651.

When a beam cracks at the mid span, the deformed shape may simplified be described by rotations at the crack and the supports as shown in Figure 4-6.

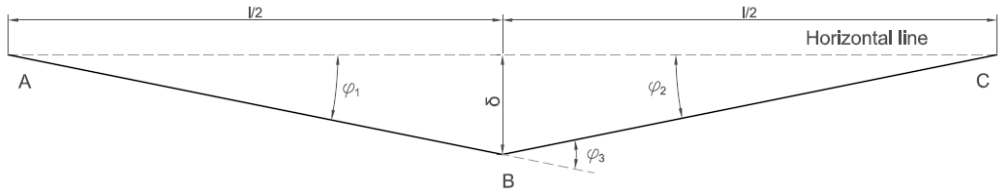

Figure 4-6 Deformed beam configuration described by rotations

The crack rotation at point B, φ_3, may be written as:

$$\varphi_3 = \frac{4}{l}\delta \qquad (4\text{-}5)$$

A NS-EN 14651 beam will always crack at the mid span, while a NSBT beam most likely will crack in other sections. For a NSBT beam, it is therefore necessary to measure the distance form the mid span to the crack to calculate the crack rotation. This distance is called crack offset, *x*. When a NSBT beam cracks with a crack offset, *x*, the rotation at the crack may be simplified as shown in Figure 4-7.

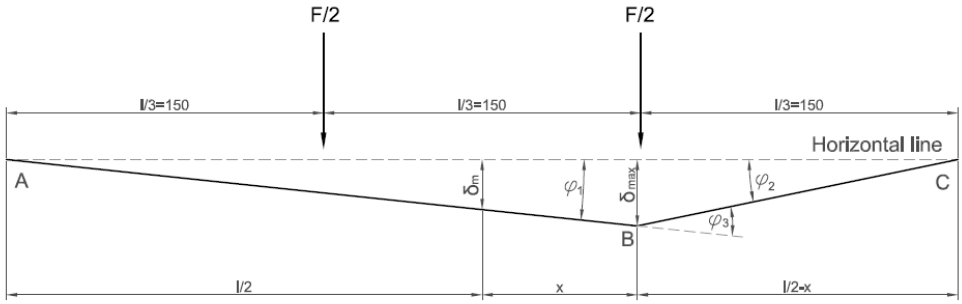

Figure 4-7 Crack offset for the NSBT method. All lengths are in mm

In Figure 4-7 the following notations are used:

δ_m: is the measured deflection [mm]
δ_{max}: is the deflection at the crack (point B) [mm]
x: is the crack offset [mm]

The expressions for the crack rotations may be written as:

$$\varphi_1 = \frac{2\delta_m}{l} = \frac{2\delta_{max}}{l+2x} \Rightarrow \delta_{max} = \frac{\delta_m(l+2x)}{l} \quad (4\text{-}6)$$

$$\varphi_2 = \frac{2\delta_{max}}{l-2x} = \frac{2\delta_m(l+2x)}{l(l-2x)} \quad (4\text{-}7)$$

$$\varphi_3 = \varphi_1 + \varphi_2 = \frac{4\delta_m}{l-2x} \quad (4\text{-}8)$$

The relationship between the CMOD, the deflection δ_m, and the crack rotation φ_3, for a NS-EN 14651 beam is shown in Figure 4-8.

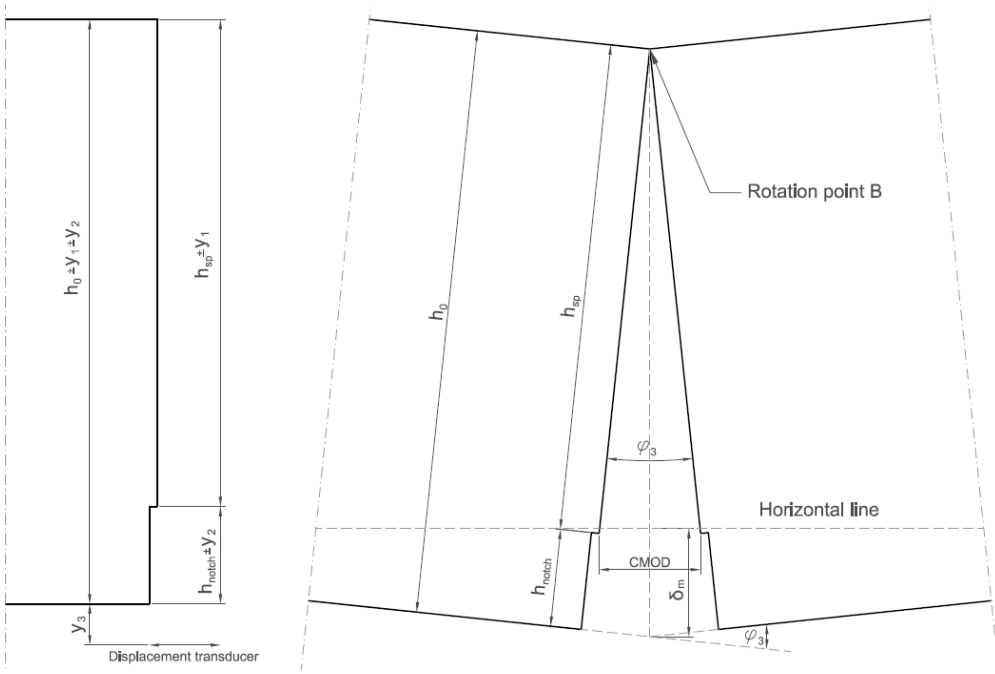

Figure 4-8 Relationship between CMOD, δ and φ_3, NS EN 14651 beam

In Figure 4-8 the following notations are used:

- h_0: is the prescribed height of the beam [150 mm]
- h_{sp}: is the prescribed distance between the tip of the notch and the top of the specimen [125 mm]
- $\pm y_1$: is the deviation from the prescribed h_{sp} [mm]
- $\pm y_2$: is the deviation from the prescribed notch depth [mm]
- y_3: is the distance from the tensile surface to the CMOD measurement location [mm]
- δ_m: is the measured deflection [mm]

The relationship between CMOD and the rotation may be written as:

$$\text{CMOD} = h_{sp}\varphi_3 \qquad (4\text{-}9)$$

CMOD is here related to the opening inside the notch, which is the real crack opening. For simplicity reasons the crack opening at the tip of the notch is called CMOD instead of CTOD (Crack Tip Opening Displacement) in the present thesis.

If the test is ran by controlling the CMOD by use of a displacement transducer placed a distance y_3 from the tensile surface, the CMOD should be corrected so that the real crack opening is calculated. The measured CMOD should also be corrected if h_0 or h_{sp} deviates from the prescribed heights.

Normally, the y_1- and y_2-term do not have to be considered because of the casting procedure; the variation in beam height should be rather small.

The relationship between CMOD and δ_m for a NS EN 14651 beam may then according to equation 4-5 be written as:

$$\text{CMOD} = 4\frac{h_{sp}}{l}\delta_m \tag{4-10}$$

The relationship between the CMOD, the deflection, δ_m, and the crack rotation, φ_3, for a NSBT beam is illustrated in Figure 4-9.

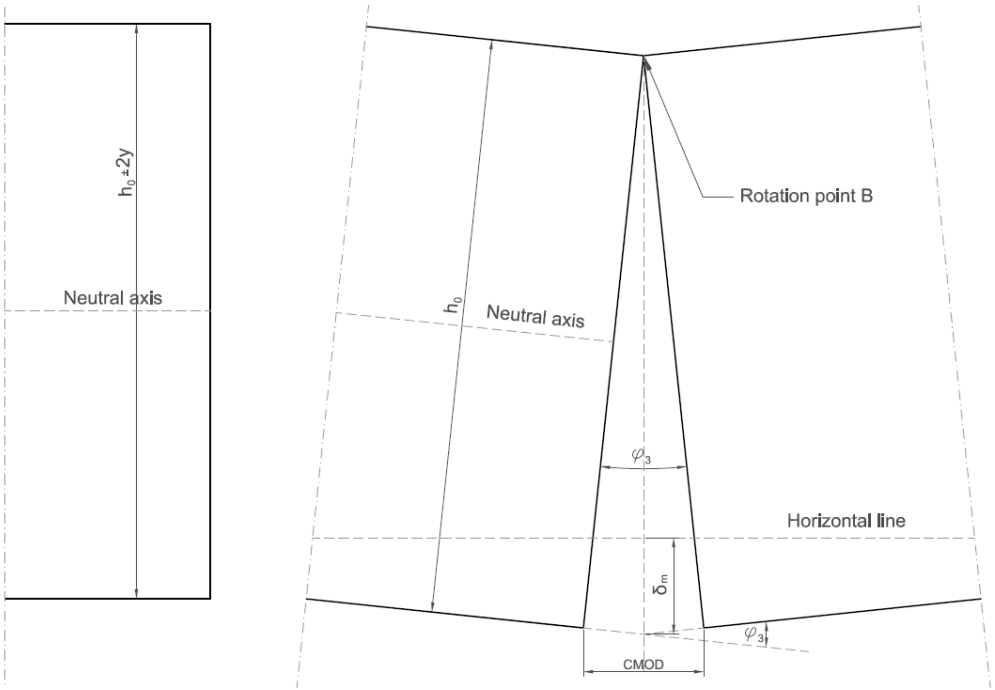

Figure 4-9 Relationship between CMOD, δ and φ_3, NSBT beam

In Figure 4-9 the following notations are used:

h_0: is the prescribed height of the beam [150 mm]
$\pm 2y$: is the deviation from prescribed h_0 [mm]
δ_m: is the measured deflection [mm]

The expression for CMOD may then be written as:

$$\text{CMOD} = (h_0 \pm 2y)\varphi_3 \tag{4-11}$$

CMOD is here related to the crack opening at the tensile surface, which is the real crack opening. The CMOD should also for NSBT beams be corrected if h_0 deviates from the prescribed height. This is more likely for NSBT beams than for NS EN 14651 beams, due to the casting procedure.

The relationship between CMOD and δ_m for the NSBT beams may then be written as:

$$\text{CMOD} = 4\frac{(h_0 \pm 2y)}{l - 2x}\delta_m \tag{4-12}$$

When the results from the NSBT and NS-EN 14651 are compared later in this chapter, they are compared by the *flexural tensile stress vs. CMOD* curves. The CMOD for a NS-EN 14651 beam is calculated according to equation 4-10, while the CMOD for a NSBT beam is calculated according to equation 4-12. Even though equation 4-10 does not give exactly equal CMOD for a given deflection as the equation in NS-EN 14651 it seems better to calculate the CMOD with similar assumptions for both test methods. Beside that, the stresses are calculated in agreement to both the NSBT procedure and the procedure in NS-EN 14651.

4.1.4 Design of ordinary reinforced concrete sections

If fibres are used in stead of conventional reinforcement in structures in bending as beams and slabs for instance, the fibre reinforced concrete must have at least equal strength as beams reinforced with the required minimum reinforcement area according to EC 2. Normally in design, the minimum concrete strength and belonging strength class is decided by the designer and the tabulated values for all other design parameters are found in table 3.1 in EC 2. The conformity criteria for compressive strength are described in NS-EN 206-1, and according to table 14 in [NS-EN 206-1], two strength criterions shall be satisfied:

- Criterion 1: $f_{cm} > f_{ck} + 4$
- Criterion 2: $f_{ci} > f_{ck} - 4$

The minimum longitudinal reinforcement for beams according to section 9 in EC 2 is calculated by the following equation:

$$A_{s,min} = 0.26 \frac{f_{ctm}}{f_{yk}} b_t d \geq 0.0013 b_t d \qquad (4\text{-}13)$$

where

f_{ctm}: is the tensile strength of the concrete, in MPa
f_{yk}: is the yield strength of the reinforcement, in MPa
b_t: is the mean width of the tension zone, in mm
d: is the effective depth of the section, in mm

Normally in design, f_{ctm} are found from table 3.1 in EC 2, where the tensile strength for different strength classes is defined.

The philosophy of the minimum reinforcement area is that the capacity after cracking shall be at least as large as the capacity prior to cracking. The intuitively implication of this philosophy, with retard to fibre reinforced beams tested according to NS-EN 14651, is that $f_{R,j}$ must be larger than $f^{f}_{ct,L}$ for all crack openings. On the other hand, this requirement is somewhat strict for fibre reinforced concrete, because the flexural tensile strength is normally larger than the tensile strength. The flexural tensile strength, $f_{ctm,fl}$, of reinforced concrete can be calculated according to equation 3.23 in EC 2 as:

$$f_{ctm,fl} = \max\left\{\left(1.6 - \frac{h}{1000}\right) f_{ctm}; f_{ctm}\right\} \qquad (4\text{-}14)$$

where

h: is the height of the specimen [mm]

For beam dimensions as prescribed in NS-EN 14651, the flexural tensile strength is expected to be nearly 50 % larger than the tensile strength, which means that a fibre reinforced beam designed to have $f_{R,j}$ larger than $f^{f}_{ct,L}$ for all crack openings most likely will have larger

capacity than a conventional beam reinforced with $A_{s,min}$. To investigate this, the two obvious possibilities are:

- To calculate the moment capacity for beams reinforced with $A_{s,min}$
- To cast and test beams reinforced $A_{s,min}$

It is actually somewhat difficult to calculate the moment capacity for a random beam or slab. To control whether a cross section has sufficient capacity with regard to the design moment, M_{Ed}, is on the other hand quite straightforward. To design a cross section to have sufficient capacity with regard to the design moment, M_{Ed}, is also quite straightforward.

The common practice, at least in Norway, is to design beams so that the strain at the compressive surface is equal to the ultimate strain, ε_{cu2}, when the steel strain in the tensile zone is equal to 5 ‰ ($2\varepsilon_{uk}$). By these limitations, the moment capacity of the compressive zone of the concrete, M_{Rd}, is easily calculated as:

$$M_{Rd} = 0{,}275 f_{cd} b d^2 \tag{4-15}$$

If M_{Rd}=M_{Ed} there is no need for steel reinforcement in the compressive zone, and the necessary cross section area of the re-bars may be calculated as:

$$A_s \geq \frac{M_{Rd}}{f_{yd} Z} \tag{4-16}$$

In this case, the moment capacity of the compressive zone and the moment capacity of the tensile zone are equal, and the concrete strain at the compressive surface will reach ε_{cu2} when the steel strain in the tensile zone is equal to 5 ‰ ($2\varepsilon_{yk}$).

If M_{Rd}>M_{Ed} it will be uneconomical to reinforce the tensile zone according to M_{Rd}, because the cross section will be strong enough if it can resist M_{Ed}. The necessary cross section area of the re-bars can then be calculated as:

$$A_s \geq \frac{M_{Ed}}{f_{yd} Z} \tag{4-17}$$

In both situations, Z is the internal moment arm, and can be calculated by force equilibrium. To calculate Z is quite difficult due to the shape of the concrete's σ vs. ε curve, and therefore Z is normally approximated to:

$$Z = \left(1 - 0.17 \frac{M_{Ed}}{M_{Rd}}\right) d \tag{4-18}$$

The factor 0.17 is only valid for strength class C20 to C45, and the factors for other strength classes can be found in several concrete reference books.

The problem by calculating the moment capacity for a random beam or slab is to find the moment arm, Z. The moment arm can be found only if the steel strain and the concrete strain at the compressive surface are known. To calculate the before mentioned strains are straight forward if the height of the compressive zone is known. The problem is that the height of the compressive zone cannot be generally described without solving equations of third degree.

In the following, a method to calculate the exact solution of the equations from EC 2 is presented. By use of this method, the moment capacity of every beams and slabs can be calculated, also if the structure is reinforced with fibres in addition to the re-bars.

In the following it is assumed that the concrete behaves as an elastic material prior to cracking, and that a crack is initiated when the flexural tensile stress reach the calculated flexural tensile strength.

To calculate the capacity of the beams after cracking, the following assumptions are used:

- There is perfect bond between the concrete and the steel reinforcement
- Navier's hypothesis is valid
- The contribution from the concrete's tensile capacity is neglected
- The stress-strain relationship is as given in EC 2

The stress-strain relationship for the concrete in compression shown in figure 3.3 in EC 2 is used, and the relationships are described as:

$$\sigma_c = f_{cd}\left[1-\left(1-\frac{\varepsilon_c}{\varepsilon_{c2}}\right)^n\right] \qquad \text{for } 0 \le \varepsilon_c \le \varepsilon_{c2} \tag{4-19}$$

$$\sigma_c = f_{cd} \qquad \text{for } \varepsilon_{c2} \le \varepsilon_c \le \varepsilon_{cu2} \tag{4-20}$$

where

n: is the exponent according to table 3.1 in EC 2

ε_{c2}: is the strain where the maximum strength according to table 3.1 in EC 2 is reached

ε_{cu2}: is the ultimate strain according to table 3.1 in EC 2

and:

$$f_{cd} = \alpha_{cc}\frac{f_{ck}}{\gamma_c} \tag{4-21}$$

where

α_{cc}: is the coefficient taking account of long term effects on the compressive strength and other unfavourable effects resulting from the way the load is applied and also that the strength in the structure may be less than the cylinder strength

γ_c: is the partial safety factor for concrete

As for concrete in compression, the stress-strain relationship for the reinforcing steel as given in EC 2 is used. There are two possibilities for calculating the steel stress, σ_s, either by strain-hardening behaviour and a maximum strain equal to ε_{ud}, or by perfect plastic behaviour and no strain limit. In the following calculation, the second alternative is chosen, which gives the following stress-strain relationships:

$$\sigma_s = \varepsilon_s E_s \qquad \text{for } 0 \le \varepsilon_s \le \frac{f_{yd}}{E_s} \tag{4-22}$$

$$\sigma_s = f_{yd} \qquad \text{for } \varepsilon_s \ge \frac{f_{yd}}{E_s} \tag{4-23}$$

where

$$f_{yd} = \frac{f_{yk}}{\gamma_s} \tag{4-24}$$

and

f_{yk}: is the yield strength, in MPa

γ_s: is the partial safety factor for reinforcing steel

ε_s: is the steel strain

The different factors that are described either in the standard text or in the National Annex are given in Table 4-1.

Table 4-1 Partial factors etc

n	ε_{c2}	ε_{cu2}	α_{cc}	γ_c	γ_s
2	0.002	0.0035	0.85	1.5	1.15

With the above mentioned assumptions and parameters, the following calculation model may be used:

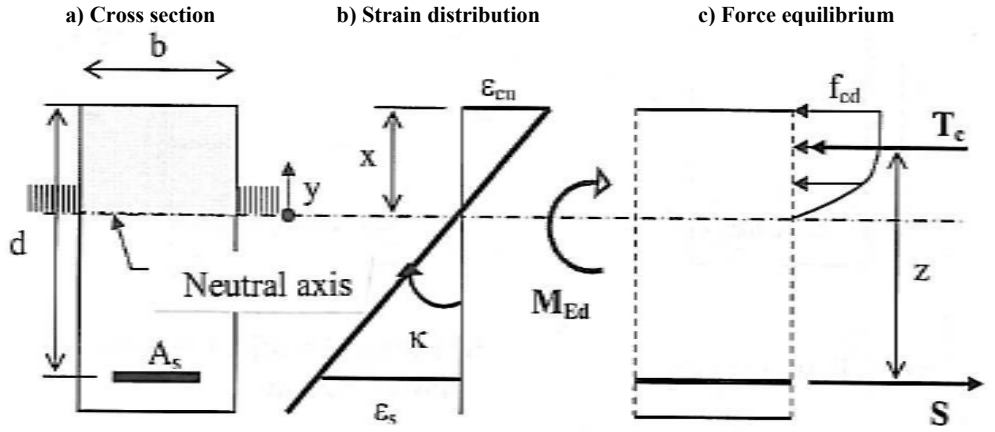

Figure 4-10 Calculation model for moment capacity [Sørensen, S.I. (2010)]

where

d: is the distance from the compressive surface of the beam to the centre of the reinforcement [mm]
A_s: is the cross section of the reinforcement steel [mm^2]
X: is the height of the compressive zone [mm]
F_s: is the force in the re-bars [N]
F_c: is the resultant of the concrete force in the compressive zone [N]
Z: is the moment arm, the distance between F_s and F_c [mm]
h: is the height of the specimen [mm]
b: is the width of the specimen [mm]
y_t: is the distance from the neutral axis to F_c

The resultant of the concrete force in the compressive zone is calculated as:

$$F_c = \int_{A_{c,c}} \sigma_c dA_{c,c} \tag{4-25}$$

where

$A_{c,c}$: is the cross sectional area of the compressive zone.

With the stress-strain relationship as given in equation 4-19 and 4-20 and beam dimension as given in Figure 4-10, F_c is written as:

$$F_c = 1000 f_{cd} bK\left(\frac{1}{2}X^2 - \frac{250}{3}KX^3\right) \quad \text{for } 0 \le \varepsilon_c \le \varepsilon_{c2} \tag{4-26}$$

$$F_c = 1000 f_{cd} bK\left(\frac{1}{2}X_1^2 - \frac{250}{3}KX_1^3\right) + f_{cd} b\left(X - X_1\right) \text{for } \varepsilon_{c2} \le \varepsilon_c \le \varepsilon_{cu2} \tag{4-27}$$

where

ε_c: is the concrete strain at the compressive surface of the beam

and:

$$K = \frac{\varepsilon_c}{d - X} \tag{4-28}$$

$$X_1 = \frac{\varepsilon_{c2}}{\varepsilon_c} X \tag{4-29}$$

F_s is written as:

$$F_s = \varepsilon_s E_s A_s \quad \text{for} \quad 0 \le \varepsilon_s \le \frac{f_{yd}}{E_s} \tag{4-30}$$

$$F_s = f_{yd} \quad \text{for} \quad \varepsilon_s \ge \frac{f_{yd}}{E_s} \tag{4-31}$$

The distance y_t is described by the following equation:

$$F_c y_t = \int_{A_{c,c}} \sigma_c y dA_{c,c} \tag{4-32}$$

Solving this integral equation gives the following expressions for y_t:

$$y_t = \frac{X\left(2 - 375KX\right)}{3 - 500KX} \quad \text{for } 0 \le \varepsilon_c \le \varepsilon_{c2} \tag{4-33}$$

$$y_t = \frac{1000KX_1^3\left(2 - 375KX_1\right) + 3\left(X^2 - X_1^2\right)}{1000K_1^2\left(3 - 500KX_1\right) + 6\left(X - X_1\right)} \quad \text{for } \varepsilon_{c2} \le \varepsilon_c \le \varepsilon_{cu2} \tag{4-34}$$

The moment capacity of a beam is found by requiring F_c=F_s, and this gives four possible combinations:

1. $0 \le \varepsilon_c \le \varepsilon_{c2}$ and $0 \le \varepsilon_s \le \frac{f_{yd}}{E_s}$
2. $0 \le \varepsilon_c \le \varepsilon_{c2}$ and $\varepsilon_s \ge \frac{f_{yd}}{E_s}$
3. $\varepsilon_{c2} \le \varepsilon_c \le \varepsilon_{cu2}$ and $0 \le \varepsilon_s \le \frac{f_{yd}}{E_s}$
4. $\varepsilon_{c2} \le \varepsilon_c \le \varepsilon_{cu2}$ and $\varepsilon_s \ge \frac{f_{yd}}{E_s}$

These four combinations correspond to different strain limitations for the concrete and the steel reinforcement, and therefore combination four gives the highest capacity because this combination fully utilize the materials.

The moment capacity, M_{cap}, for the different strain limitations can then be found by use of the following equation:

$$M_{cap} = F_c Z = F_s Z \tag{4-35}$$

The calculation model in Figure 4-10 can easily be expanded to be valid also for members reinforced with fibres (adding a tensile block of random shape in the tensile zone) and members with re-bars in the compressive zone (adding a compressive force at the re-bars location).

By use of equation 4-35 and combination 1 to 4, a M_{cap} *vs.* ε_s curve can be calculated. This curve will be valid after cracking, because the capacity is calculated according to the theory for cracked concrete sections. It should also be noted that the equations for the compressive zone are valid only if ε_{c2}, ε_{cu2} and n are equal to 0.002, 0.0035 and 2 respectively, which means for strength class up to C60/50. The moment capacity of plain concrete can be calculated according to elastic theory as:

$$M_{cap}(X) = \frac{2}{3} b X^2 \sigma_{ct} \tag{4-36}$$

where

σ_{ct}: is the concrete stress at the tensile surface or at the tip of the crack in the post-cracking phase.

The concrete strain at the compressive surface can be calculated as:

$$\varepsilon_c = \frac{\sigma_c}{E_{cm}} \tag{4-37}$$

where

σ_c: is the concrete stress at the compressive surface, and equal to σ_{ct}

The tensile strain at the depth of the re-bars can then be calculated as:

$$\varepsilon_s = \frac{\varepsilon_c (d - X)}{X} \tag{4-38}$$

By use of the above mentioned calculation method, the moment capacity for a beam can be calculated for all possible ε_s and also in the pre-cracked phase. If the calculated M_{cap} shall be compared with results from beam tests the steel strain must somewhat be related to deflection. In chapter 4.1.3 a method to calculate the CMOD from the measured deflection on tested beams is shown, but as mentioned in chapter 3.9, it is quite problematic to estimate the CMOD from a theoretical calculation of the capacity.

One possibility is to use the assumptions from chapter 4.1.3, which means that the beams after cracking behave as rigid bodies rotating at the compressive surface, meaning that there is no compressive zone. The total elongation of the steel reinforcement with constant strain can then be calculated as:

$$\Delta l_s = l_s \varepsilon_s \tag{4-39}$$

Because the steel strain is not constant due to the fact that the bending moment varies over the span and the steel strain is only significant close to the crack, it is somewhat difficult to calculate the total elongation of the steel. With the assumption that the average steel strain corresponds to the average bending moment, it may be assumed that the average steel strain is

50 % of maximum steel strain for beams tested according to NS-EN 14651, and 67 % of the maximum steel strain for beams tested according to the NSBT-procedure.

By these assumptions, the CMOD may be calculated as:

$$\mathrm{CMOD}_1 = \varepsilon_{\mathrm{s,mean}} l \frac{h}{d} \tag{4-40}$$

where

l: is the length of the beam
$\varepsilon_{\mathrm{s,mean}}$: is the average steel strain

To assume that the height of the compressive zone is zero when calculating the CMOD is in agreement with the deflection vs. CMOD relationship as described in chapter 4.1.3. Because the intention is to compare the *estimated capacity* at different CMODs with the *measured capacity* at different CMODs, it is advantageous to calculate the CMOD with equal assumptions. Nevertheless, it seems somewhat meaningless to first calculate the capacity in an iterative process where X is found by requiring $F_c = F_s$ and then to assume that $X = 0$ to calculate the CMOD.

A second possibility is to assume that the beams rotate as rigid bodies, but that the two parts rotates at the location of the neutral axis. The depth of the compressive zone, X, is already found if the calculation method described earlier in this chapter is used. The expression for the second possibility will then be:

$$\mathrm{CMOD}_2 = \varepsilon_{\mathrm{s,mean}} l \frac{h - X}{d - X} \tag{4-41}$$

A third possibility is to use the expression from [Löfgren (2003)]. Also by this method, it is necessary to estimate the average steel strain, and in addition, the length of the hinge must be assumed. Because the beams only have one crack, it may be possible to use the beam length as the length of the hinge. The expression for the third possibility will then be:

$$\mathrm{CMOD}_3 = \varphi(h - X) - \frac{f_{\mathrm{ct}}}{E_{\mathrm{cm}}} l \tag{4-42}$$

where

$$\varphi = \kappa^* \cdot l = \frac{\varepsilon_{\mathrm{s,mean}}}{X} l \tag{4-43}$$

The curvature is calculated by use of the concrete strain at the compressive surface and X, which in turn is calculated by use of steel strain. Due to the fact that the steel strain varies over the length of the beam, the curvature will also vary, which means that it might be more correct to use the assumption that the average steel strain corresponds to the average bending moment, which is why the curvature is written as κ^*.

The difference in CMOD_2 and CMOD_3 is only the second term of equation 4-42, which represents the elastic deformation in the non-linear hinge. The difference between CMOD_1 and CMOD_2 (and CMOD_3) varies with the depth of the neutral axis.

The CMOD from immediately after cracking and until the reinforcement starts to give a contribution to the strength may be calculated as:

$$\text{CMOD} = \varepsilon_{\text{ct,fict}} l \tag{4-44}$$

where

$\varepsilon_{\text{ct,fict}}$: is the fictitious concrete strain at the tensile surface that would have been present if the concrete did not crack, and calculated as:

$$\varepsilon_{\text{ct,fict}} = \varepsilon_{\text{c}} \frac{h - X}{X} \tag{4-45}$$

This calculation method is used to calculate the moment capacity for beams reinforced with conventional reinforcement tested according to NS-EN 14651 and the NSBT procedure presented in chapter 4.2.6, and also to find *the moment capacity vs. curvature* diagrams in chapter 8.7.

4.2 Experimental part

In this chapter, results from the beam tests are reported and evaluated. Beams have been cast with steel- and synthetic fibres, and in addition, 6 beams have been reinforced with conventional re-bars.

Contractors are often interested in the amount of synthetic fibre that has to be used to achieve the same properties as a given amount of steel fibre. This is a difficult question to answer amongst others because different test methods give different relationships. The steel/synthetic fibre relationship found by use of the Norwegian sawn beam test is reported in chapter 4.2.2 while the steel/synthetic fibre relationship found by use of NS-EN 14651 is reported in chapter 4.2.3. Finally, comparison of results from both beam test methods is reported in chapter 4.2.4.

The steel fibres used in these tests are Dramix 6560 while the synthetic fibres are Barchip Shogun. Both fibre types are described in chapter 2.

Three beams with steel fibre content 0.7 vol% and three beams with synthetic fibre content 1.0 vol% were produced and tested by both test methods. In addition, three beams with steel fibre content 0.7 vol% and three beams with synthetic fibre content 1.0 vol% were cast according to NS-EN 14651 but tested according to the NSBT procedure. In an earlier test program, six beams with steel fibre content 0.5 vol% were tested according to NS-EN 14651 to gain experience with the test method, and the results from this series are also reported. An overview of the tested beams is shown in Table 4-2.

Table 4-2 Overview of tested beams

Beam name	Fibre dosage and fibre type	Casting procedure	Testing procedure
090210-1, -2 and -3	0.7 vol% Dramix 6560	NS-EN 14651	NSBT
090210-4, -5 and -6		NS-EN 14651	NS-EN 14651
090210-7, -8, and -9		NSBT[1]	NSBT
160210-1, -2 and -3	1.0 vol% Barchip Shogun	NS-EN 14651	NSBT
160210-4, -5 and -6		NS-EN 14651	NS-EN 14651
160210-7, -8, and -9		NSBT[1]	NSBT
261109-1 to -6	0.5 vol% Dramix 6560	NS-EN 14651	NS-EN 14651
[1]Cast as horizontal slabs			

The main purpose of these tests was to compare the results from beams tested according to the NSBT and NS-EN 14651. The six beams reinforced with 0.5 vol% Dramix 6560 were initially tested to be familiar with the NS-EN 14651.

All beams are made of concrete D described previously in chapter 2.1. Casting date, testing date and compressive strength are shown in Table 4-3.

Table 4-3 Casting date, testing date and compressive strength

Fibre type/dosage	Casting date	Testing date	Compressive strength
0.5 vol% Steel fibre	26.Nov.09	14.Jan.10	52 MPa[1]
0.7 vol% Steel fibre	09.Feb.10	09.Mar.10	52 MPa
1.0 vol% Synthetic fibre	16.Feb.10	16.Mar.10	54 MPa
[1]Compressive strength after 28 days: ~52 MPa. Age at testing: 49 days			

The number of beams in this test series is rather limited. Due to a coefficient of variation up to 25%, it is difficult to draw some definitive conclusions. What seems to be a trend when the average values are compared might be due to statistical deviation. Nevertheless, it is considered to be better to try to find some trends that eventually are found to be incorrect in later studies, than to hide behind statistical uncertainties.

In addition to the 24 beams shown in Table 4-2 a large number of beams have been tested according to NS-EN 14651 in connection with the *ductile high tensile strength all round concrete*-project. The results from these beam tests are reported in chapter 8

4.2.1 Fibre counting

After testing the beams with 0.7 vol% steel fibres and 1.0 vol% synthetic fibres, the beams were cut 50 mm to the side of the crack, and the amount of fibres in the cross section was counted. This was done to see if the number of fibres in the cross section was equal in all beams, and to find out if there is a correlation between the flexural tensile strength and the amount of fibre. The results from the fibre counting are shown in Figure 4-11 and Figure 4-12, for the steel fibre and synthetic fibre reinforced beams respectively.

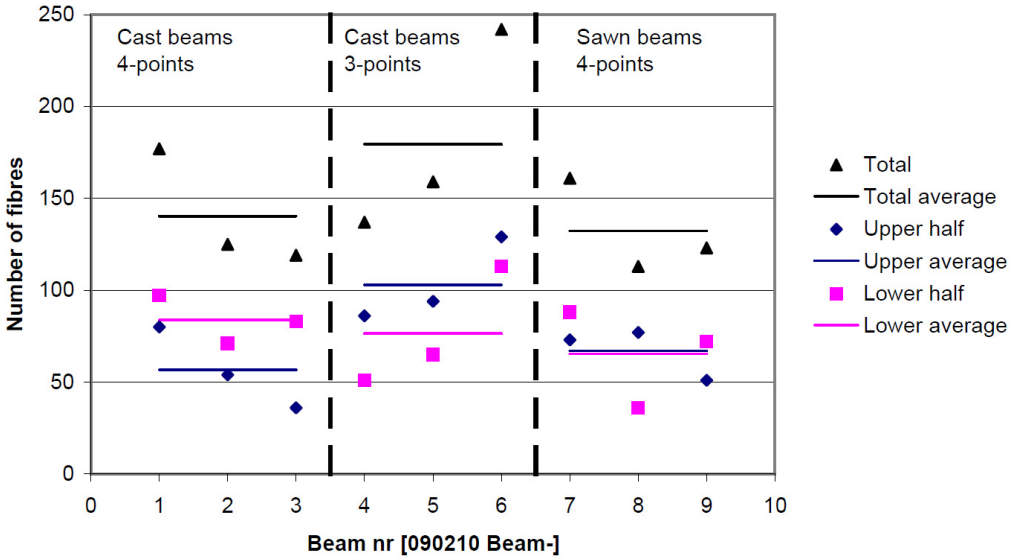

Figure 4-11 Fibre counting, steel fibre

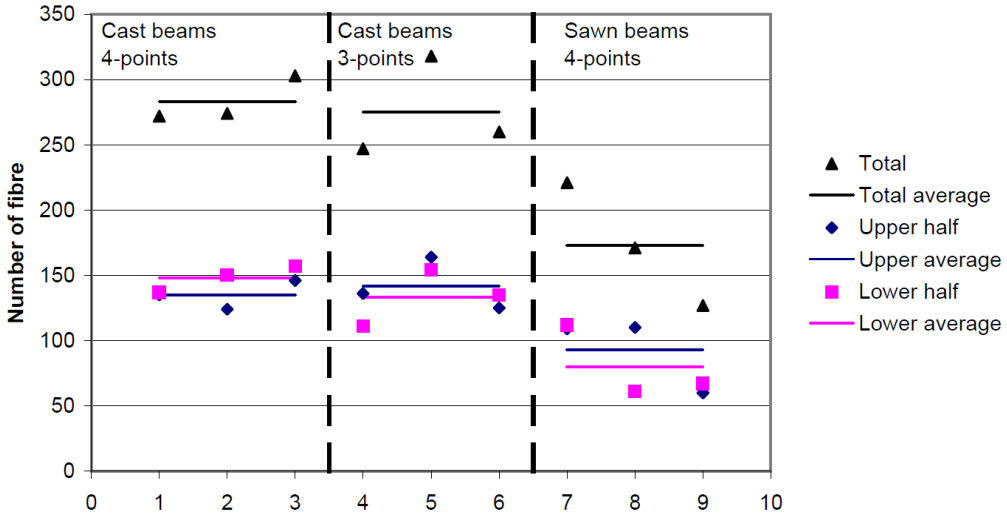

Figure 4-12 Fibre counting, synthetic fibre

As seen in Figure 4-11 and Figure 4-12, the amount of fibres in the cross section is not equal for all beams. The fibre density in the lower half of the beam is considered to be more important than the fibre density in the upper half, because the fibres are transferring tensile stresses across the cracks.

The most important findings from the fibre counting can be summarized as:

- *090210 Beam 6* had considerably more fibres than all the other steel fibre reinforced beams.

- *090210 Beam 7* had also more fibres in the lower half than the two other beams cast and tested the same way, but it is shown in later chapters that both beam 6 and 7 also had higher capacity in bending than the similar beams.
- *160210 Beam 7, 8* and *9* had fewer fibres than the other synthetic fibre reinforced beams, and this may be the explanation why these beams had less capacity in bending than expected. This will also be further discussed in later chapters.

4.2.2 Norwegian sawn beam test

The flexural tensile stress vs. deflection curves for the three beams with 0.7 vol% steel fibre are shown in Figure 4-13 and the calculated results are shown in Table 4-4.

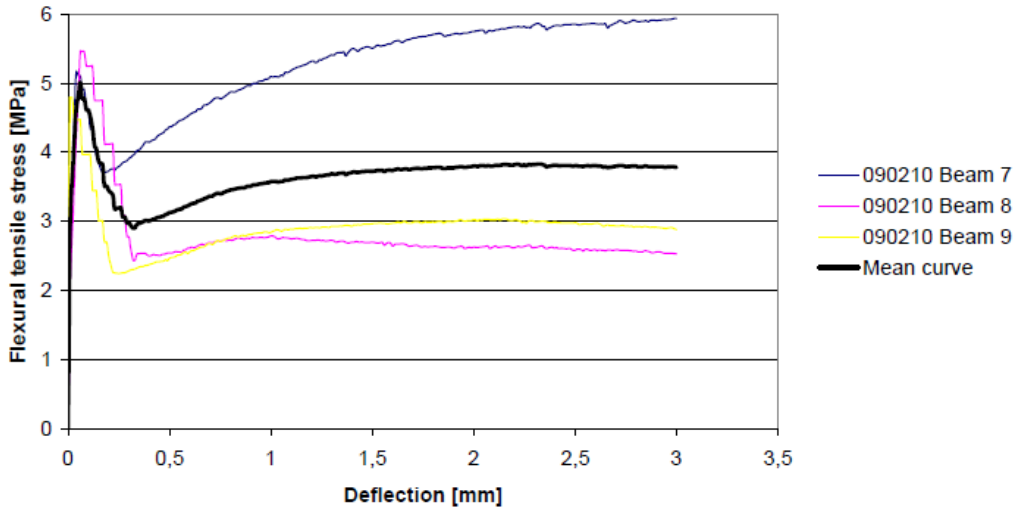

Figure 4-13 0.7 vol% Steel fibre, Norwegian sawn beam test

Table 4-4 Results, 0.7 vol% steel fibre, Norwegian sawn beam test

	090210 Beam 7	090210 Beam 8	090210 Beam 9	**Mean value**	Coefficient of variation
b [mm]	150.0	150.5	151.0	150.5	0.3%
h_{sp} [mm]	151.0	152.0	153.0	152.0	0.7%
l [mm]	450.0	450.0	450.0	450.0	0.0%
f_{crack} [MPa]	5.16	5.46	4.87	**5.2**	5.7%
f_{ult} [MPa]	5.96	5.46	4.87	**5.4**	10.0%
$f_{\delta 1}$ [MPa]	4.37	2.54	2.46	**3.1**	34.5%
$f_{\delta 2}$ [MPa]	5.85	2.58	2.98	**3.8**	46.9%
$f_{\delta 12}$ [MPa]	5.38	2.67	2.89	**3.6**	41.2%

The beam marked with *090210 Beam 7* had considerably higher capacity than the other two beams. After testing the beams, they were cut in half and the number of fibres was counted. *090210 Beam 7* had 63 % more fibres in the lower half of the beam than the other two beams.

The flexural tensile stress vs. deflection curves for the three beams with 1.0 vol% synthetic fibre are shown in Figure 4-14 and the calculated results are shown in Table 4-5.

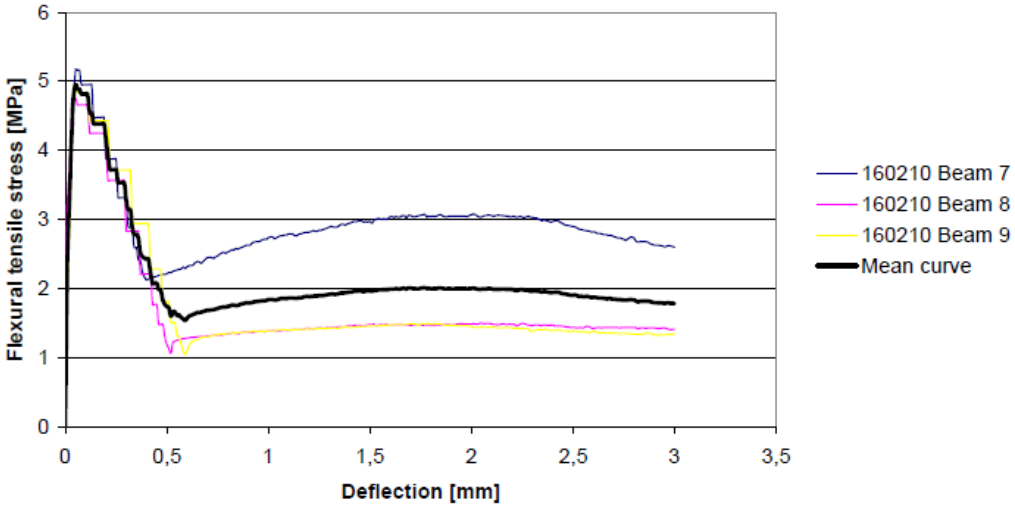

Figure 4-14 1.0 vol% synthetic fibre, Norwegian sawn beam test

Table 4-5 Results, 1.0 vol% synthetic fibre, Norwegian sawn beam test

	160210 Beam 7	160210 Beam 8	160210 Beam 9	**Mean value**	Coefficient of variation
b [mm]	150.5	151.0	151.0	150.8	0.2%
h_{sp} [mm]	152.5	153.0	152.0	152.5	0.3%
l [mm]	450.0	450.0	450.0	450.0	0.0%
f_{crack} [MPa]	5.17	4.76	4.92	**5.0**	4.2%
f_{ult} [MPa]	5.17	4.76	4.92	**5.0**	4.2%
$f_{\delta 1}$ [MPa]	2.21	1.20	1.81	**1.7**	29.4%
$f_{\delta 2}$ [MPa]	2.90	1.43	1.38	**1.9**	45.2%
$f_{\delta 12}$ [MPa]	2.84	1.41	1.43	**1.9**	43.3%

Also one beam with synthetic fibres shows untypical behaviour. After fibre counting, it was found that *160210 Beam 7* had 75 % more fibres in the lower half of the beam than the other two beams. Even though, as seen from the number of fibre in Figure 4-12, it may be that *160210 Beam 7* is the most relevant beam from the NSBT-series to compare with the other tests series.

In Figure 4-15 the two mean curves are shown to compare the effect of adding 0.7 vol% steel fibre and 1.0 vol% synthetic fibre, respectively. The belonging calculated mean results are shown in Table 4-6.

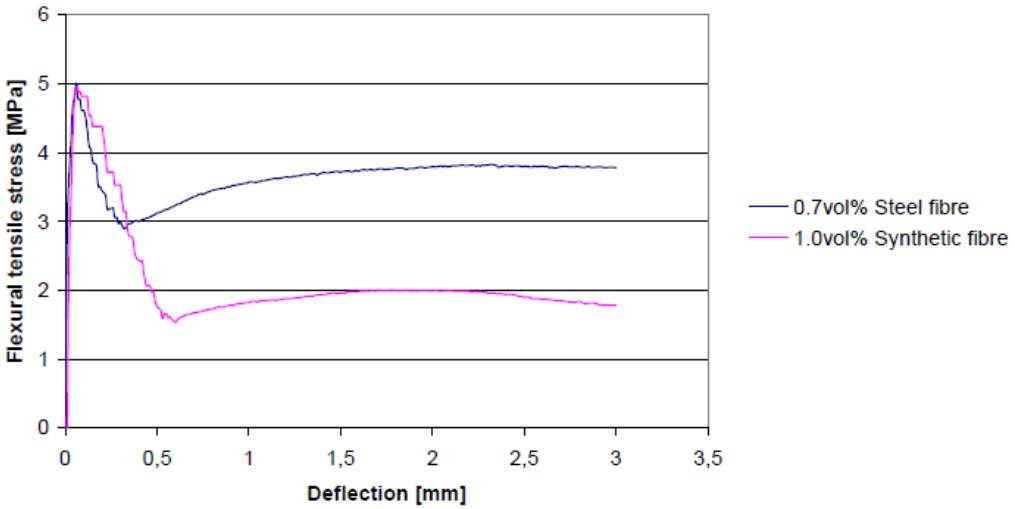

Figure 4-15 Comparison 0.7 vol% steel fibre and 1.0 vol% synthetic fibre, NSBT test

Table 4-6 Comparison 0.7 vol% steel fibre and 1.0 vol% synthetic fibre, NSBT

	0.7 vol% Steel fibre		1.0 vol% Synthetic fibre		Ratio synthetic/steel
	Mean value	Coefficient of variation	Mean value	Coefficient of variation	
f_{crack} [MPa]	5.2	5.7 %	5.0	4.2 %	96 %
f_{ult} [MPa]	5.4	10.0 %	5.0	4.2 %	93 %
$f_{\delta 1}$ [MPa]	3.1	34.5 %	1.7	29.4 %	55 %
$f_{\delta 2}$ [MPa]	3.8	46.9 %	1.9	45.2 %	50 %
$f_{\delta 12}$ [MPa]	3.1	41.2 %	1.9	43.3 %	61 %

The Norwegian sawn beam test shows that adding 0.7 vol% Dramix 6560 fibre into concrete D gives almost twice the flexural tensile strength than adding 1.0 vol% Barchip Shogun fibre.

From Figure 4-12 it can be seen that the number of fibres in the lower half of *160210 Beam 8* and *9* is approximately 50 % of the average for the synthetic fibres. This means that the calculated strengths for these beams may be half the strength they would have had if the fibre amount had been as for the other beams.

The numbers of beams are as already mentioned too small, and the variation in fibre density is too large to draw a definitive conclusion, but the trend is that the steel fibres are more effective than the synthetic fibres when these two fibre types are tested according to the NSBT procedure. The steel fibre beams had approximately twice the strength of the synthetic fibre beams. Once again, it may be that the synthetic fibre beams would have had flexural tensile strengths closer to the steel fibre beams if the fibre amount was the same as for the *cast beams 4-points* and the *cast beams 3-points* shown in Figure 4-12.

The relationship between these two fibre types may be different in other concrete mixes, for instance in a concrete with different strength.

4.2.3 NS-EN 14651

The tests performed at NTNU/SINTEF differ from NS-EN 14651 in two ways:

1. The rate of increase of CMOD
2. The rate of data recording

The rate of increase of CMOD

According to NS-EN 14651, "*the machine shall be operated so that CMOD increases at a constant rate of 0.05 mm/min. When CMOD=0.1 mm, the machine shall be operated so that CMOD increases at a constant rate of 0.2 mm/min. In case of a testing machine controlling the rate of increase of deflection, the above testing procedure shall be applied provided that the CMOD related parameters are transformed into deflection related parameters.*

The relation between CMOD and deflection, δ, may be approximated by

$$\delta = 0.85\text{CMOD} + 0.04\text{ }''\qquad(4\text{-}46)$$

The δ *vs. CMOD* relationship shown in Table 4-7 are also found in NS-EN 14651, and may be used in stead of equation 4-46.

Table 4-7 Relationship between CMOD and δ [NS-EN 14651]

CMOD [mm]	δ [mm]
0.05	0.08
0.1	0.13
0.2	0.21
0.5	0.47
1.5	1.32
2.5	2.17
3.5	3.02
4.0	3.44

At the laboratory at SINTEF/NTNU, it is not possible to perform the tests by controlling the increase of CMOD. The machine can only be operated so that the deflection rate is controlled. It is also easier to measure the deflection by help of LVDTs than to measure the CMOD. Because of this, the tests are performed deflection-controlled, and not CMOD-controlled. In addition, the deflection rate is set to 0.21 mm/min during the whole test. This is done because it is not possible to program the machine at the laboratory at SINTEF/NTNU to increase the deflection rate at a specified deflection value. It is considered more important to test every beam equally, than to have a lower deflection rate in the beginning of the test.

The deflection rate is controlled by the internal deflectometer. In addition to this, two LVDTs are mounted at the beam, one at each side, and the mean value of these deflection measurements is used when the load vs. deflection curve is drawn.

The rate of recording

According to NS-EN 14651, the load and corresponding CMOD shall be recorded at a rate not less than 5 Hz during the first two minutes, and not less than 1 Hz during the rest of the test. At SINTEF/NTNU the load and corresponding deflection is recorded at a rate of 2 Hz during the whole test. This is done to reduce the amount of data in the logging file.

The flexural tensile stress vs. CMOD curves for the six beams with 0.5 vol% steel fibre are shown in Figure 4-16 and the calculated results are shown in Table 4-8. The CMOD is calculated according to equation 4-46, and the flexural tensile stress is calculated according to equation 4-4.

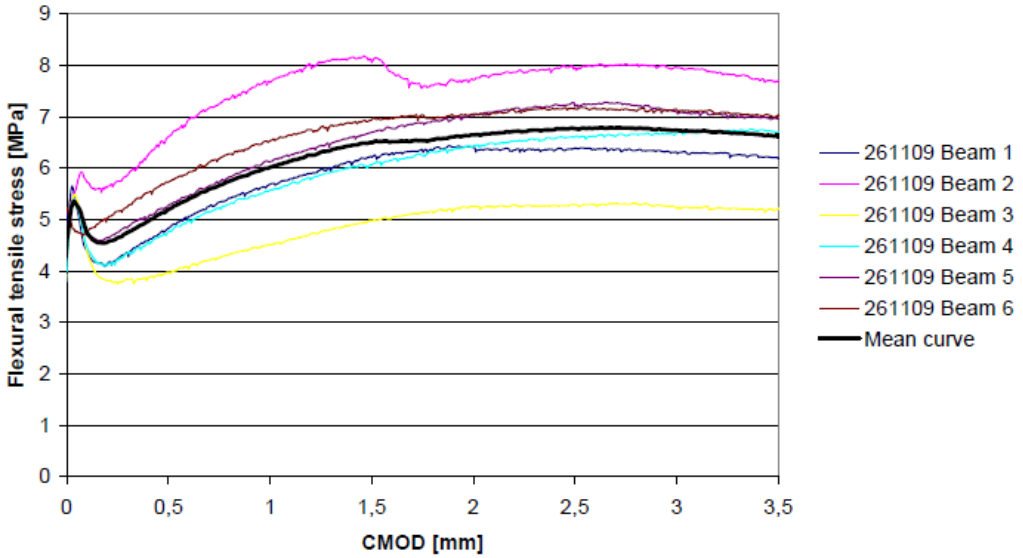

Figure 4-16 0.5 vol% Steel fibre, NS-EN 14651

Table 4-8 Results, 0.5 vol% steel fibre, NS-EN 14651

	261109 Beam 1	261109 Beam 2	261109 Beam 3	261109 Beam 4	261109 Beam 5	261109 Beam 6	**Mean value**	Coefficient of variation
b [mm]	150.5	151.5	151.5	152.5	152.0	151.0	**151.5**	0.5 %
h_{sp} [mm]	125.5	124.0	125.0	126.0	125.5	125.5	**125.3**	0.6 %
l [mm]	500	500	500	500	500	500	**500**	0.0 %
$f^{f}_{ct,L}$ [MPa]	5.65	5.60	5.49	5.40	5.39	5.25	**5.5**	2.7 %
$f_{R,1}$ [MPa]	4.84	6.62	3.97	4.77	5.29	5.75	**5.2**	17.5 %
$f_{R,2}$ [MPa]	6.23	8.08	4.98	6.07	6.70	6.95	**6.5**	15.9 %
$f_{R,3}$ [MPa]	6.39	7.92	5.29	6.63	7.22	7.15	**6.8**	13.3 %
$f_{R,4}$ [MPa]	6.20	7.69	5.21	6.71	6.97	7.03	**6.6**	12.8 %

261109 beam 2 had a local maximum at $\delta_{peak} = 0.1$ mm, and the corresponding fictitious stress at the tip of the notch, f_{peak}, was 5.92 MPa. According to NS-EN 14651, the $f^{f}_{ct,L}$ are to be found at a CMOD not larger than 0.05 mm, which according to Table 4-7 corresponds to a deflection not larger than 0.08 mm. Therefore, $f^{f}_{ct,L}$ for *261109 Beam 2* shown in Table 4-8 is less than the peak stress shown in Figure 4-16.

The flexural tensile stress vs. deflection curves for the three beams with 0.7 vol% steel fibre are shown in Figure 4-17 and the calculated results are shown in Table 4-9.

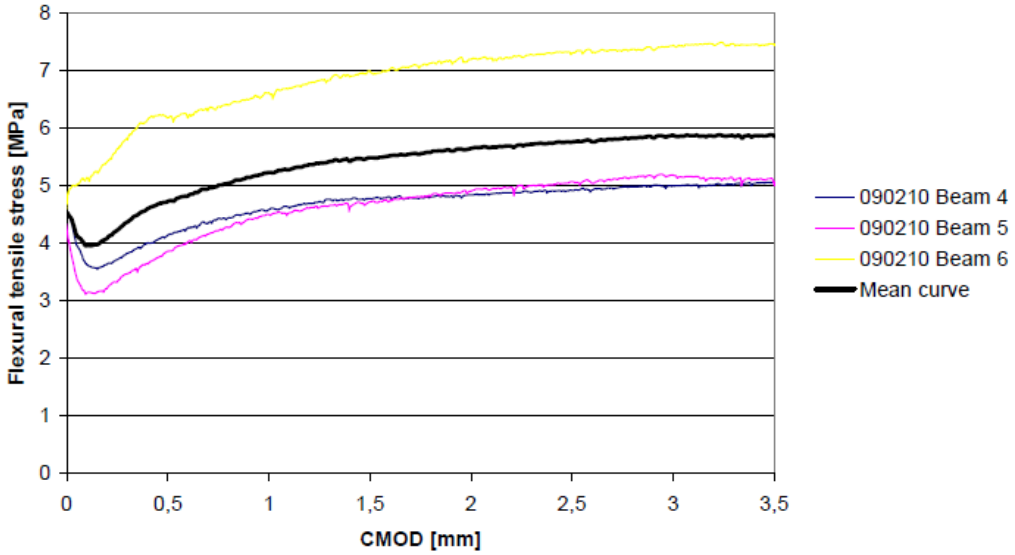

Figure 4-17 0.7 vol% Steel fibre, NS-EN 14651

Table 4-9 Results, 0.7 vol% steel fibre, NS-EN 14651

	090210 Beam 4	090210 Beam 5	090210 Beam 6	**Mean value**	Coefficient of variation
b [mm]	151.0	151.5	151.0	151.2	0.19 %
h_{sp} [mm]	125.0	125.0	125.0	125.0	0.00 %
l [mm]	500	500	500	500	0.00 %
$f^{f}_{ct,L}$ [MPa]	4.54	4.46	5.01	**4.7**	6.4 %
$f_{R,1}$ [MPa]	4.16	3.87	6.19	**4.7**	26.7 %
$f_{R,2}$ [MPa]	4.78	4.73	6.97	**5.5**	23.4 %
$f_{R,3}$ [MPa]	4.92	5.07	7.32	**5.8**	23.3 %
$f_{R,4}$ [MPa]	5.06	5.06	7.46	**5.9**	23.6 %

As seen from Figure 4-17 and Table 4-9, it seems like *090210 Beam 6* has an untypical behaviour. After testing the beams, they were cut in half and the number of fibres was counted. *090210 Beam 6* had 95 % more fibres in the lower half of the beam than the other two beams, as previously shown in Figure 4-11

The flexural tensile stress vs. deflection curves for the three beams with 1.0 vol% synthetic fibre are shown in Figure 4-18 and the calculated results are shown in Table 4-10.

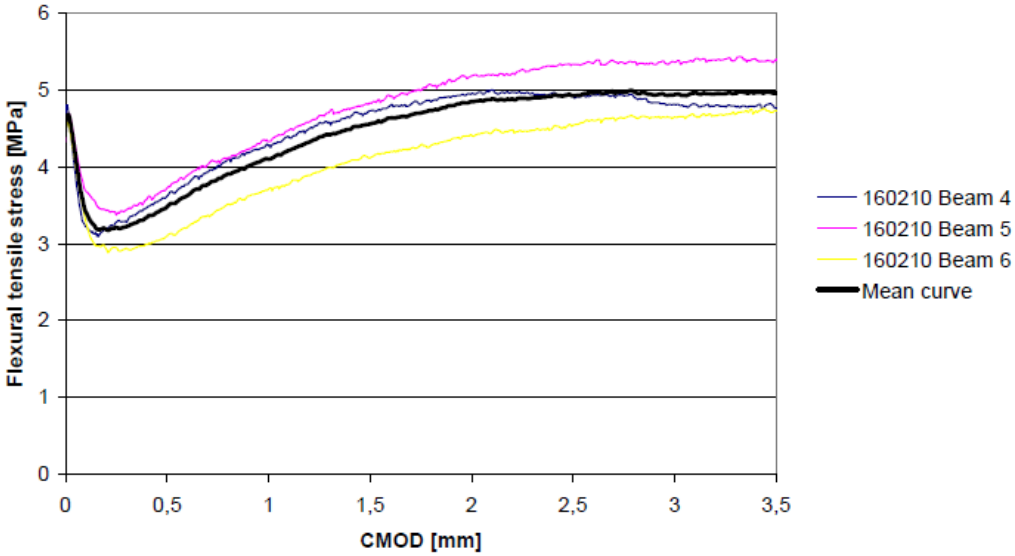

Figure 4-18 1.0 vol% Synthetic fibre, NS-EN 14651

Table 4-10 Results, 1.0 vol% synthetic fibre, NS-EN 14651

	160210 Beam 4	160210 Beam 5	160210 Beam 6	**Mean value**	Coefficient of variation
b [mm]	150.5	151.0	150.5	150.7	0.19 %
h_{sp} [mm]	125.0	125.5	125.0	125.2	0.23 %
l [mm]	500	500	500	500	0.00 %
$f^{f}_{ct,L}$ [MPa]	4.80	4.68	4.58	**4.7**	2.3 %
$f_{R,1}$ [MPa]	3.62	3.74	3.11	**3.5**	9.5 %
$f_{R,2}$ [MPa]	4.73	4.82	4.12	**4.6**	8.4 %
$f_{R,3}$ [MPa]	4.90	5.32	4.54	**4.9**	8.0 %
$f_{R,4}$ [MPa]	4.75	5.39	4.73	**5.0**	7.5 %

The results from the six beams with 0.5 vol% steel fibre are not analyzed further because they were tested after 49 days of curing. The results are shown here mostly to highlight that the coefficient of variation may be quite large, and that the residual flexural strengths are dependent on the concrete age. The reason why the 0.5 vol% steel fibre concrete had higher residual flexural tensile strength than the 0.7 vol% steel fibre concrete is most likely increased concrete strength as a consequence of higher concrete age.

In Figure 4-19 the mean curve from the beams with synthetic fibres are plotted together with the mean curve from the beams with steel fibres, and the belonging mean results are shown in Table 4-11.

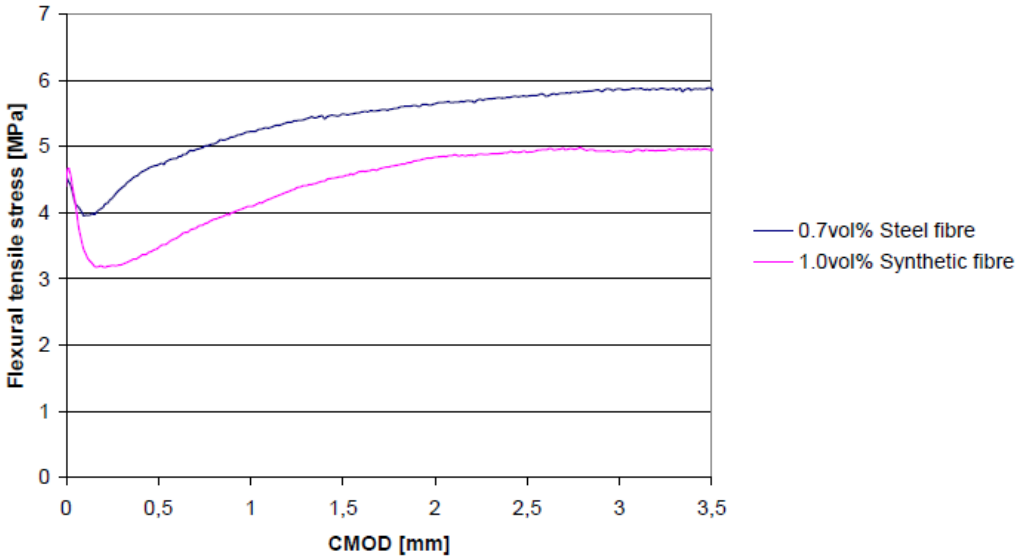

Figure 4-19 Comparison between steel fibres and synthetic fibres

Table 4-11 Comparison 0.7 vol% steel fibre and 1.0 vol% synthetic fibre, NS-EN 14651

	0.7 vol% Steel fibre		1.0 vol% Synthetic fibre		Ratio synthetic/steel
	Mean value	Coefficient of variation	Mean value	Coefficient of variation	
$f^{f}_{ct,L}$ [MPa]	**4.7**	6.4 %	**4.7**	2.3 %	100%
$f_{R,1}$ [MPa]	**4.7**	26.7 %	**3.5**	9.5 %	74%
$f_{R,2}$ [MPa]	**5.5**	23.4 %	**4.6**	8.4 %	84%
$f_{R,3}$ [MPa]	**5.8**	23.3 %	**4.9**	8.0 %	84%
$f_{R,4}$ [MPa]	**5.9**	23.6 %	**5.0**	7.5 %	85%

If not tricked by statistical variations, the test method described in NS-EN 14651 shows that adding 1 vol% Barchip Shogun fibre into Concrete D gives about 85 % the flexural tensile strength that adding 0.7 vol% Dramix 6560 fibre at CMOD larger than 1.5 mm.

As for the *steel vs. synthetic fibre* relation when tested according to NSBT, the relationship between these two fibre types may be different in other concrete mixes. Further, the relationship is dependent by how the beams are tested.

4.2.4 Comparison NS-EN 14651 vs. NSBT

As already mentioned, to compare the results from beam tests according to NS-EN 14651 and the NSBT procedure, three beams were cast and tested according to NS-EN 14651, three beams were cast and tested according to the NSBT procedure, and three beams were cast according to NS-EN 14651 but tested according to the NSBT procedure. This test was done both with 0.7 vol% steel fibres and with 1.0 vol% synthetic fibres. To compare the results from the two different test methods, stress vs. CMOD diagrams are made, and CMOD is calculated according to the equations in chapter 4.1.3, which means that the deflection vs. CMOD relation is not exactly as in NS-EN 14651.

To compare results from different test methods, it seems more important to calculate the peak stress, f_{peak}, than the $f^{f}_{ct,L}$ even though f_{peak} is achieved at a deflection larger than 0.08 mm.

The calculated residual flexural strengths for each beam are summarized in appendix A.

The average flexural tensile stress vs. CMOD curves are shown in Figure 4-20 a) and b) for the steel- and synthetic fibre reinforced beams, respectively.

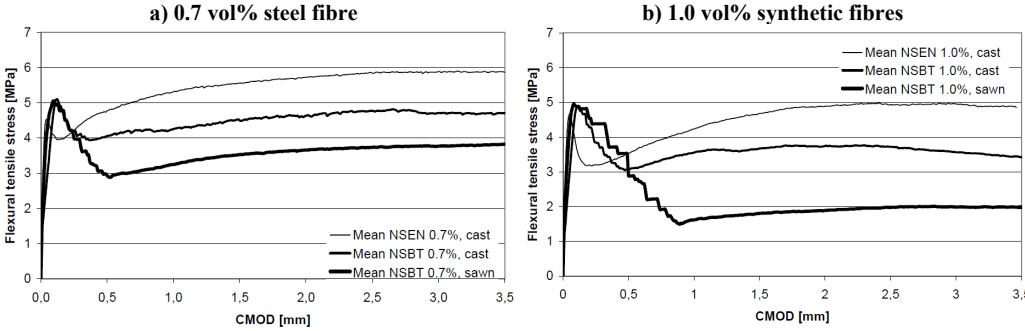

Figure 4-20 Mean curves beams reinforced with

For both fibre types, the NS-EN 14651 method gives higher residual flexural strength than the NSBT method. The mean curves for beams cast according to the description in NS-EN 14651 but tested according to the NSBT description lie between the two other curves. For the steel fibre reinforced beams, the three average curves are more or less parallel when the CMOD is larger than about 0.6 mm. The residual flexural tensile strength for beams tested according to NS-EN 14651 is about 2 MPa higher than the beams tested according to the NSBT procedure, while the beams cast according to the description in NS-EN 14651 and tested according to the NSBT procedure have strength of about 1 MPa less then the NS-EN beams. It seems like the casting procedure contributes to around 50 % of the difference between the NS-EN method and the NSBT-method, while the remaining 50 % of the difference then should be related to the testing procedure.

The results from beam tests with synthetic fibres do not show the same relation between the NS-EN 14651 method and the NSBT method. What seems to be relatively clear is that when 4-point bending tests are performed the capacity drop directly after cracking is larger than when 3-point bending tests are performed. Figure 4-21 shows the flexural tensile stress vs. CMOD curves when CMOD is less than 1.0 mm.

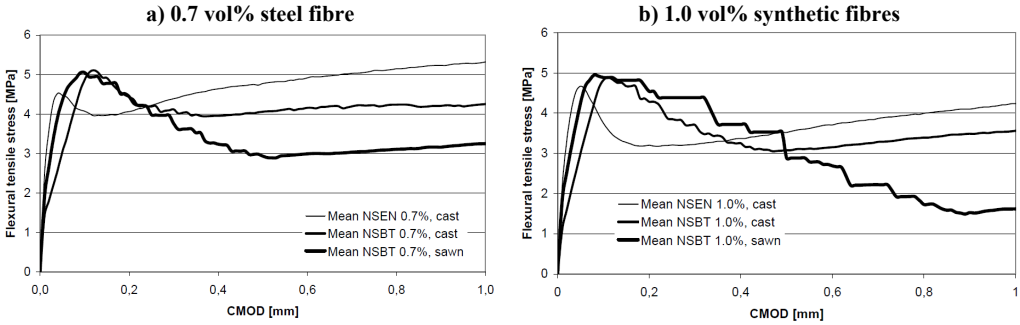

Figure 4-21 CMOD less than 1.0mm

For both fibre types, there was a large drop in capacity directly after cracking when 4-point bending test was performed, and beams with synthetic fibres needed larger CMOD than beams with steel fibres to be effective.

As mentioned in the introduction of this chapter, the major advantage of the NSBT-method is that this method makes it possible to use sawn beams from a real structure to document the in-situ residual flexural strength. More research involving larger number of specimens due to the relatively large scatter is needed to fully understand the relation between the NSBT-method and NS-EN 14651, and it is important to investigate the relation also for different fibre types.

4.2.5 Comparison steel fibres vs. synthetic fibres

As for the relation between the two types of beam test, it is difficult to quantify the relation between the residual strength per fibre volume achieved by the two different fibre types. In Figure 4-22 this *steel vs. synthetic fibre* ratios are shown for beams with 0.7 vol% steel fibres and 1.0 vol% synthetic fibres.

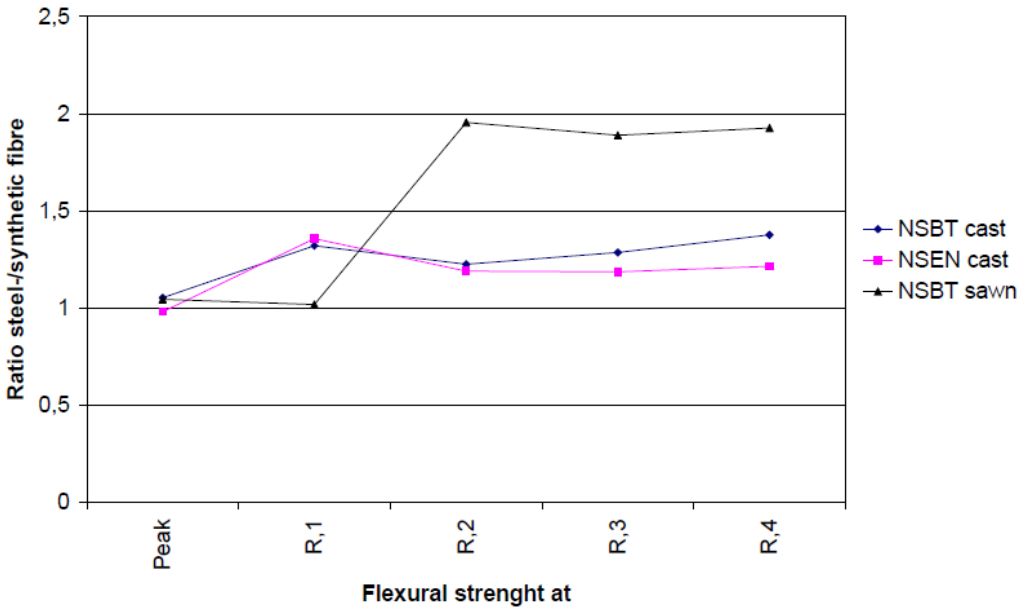

Figure 4-22 Relation between residual strength of steel fibre reinforced beams (0.7 vol%) and synthetic fibre reinforced beams (1.0 vol%)

As seen from the figure, 3-point bending tests give a ratio of about 1.2 to 1.4, while the 4-point bending tests give a ratio of nearly 2.

Once again, the number of beams in this study is small, and the coefficient of variation is large, which means that it is not possible to draw a definitive conclusion on neither the fibre effect nor the test method relation, but it seems like the steel- vs. synthetic fibre ratio is dependent on the test method.

4.2.6 Fibres as minimum reinforcement

If fibres shall be used as an alternative to conventional reinforcement in members reinforced with the minimum required reinforcement area, the fibre reinforced concrete must have equal capacity as conventional reinforced concrete. In that respect, it is interesting to determine the behaviour of conventional reinforced concrete when it is tested similarly to fibre reinforced concrete. Therefore, an experimental work involving beams with conventional steel reinforcement tested as NSEN-beams and NSBT-beams as described in chapter 4.1.3 is performed. These beams are also used to control the calculation model described in chapter 4.1.4.

The minimum longitudinal reinforcement according to EC 2 in beams made of concrete D, with the dimensions according to the description in NS-EN 14651 and the NSBT-method is shown in Table 4-12. The distance from the tensile surface to the centre of the reinforcement is in both cases set to 34 mm.

Table 4-12 $A_{s,min}$ according to [NS-EN 1991-1-1]

Beam type	f_{ctm} [MPa]	f_{yk} [MPa]	b_t [mm]	d [mm]	$A_{s,min}$ [mm^2]
NSEN	3.5	500	150	91	24.8
NSBT				116	31.7

Concrete D, which had an average 28-days compressive strength, f_{cm}, of 46 MPa was used in these beams. The cylinder with minimum strength had f_{ci} = 44.2 MPa, which means that the concrete belongs to the strength class C40/50 according to NS-EN 206-1.

The smallest reinforcement bar that was available at the laboratory was Ø8 mm. A diameter of 8 mm corresponds to a cross section area of 50 mm^2, which is 2 times and 1.6 times the required minimum reinforcement for the NSEN- and NSBT- beams respectively. A distance d from the notch top equal to 34 mm is used simply because the spacers were 30 mm, and the remaining 4 mm is half the diameter of the reinforcement.

4.2.6.1 Beam test with Ø8 steel bar reinforcement

The flexural tensile stress vs. CMOD diagrams for the beam tests with one Ø8 mm re-bar is shown in Figure 4-23. The CMOD is calculated according to equation 4-41 for the theoretical curves, while the crack opening for the experimental curves are calculated according to equation 4-10 and 4-12 for the NSEN Ø8 curve and NSBT Ø8 curve respectively. The flexural tensile stress is calculated according to equation 4-2 for the NSBT-curves and according to equation 4-4 for the NSEN curves.

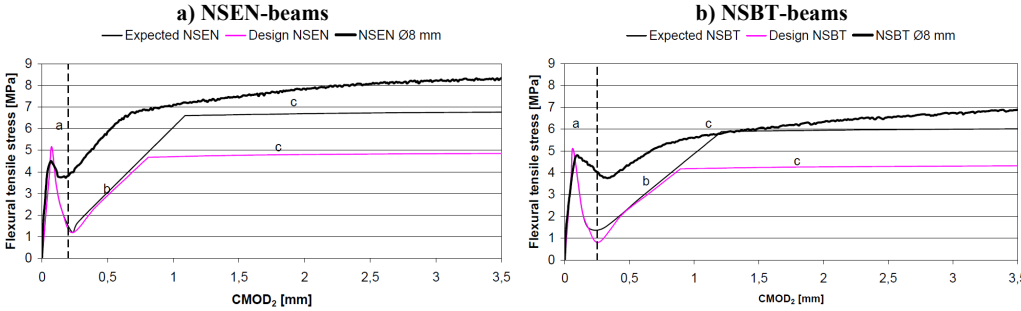

Figure 4-23 Calculated and experimental stress vs. CMOD diagrams

The calculation according to EC 2 with no partial factors etc (i.e. the expected curve) gives relatively correct results for the cracking load and the load at which the reinforcement starts yielding. The calculated curves may be divided in three parts, a, b and c:

a. This part is calculated from elastic theory; the flexural tensile stress at cracking is simply $f_{ctm,fl}$ as given by equation 4-14, and the corresponding CMOD is calculated as given by equation 4-44. After cracking, the flexural tensile stress is calculated with increasing crack depth and a stress value $f_{fcm,fl}$ where the crack stops (almost at the neutral axis).
b. When the depth of the crack reaches the reinforcement, the reinforcement starts to be effective. The flexural tensile stress is found by use of equation 4-4, where the moment capacity is calculated by equation 4-35 and combination 1. The corresponding crack opening is calculated by equation 4-41. Part b of the curves ends when the reinforcement starts yielding. When the stress is about 6.7 MPa and 5.3 MPa (for NSEN Ø8 mm and NSBT Ø8 mm respectively), the gradient of the experimental curve is reduced, which most likely is the point where the reinforcing steel starts to yield.
c. The calculated curves are almost horizontal in part c, because the only increase in calculated capacity is due to increased internal moment arm. The increase in stress at further CMODs for the experimental curve is most likely due to strain hardening

behaviour of the reinforcing steel, which is not taken into consideration when the capacity of the beams is calculated. The flexural tensile stress for part c of the calculated curves is the solution of equation 4-4, where the moment capacity is calculated by equation 4-35 and combination 2. The corresponding CMOD is calculated by equation 4-41 as for part b. Combination 3 holds for over reinforced beams, and thus cannot be solved for these beams. To reach a concrete strain level of ε_{c2}, which means combination 4, the height of the compressive zone must be less than 7 mm, which corresponds to a CMOD equal to approximately 9 mm and 13 mm for the NSEN- and NSBT- beams respectively (for the *expected* results calculations).

As mentioned in chapter 4.1.4, it is quite complicated to find a theoretically correct approach to calculate the CMOD, both from the theoretical calculation of the strength vs. CMOD relation, and when measured deflections are transformed to crack opening. As shown in Figure 4-23 the flexural tensile stress values corresponds well both at cracking and when the reinforcement starts to yield, which means that the strength-calculations are correct, even though there are some uncertainties with regard to the CMOD calculations.

From the theoretical calculations, the moment capacity is calculated for a given steel strain, which means that a M_{cap} *vs.* ε_s curve will be theoretically correct. When a beam test is performed, the load and corresponding deflection is measured. The applied bending moment can be found by the static system, which means that a M_E *vs.* δ curve will not be encumbered with errors due to simplifications in the calculations, and can be considered theoretically correct. Figure 4-24 shows these curves for beams reinforced with one Ø8 mm re-bar.

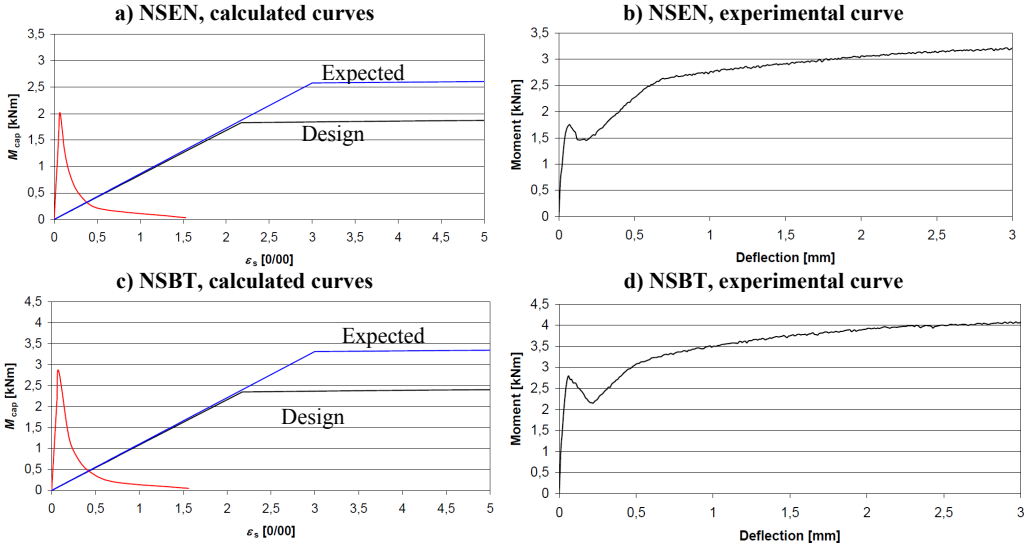

Figure 4-24 Bending moment vs. steel strain and bending moment vs. deflection

The red curve is the moment capacity of concrete without reinforcement, and to be able to draw this curve in the same diagram as for the black and blue curves, the strain at the location of the re-bars is calculated. The main point with regard to Figure 4-23 and Figure 4-24 is that even though it is difficult to find a correct relation between the calculated CMOD and steel strain, and between measured deflection and CMOD, the calculated strengths seem to be reasonably accurate.

To summarize this comparison, it may be stated that the theoretical method based on EC 2 gives relatively good agreement with the experimental behaviour both at cracking, when the reinforcement starts yielding and further for increasing CMOD. This implies that the present method also should give reasonably correct capacity if the cross section of the reinforcement is reduced to $A_{s,min}$ as previously calculated in Table 4-12.

4.2.6.2 Capacity of $A_{s,min}$

The calculated flexural tensile stress vs. CMOD relations for NSEN- and NSBT- beams with longitudinal reinforcement bar area equal to $A_{s,min}$ are shown in Figure 4-25.

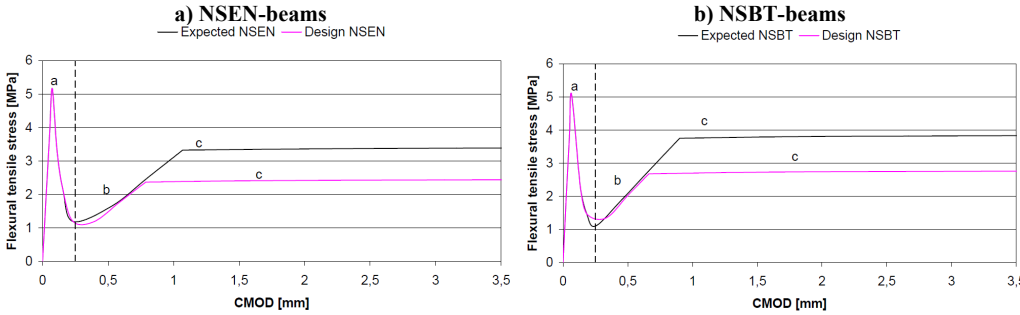

Figure 4-25 Calculated stress vs. CMOD diagrams, minimum reinforcement

The parts a, b and c are calculated similarly as described in chapter 4.2.6.1.

One interesting point is that beams reinforced with the minimum required reinforcement ratio according to EC 2, is expected to have less capacity after cracking than before cracking.

Table 4-13 Calculated flexural tensile stress when reinforced with the required minimum reinforcement

	Calculated flexural tensile stress [MPa]				
		Including partial factors etc		No partial factors etc	
	At cracking, $f_{ctm,fl}$	$\varepsilon_s = 0.00217$	No steel strain limit	$\varepsilon_s = 0.003$	No steel strain limit
NSEN	5.2	2.4	2.5	3.3	3.4
NSBT	5.1	2.7	2.8	3.8	3.9

What is seen from the numbers in Table 4-13 is that beams reinforced with $A_{s,min}$ actually are expected to have a deflection-softening behaviour in bending, even though the capacity is calculated with the factors α_{cc}, γ_s and γ_c all equal to 1. Further, if fibre reinforced beams made of concrete in strength class C40/50 shows larger capacity than 3.5 MPa for all $f_{R,j}$ when tested as described in NS-EN 14651, then the capacity for the fibre reinforced beams will be larger than the calculated capacity for beams reinforced with $A_{s,min}$. It should be noted though, that the effective depth of the section, d, is small compared to the total height, h. In real structures, the typical nominal concrete cover, c_{nom}, is about 35 mm, which means that the NSBT-beams actually have a d vs. h ratio that is not that untypical for slabs on ground. A more realistic thickness of a slab is about 200 mm. Even so, the post cracking capacity will still be less than the cracking load, meaning that such a slab will still show deflection-softening behaviour.

From the experimental curves from tests on beams with one Ø8 mm re-bar it is shown that the calculated capacity is more or less correct when the reinforcement starts yielding, and that the capacity is larger than expected with increasing CMOD.

If it shall be allowed to use fibres as minimum reinforcement in bending, it seems reasonable to require that the flexural tensile strength shall be larger than the cracking strength for all CMODs when tested according to NS-EN 14651. This is actually a quite strict requirement, because a beam reinforced with $A_{s,min}$ will most likely not fulfil it. Even so, this requirement is the basis for developing an all-round fibre reinforced concrete with high tensile strength and ductility reported in chapter 8.

4.3 Summary of the beam tests

Different beam test methods are basically measuring the same parameter, namely the post cracking moment capacity. The moment capacity is then used to find the residual flexural tensile stress, which is determined by a stress configuration, which corresponds to a linear elastic material. The residual flexural tensile strengths are therefore fictitious values.

It is in general large scatter in results from beam testing, and the scatter is larger for the NSBT-method than the method described in NS-EN 14651. The scatter may partly be explained by variation of the number of fibres crossing the crack, and partly by the fibre orientation. Even though beam tests according to NS-EN 14651 have less scatter than beam tests according to the NSBT-method, the NSBT-method has the advantage that there will be no wall effect during casting, which may be favourable with regard to predicting the behaviour of a larger specimen. However, it might be a good idea to test the sawn beams according to NS-EN 14651, but then the notch should be sawn on the surface that will be subjected to flexural tensile stresses. Even though the four point bending test ensures that the weakest point is found, it is rather unlikely that a larger specimen, as for instance a basement wall, will be subjected to largest stresses at the location of the weakest point. Even so, the weakest point of a small beam is most likely not representative for the whole area subjected to external loads, which might justify the use of notched beams.

It is shown that 0.7 vol% steel fibre may be sufficient to have larger residual flexural tensile strength than the limit of proportionality, and with the exception of a small region directly after cracking 0.7 vol% steel fibre is sufficient to show deflection hardening behaviour in bending. This means that 0.7 vol% steel fibre is sufficient to fulfil the philosophy of the minimum reinforcement area required according to EC 2. It is shown that the calculated residual flexural strength for beams reinforced with the minimum required reinforcement area is less than the residual flexural strength for beams reinforced with both 0.7 vol% steel fibres and 1.0 vol% synthetic fibres if tested as described in NS-EN 14651. For the steel fibre reinforced beams, the flexural tensile strength was larger also when tested as described in the NSBT-method.

5 Panel test

5.1 Theoretical part

Panel tests can be performed in several different ways. NB 7 prescribes circular panels with diameter and thickness equal to 600 mm and 100 mm, respectively [NB 7 (2003/2011)]. The panels shall be placed on a ring, which provides continuous support (CS) until cracking. ASTM C 1550 prescribes circular panels with diameter and thickness equal to 800 mm and 75 mm, respectively [ASTM C 1550 (2008)]. The panels shall be placed on 3 point supports, and the method is therefore called 3-point determinate support. A third alternative is NS-EN 14488-5, which prescribes square panels with dimension 600×600×100 mm [NS-EN 14488-5]. The panels shall be tested on a square frame, which provides continuous support until cracking similar to panels tested according to NB 7.

In general, the objective to perform panel tests is to measure the flexural toughness by means of the energy absorbed by the specimen when it has reached a predefined failure state. The energy absorbed by the specimen (E) is simply the area under the load vs. deflection curve until a deflection limit, and it is calculated as:

$$E = \sum_{i=0}^{i=\delta_m} \left[\left(\delta_{i+1} - \delta_i\right) \frac{F_i + F_{i+1}}{2} \right] \tag{5-1}$$

where

F_i: is the load corresponding to a deflection equal to δ_i

δ_m: is the upper deflection limit [mm]

Different codes prescribe different deflection limits and various methods for corrections of the results for deviating specimen dimensions.

In this work, three different test methods have been used:

- ASTM C 1550
- 3-point roller support method, modified ASTM C 1550-method
- NB 7

A short presentation of each test method is given in chapter 5.1.1.-5.1.3.

Because the different codes prescribe different support conditions and deflection limits, it is impossible to compare results from tests performed according to the different codes directly. Nevertheless, if it is a real material property that is investigated in all test methods, it should be possible to establish a relation between them. According to the working hypothesis, it should be possible to describe the fibres' contribution to the concrete properties with respect to the crack opening. To do so, a relation between the deflection and the crack opening must be established, and the load capacity must be related to the dimension of the panels.

By use of yield line theory the internal energy can be calculated, and it is also possible to calculate the residual flexural tensile strength of the fibre reinforced concrete under certain assumptions. The yield line theory is based on the principle that the work done in rotating yield lines is the same as the work done by moving loads [Kennedy and Goodchild (2003)], as written in equation 5-2:

$$E_{\text{int}} = E_{\text{ext}} \Rightarrow \sum_{\theta=0}^{\theta=\theta_m} (m_l l\theta) = \sum_{\delta=0}^{\delta=\delta_m} (F\delta) \tag{5-2}$$

where

m_l: is the bending moment pr unit length of the yield line (kNmm/mm)
l: is the length of the yield line, or its projected length onto the axis of rotation for the actual region (mm)
θ: is the rotation of the region about its axis of rotation (mm/mm)
F: is the external load acting within a particular region (kN)
δ: is the displacement of the load on each region (mm)

The work done by deflecting loads is exactly the same as the energy absorbed by the specimen (E) from equation 5-1.

The use of yield line theory and the principles described above to calculate the residual flexural tensile strength is further explained in chapter 5.1.5, while a method to calculate the crack opening is described in chapter 5.1.6.

5.1.1 ASTM C 1550

According to ASTM C 1550 circular panels with diameter 800 mm and thickness 75 mm shall be cast or sprayed. The load shall be applied through a hemispherical-ended steel piston, with a displacement rate of 4 mm/min. The load and corresponding deflection shall be recorded until the deflection is at least 40 mm. The measured energy absorption, W', is the area under the load deflection curve and can be calculated according to equation 5-1. The measured energy is corrected for geometry deviations by the following equation:

$$W = W' \left(\frac{t_0}{t} \right)^{\beta} \left(\frac{d_0}{d} \right) \tag{5-3}$$

where

$$\beta = 2.0 - \frac{\delta - 0.5}{80}$$

and

W: is the corrected energy absorption [J]
t: is the average thickness [mm]
t_0: is the nominal thickness of 75mm
d: is the average diameter [mm]
d_0: is the nominal diameter of 800mm
δ: is the specified central deflection limit for absorbed energy determination [mm]

The notations in equation 5-3 are adopted from ASTM C 1550, and in the present thesis E is used as notation for the absorbed energy in stead of W.

5.1.2 The 3-point roller support method, the modified ASTM C 1550-method

The 3-point roller support method is based on ASTM C 1550. The only difference is that in ASTM C 1550 the 3 supporting points are fixed in the horizontal plane, while in the modified method the 3 supports can slide outwards during the test. Figure 5-1 shows the free support arrangement.

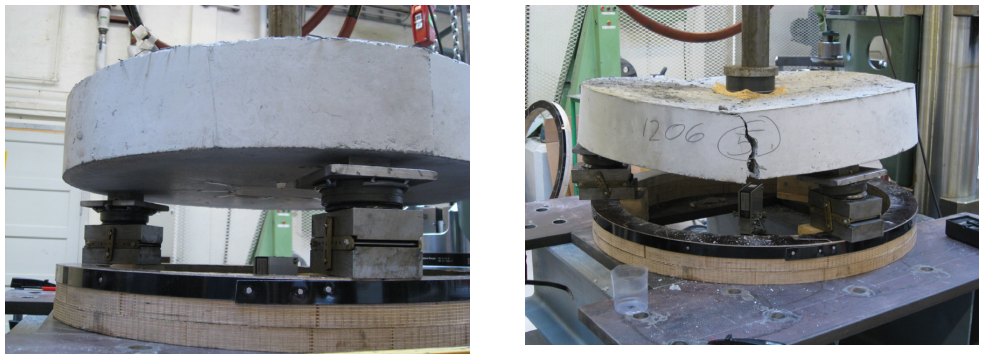

Figure 5-1 Movable support arrangement

The measured absorbed energy is calculated according to equation 5-1. To compensate for deviating dimensions, the method in ASTM C 1550 may be used, or alternatively the method from NB 7 presented in the next chapter may be used.

The 3-point roller support method was designed especially for this work. Bernard has reported that the friction between the support and the concrete contributes to approximately 15-20 % of the absorbed energy for the ASTM-method [Bernard (2005)]. The idea of the 3-point roller support method was to reduce the influence of friction, by allowing the support to slide outwards during the test. Even so, if a panel does not crack in three equally sized sectors with the support half way between the cracks, a tangential movement at the support does also occur, and the friction effect of this tangential movement will not be reduced.

In the following, 3P is the abbreviation for *3-point roller support*.

5.1.3 Norwegian Concrete Association Publication nr 7 (2003/2011)

NB 7 prescribes a circular panel with diameter 600 mm and height 100 mm. Actually; the method is developed for sprayed concrete, so the panels shall be sprayed at the building place. The panels shall be tested on CS with the sprayed surface down, and the concentrated load is applied at the centre of the panel. On top of the panel, a circular steel plate with diameter 100 mm shall be placed to distribute the load. The load is applied with a displacement rate of 1.5 mm/min, and the load, F, and the corresponding deflection, δ, is recorded.

The main test result is the absorbed energy determined from 0 to 25 mm deflection.

According to NB 7, the absorbed energy shall be corrected for deviating height. This is done in two steps. First the maximum deflection, δ_m, shall be corrected by a factor of 100/h to ensure that the maximum crack width is equal even if the height varies. Secondly the *measured* energy shall be corrected by a factor of 100/h to take into account the effect of increased or decreased cross section area.

Actually, the correction of the deflection limit, δ_m, as explained above will only ensure that the maximum crack width is equal if the number of cracks is constant. This matter will be discussed in details in chapter 5.1.7.

In the tests in this work, the panels were always tested with the cast surface up. This was done simply because it is easier to place the panels when the smooth surface is placed on the

support, and because the variation in friction effect will be less when the surface is smooth. It should be noted that after the tests reported in this work was performed, a new revision of NB7 was made. In the new revision, finished in 2011, it is written that the panels shall be tested with the smooth surface placed on the support [NB 7 (2011)].

A typical load vs. deflection curve from a NB7 panel test is shown in Figure 5-2 together with the calculation procedure for measured and corrected capacity to absorb energy.

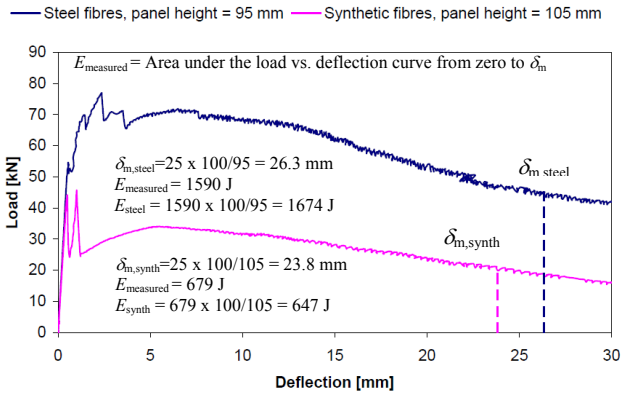

Figure 5-2 Typical load deflection curves NB7, specimens with 0.5 vol% steel fibres and 0.5 vol% synthetic fibres

As shown in Figure 5-2, the panel's ability to resist load is clearly influenced by the deflection and fibre type, and the post cracking behaviour is strongly influenced by both fibre dosage and fibre type. The cracking load is a concrete parameter, which normally is considered to be insignificantly influenced by the fibre type and dosages used in sprayed concrete. Still, as seen from the figure, the steel fibre reinforced panel cracked about 54 kN, while the synthetic fibre reinforced panel cracked at about 45 kN.

5.1.4 Advantages and disadvantages with the different test methods

There are advantages and disadvantages with the different test methods. With regard to testing the panels, it is easier to handle NB 7 panels than panels according to the other codes, simply because the panels are smaller and the weight is less.

The crack pattern in panels tested according to ASTM C 1550 and the 3-point roller support method is more consistent than for panels tested according to NB 7 and NS-EN 14448-5, and the scatter in results are less. Nevertheless, panels tested according to ASTM C 1550 will sometimes have only one diagonal crack like in a beam, which is insufficient for energy determination, and makes it necessary to spray or cast more panels than prescribed to secure the minimum number of successful tests. This situation occurs more often when high concrete quality is combined with relatively low amount of fibres. In one tests series by Bjøntegaard & Myren, 3 out of 18 panels had only one diagonal crack, which is approximately 17 % [Bjøntegaard & Myren (2011)]. Still, compared to the other test methods, the variation of the crack geometry is rather small. Another advantage with the ASTM-method is that the result is not affected by flatness distortions on the underside of the panels, because the panel will in any case be uphold by three supports. Panels tested according to NB 7 or NS-EN 14488-5 will only be truly continuously supported if the underside of the panel is completely flat, and only

when the deflection is small. With increasing deflections, the panels will only be supported where the cracks reach the supporting ring.

The typical crack pattern for ASTM/3P-panels and NB 7-panels is shown in Figure 5-3.

a) ASTM-panels and 3P-panels **b) CS-panels**

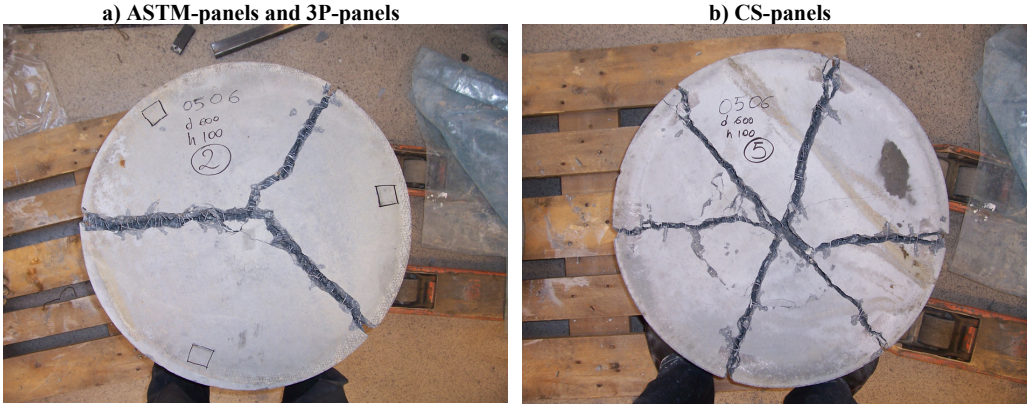

Figure 5-3 Typical crack pattern, panels reinforced with 0.5 vol% steel fibres

The number of cracks in the panels tested according to NB 7 may vary quite much. For the synthetic fibre panels tested at NTNU/SINTEF the number of cracks are usually either 4 or 5. The length of every crack is equal, because the cracks normally start in the centre of the panel and the panels are circular. For the steel fibre panels tested at NTNU/SINTEF, the number of cracks may vary between 4 and 8, and in addition, some punching shear cracks may be formed. As for the synthetic fibre panels, the length of every crack is roughly equal.

As seen in Figure 5-3 the length of all cracks in one panel is not always exactly equal, still 5 of 6 cracks have equally length, and another panel with six cracks will have approximately equal total crack length.

The panels tested according to NS-EN 14488-5 may crack in several ways. It is reasonable to believe that the number of cracks may vary similar to the NB 7-method, but in addition the length of each crack will vary because the panels are quadratic.

Some of the advantages and disadvantages by the different methods are summarized in Table 5-1.

Table 5-1 Advantages and disadvantages

	Concrete volume / weight	Effect of friction (%)	Variation of crack geometry
NB7	28 l / 67 kg	35-40[1]	Medium
ASTM C 1550	38 l / 91 kg	15-20[2]	Small
NS-EN 14488-5	36 l / 86 kg	35-40[1]	High

[1] According to Bjøntegaard [Bjøntegaard (2009a] and [Bjøntegaard (2009b)]
[2] According to Bernard [Bernard (2005)]

5.1.5 Yield line theory for flexural strength determination

First of all, *yield line theory* is only valid once a crack pattern is established, which means that yield line theory cannot be used to estimate the crack load. The following equations are therefore valid only after cracking.

In the present thesis, the following abbreviations are used:

NB 7-panels: Circular panels with diameter and height equal to 600 mm and 100 mm respectively, tested at continuous support.

3P-panels: Circular panels with random dimension and tested at 3 point roller support

ASTM-panels: Circular panels with diameter and height equal to 600 mm and 75 mm respectively, and tested as prescribed in ASTM C 1550

CS-panels: Circular panels with random dimension and tested at continuous support. NB 7-panels are then a CS-panel.

The experimental work involves two different panel diameters, and two different panel heights. The panel diameter was either 600 mm or 800 mm, and the height was either 75 mm or 100 mm.

The 3 roller supports were placed 50 mm from the outer edge of the panel, which means that the distance from the supports to the centre of the panel was 250 mm and 350 mm for panel with diameter 600 mm and 800 mm respectively. The following equations for 3P-panels are therefore only valid if the roller supports are placed relative to the panel dimensions, and not if a panel with diameter 800 mm are placed on a support configuration where the distance from the supports to the centre is for instance 250 mm.

Similar to the 3P-tests, two different supporting rings were used for the panels tested at CS. The panels with diameter equal to 600 mm were placed on a supporting ring with internal diameter equal to 250 mm, while the panels with 800 mm diameter were placed on a supporting ring with internal diameter equal to 350 mm. Because the NB 7-panels are one type of CS-panels, the equations for all CS-panels (including the NB 7-panels) are described together. The equations for the CS-panels are only valid if the diameter of the supporting ring is changed similar to the diameter of the panels.

The equations for both 3P-panels and CS-panels can easily be expanded to be valid also when the support configuration does not change when the panel diameter changes. For the equations in the present thesis, the only difference will be that the radius of the support configuration cannot be described as a function of the panel radius.

The theoretical basis for the use of yield line theory presented in this work is mostly found in a publication by Gerard Kennedy and Charles Goodchild [Kennedy and Goodchild (2003)].

The work done by rotating yield lines is the *internal energy*, and the expression for the internal energy (E_{int}) is:

$$E_{int} = \sum_{\theta=0}^{\theta=\theta_m} \left(m_1 l \theta \right) \tag{5-4}$$

m_l and l must be projected to a line parallel to the axes of rotation, so that the whole yield line has the same rotation θ. If the moment resistance is considered to be an average value from zero rotation to a rotation θ_m corresponding to δ_m, the equation for E_{int} may be expressed as:

$$E_{int} = m_l l \theta_m \tag{5-5}$$

where

$$\theta_m = \frac{\delta_m}{r_r} \tag{5-6}$$

and

δ_m: is the maximum deflection

r_r: is the distance from the axes of rotation to the load as illustrated in Figure 5-7 and Figure 5-11 (CS) and Figure 5-9 (3P)

If the moment resistance per unit length of the cracks and the deflection are independent of the number of cracks, equation 5-5 may be written more generally as:

$$E_{int} = \sum_{i=1}^{n} m_l l_i \frac{\delta_m}{r_{r,i}} = m_l \delta_m \sum_{i=1}^{n} \frac{l_i}{r_{r,i}} \tag{5-7}$$

where

n: is the number of regions/cracks

The work done by the external load is the *external energy,* E_{ext}, which can be expressed as:

$$E_{ext} = \sum_{0}^{\delta_m} F\delta \tag{5-8}$$

As for the internal energy, if the load F is considered to be the average load from zero deflection to a deflection equal to δ_m, the equation for E_{ext} may be written as:

$$E_{ext} = F\delta_m \tag{5-9}$$

Since E_{int}=E_{ext} the following equation for the moment capacity may be written:

$$m_l = \frac{F}{S} \tag{5-10}$$

where

$$S = \sum_{i=1}^{n} \frac{l_i}{r_{r,i}} \tag{5-11}$$

With n cracks, the panel is divided into n regions. If all regions have the same size, the total length of the yield lines projected parallel to their axes of rotation, l, is expressed as

$$l = n \cdot 2R \sin\frac{180}{n} \tag{5-12}$$

where

R: is the radius of the concrete panel

The only unknown value in equation 5-11 is the r_r-term. The expression for the r_r-term is not equal for ASTM-panels, 3P-panels and CS-panels, so it has to be expressed in different equations.

ASTM-panels and 3P-panels

Figure 5-4 shows the yield line pattern and the axes of rotation for an ASTM C 1550 or a 3P-panel.

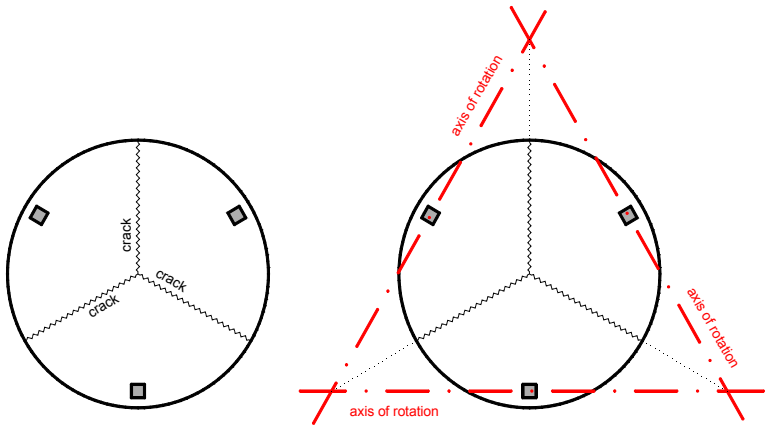

Figure 5-4 Yield line pattern and axes of rotation

Considering the panels in an axonometric point of view as in Figure 5-5 and Figure 5-6, it is easier to see that every segment turns with an angle θ.

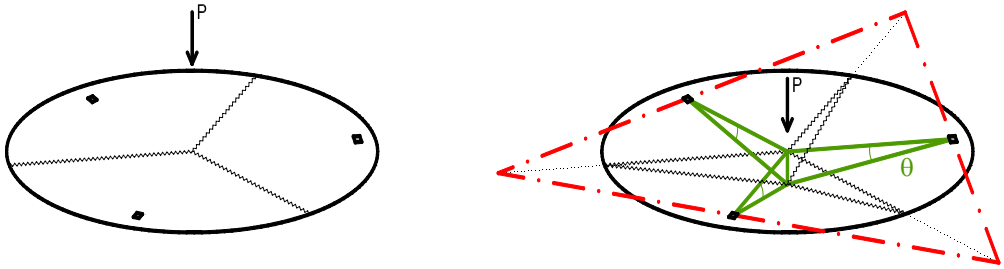

Figure 5-5 Axonometric point of view

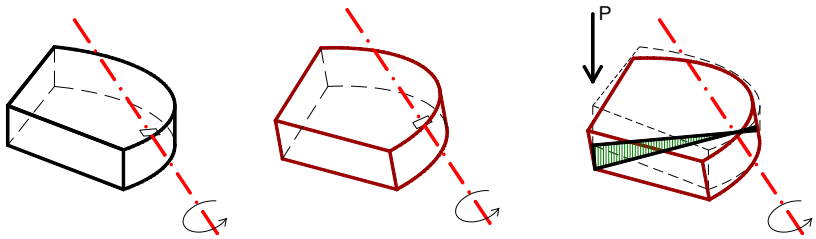

Figure 5-6 Rotation of one segment

The test setup described in ASTM C 1550 ensures that the distance r_r is equal to 375 mm, because the code prescribes in chapter 6.2 that "*the fixture supporting the panel during testing shall consist of any configuration that includes three symmetrical arranged pivots on a pitch circle diameter of 750 mm"*. Further, the number of cracks shall always be three (other ways the result shall be discarded). Therefore, the expression for S for ASTM-panels is simplified to:

$$S = 3\frac{l_i}{r_r} = 3\frac{\sqrt{3}R}{375} = R\frac{\sqrt{3}}{125} \tag{5-13}$$

The test setup for the 3-point roller support method does not ensure that the distance r_r is constant because the support slide outwards, but the number of cracks is always three (or the specimen is discarded). Initially the supports are always placed the same distance (50 mm) from the panel edge and the length r_r can therefore simplified be expressed as:

$$r_r = r = R - 50 \tag{5-14}$$

The expression for S for 3P-panels is then:

$$S = 3\frac{l_i}{r_r} = 3\frac{\sqrt{3}R}{R-50} \tag{5-15}$$

CS-panels

For the CS-panels, the number of cracks is not known prior to the test. Figure 5-7 shows the crack pattern and the axes of rotation for a CS-panel with three cracks.

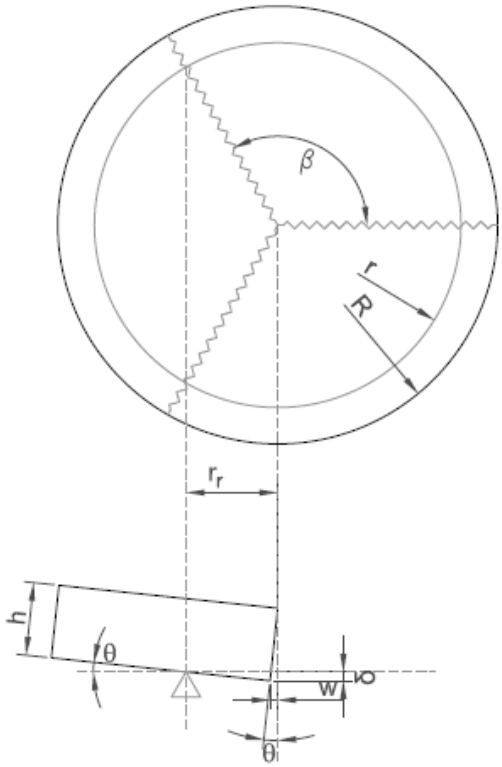

Figure 5-7 CS-panel with three cracks

The total length of the projected yield lines is expressed as in equation 5-12 for the ASTM and 3P-panels, but the expression for r_r for the CS-panels is different and written as:

$$r_r = r\cos\frac{360}{2n} = r\cos\frac{180}{n} \tag{5-16}$$

The expression for S for CS-panels is then written as:

$$S = n\frac{2R\sin\frac{180}{n}}{r\cos\frac{180}{n}} = 2n\frac{R}{r}\tan\frac{180}{n} \qquad (5\text{-}17)$$

In Table 5-2 S is calculated for some different panel diameters and the typical numbers of cracks. These panel dimensions are shown because panels with these dimensions are tested, and the results are shown and evaluated in chapter 5.2 .

Table 5-2 Possible values of *S*

	CS		3P		ASTM
Nr of cracks	d600	d800	d600	d800	d800
3	12.47	11.88	6.24	5.94	5.54
4	9.60	9.14	Discarded		
5	8.72	8.30			
6	8.31	7.92			
7	8.09	7.71			
8	7.95	7.57			

By use of equation 5-10 and the observed number of cracks and the corresponding S-value in Table 5-2, it is possible to estimate the panels' moment capacity based on the results from panel tests.

When the moment capacity is found, it is possible to calculate the flexural tensile strength based on an assumed linear stress distribution shown in Figure 5-8 [NS-EN 14651].

a) Real stress distribution **b) Assumed stress distribution**

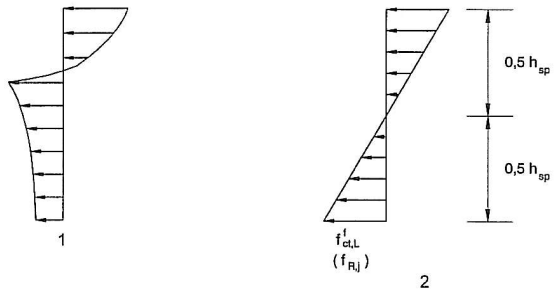

Figure 5-8 Stress distribution according to [NS-EN 14651]

If a linear stress distribution is assumed, the relationship between the moment capacity and the residual tensile flexural strength, $f_{R,j}$, is expressed as [NS-EN 14651]:

$$f_{R,j} = \frac{m_j}{\frac{1}{6}bh^2} \qquad (5\text{-}18)$$

where

$f_{R,j}$: is the residual flexural tensile strength [MPa]
m_j is the moment capacity (equal to m_1 found from a panel test)
j: is the deformation at which the moment capacity is calculated

It is shown in chapter 3 that the fibres ability to resist loads is dependent on the slip, which may be related to the CMOD. Bernard et al. have stated that "*two hypothetically identical beams will only show the same post-crack performance in a third-point loaded beam test if the crack occurs at the same offset because only then will the angle of crack rotation suffered at a given central deflection be the same*" [Bernard, Tutlu and Diamant1idis (2003)]. To overcome the problem with varying offsets, a simple adjustment to the central deflection to maintain the same crack rotation was suggested. The method of comparing beams or panels at equally rotation is actually not in conflict with the assumption that the beams or panels should be compared at equal CMOD, because if only the crack offset varies, the CMOD-correction and the rotation-correction are identical. If the height also varies, then the CMOD will vary even though the crack rotation is unchanged.

To compare results from tests on panels with different diameters, heights and support arrangement, the resistance should therefore be calculated at specified CMODs and not at a specified deflection.

5.1.6 Calculation of CMOD and rotation angle from the panel tests

Because the ASTM- and 3P-panels have different support configuration than the panels tested at CS, the calculation procedure are somewhat different and has to be described separately.

ASTM- and 3P-panels
Figure 5-9 shows a simplified model for the rotation of an ASTM/3P-panel.

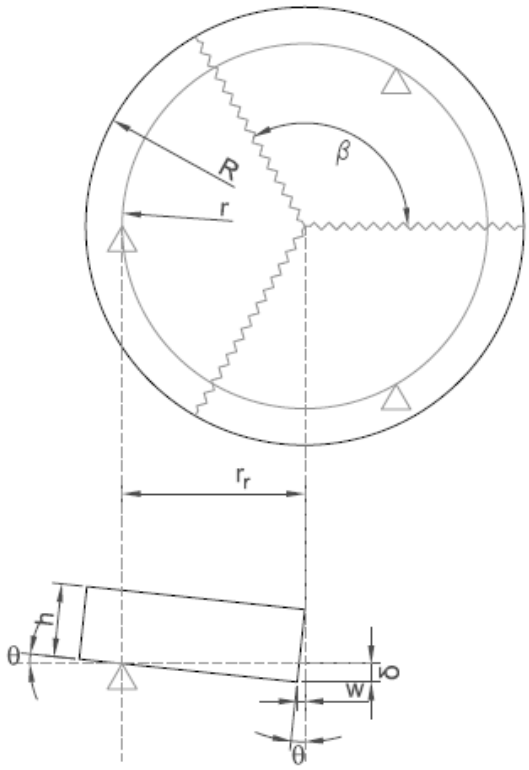

Figure 5-9 ASTM/3P-panel

In Figure 5-9 the following notations are used:

h: is the height of the panel

w: is the horizontal displacement of the crack mouth

θ, r_r and δ are already defined.

The horizontal displacement of the crack mouth, *w*, is expressed as:

$$w = h\frac{\delta}{r_r} \tag{5-19}$$

The relationship between *w* and CMOD is shown in Figure 5-10.

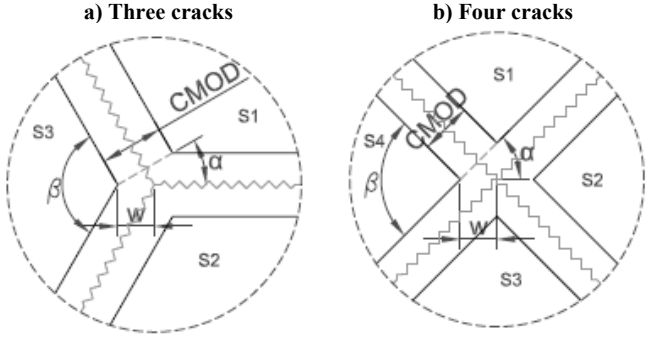

Figure 5-10 CMOD vs. *w*

In Figure 5-10 the following notations are used:

α: is the angle between *w* and CMOD

β: is the angle between each crack

The expression for CMOD is:

$$\text{CMOD} = 2h\frac{\delta}{r_r}\cos\alpha \tag{5-20}$$

where

$$\alpha = 90^\circ - \frac{\beta}{2}$$

r_r is always 375 mm for an ASTM panel, and as defined in equation 5-14 for a 3P-panel.

The support for the 3P-panels will slide outwards during the test, which results in an increased distance from the support to the centre of the panel (increased r_r). This increase in r_r is not taken into consideration, because it will not influence the CMOD. Also the ASTM-panels will slide outwards, and it is this horizontal movement that causes the friction contribution. When r_r is increased, the applied moment is increased for a constant load, but this increase is considered to be neglectable.

Bernard and Xu have made similar calculations, and shown that the crack width for an ASTM-panel based on a rigid plate model is [Bernard and Xu (2010)]:

$$w = \frac{\sqrt{3}\delta \cdot t}{r} \tag{5-21}$$

Where *w*, δ, *t* and *r* are crack width, deflection, thickness of the panel and distance from the axes of rotation to the load, respectively (the notations are as in [Bernard and Xu (2010)]). Equations 5-20 and 5-21 are identical when the angle between each crack, β, is 120º. In addition, Minelli and Plizzari have found an identical relationship as Bernard and Xu between crack opening and deflection [Minelli and Plizzari (2010)].

In [Bernard and Xu (2010)] and [Minelli and Plizzari (2010)] it is reported that the actual crack widths at large deflections are wider near the centre and narrower near the edge of the specimen than predicted by equation 5-20 and 5-21. Their explanation for this is that the post-crack residual strength makes the un-cracked portions of the panel curved and that the neutral axis is typically not located at the upper surface of the panel. Even so, by comparing the

results from the measured crack openings reported in [Sandbakk et al (2010)] with the calculated crack openings, the predicted CMOD is actually quite close to the measured CMOD, at least for CMOD not larger than 20 mm.

CS-panels
Figure 5-11 shows a simplified model for the rotation of a CS-panel with 4 cracks.

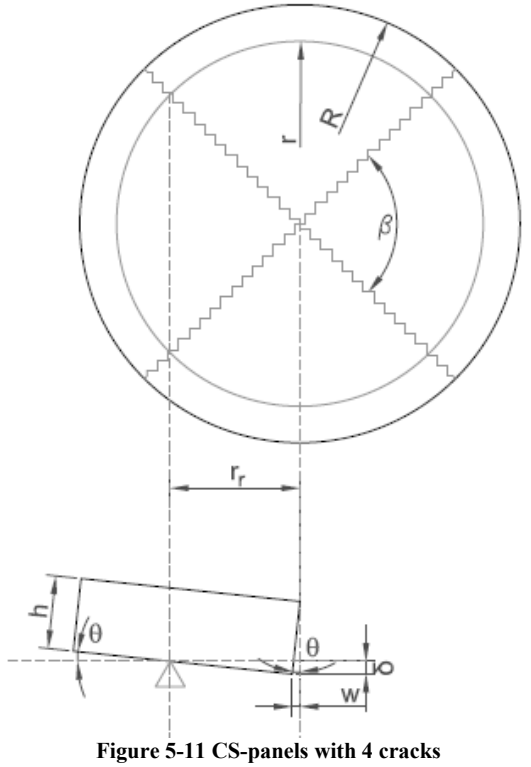

Figure 5-11 CS-panels with 4 cracks

All notations and expressions are identical for the CS and the ASTM/3P-panels, except the expression for r_r, which is as defined in equation 5-16 for the CS-panels.

The calculation of CMOD is summarized in Table 5-3.

Table 5-3 Calculation of CMOD, summarized

	ASTM	3P	CS
r_r [mm]	*375*	*r*	$r\cos\frac{180}{n}$
α	*30°*		*90 °- (180 °/n)*
CMOD [mm]	$2h\frac{\delta}{r_r}\cos\alpha$		
θ [rad]	$\frac{\delta}{r_r}$		

5.1.6.1 CMOD and rotation angle vs. deflection for the panel dimensions in the preset thesis

As mentioned previously the ASTM- and 3P-panels are discarded if the number of cracks is unlike three. Calculated values for CMOD and rotation angle, θ, at 25 mm deflection for the different panels in the present test series are shown in Table 5-4. These theoretical values will later be evaluated against the experimental behaviour.

Table 5-4 CMOD and rotation angle θ at deflection equal to 25 mm

Panel type	Nr of cracks	d600 h75		d600 h100		d800 h75		d800 h100	
		CMOD	θ °	CMOD	θ °	CMOD	θ °	CMOD	θ °
3P	3	13.0	5.73	17.3	5.73	9.3	4.09	12.4	4.09
ASTM	3	11.8	5.21	15.7	5.21	8.7	3.82	11.5	3.82
CS	4	15.0	8.10	20.0	8.10	10.7	5.79	14.3	5.79
	5	10.9	7.08	14.5	7.08	7.8	5.06	10.4	5.06
	6	8.7	6.62	11.5	6.62	6.2	4.73	8.2	4.73
	7	7.2	6.36	9.6	6.36	5.2	4.54	6.9	4.54
	8	6.2	6.20	8.3	6.20	4.2	4.43	5.9	4.43

With regard to the calculated CMOD and corresponding rotation angles, it should be noted that some approximations are used. First off all, the rotation angles are considered to be small enough to consider $\sin\theta = \tan\theta = \theta$. As seen from Table 5-4 the panel with largest rotation angle will be a d600h100 panel with 4 cracks. The correct expression for CMOD with the present models will be:

$$\text{CMOD} = 2h\sin\left(\arctan\frac{\delta}{r_r}\right)\cos\alpha \qquad (5\text{-}22)$$

By use of equation 5-22, the crack opening will be 19.8 mm instead of 20 mm, which means that the error margin is 1 %. For all other panels the error margin will be less because the rotation angle is less.

Another point, which is not taken into consideration in the present models, is due to the fact that the panels will slide outwards during the test. For the CS and ASTM panels the distance r_r remains the same, but for the 3P-panels the supports will slide together with the panel sectors. This means that the moment arm will increase, and the applied moment will therefore be larger at increasing deflection, even if the applied load is constant. Also this effect is considered to be of minor influence.

5.1.7 Energy absorption related to a specified CMOD

The fibres ability to transfer stresses across cracks are dependent on the crack width. It seems therefore reasonable to relate the upper deflection limit, δ_m, to a fixed CMOD and not a fixed deflection. As already described, the relation between the CMOD and the deflection are dependent on both the height and the diameter of a panel.

If the prescribed dimensions and δ_m are d_0, h_0 and $\delta_{m,0}$, then δ_m should be corrected to maintain the same CMOD for deviating dimensions as:

$$\frac{\mathrm{CMOD_n}}{\mathrm{CMOD_0}} = \frac{2h_\mathrm{n}\dfrac{\delta_\mathrm{m,n}}{r_\mathrm{r,n}}\cos\alpha_\mathrm{n}}{2h_0\dfrac{\delta_\mathrm{m,0}}{r_\mathrm{r,0}}\cos\alpha_0} \Rightarrow \delta_\mathrm{m,n} = \frac{h_0}{h_\mathrm{n}}\cdot\frac{r_\mathrm{r,n}}{r_\mathrm{r,0}}\cdot\frac{\cos\alpha_0}{\cos\alpha_\mathrm{n}}\cdot\delta_\mathrm{m,0} \tag{5-23}$$

For the ASTM-panels, r_r is always 375 mm, and α always 30º. For the CS-panels, r_r is dependent on both the diameter of the supporting ring and the number of cracks, while α is dependent on the number of cracks. For the 3P-panels, r_r is dependent on the diameter of the concrete panel, while α always is 30º.

From equation 5-4, it is clear that also the internal energy is affected by change in dimensions through the l and θ-terms. From equation 5-18, it is seen that also the m-term is affected by deviations in height.

The expression for the measured energy for a panel with planned dimensions can be written as:

$$E_0 = \sum m_\mathrm{l} l\theta = \frac{1}{6}bh_0^2 f_\mathrm{R,j}\cdot S_0\cdot\delta_\mathrm{m,0} \tag{5-24}$$

The relationship between the measured internal energy for a panel with planned dimensions and random dimensions is then:

$$\frac{E_\mathrm{n}}{E_0} = \frac{h_\mathrm{n}^2 S_\mathrm{n}\delta_\mathrm{m,n}}{h_0^2 S_0\delta_\mathrm{m,0}} \tag{5-25}$$

To be able to compare the energy from panels with different dimensions, the measured energy, E_measured, should be calculated up to a deflection of $\delta_\mathrm{m,n}$ and the corrected energy, E_corr, should be calculated as:

$$E_\mathrm{corr} = \frac{h_0^2 S_0\delta_\mathrm{m,0}}{h_\mathrm{n}^2 S_\mathrm{n}\delta_\mathrm{m,n}}\cdot E_\mathrm{measured} \tag{5-26}$$

As for the CMOD calculations, the expressions for correcting the absorbed energy are somewhat different for the different types of panel tests and have to be described separately.

5.1.7.1 ASTM-panels

The support system for the ASTM-panels is always the same. A change in diameter will only affect the total length of cracks, which of course will influence the measured energy, E_measured. If the radius of the panel, R, increases by a factor k, the total length of the projected yield lines is also increased by a factor k, which makes it reasonable to add a *radius-adjustment factor* to the expression for the calculated energy absorption. In ASTM C 1550, this is taken care of by multiplying the measured energy absorption by a factor d_0/d, where d_0 and d are the nominal and measured diameter, respectively.

If the height is changed, both the CMOD and the moment capacity are changed. In ASTM C 1550 the expression for the corrected energy, when written with the present notations, is:

$$E_\mathrm{corr} = E_\mathrm{measured}\left(\frac{h_0}{h}\right)^\beta\left(\frac{R_0}{R}\right) \tag{5-27}$$

where

$\beta = 2.0-(\delta-0.5)/80$

δ: is the specified central deflection (in mm) at which the capacity to absorb energy is measured

Whether the ratio d_0/d or R_0/R is used is of course of no consequence because the ratios are equal.

Bernard and Pircher have investigated the influence of varying thickness in panels tested according to the description in ASTM C 1550. The thickness varied from 55 to 95 mm, in increments of 10 mm. With $\beta = 2.0-\delta/80$ the curve fitting to experimental data had a mean coefficient of determination (r^2) equal to 0.7932 [Bernard and Pircher (2001)]. Even though this suggests a mediocre fit, they assumed that the variability within each set of panels was responsible for the relatively low value of r^2. (Other β-values for equally simple equations had only marginally higher values of r^2).

5.1.7.2 3P-panels

In contrast to the ASTM method, the support system for the 3P-panels is located relative to the concrete panel. The panels should always crack in three segments similar to the ASTM-panels, which simplifies the general expression for $\delta_{m,n}$ (equation 5-23) and E_{corr} (equation 5-26) because α, r_r and S in general are functions of the number of cracks. The $\cos\alpha_0/\cos\alpha_n$-term in equation 5-23 will always be 1 for 3P-panels, because α is considered to be uniquely determined by the number of cracks, which leads to the simplified equation for $\delta_{m,n}$ as:

$$\delta_{m,n} = \frac{h_0}{h_n} \cdot \frac{r_n}{r_0} \cdot \delta_{m,0} \qquad (5\text{-}28)$$

Further, r_r is always equal to r for the 3P-panels, in contrast to the CS-panels where r_r is a function of the number of cracks, which means that the expression for S is as given in equation 5-15, and E_{corr} can than be written as:

$$E_{corr} = \frac{h_0^2}{h_n^2} \cdot \frac{R_0 r_n}{R_n r_0} \cdot \frac{\delta_{m,0}}{\delta_{m,n}} \qquad (5\text{-}29)$$

Finally, by replacing $\delta_{m,0}/\delta_{m,n}$ in equation 5-28 with the relation from equation 5-29, the expression for corrected energy can be written as:

$$E_{corr} = \frac{h_0}{h_n} \cdot \frac{R_0}{R_n} \cdot E_{measured} \qquad (5\text{-}30)$$

If the nominal height and diameter is 75 mm and 800 mm respectively, the correction factors according to equation 5-28 and 5-30 for deflection and absorbed energy, respectively, is like shown in Table 5-5. These correction factors can be used to convert 3P-results to ASTM-results.

Table 5-5 Correction coefficient for 3P-panels to be compared with ASTM C 1550

Nr of cracks	$\delta_{m,n}/\delta_{m,0}$				$E_{corr}/E_{measured}$			
	h = 75 mm		h = 100mm		h = 75mm		h = 100mm	
	R = 300	R = 400	R = 300	R = 400	R = 300	R = 400	R = 300	R = 400
3	0.67	0.93	0.50	0.70	1.33	1.00	1.00	0.75

This means that to compare results for a panel with diameter equal to 600 mm and thickness equal to 75 mm tested at 3 point roller support, with results from tests performed on support conditions as described in ASTM C 1550, the following procedure should be carried out:

- The energy should be measured to a deflection $\delta_{m,n} = \delta_{m,0}$ x 0.67, corresponding to 26.7 mm for $\delta_{m,0} = 40$ mm.
- The measured energy should be corrected as $E_{corr} = E_{measured}$ x 1.33

5.1.7.3 CS-panels

As for the ASTM-panels, the support arrangement for the CS-panels is fixed; hence the length r_r is not affected by the dimension of the panel. This means that if the panel's diameter is increased by a factor of k, the total length of the projected yield lines is also increased by a factor k, and a *radius-adjustment factor* should be added to the expression for energy absorption.

If also the diameter of the supporting ring is changed, both l and r_r are changed.

In contrast to the ASTM- and 3P-panels, the numbers of cracks are not known before testing the panels, and therefore $\delta_{m,n}$ are known first when the crack pattern is developed.

In Table 5-6 the correction factors according to equation 5-23 and 5-26 for deflection and absorbed energy, respectively, are listed. Both factors are 1.0 for panels tested according to the ASTM-procedure.

By use of these factors, the energy absorption will be calculated for equal CMOD and for the same CMOD as for the panels tested at 3-point roller support and panels tested according to ASTM C 1550.

Table 5-6 Correction coefficient for CS-panels to be compared with ASTM C 1550

Nr of cracks	$\delta_{m,n}/\delta_{m,0}$				$E_{corr}/E_{measured}$			
	h = 75mm		h = 100mm		h = 75mm		h = 100mm	
	R/r = 300/250	R/r = 400/350	R/r = 300/250	R/r = 400/350	R/r = 300/250	R/r = 400/350	R/r = 300/250	R/r = 400/350
4	0.58	0.81	0.43	0.61	1.00	0.75	0.75	0.56
5	0.79	1.11	0.60	0.83	0.80	0.60	0.60	0.45
6	1.00	1.40	0.75	1.05	0.67	0.50	0.50	0.38
7	1.20	1.68	0.90	1.26	0.57	0.43	0.43	0.32
8	1.39	1.95	1.05	1.46	0.50	0.38	0.38	0.28

This means that to compare results for a panel with diameter equal to 600 mm and thickness equal to 100 mm tested at CS-support with 6 cracks, with results from tests performed on support conditions as described in ASTM C 1550, the following procedure should be carried out:

- The energy should be measured to a deflection $\delta_{m,n} = \delta_{m,0}$ x 0.75, corresponding to 30 mm for $\delta_{m,0} = 40$ mm.
- The measured energy should be corrected as $E_{corr} = E_{measured}$ x 0.50

5.2 Experimental part

5.2.1 Introduction

The test program was first designed to analyze and compare the results from panels tested according to NB 7 (2003) and ASTM C 1550. Both codes describe that the test shall be run displacement controlled, but while NB 7 (2003) prescribes a displacement rate of 1.5 mm/min, ASTM C 1550 prescribes 4 mm/min. (As already mentioned, a new revision of NB 7 was finished in 2011. In the 2011 version, a deflection rate of 3 mm/min is prescribed) To evaluate whether the displacement rate influences the results, the first test series included 12 panels with diameter 600 mm and thickness 100 mm. 6 of these panels were reinforced with 0.5 vol% steel fibre, while the remaining 6 panels were reinforced with 0.5 vol% synthetic fibre. Three of both the steel and synthetic fibre reinforced panels were tested with displacement rate of 1.5 mm/min, while the remaining panels were tested with a rate of 4 mm/min. An overview of the tested panels in the first test series is given in Table 5-7.

Table 5-7 Overview of tests with two different displacement rates

Panel name	Displacement rate	Nr of cracks	Comments
2305-d600h100-1	4 mm/min	6	Punching shear crack, steel fibres
2305-d600h100-2		7	Punching shear crack, steel fibres
2305-d600h100-3		6	Punching shear crack, steel fibres
2305-d600h100-4	1.5 mm/min	6	Punching shear crack, steel fibres
2305-d600h100-5		6	Punching shear crack, steel fibres
2305-d600h100-6		6	No punching shear crack, steel fibres
2905-d600h100-1	4 mm/min	4	No punching shear crack, synthetic fibres
2905-d600h100-2		4	No punching shear crack, synthetic fibres
2905-d600h100-3		4	No punching shear crack, synthetic fibres
2905-d600h100-4	1.5 mm/min	4	No punching shear crack, synthetic fibres
2905-d600h100-5		4	No punching shear crack, synthetic fibres
2905-d600h100-6		4	No punching shear crack, synthetic fibres

Because the two codes also prescribe different geometry and different supporting system, the second test series included the following panels, both with steel and synthetic fibres:

- 6 panels with diameter 600 mm and thickness 100 mm
- 6 panels with diameter 600 mm and thickness 75 mm
- 6 panels with diameter 800 mm and thickness 100 mm
- 6 panels with diameter 800 mm and thickness 75 mm

Three panels of each dimension were tested on CS, while the other three panels were tested on 3P. (The 3P-method was chosen because the support system described in ASTM C 1550 was not available at the testing time.) The whole test program was carried out with both steel- and synthetic fibre (0.5 vol%). A detailed overview of the tested panels in the second series is given in Table 5-8 and Table 5-9, for the steel fibre reinforced and synthetic fibre reinforced panels, respectively.

Table 5-8 Overview of tests on steel fibre reinforced concrete, second series (0.5 vol%)

Panel name	CS or 3P	Nr of cracks	Comments
Steel-d600h100-1	3P	3	
Steel-d600h100-2	3P	3	
Steel-d600h100-3	3P	3	
Steel-d600h100-4	CS	7	Punching shear crack
Steel-d600h100-5	CS	6	Punching shear crack
Steel-d600h100-6	CS	5	
Steel-d600h75-1	3P	3	
Steel-d600h75-2	3P	3	
Steel-d600h75-3	3P	3	Almost like beam failure. Discarded
Steel-d600h75-4	CS	6	Punching shear crack
Steel-d600h75-5	CS	5	Punching shear crack
Steel-d600h75-6	CS	4	Low amount of fibre in the cracks. Discarded
Steel-d800h100-1	3P	3	
Steel-d800h100-2	3P	2 (4)	Beam failure, one major crack, and two minor cracks.
Steel-d800h100-3	CS	6	Punching shear crack
Steel-d800h100-4	CS	4	Considered not to be representative. Discarded
Steel-d800h100-5	CS	7	Punching shear crack
Steel-d800h100-6	CS	8	Punching shear crack, laser did not measure deflection. Discarded
Steel-d800h75-1	CS	6	Punching shear crack
Steel-d800h75-2	CS	7	Punching shear crack
Steel-d800h75-3	CS	7	Punching shear crack
Steel-d800h75-4	3P	2 (3)	Beam failure. The third crack is small, and do not reach the centre of the panel. Discarded
Steel-d800h75-5	3P	3	Two minor cracks near one major
Steel-d800h75-6	3P	2 (3)	Beam like failure. The third crack is small, but reached the centre of the panel

Table 5-9 Overview of tests on synthetic fibre reinforced panels, second series (0.5 vol%)

Panel name	CS or 3P	Nr of cracks	Comments
Synth-d600h100-1	CS	4	
Synth-d600h100-2	CS	5	
Synth-d600h100-3	CS	5	
Synth-d600h100-4	3P	3	Measurement stopped at 23mm deflection
Synth-d600h100-5	3P	3 (2)	Almost like beam failure. The third crack is less than the others. Discarded
Synth-d600h100-6	3P	3	
Synth-d600h75-1	3P	3	
Synth-d600h75-2	3P	3	
Synth-d600h75-3	3P	3	
Synth-d600h75-4	CS	4	
Synth-d600h75-5	CS	4	
Synth-d600h75-6	CS	4	
Synth-d800h100-1	3P	3	
Synth-d800h100-2	3P	3	
Synth-d800h100-3	3P	3	
Synth-d800h100-4	CS	4	
Synth-d800h100-5	CS	4	
Synth-d800h100-6	CS	4	
Synth-d800h75-1	3P	2 (3)	Beam failure. The third crack is small. Discarded
Synth-d800h75-2	3P	3	
Synth-d800h75-3	3P	3	
Synth-d800h75-4	CS	4	
Synth-d800h75-5	CS	4	
Synth-d800h75-6	CS	4	

Pictures of all panels in series 1 and 2 can be found in appendix B.

5.2.2 Results from tests according to NB 7 (2003)

The load vs. deflection curves for the 12 panels in series 1 are shown in Figure 5-12 together with the curves for the 6 panels from series 2 with equal dimension.

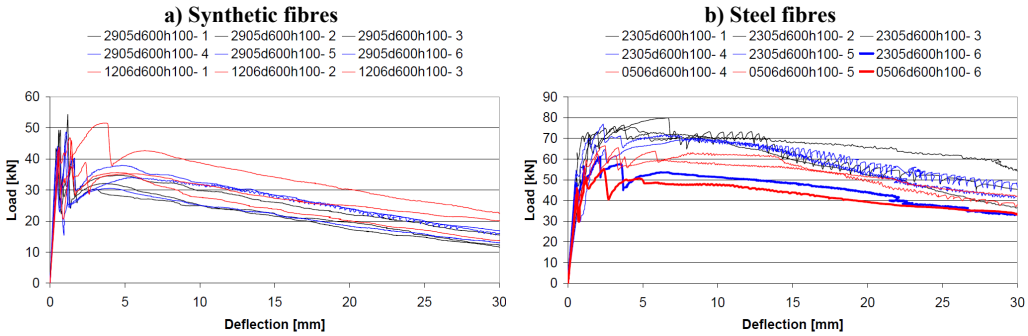

Figure 5-12 Different rate of displacement, blue curves corresponds to 1.5 mm/min and black and red curves corresponds to 4 mm/min

Note that panel *2305d600h100-6* and *0606d600h100-6* had considerable less capacity than the other panels with steel fibres, at least at small deflection. These panels were the only panels with dimension as prescribed in NB 7 that did not have any punching shear cracks. The consequence of shear cracks will be discussed later.

The absorbed energy shown in Table 5-10 and Table 5-11 is calculated in accordance with the procedure in NB 7, which means that the absorbed energy is summarized to $\delta_{m,n}=25(100/h)$ and the measured energy is corrected for the actual height of the panels as $E_{corr}=E_{measured}(100/h)$. There is actually a third correction factor prescribed in NB 7 (2011), which is a reduction factor due to friction. This correction is not included in the results in Table 5-10 and Table 5-11.

Table 5-10 NB 7-results synthetic fibres

Rate of displacement [mm/min]	Concrete strength [MPa]	Panel name	E_{corr} [J]	E_{corr} Average [J]	CoV [%]	E_{corr} Average all panels [J]	CoV all panels [%]
4[1]	57	2905-1	544	592	13	667	17
		2905-2	683				
		2905-3	548				
1.5[1]		2905-4	709	656	12		
		2905-5	562				
		2905-6	696				
4[2]	48	1206-1	632	754	17		
		1206-2	887				
		1206-3	744				
[1]Test series 1 [2]Test series 2							

Table 5-11 NB 7-results steel fibre

Rate of displacement [mm/min]	Concrete strength [MPa]	Panel name	E_{corr} [J]	E_{corr} Average [J]	CoV [%]	E_{corr} Average all panels [J]	CoV all panels [%]
4[1]	55	2305-1	1561	1541	2	1388	12
		2305-2	1547				
		2305-3	1514				
1.5[1]		2305-4	1469	1353	13		
		2305-5	1431				
		2305-6	1159				
4[2]	50	0506-4	1424	1272	14		
		0506-5	1324				
		0506-6	1067				
[1]Test series 1 [2]Test series 2							

As seen from the calculated E_{corr} and the load vs. deflection curves, it is impossible to state whether the displacement rate really affects the absorbed energy or not, based on the limited numbers of panels in the present study. For the synthetic fibre reinforced panels in test series 1, it seems like a displacement rate of 4 mm/min give less absorbed energy than a

displacement rate of 1.5 mm/min. The synthetic fibre reinforced panels from series 2, which were tested with 4 mm/min as displacement rate, had less compressive strength; nevertheless, the absorbed energy was larger. For the steel fibre reinforced panels, the situation was completely opposite, even if the "no shear crack" panels are excluded.

Bernard has investigated the influence of displacement rate where the rates of central deflection varied in logarithmic increments from 0.36 mm/min up to 360 mm/min [Bernard (2001)]. In this investigation, Bernard found out that in one of two series involving steel fibre reinforced panels the energy absorption up to 40 mm deflection increased by 12 % between the slowest and the fastest deflection rate. The other steel fibre reinforced set had negligible variation. One of the two synthetic fibre reinforced sets had a 20 % drop in energy absorption with increasing deflection rate, while the other set showed a 66 % increase with increasing deflection rate. Nevertheless, the synthetic fibre reinforced set that showed highest deflection rate sensitivity, had only 15 % variation in energy absorption in the range from 0.8 to 7.8 mm/min, while the other sets showed less than 5 % variation within this range.

The remaining panels in the present test series were tested at a deflection rate of 4 mm/min. The different dimensions and support systems will clearly affect the rate of crack opening, but this difference is considered to be of minor significance because the variation in crack opening rate is relatively small. The variation in crack opening rate is identical with the correction factors given in Table 5-5 and Table 5-6 for 3P-panels and CS-panels, respectively. A deflection rate of 4 mm/min corresponds to a crack opening rate between 3.2 mm/min (CS-panel d600h100, 4 cracks) and 0.71 mm/min (CS-panel d800h75, 8 cracks).

5.2.3 The influence of panel geometry

To compare the results from test on panels with various dimensions the nominal values of the height (h_0), diameter (d_0) and upper deflection limit ($\delta_{m,0}$) are set to:

h_0: 75 mm
d_0: 800 mm
$\delta_{m,0}$: 22.5 mm

$\delta_{m,0}$ =22.5 mm corresponds to a CMOD = 7.79 mm for a panel with the nominal dimensions tested according to ASTM C 1550 (equation 5-20). These nominal values are chosen simply because the largest CMOD all panels are tested to is 7.79 mm. A CMOD equal to 7.79 mm corresponds to 13.41 mm deflection for a panel tested according to NB 7 with 5 cracks. The correction coefficients shown in Table 5-5 and Table 5-6 are used, which means that the resulting E_{corr} values are comparable with the absorbed energy from ASTM-panels tested to 22.5 mm deflection.

In total 9 steel- and 9 synthetic fibre reinforced panels with diameter 600 mm and thickness 100 mm were tested at continuous support. In the following, only the 3 steel fibre reinforced panels named 0506-4 to -6, and the 3 synthetic fibre reinforced panels named 1206-1 to -3 are evaluated. For some reason, which is not known, the concrete strength of the panels named 2305-1 to-6 and 2905-1 to 6 was higher than the concrete in the remaining panels, and they are therefore left out of the panel geometry investigation.

5.2.3.1 Energy absorption

There are several ways to adjust the measured energy for panels with different geometry so that they can be compared, and in this thesis, four different methods are used.

Method 1

As shown in chapter 3, the fibre's ability to resist loads is strongly influenced by the fibre slip. The load vs. deflection curves from panel tests show that the panel's ability to resist loads is strongly influenced by the deflection. The results from beam tests reported in chapter 4 show that the CMOD most likely is more important than the rotation. The theoretically correct method to compare the absorbed energy from different panels seems therefore to be to analyze the absorbed energy to a specified CMOD. This can be done by measuring the absorbed energy to a deflection $\delta_{m,n}$ as given in equation 5-23, and then correct the absorbed energy as in equation 5-26.

Method 2

Assumption 1: All panels have the same crack pattern, which means the crack pattern has no consequence.

If all panels crack equally, the number of cracks is equal, and thereby the expressions for $\delta_{m,n}$ and E_{corr} are simplified to:

$$\delta_{m,n} = \frac{h_0}{h_n} \cdot \frac{d_n}{d_0} \cdot \delta_{m,0} \tag{5-31}$$

$$E_{corr} = \frac{h_0}{h_n} \cdot \frac{d_0}{d_n} \cdot E_{measured} \tag{5-32}$$

The assumption that all panels cracks equally is a correct assumption for panels tested according to the 3-point roller support method and ASTM C 1550 (because panels that do not have three cracks shall be discarded), and a quite good assumption for synthetic fibre reinforced panels (because these normally have four cracks). For steel fibre reinforced concrete on the other hand, this assumption is strongly questionable, because the crack pattern varies largely. The number of cracks in the present test program is reported in Table 5-8 and Table 5-9.

Method 3

Assumption 1: All panels have the same crack pattern, which means the crack pattern has no consequence.

Assumption 2: The change in diameter is of no consequence for the absorbed energy, because the absorbed energy up to cracking is small compared to the absorbed energy up to $\delta_{m,n}$, and variations in energy up to cracking can be neglected.

From equation 5-26, the correction due to different diameter is through the S-term, which is defined in equation 5-16. With the two assumptions mentioned above, the relationship S_0/S_n is according to yield line theory:

$$\frac{S_0}{S_n} = \frac{R_0}{r_0}\frac{r_n}{R_n} \tag{5-33}$$

If R_0, R_n, r_0 and r_n are 400 mm, 300 mm, 350 mm and 250 mm, respectively, the relationship $S_0/S_n = 20/21$, which means that the panels with diameter equal to 600 mm should absorb 5 % more energy than the d800-panels. The moment capacity per unit length of crack should be

somewhat larger for the d800-panels because the CMOD is less at the same deflection. The yield line theory is valid first when the crack pattern is established, so the crack load may be larger for d600-panels than for d800-panels with equal thickness because the span is larger for the d800-panels.

Summarized:

- S-term: EABS(d600) > EABS(d800)
- Moment capacity: EABS(d600) < EABS(d800)
- EABS at cracking: EABS(d600) > EABS(d800)

The sum of these effects may be that the change in diameter is of no consequence for the absorbed energy, and the expression for $\delta_{m,n}$ and E_{corr} is simplified to:

$$\delta_{m,n} = \frac{h_0}{h_n} \cdot \delta_{m,0} \tag{5-34}$$

$$E_{corr} = \frac{h_0}{h_n} \cdot E_{measured} \tag{5-35}$$

This correction method is the method described in NB 7 (2011). NB 7 (2011) prescribes circular panels with diameter 600 mm and the supporting ring shall have an internal diameter of 500 mm. The tolerance in diameter of the concrete panel is 5 mm, so the deviation in the S-term for the round panels can be neglected. Nevertheless, NB 7 (2011) allows square panels as prescribed in NS-EN 14488-5 to be tested instead of circular panels. NS-EN 14488-5 does not describe any correction of neither the deflection limit nor the absorbed energy, but if square panels are tested according to NB 7 (2011), the correction of deflection limit and absorbed energy according to equation 5-33 and 5-34 shall be performed. To treat square and circular panels equally may be justified by the work done by Bjøntegaard [Bjøntegaard (2009a)]. NS-EN 14488-5 prescribes panel tests on square panels with dimensions 600×600×100 mm, placed on a square continuous support with internal dimension 500×500 mm. A square NS-EN 14488-5-panel with 4 cracks perpendicular to the support will have exactly the same S-term as a round NB 7-panel with 4 cracks. On the other side, a square NS-EN 14488-5-panel with 4 cracks having an angle of 49º to the support will have the quite similar S-term as a round panel with diameter 800 mm. As already mentioned, the S-term and absorbed energy at cracking favours the d600-panels, while the reduced CMOD at equal deflection favours the d800-panels, which is analogous with square panels with different crack vs. support angle.

Method 4

Assumption 1: All panels have the same crack pattern, which means the crack pattern has no consequence.

Assumption 2: The change in diameter is of no consequence for the absorbed energy, because the absorbed energy up to cracking is small compared to the absorbed energy up to $\delta_{m,n}$, and variations in energy up to cracking can be neglected.

Assumption 3: The variation in load capacity from $\delta_{m,0}$ to $\delta_{m,n}$ is small and can be neglected.

With these three assumptions the expression for $\delta_{m,n}$ and E_{corr} is simplified to:

$$\delta_{m,n} = \delta_{m,0} \tag{5-36}$$

$$E_{corr} = \left(\frac{h_0}{h_n}\right)^2 \cdot E_{measured} \tag{5-37}$$

The correction method in ASTM C 1550 is actually quite similar to method 4. The correction of the measured energy includes a diameter factor, but the deflection limit is not corrected either for deviating heights nor for diameter. The height correction of absorbed energy is not in the second power, but rose to the power β=2.0-(δ-0.5)/80 [ASTM C 1550 (2008)], which is approximately 1.5 at 40 mm of deflection.

Method 2, 3 and 4 may be considered to be methods to compare the panels' capacity to absorb energy corrected for deviating dimensions. In this case, the crack pattern is not so important, because the interesting part is the panels' ability to absorb energy limited to a specified deflection. In which way the panels cracks to absorb the energy is in that respect not of interest.

Method 1 may be considered to be a method to analyze the flexural tensile strength at different CMODs.

The corrected EABS values for the four calculation methods are summarized in Table 5-12 and Table 5-13, synthetic fibres and steel fibres respectively.

Table 5-12 E_{corr} synthetic fibre reinforced concrete panels, in Joule

		E_{corr}							
		Method 1		Method 2		Method 3		Method 4	
	Panel nr	3P	CS	3P	CS	3P	CS	3P	CS
Synthetic, d600h100	1		222		377		356		329
	2		318		507		488		460
	3		271		424		406		386
	4	213		235		214		190	
	5	247		273		251		221	
	6	241		265		240		210	
	Average	**234**	**270**	**257**	**436**	**235**	**416**	**207**	**392**
	CoV [%]	8 %	18 %	8 %	15 %	8 %	16 %	8 %	17 %
Synthetic, d600h75	1	190		205		187		188	
	2	156		173		160		159	
	3	171		185		165		165	
	4		211		352		336		336
	5		233		391		373		374
	6		205		342		323		323
	Average	**172**	**216**	**188**	**361**	**171**	**344**	**170**	**344**
	CoV [%]	10 %	7 %	8 %	7 %	9 %	8 %	9 %	8 %
Synthetic, d800h100	1	182		192		192		177	
	2	178		193		193		175	
	3	210		225		225		205	
	4		193		315		315		296
	5		216		348		348		319
	6		239		391		391		370
	Average	**190**	**216**	**203**	**351**	**203**	**351**	**186**	**328**
	CoV [%]	9 %	11 %	9 %	11 %	9 %	11 %	9 %	12 %
Synthetic, d800h75	1[1]	189		197		197		197	
	2	204		215		215		215	
	3	176		190		190		189	
	4		178		290		290		289
	5		250		412		412		410
	6		284		467		467		466
	Average	**189**	**237**	**200**	**389**	**200**	**389**	**200**	**388**
	CoV [%]	7 %	23 %	7 %	23 %	7 %	23 %	7 %	23 %

[1] Crack pattern established before the load and deflection recording started. The panel was unloaded, load and deflection recording started, and the panel was then reloaded. This panel did also crack almost in a beam-like mode; discarded from further evaluation.

Table 5-13 E_{corr} steel fibre reinforced concrete panels, in Joule

		E_{corr}							
		Method 1		Method 2		Method 3		Method 4	
	Panel nr	3P	CS	3P	CS	3P	CS	3P	CS
Steel, d600h100	1	470		517		490		450	
	2	498		552		524		482	
	3	462		526		517		489	
	4		515		760		757		735
	5		467		701		700		684
	6		362		576		567		548
	Average	**477**	**448**	**532**	**679**	**510**	**675**	**473**	**656**
	CoV [%]	4 %	18 %	3 %	14 %	3 %	14 %	4 %	15 %
Steel, d600h75	1	451		517		484		478	
	2	504		574		544		541	
	3[1]	362		412		393		390	
	4		530		820		819		819
	5		441		713		703		701
	6[2]		208		364		354		352
	Average	**439**	**393**	**501**	**632**	**473**	**625**	**470**	**624**
	CoV [%]	16 %	42 %	16 %	38 %	16 %	39 %	16 %	39 %
Steel, d800h100	1	440		469		469		438	
	2	518		557		557		525	
	3		457		673		673		663
	4[3]		312		521		521		504
	5		525		750		750		751
	6[4]								
	Average	**479**	**432**	**513**	**648**	**513**	**648**	**481**	**639**
	CoV [%]	11 %	25 %	12 %	18 %	12 %	18 %	13 %	20 %
Steel, d800h75	1		547		815		815		817
	2		446		671		671		672
	3		453		652		652		651
	4[5]	241		257		257		256	
	5[6]	449		476		476		476	
	6[5]	417		449		449		448	
	Average	**369**	**482**	**394**	**713**	**394**	**713**	**393**	**713**
	CoV [%]	30 %	12 %	30 %	13 %	30 %	13 %	30 %	13 %

[1] The panel cracked almost in a beam-like mode, and the capacity was less than for the other panels. Discarded from further evaluation.
[2] Untypical crack pattern and extremely low capacity related to the other steel fibre panels. Considered to be an underachiever and discarded from further evaluation.
[3] Untypical crack pattern and low capacity related to the other steel fibre panels. Considered to be an underachiever and discarded from further evaluation.
[4] No laser-record. As a result was panel d800h100-3 tested at CS instead of 3P
[5] Cracked in a beam-like mode. Discarded as described in ASTM C 1550.
[6] Three major cracks and in addition two minor ones.

As seen from Table 5-13, none of the steel fibre reinforced panels tested at 3P with dimension d800h75 was successful. To have one panel to compare with the other dimensions, d800h75-5 is used in further evaluation, but the result is not to any great extent trustworthy.

In Table 5-7 and Table 5-8 information of the number of cracks and which panels that had shear cracks for the steel fibre reinforced panels are given for the panels in series 1 and 2, respectively. The following panels did not have any shear cracks:

- *2305d600h100-6*
- *d600h100-6*
- *d600h75-6*
- *d800h100-4*

As shown in Table 5-11 and Table 5-13, these panels also absorbed less energy than the other panels tested equally. This is an example of the classical "cause and effect" question. It seems reasonable to believe, based on the panels tested in the present thesis, that it is a relation between whether shear cracks occur or not and the capacity to absorb energy. Whether high EABS is an effect of shear cracks, or shear cracks are an effect of high EABS is not investigated. The former may be explained by reduced crack opening in the cracks going from the centre of a panel to the support for a given deflection, resulting in higher capacity because fibres are more effective when crack openings are limited. An explanation for the latter may be that if the fibres are sufficiently effective in transferring stresses across the bending cracks, the concrete's capacity to resist shear force is reached in other areas, resulting in shear cracks.

From the information in Table 5-6 to Table 5-13 it also seems like the number of cracks and the EABS varies simultaneously, another example of the "cause and effect" question.

The coefficient of variation is in general less for the 3P-tests than for the CS-tests. One explanation for this is that the panels tested at 3P should theoretically always have three cracks, and therefore the behaviour after cracking should be more similar for these panels than for CS-panels.

Average values when the discarded panels are left out are shown in Table 5-14 and Table 5-15.

Table 5-14 Average E_{corr} synthetic fibre reinforced concrete panels, in Joule

	E_{corr}							
	Method 1		Method 2		Method 3		Method 4	
Panel dimension	3P	CS	3P	CS	3P	CS	3P	CS
d600h100	234	270	257	436	235	416	207	392
d600h75	172	216	188	361	171	344	170	344
d800h100	190	216	203	351	203	351	186	328
d800h75	190	237	202	389	202	389	202	388

Table 5-15 Average E_{corr} steel fibre reinforced concrete panels, in Joule

	E_{corr}							
	Method 1		Method 2		Method 3		Method 4	
Panel dimension	3P	CS	3P	CS	3P	CS	3P	CS
d600h100	477	448	532	679	510	675	473	656
d600h75	478	485	545	766	514	761	510	760
d800h100	479	491	513	711	513	711	481	707
d800h75	449	482	476	713	476	713	476	713

The results from Table 5-14 and Table 5-15 are shown graphically in Figure 5-13.

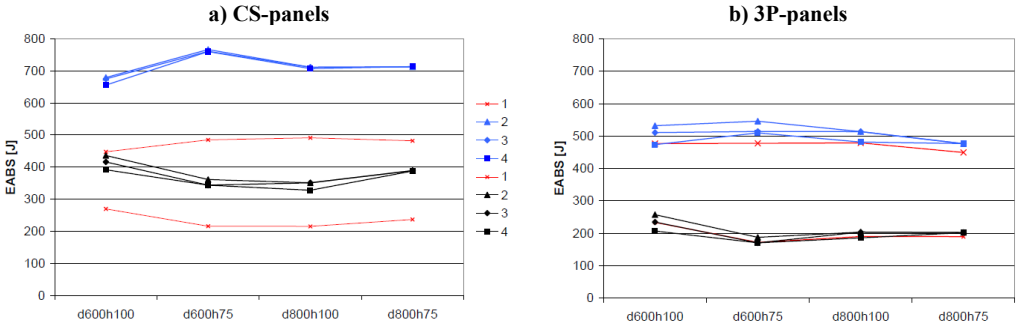

Figure 5-13 Comparison method 1-4. The four upper curves (three blue, one red) are steel fibre reinforced panels, the four lower curves are synthetic fibre reinforced panels, and red curves are method 1

As seen from Figure 5-13, the EABS is more or less constant for all panel dimensions regardless of calculation method. For the panels tested at 3P, all four correction methods give almost exactly the same corrected energy absorption as well. For the panels tested on CS correction method 1 gives less absorbed energy than the three other methods. In addition, the panels tested at CS corrected by method 1 gives approximately the same absorbed energy as the panels tested at 3P, which is shown in Figure 5-14.

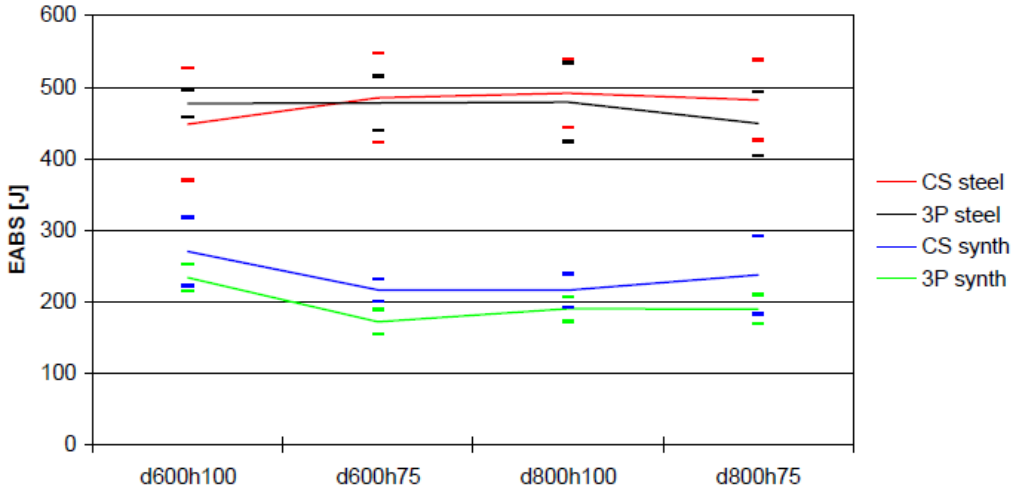

Figure 5-14 Comparison correction method 1, inclusive ± 1 STD

If the assumption that the energy absorption should be calculated to the same CMOD is correct (i.e. method 1 is correct), the EABS-curves in Figure 5-14 should be horizontal. If panels tested at CS and 3P are equally influenced by friction, the CS- and 3P-curves should coincide in addition. The 3 point roller support was introduced to reduce the friction, and if the panels crack in three equally sized sectors and the cracks are localized midway between the supports, the roller supports will reduce the friction. Panels that crack asymmetrically will have a tangential displacement relative to the support, and this tangential contribution to the friction will not be reduced by the roller supports. Another important point is that there is a certain scatter in the results. In addition to the average EABS, the range ± 1 standard deviation (STD) is shown in Figure 5-14.

As seen, with the exception of d600h75 with synthetic fibres, the results more or less overlap each other. As already mentioned, it is reported that the ASTM-procedure involves 15-20 % contribution from friction, while the NB 7 procedure involves 35-40 % contribution from friction. In connection with a Round Robin test program involving panels tested according to ASTM C 1550 [Sandbakk et al. (2010)], 2 panels were tested at the ASTM-support system, while 3 panels were tested at 3P-roller support. This was originally done to gain experience with the test methods, and the number of panels are very limited, and not reported in [Sandbakk et al. (2010)]. Nevertheless, it was found that panels tested at 3P-roller support absorbed about 15 % more energy than panels tested at ASTM-support when the energy was summarized to a CMOD = 8.66 mm, corresponding to a deflection equal to 25 mm and 23.33 mm, ASTM-procedure and 3P-procedure respectively. (The 5 tested panels were reinforced with 0.5 vol% steel fibres.) If this relationship between the ASTM-results and the 3P results are generally valid, this means that the friction contribution to the 3P-panels should be about 30 %. (If the absorbed energy for an ASTM-panel is 1 and the friction contributes to 15-20 %, the energy absorbed by fibres is 0.80-0.85. If the 3P-panel shows 15% higher absorbed energy (1.15), and the energy absorbed by fibres is still 0.80-0.85, this means that the energy absorbed by fibres in percent of the total energy should be in the range from (0.8/1.15 =) 0.7 to (0.85/1.15=) 0.74. The remaining 26-30% should then be attributed to the friction). Compared with the 35-40 % for the CS-panels this means that the CS-panels should absorb somewhat more energy than the 3P-panels.

The synthetic fibre reinforced panels tested at CS absorbed 13-26 % more energy than the 3P-panels; while the CS/3P-ratio for the steel fibre reinforced panels were 0.97-1.04. The author's explanation to this is that the synthetic fibre reinforced panels is more likely to crack in three equally sized sectors than the steel fibre reinforced panels, which let the roller support to be effective when it comes to reducing the friction.

5.2.3.2 Load at first crack

The average load at first crack is summarized in Table 5-16. In agreement with the theory of linear elasticity, the measured loads are multiplied by $(75/h)^2$ to compensate for different panel thickness. The discarded panels are not taken into consideration, even though the loads are registered.

Table 5-16 Load at first crack, in kN

	Synthetic fibre		Steel fibre	
Panel dimension	3P	CS	3P	CS
d600h100	29	24	31	25
d600h75	29	25	32	25
d800h100	25	23	31	22
d800h75	25	20	27	24

One interesting observation is that the panels tested at 3P cracked at higher load than the panels tested at CS. Figure 5-15 shows the relation between panel dimension and load at first crack for all panels together with the average curve.

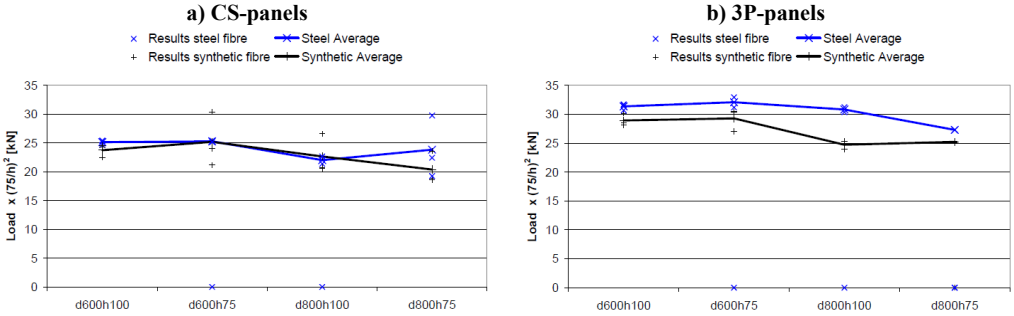

Figure 5-15 Load at first crack

Summarized:

- The CS-panels had more or less the same load at cracking for steel and synthetic fibres, which is expected based on the assumption that fibres do not affect the pre-cracked behaviour in bending.
- The 3P-panels with steel fibres had higher cracking load than those with synthetic fibres, in contrast to the CS-panels
- The 3P-panels had higher cracking load than the CS-panels
- Steel fibre reinforced panels: Except CS-d800h100, the crack load seems independent by the diameter of the panels (3P-d800h75 involves only one panel, and the crack pattern was not as expected, not trustworthy result)
- Synthetic fibre reinforced panels: The load at cracking decreased when the panel diameter increased, not surprisingly because the span increases.
- The reason why the panels cracked at higher loads when tested at 3P is most likely that the supporting system decides where the crack arises. For the panels tested at CS, the concrete cracks at the locations where the concrete is weakest.
- It is the stress distribution according to elastic theory, which decides when the first crack comes. This is different for ASTM/3P and CS-panels.

Crack load vs. EABS

A two way slabs ability to resist a point load is theoretically independent of the span. This means that the capacity after cracking should be independent of the span, but if the contribution to the total EABS of the pre-cracked phase is large enough, it should be possible to find a correlation between the cracking load and the total EABS. In Figure 5-16 the crack load vs. EABS relations are shown when the EABS are calculated according to method 4 and method 1.

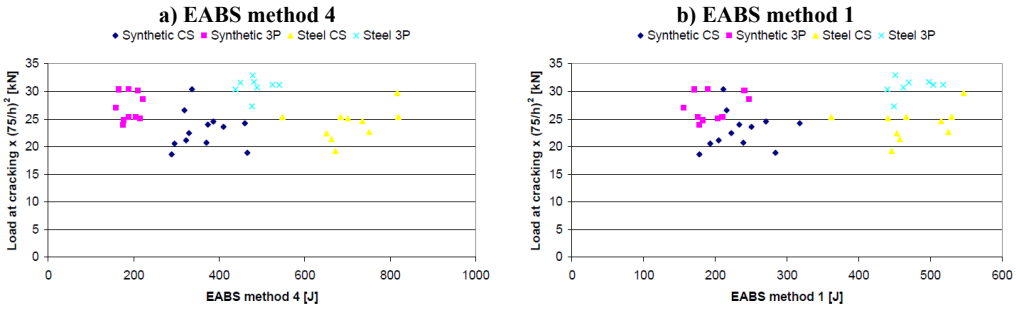

Figure 5-16 Load at cracking vs. EABS

As seen from Figure 5-16, there seems to be no correlation between the load at cracking and the absorbed energy, regardless of calculation method, fibre type and support condition.

5.2.3.3 Maximum load

The maximum loads are summarized in Table 5-17. As for the cracking loads, the measured loads are multiplied by $(75/h)^2$ to compensate for different panel thickness. The discarded panels are not taken into consideration, even though the loads are registered.

Table 5-17 Maximum load, in kN

	Synthetic fibre		Steel fibre	
Panel dimension	3P	CS	3P	CS
d600h100	29	26	31	35
d600h75	29	27	32	37
d800h100	25	25	31	36
d800h75	25	22	27	36

For the 3P-panels, the maximum load was reached when the cracking occurred. For the CS-panels, the maximum load was reached after the first crack. Figure 5-17 shows the relation between panel dimension and the maximum load for all panels together with the average curve.

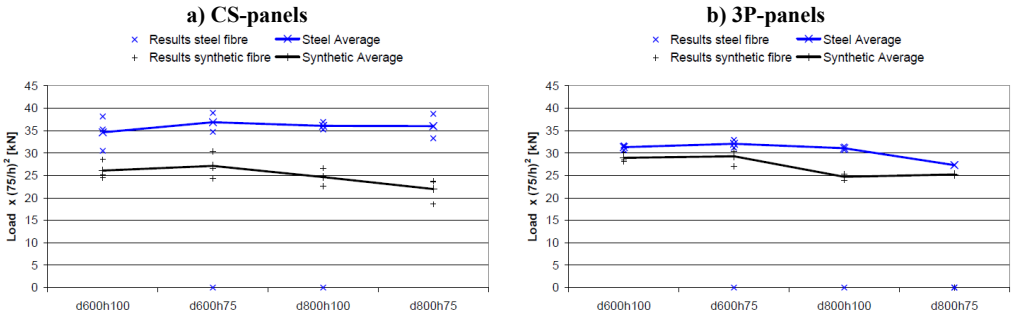

Figure 5-17 Maximum load

Summarized:

- The maximum load for the steel panels seems to be independent of the dimension of the panels (3P-d800h75 is not trustworthy, only one panel)

- The maximum load for the synthetic fibre panels seems to decrease when the diameter increase.

Maximum load vs. EABS

Even though it is shown that the cracking load does not influence the capacity to absorb energy, it is likely to believe that a panel that shows high maximum load should be able to absorb more energy than a panel with less maximum load. The maximum load vs. EABS relations are shown in Figure 5-18.

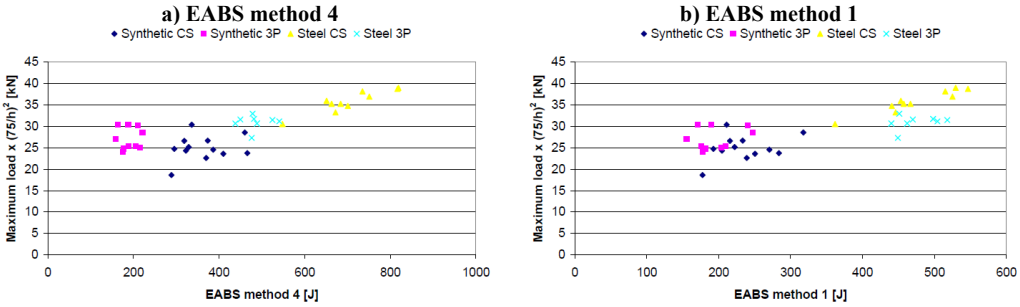

Figure 5-18 Maximum load vs. EABS

As seen in Figure 5-18 it seems to be a correlation between the maximum load and EABS for the steel fibre reinforced panels, at least if the panels are tested at CS. For the synthetic fibre reinforced panels, the maximum load seems to have no influence on the ability to absorb energy. This is mainly because the maximum load is equal to the cracking load for the panels tested at 3P, and also for the synthetic fibre reinforced panels tested at CS.

5.2.3.4 Flexural tensile strength

The flexural tensile strength may be related to deflection, crack rotation or CMOD. Clearly, this is better than making diagrams including the load, which makes it difficult to compare results if the panel thickness is not equal for all panels.

Figure 5-19 shows flexural tensile stress vs. CMOD and flexural tensile stress vs. rotation curves. The curves in Figure 5-19 are average curves for all panels in each series.

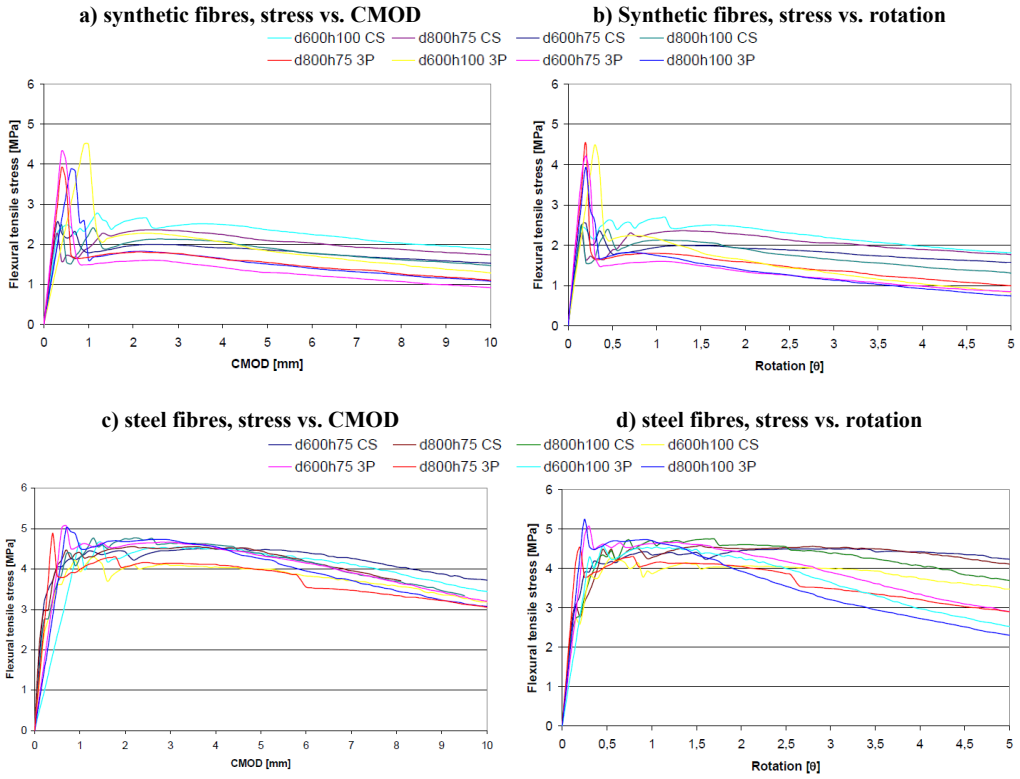

Figure 5-19 Flexural tensile stress vs. CMOD and rotation

From Figure 5-19 it seems to be better agreement between the different panel dimensions when the results are expressed as *flexural tensile tress vs. CMOD* than for *flexural tensile stress vs. rotation*. This implies that when for instance beams are tested, the crack offset correction should be related to CMOD and not only rotation. The reason why a *rotation-related* crack offset correction seems to be correct in beam tests is that the beam heights do not vary to any great extent, which means that the correction due to rotation or CMOD will give similar results.

As already mentioned, the following steel fibre reinforced panels are discarded (for different reasons, which are explained in Table 5-9): d600h75-4, d800h100-4, d800h100-6, d600h75-3 and d800h75-4. The synthetic reinforced panels that are discarded are d600h100-5 and d800h75-1.

In Figure 5-20, four average stress vs. CMOD curves are shown. These curves are simply the average of every panel tested similarly and with the same fibre type, which means that the *3P Steel*-curve, for instance, represents the average stress vs. CMOD curve for all steel fibre reinforced panels tested at 3P regardless of the dimensions.

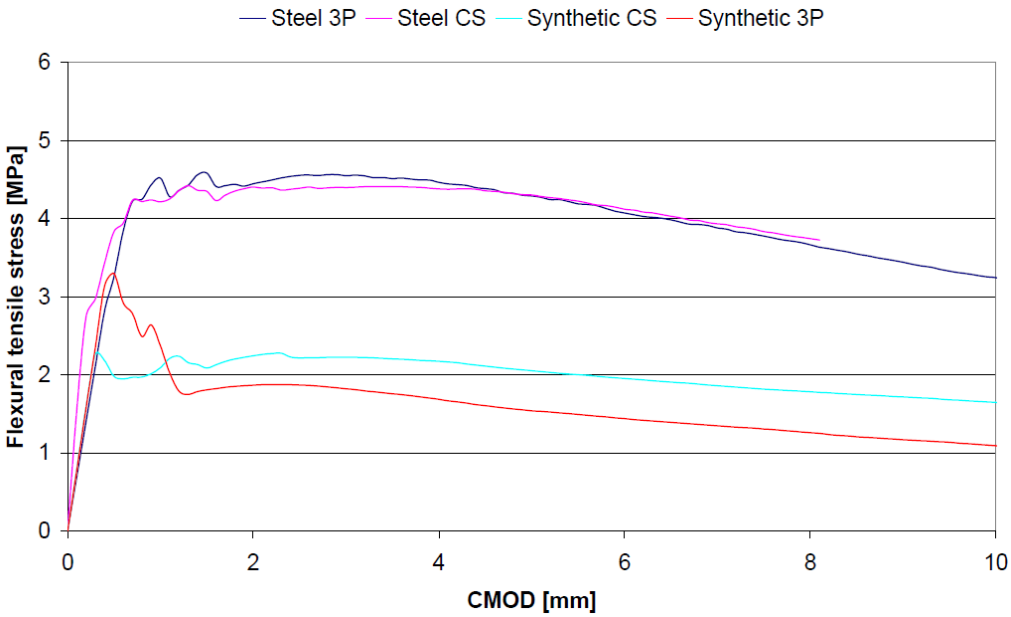

Figure 5-20 Comparison steel fibre reinforced and synthetic fibre reinforced panels

Based on these findings, it seems like the 3-point roller support did not reduce the friction compared to the CS-method. As already mentioned, the author's conviction is that the calculation method is correct, meaning that it is possible to compare both EABS and flexural tensile stress from panels tested at different support conditions, but that the steel fibre reinforced panels did not crack in a way that made the roller support effective in reducing the friction.

As mentioned earlier, CMOD in the pre-cracked phase is a self-contradiction. From the measured CMOD in the Round Robin program reported in [Sandbakk et al. (2010)] involving panel tests according to ASTM C 1550, the crack opening was measured at in total 19 panels. When comparing the measured *crack vs. deflection* curves with the *load vs. deflection* curve for every panel, it seems clear that the cracks start to develop first when the maximum load is reached, which is obvious. The registered CMOD before the maximum load was reached must then be elastic elongation. Figure 5-21 shows the *crack vs. deflection* curves together with the corresponding *load vs. deflection* curve for a panel reinforced with 40 kg/m^3 steel fibres tested according to ASTM C 1550. This panel is named MF40-1-3 in [Sandbakk et al. (2010)].

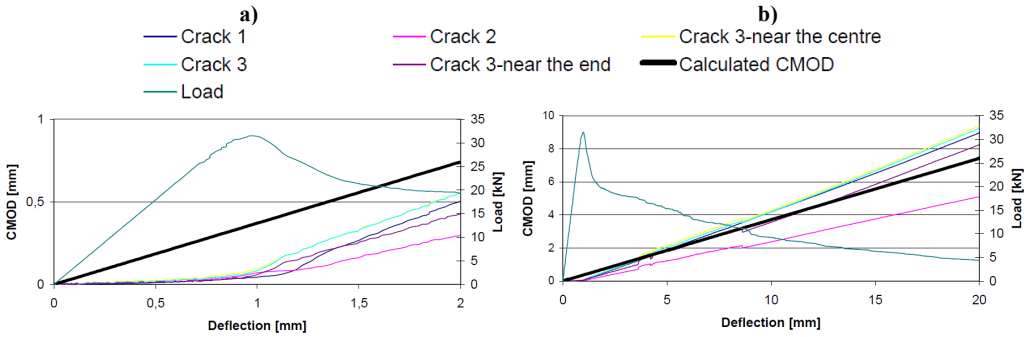

Figure 5-21 Crack development in a panel tested according to ASTM C 1550

Similar curves may be made for every 19 panels, and the overall impression is that the calculated CMOD overestimate the crack opening immediately after cracking by approximately 0.25 mm. If the *calculated CMOD* curve is adjusted by subtracting 0.25 mm due to the overestimation before cracking, it will still be within the 3 curves representing the measured crack opening in the three different cracks.

5.2.4 The relationship between steel fibres and synthetic fibres

As for the beam tests shown in chapter 4.2.5, the results from panel tests may be used to quantify the relation between the energy absorption capacity per fibre volume achieved by the two different fibre types. Because the EABS normally is measured to relatively large deflection compared to residual flexural strength tests, and the fact that the number of cracks are not considered neither in NB 7 nor NS-EN 14488-5, calculation method 4 described in chapter 5.2.3 is most suitable to quantify the ratio. Actually, calculation method 3 is identical with the calculation methods in the two previously mentioned codes, but for the panels with 100 mm thickness the deflection limit, $\delta_{m,n}$, was reduced from 22.5 mm to 16.9 mm due to equation 4-32 when the EABS was calculated.

Table 5-18 Relation between the energy absorption capacity of steel fibre reinforced panels (0.5 vol%) and synthetic fibre reinforced panels (0.5 vol%)

Panel dimension	Ratio steel-/synthetic fibre	
	CS	3P
d600h100	1.67	2.29
d600h75	2.21	2.99
d800h100	2.15	2.59
d800h75	1.84	2.36
Total	1.97	2.56

As seen from Table 5-18 it is almost impossible to quantify the relation between steel fibres and synthetic fibres with regard to EABS. The ratio varies with respect to both panel dimensions and support conditions. What is relatively clear is that one might expect a NB 7-panel reinforced with steel fibres to have about 1.7 times the capacity to absorb energy relative to equal vol % of synthetic fibres. Even though the 3P-method is quite similar to the ASTM-method, the relation for panels with diameter and height equal to 800 mm and 75 mm respectively, cannot be used as a steel vs. synthetic relation for ASTM-panels because the

prescribed deflection limit in ASTM is 40 mm, while the relations in Table 5-18 are calculated for EABS summarized to 22.5 mm deflection.

From Figure 5-20 it is shown that the steel vs. synthetic fibre relation varies as a function of the CMOD, which off course will influence the ratio for different panel dimensions. What is beyond doubt is that steel fibres are more effective than synthetic fibres when the volume percent of fibres is equal.

5.3 Summary of the panel tests

Even though panel tests are designed to determine the energy absorption capacity, the residual flexural tensile strength is tested. By counting the number of cracks, it is possible to calculate both the crack opening and the corresponding flexural tensile strength. From the tests with two different panel diameters, it is shown that the cracking strength does not influence the total energy absorption capacity. The general impression is that it is a correlation between the number of cracks and the energy absorption capacity, but whether a large number of cracks result in high energy absorption capacity or high energy absorption capacity result in large number of cracks are not investigated.

Four different methods to correct the measured energy absorption capacity are described, where the method that is related to the crack opening is considered theoretically correct. The three other methods are simplifications of the theoretically correct method, and it is shown which assumptions that lead to the calculation method that is used in NB 7 (2011).

It is shown that the panel geometry has no influence on the residual flexural tensile stress vs. CMOD curve, which of course means that the calculated capacity to absorb energy will be independent on the panel geometry when the correction method for EABS that is related to the crack opening is used. If the residual flexural tensile strength is a material property, it should be of no consequence in which way it is determined, which means that the residual flexural tensile strength determined from beam tests should be comparable with the residual flexural tensile strength determined from panel tests. This comparison is shown in chapter 6

In other words, chapter 6 is basically a continuation of the beam- and panel chapters.

6 Comparison beam and panel tests

Because panel tests and beam tests basically are measuring the flexural tensile strength, it should be possible to relate the results from panel tests with results from beam tests. When the results from both test methods are expressed as *flexural tensile stress vs. CMOD* curves, it is possible compare the results directly. The idea of doing this comparison came after casting and testing the beams and the panels. Originally, the beam study and the panel study were two totally different studies. The fibre content in the beams was decided to be different for Dramix and Barchip fibres because more synthetic fibres than steel fibres are needed to have equally behaviour in bending. One of the objectives was to see whether concrete reinforced with 1.0 vol% synthetic fibres had equally strength as concrete reinforced with 0.7 vol% steel fibres. These volumes were simply chosen due to information from contractors within COIN.

For the panel tests, the main objective was to analyze in which way different panel dimensions and support conditions affect the capacity to absorb energy. To be wise after the event one may say that the fibre content should have been kept constant for both beam and panel tests. Nevertheless, it is possible to use the results from beam and panel tests in order to investigate the relation between them.

The tested beams reported in chapter 4.2 and panels reported in chapter 5.2, are all made of concrete D, and the mix design of this concrete was shown in Table 2-1 in chapter 2.1. The fibre content in the specimens tested after 28 days of curing is summarized in Table 6-1.

Table 6-1 Fibre type and dosage in beam and panel tests

	Dramix 6560	Barchip Shogun
Beams	0.7 vol%	1.0 vol%
Panels	0.5 vol %	0.5 vol%

The method for calculating the flexural tensile stress vs. CMOD curves for beam tests and panel tests are presented in chapter 4.1 and chapter 5.1 respectively.

The flexural tensile stress vs. CMOD curves from beam tests (according to NS-EN 14651) have already been shown in Figure 4-16 to Figure 4-18, and the flexural tensile stress vs. CMOD curves from panel tests were shown in Figure 5-19. In Figure 4-16 to Figure 4-18, the CMOD was calculated from the measured deflection according to equation 4-46, while the CMOD for the panels were calculated with the assumption of rigid body movement and contact point between the sectors at the compressive surface. To compare results from beam and panel tests in the same stress vs. CMOD diagram, it seems reasonable to calculate the CMOD with identical assumptions. For that reason, the CMOD for the beams in the present chapter are calculated according to equation 4-10.

As shown in Figure 5-21, the calculated CMOD according to equation 5-20 seems to overestimate the crack opening at first crack with approximately 0.25 mm for panels tested according to ASTM C 1550. By assuming that the calculated crack opening is overestimated with 0.25 mm also for panels tested at CS- and 3P- support, the flexural tensile stress vs. CMOD curves as shown in Figure 6-1 is made.

In Figure 6-1 the average curves from beam- and panel tests are drawn in the same flexural tensile stress vs. CMOD- diagram.

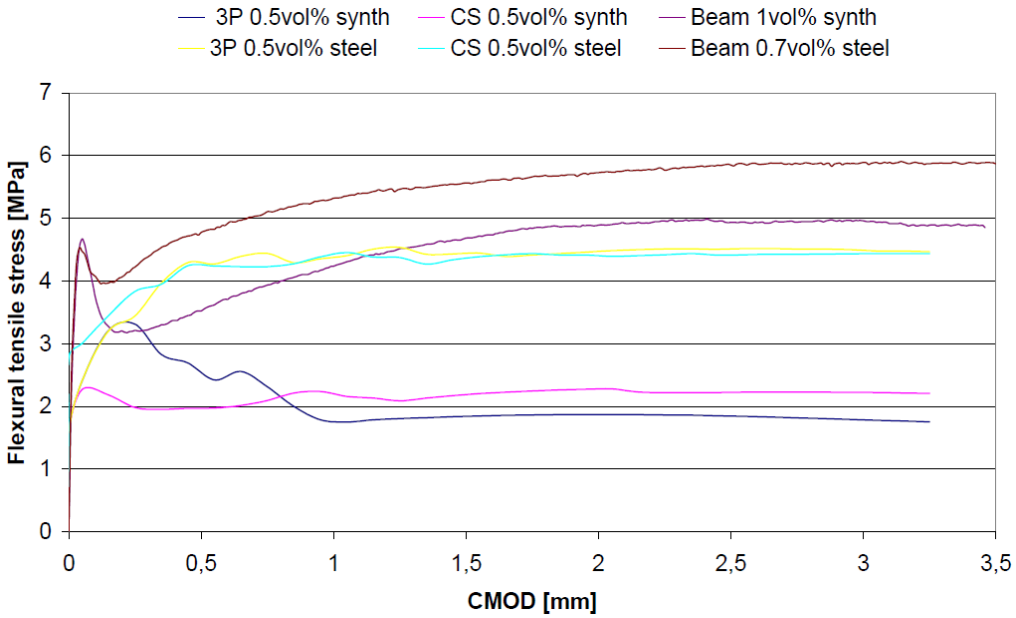

Figure 6-1 Stress vs. CMOD diagram for beam and panel tests

Because the flexural tensile stress vs. CMOD diagram in Figure 6-1 consist of average results, the stress at cracking for the panels in the figure is not correct. From Figure 5-19 it is seen that the cracking stress was about:

- 3 MPa for the synthetic fibre reinforced panels tested at CS
- 4.5-5 MPa for the synthetic fibre reinforced panels tested at 3P
- 4-5 MPa for the steel fibre reinforced panels tested at CS
- 5-5.5 MPa for the steel fibre reinforced panels tested at 3P

Because the first maximum of the stress vs. CMOD curves is reached at different CMODs for the different panels, the stress values are smoothened out when the average curves are made. (For panels tested at 3P, the first maximum is also the absolute maximum, while for CS-panels the absolute maximum is sometimes located at larger CMODs.)

The general trend is that panels tested at 3P show higher cracking strength than panels tested at CS. The reason for this is most likely that 3P-panels crack where the stresses are highest (due to the support arrangement) while the CS panels crack in their weakest zones. In addition, the stress distribution before cracking is different for panels tested at the two different support arrangements. A cracking stress of about 4.5-5.5 MPa is quite near the measured cracking stress determined from the beam tests.

It should also be emphasized that:

- Yield line analysis is only valid when the crack pattern is established, which means that the flexural tensile stress before cracking cannot be calculated.
- Panels tested at CS normally do not have the same number of cracks during the whole test if they crack in more than 4 sectors. It is possible that they first crack in 4 sectors, and that more cracks occur during the test. To calculate both the stress and the CMOD, the number of cracks after testing is counted, and because it is possible that

the number of cracks is increasing during the test, it is obvious that the calculations may be somewhat wrong.

- It is obvious that before panels or beams are cracking, the CMOD is zero. Because the CMOD is calculated with the assumption of rigid body movement, the calculated CMOD before cracking is of course fictitious. One might suggest just subtracting the calculated CMOD at cracking from the CMOD-curve, which means to shift the curve horizontally. This will also be incorrect, because of the energy that is released once the concrete is cracking, so even though the CMOD 1 second before cracking should be zero, the CMOD 1 second after cracking may be much larger than expected from the displacement rate of the load cell.
- The panels tested at CS are placed on a ring made of plywood with a smooth surface. After cracking, the only place they are in contact with the support is near the cracks, which means that the contact area is quite small, which in turn result in the possibility for the panels to be pushed down into the support. Because the deflection is measured relative to the support, this may give a contribution to the measured deflection that is false. Another source of error is radial cracks due to punching shear. Panels tested at CS can have some punching shear cracks in addition to the cracks that go from the centre to the support. When the moment capacity is calculated, the punching shear cracks are not taken into consideration. The punching shear cracks may also increase the measured deflection, and this extra deflection will be calculated as a crack opening between the rotating sectors. It is also possible that the shear cracks reduce the measured deflection, which also will interrupt the calculated crack opening.
- Bernard [Bernard, E. S.(2005)] has reported that the influence of friction for panels tested according to ASTM C 1550 is about 15-20%, while Bjøntegaard [Bjøntegaard, Ø. (2009a)], [Bjøntegaard, Ø. (2009b)] has shown that the influence of friction for panels tested according to NB 7 (both the 2003 version and the 2011 version) is about 35-40%. Even though the roller support in the present 3P-tests was introduced to reduce the effect of friction, it is obvious that if the panels do not crack in three equally sized sectors with the support located halfway between the cracks, the sectors will slide on the support. Nevertheless, it is reasonable to believe that panels tested at the present 3P should be less influenced by friction than panels tested at CS. It seems like the steel fibre reinforced panels show the same results regardless of support conditions, while the synthetic fibre reinforced panels show larger capacity at CS than 3P. In general steel fibre reinforced panels cracked in more sectors than the synthetic fibre reinforced panels did.

Thorenfeldt [Thorenfeldt E. V. (2003)] has introduced a simplified expression that can be used to determinate the residual tensile strength of steel fibre reinforced concrete, $f_{\mathrm{ft,res}}$, which is written as:

$$f_{\mathrm{ft,res}} = \eta_0 v_{\mathrm{f}} \eta_1 \sigma_{\mathrm{f,max}} = \eta_0 v_{\mathrm{f}} \sigma_{\mathrm{f,mean}} \tag{6-1}$$

where

η_0: is a capacity factor representing the theoretical normal resultant of fibres with known mean stress assuming unchanged direction of fibres crossing a tensile crack, with values 1/3 for random 3D-oriented fibres, 1/2 for random 2D-oriented fibres in planes parallel to tension direction, and 1.0 for distributed one-directional fibres in the tension direction

v_{f}: is the volume fraction of fibres

η_1: is the ratio of mean to max stress in fibres with random anchorage length

$\sigma_{\mathrm{f,max}}$: is the maximum fibre stress in fibre with fully developed anchorage length

$\sigma_{f,mean}$: is the average stress in all fibres crossing a given crack

Thorenfeldt has also established a relation between the capacity factor, η_0, and the fibre orientation factor, α [Thorenfeldt E. V. (2003)]. According to this relation, the capacity factor can be estimated by counting the number of fibres and calculating the section ratio and corresponding fibre orientation factor. The expression for α is written as:

$$\alpha = n\frac{A_f}{A_c v_f} = \frac{\rho_f}{v_f} \tag{6-2}$$

where

n: is the number of counted fibres
A_f: is the cross section area of one fibre
A_c: is the cross section area of the concrete
v_f: is the fibre volume ratio
ρ_f: is the fibre section ratio

When the orientation factor is calculated, the capacity factor, η_0, can be estimated as:

$$\eta_0 = \frac{2}{3}\alpha \quad \text{for} \quad 0 < \alpha \le 0.5 \tag{6-3}$$

$$\eta_0 = \frac{4}{3}\alpha - \frac{1}{3} \quad \text{for} \quad 0.5 < \alpha \le 1.0 \tag{6-4}$$

The residual flexural tensile stresses calculated according to linear stress distribution as defined in NS-EN 14651, and shown in Figure 5-8 are of course fictitious. The relation between this fictitious residual flexural tensile stress and the residual tensile stress as given in [Kanstad et al (2011)] is written as:

$$f_{ft,res} = 0.37 f_R \tag{6-5}$$

By combining equation 6-1 and 6-5, the average mean stress in fibres at the crack can be calculated. If η_0 is assumed to be 0.5, which corresponds to plane oriented fibres (α=0.625), *the mean fibre stress vs. CMOD* curves are as shown in Figure 6-2.

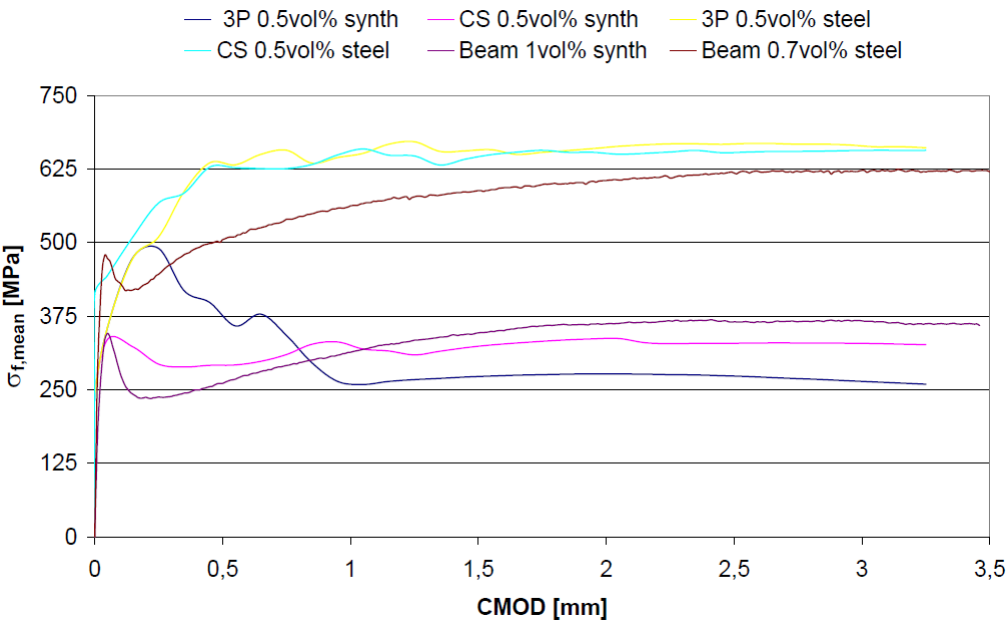

Figure 6-2 Mean fibre stress vs. CMOD curves

With regard to the relatively large scatter in the results from both beam and panel tests, the calculated mean stress in the fibres is surprisingly equal. Surely, some deviations exist, but when the input from beam and panel tests is encumbered with deviations, the output cannot be less encumbered. The overall impression is that it is quite likely that the capacity actually may be described by average fibre stress, $\sigma_{f,mean}$, the volume fraction of fibres, v_f, and the capacity factor, η_0, and further that the average fibre stress varies with regard to the CMOD, or more correctly; by the slip.

7 Relation EABS from ASTM C 1550 tests vs. EABS from NB 7 tests

As shown in the earlier chapters, it seems reasonable to believe that the fibre efficiency really may be described by the fibre slip, which again can be related to crack openings. By use of the equations and results from chapter 5, it should then be possible to find a theoretical relation for the energy absorbed in panel tests according to ASTM C 1550, NB 7 and NS-EN 14488-5.

Consider the ASTM C 1550 as reference. The deflection limit and measured EABS for a panel with diameter 600 mm and thickness 100 mm, as prescribed in NB 7, should then be corrected by the factors given in Table 5-6.

The correction factors for deflection and EABS for a NB 7 panel relative to ASMT C 1550 varies as a function of the number of cracks as described in chapter 5.1.7.3 and the deflection limit and correction factors are summarized in Table 7-1.

Table 7-1 Deflection limit and correction factors for EABS measured by NB 7 related to ASTM C 1550 ($\delta_{m,0}$=40 mm)

Nr of cracks	$\delta_{m,n}$ [mm]	$E_{corr}/E_{measured}$ [-]
4	17.32	0.750
5	23.84	0.600
6	30.00	0.500
7	35.97	0.429
8	41.82	0.375
d800h100, 4 cracks[1]	24.25	0.563
[1]Corresponds to a NS-EN 14488-5 panel with crack vs. support angle equal to 49º		

When panels are tested and results reported as prescribed in NB 7, the reported EABS are summarized to 25×(100/h) mm, which means that it is impossible to calculate the energy absorbed to a deflection larger than about 25 mm based on the reported NB 7 results. In connection with the revision of NB 7, in total 20 steel fibre reinforced panels were cast at the laboratory at SINTEF/NTNU. These panels were tested at 4 different laboratories (SINTEF/NTNU in Trondheim, SINTEF in Oslo, Norwegian Public Roads Administration in Oslo and Mannvit in Iceland). The results from this Round Robin programme will be reported as a COIN-report later. Even though NB 7 prescribe that the panels shall be tested to a deflection of 30 mm, and the absorbed energy shall be summarized to 25 mm, the 5 panels tested at the laboratory in Trondheim were tested to 35 mm, and the normalized average curve of these 5 panels are shown in Figure 7-1. The average curve is normalized by dividing the absorbed energy by the absorbed energy at 25 mm, which makes it possible to calculate the absorbed energy at different deflections relative to the NB 7-result.

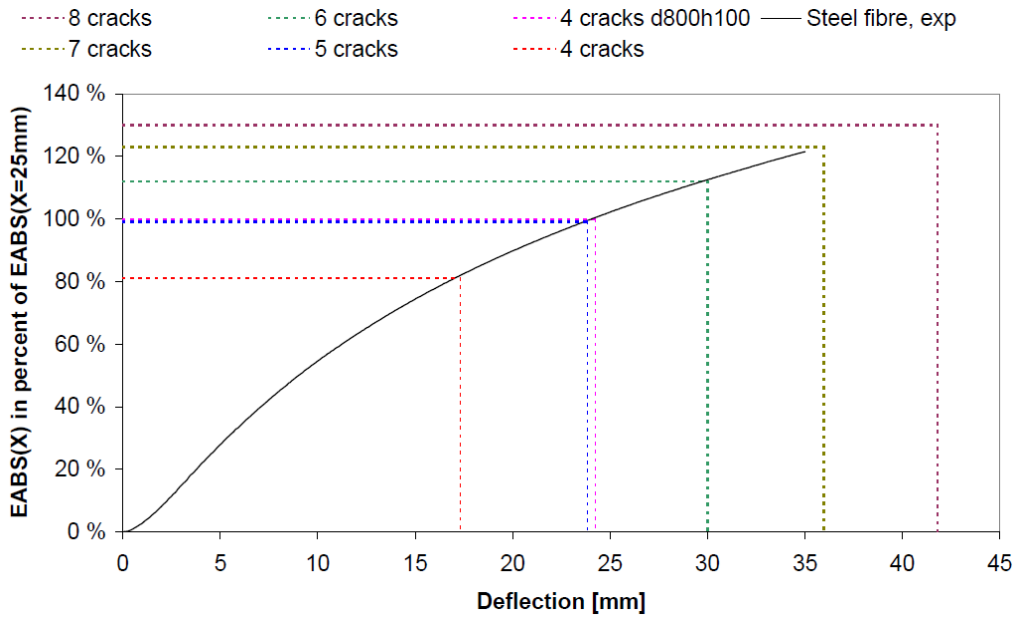

Figure 7-1 Normalized EABS, steel fibre reinforced panels tested according to NB 7 (2011) (Average of 5 panels)

In Table 7-2 the absorbed energy at the relevant deflection limits are summarized. These values are also illustrated graphically in Figure 7-1. The correction factors for absorbed energy in Table 7-2 are simply the correction factors from Table 7-1 multiplied by the belonging percentual values.

Table 7-2 Energy capacity at $\delta_{m,n}$ in percent of NB 7- results

Nr of cracks	EABS at $\delta_{m,n}$ in % of total EABS at 25 mm	$E_{corr}/E_{measured}$ [-]
4	81.0	0.608
5	99.0	0.594
6	112.0	0.560
7	123.0[1]	0.527
8	130.0[1]	0.488
d800h100, 4 cracks[2]	99.8	0.561

[1]Extrapolated from the EABS vs. deflection curve, the panels were tested to a deflection equal 35 mm
[2]Corresponds to a NS-EN 14488-5 panel with crack vs. support angle equal to 49º

To sum up, if a NB 7 panel have 5 cracks, the energy should be summarized to 23.84 mm deflection before corrected. The reported EABS are always summarized to 25 mm deflection, which means that reported EABS may be multiplied with 0.99 to find the EABS at 23.84 mm deflection, and thereafter by 0.600 to relate it to the ASTM values, or as shown in Table 7-2; the NB 7 result may just be multiplied with 0.594.

As already mentioned, [Bernard, E. S.(2005)] has found that friction contributes to about 15-20 % of the absorbed energy for panels tested according to ASTM C 1550, while [Bjøntegaard, Ø. (2009b)] has found the friction effect to be about 35 % for the NB 7 (2011) method. Because E_{corr} is corrected to be similar to the energy absorbed by ASTM-panels, and $E_{measured}$ is the energy absorbed according to NB 7, the expected ratios between them when the

difference in friction contributions are included are shown in Table 7-3 for the different number of cracks. The friction effect is named $k_{friction}$ in Table 7-3 and equation 7-1.

Table 7-3 Theoretical relation between results from panel tests according to NB 7 and ASTM C 1550

Nr of cracks	Ratio NB 7/ASTM	
	$k_{friction,ASTM}$: 0.2	$k_{friction,ASTM}$: 0.15
	$k_{friction,NB7}$: 0.35 – 0.40	$k_{friction,NB7}$: 0.35 – 0.40
4	2.03 – 2.19	2.15 – 2.33
5	2.07 – 2.24	2.20 – 2.38
6	2.20 – 2.38	2.34 – 2.53
7[1]	2.33 – 2.53	2.48 – 2.69
8[1]	2.52 – 2.74	2.68 – 2.91
d800h100, 4 cracks[2]	2.19 – 2.38	2.33 – 2.52

[1]Extrapolated from the EABS vs. deflection curve, the panels were tested to a deflection equal 35 mm

[2]Corresponds to a NS-EN 14488-5 panel with crack vs. support angle equal to 49º

The numbers in Table 7-3 are found by the following calculations:

- Consider the result from NB 7 test to be $E_{result,NB7}$
- The fibre contribution is: $E_{fibre,NB7} = (1-k_{friction,NB7}) \times E_{result,NB7}$
- The theoretical absorption capacity for an ASMT panel should then be: $E_{fibre,ASTM} = (E_{corr}/E_{measured}) \times E_{fibre,NB7}$
- And the result from a panel test performed according to ASMT C 1550 should then be $E_{result,ASTM} = E_{fibre,ASTM} /(1-k_{friction,ASTM})$

The NB 7 vs. ASTM relation can then be written as:

$$\frac{E_{result,NB7}}{E_{result,ASTM}} = \frac{1-k_{friction,ASTM}}{1-k_{friction,NB7}} \cdot \frac{E_{measured}}{E_{corr}} \qquad (7\text{-}1)$$

As seen from Table 7-3, a NS-EN 14488-5 panel with four cracks and a crack vs. support angle equal to 49 º, should theoretically have about the same capacity to absorb energy as a NB 7 panel with 6 cracks, if the friction effect does not change with the number of cracks.

Bjøntegaard has shown from an experimentally investigation that the EABS determined from square and round panels corresponds well [Bjøntegaard, Ø. (2009a)]. Based on the results from Table 7-3 this is not surprising, because:

- A square panel with four cracks, and crack vs. support angle equal to 90º shall theoretically have exactly the same capacity to absorb energy as a circular panel with four cracks
- A square panel with four cracks, and crack vs. support angle equal to 49º shall theoretically have almost equally capacity as a NB 7 panel with 6 cracks, and about 6 % larger capacity than a NB 7 panel with 5 cracks.

The author's experience from testing panels according to the 2003 revision of NB 7 is that 6 cracks are not unusual for fibre reinforced panels designed for EABS equal to 1000 J, even though 4 or 5 cracks are most common for synthetic fibre reinforced panels. As shown in Table 5-8, the largest number of cracks in the steel fibre reinforced NB 7 panels in that series was 7. In the long run, one might expect square panels to show larger absorption capacity than circular panels, but the square vs. circular ratio (4 cracks) is not larger than the 4 cracks vs. 6

cracks ratio for NB 7 panels, which means that the difference will most likely be "hidden" in the "within series" scatter. If experience from the 2011 revision of NB 7 shows that, the number of cracks is limited to 4 or 5, it seems more reasonable to find square panels to absorb more energy. In that case, a reduction factor for square panels should be implemented in NB 7 if square panels shall be allowed instead of circular ones.

Bernard has examined the relation between ASTM-panels and EFNARC-panels experimentally by testing in total 372 panels [Bernard, E. S. (2002)], which may be used to compare the experimental relation with the theoretical relation described earlier. Panel tests according to the EFNARC Guidelines [EFNARC (1999)] are in principle identical to panel tests according to NS-EN 14488-5, which means that argument that holds for EFNARC panels should also hold for NS-EN 14488-5 panels. The EFNARC vs. ASTM relation from [Bernard, E. S. (2002)] is shown graphically in Figure 7-2.

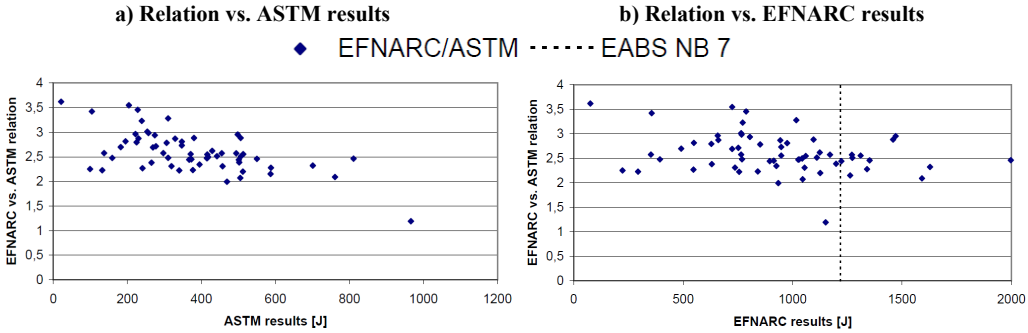

Figure 7-2 Relation between energy absorption capacity from tests according to EFNARC and ASTM C 1550 [Bernard (2002)]

The theoretical NB 7 vs. ASTM C 1550 relations shown in Table 7-3 are in quite good agreement with the empirical relation found by Bernard. The average absorption capacity for the 5 panels tested to find the average curve in Figure 7-1 was 1218 J. As seen in Figure 7-2b), the EFNARC vs. ASTM relation from Bernard's investigation was about 2.5 when the EFNARC result was about 1218 J, which is in good agreement with the prediction from Table 7-3. Another interesting finding is that the EFNARC vs. ASTM relation seems to decrease slightly by increasing ASTM result.

8 Ductile high tensile strength all round concrete

8.1 Introduction

The main goal of this experimental work was to develop fibre reinforced concretes, which show strain hardening behaviour in bending, and are suitable for use in load carrying concrete structures. The title of the chapter reflects that this is a step towards the overall goal of the fibre project in COIN, which is to develop concretes with very high residual strengths.

Three criterions may be stated to have a successful concrete mix:

1. Strength criterion; the post cracking strength shall be larger than the cracking strength.
2. Ductility criterion; the deformation at maximal load must be relatively large.
3. Practical concrete criterion; the concrete must be possible to use in the field.

The strength criterion ensures that a given concrete structure has sufficient capacity even if the concrete cracks due to shrinkage or other imposed deformations. The deformation criterion ensures that the ductility is sufficient. The practical concrete criterion ensures that the concrete is possible to use by contractors in real structures. With high dosages of fibres, the workability of the concrete is reduced. If fibre reinforcement shall be used as structural reinforcement, the fibre amount has to be relatively large, and therefore influence the workability of the concrete. To make SCC with fibre amounts necessary to fulfil criterion 1) and 2) is very difficult because the fibres reduce the workability, which is why the practical concrete criterion is stated.

Beam tests according to NS-EN 14651 were used to decide whether the strength- and ductility criterion is fulfilled. Whether the different concrete mixes are applicable in real constructions is evaluated based on the experience when the beams were cast.

The particle-matrix model, described by Mørtsell [Mørtsell (1996)], was used when the mix designs were worked out. In the particle-matrix model, the concrete is considered a two-phase composite; the particle phase and the matrix phase. The particle phase is considered to be a friction material, while the matrix phase is considered to be a viscous material. Because the particles with maximum particle size, d_{max}, less than 125 μm has shown to influence the concrete properties basically due to its effective volume, surface properties and total surface area, these particles are considered to be within the matrix phase [Mørtsell (1996)]. The particle phase contains all solids with d_{max} larger than 125 μm, and the matrix phase contains all liquids and particles with d_{max} less than 125 μm. The particle-matrix model assumes that the rheological properties of the concrete may be expressed as a function of the properties of the particle and the matrix phases and the volume relations between them.

There are several papers available in the literature regarding fibre reinforced concrete with high tensile strength and large strain capacity. Jorun Marie Hisdal has made a state of the art report on this topic [Hisdal (2011)], and the most important finding with regard to the *ductile high tensile strength all round concrete*-project is that it is essential to reduce the maximum aggregate size to reduce the concrete porosity. In Norway, at least, cement composite where the maximum aggregate size is less than 4 mm is called *mortar* [Maage (2003)], while the name *concrete* is used when d_{max} is at least 8 mm.

What seems to be less investigated is the possibility to make an all round fibre reinforced concrete with high enough post-cracking tensile strength to be used as an alternative to

ordinary reinforced structures. The principle of minimum reinforcement ratio according to EC 2 is that the steel reinforcement shall be able to carry the tensile stresses that are released when the concrete cracks. If this principle is used for beams tested according to NS-EN 14651, it means that the capacity after cracking must be at least as large as when cracking occurs. It seems therefore obvious that it should be easier to make such a concrete if the cracking capacity is not to large. Li et al. have shown that the sand content must be limited in the matrix mix for design of a strain hardening composite [Li et al. (1995)], and that low matrix toughness is favourable for multiple cracking [Li et al. (1992)]. Even though Li's study [Li et al. (1995)] was based on cementitious composites where d_{max} of the sand was less than 0.3 mm, it is possible that reducing d_{max} from 16 mm to 8 mm will have beneficial effect on the post cracking behaviour.

The experience from several tests at NTNU and the results from pull-out tests on single fibres reported in chapter 3, show that the synthetic fibres need larger deformations to be fully effective than steel fibres. Steel fibres on the other hand may give a large increase in capacity at small deformations, and then show a reduced capacity, which may result in a strain softening behaviour. It seems reasonable that it might be possible to utilize the best properties of different fibre types by combining them.

To reach the goal of a ductile high tensile strength all round fibre reinforced concrete it was decided to start with making a concrete with low compressive strength to reduce the cracking stress, and thereby reduce the necessary residual flexural strength of the fibre reinforced concrete to fulfil the strength and ductility criterion. First after finding a concrete- fibre composition that fulfils these criterions, the work should continue with concretes with higher compressive and tensile strengths.

So far, the *ductile high tensile strength all round concrete* project involves concrete mixes in three strength classes:

1. C25/20; the ductile low tensile strength concrete
2. C45/35; the ductile medium tensile strength concrete
3. C75/60; the ductile high tensile strength concrete

This *ductile high tensile strength all round concrete* project is part of a larger experimental work, which also involves replacing cement with limestone powder, fly ash, calcined clay or a combination of them [Vikan et al. (2011)]. The numbering of concrete mixes in the present chapter follows the numbering in [Vikan et al. (2011)] for simplicity reasons. The total parameter variations of the original experimental work are shown in Table 8-1.

Table 8-1 Parameter variations in the original work [Vikan et al. (2011)]

Mix no.	d_{max}	Paste [l/m^3]	Matrix [l/m^3]	Cement [vol%]	Fly ash [vol%]	Limestone powder [vol%]	Clay [vol%]	Silica fume [vol%]
11	8 mm	346	393	80	-	20	-	-
12	16 mm	339		100	-	-	-	-
13				70	-	30	-	-
14					20	10	-	-
15					-	10	20	-
16					-	20	10	-
17					-	20	-	10

The 11 mix (with reduced d_{max}) was added to the parameter variation after deciding the parameter variation of mix 12-17. At that stage it was not decided which mixes that should be further analyzed, and because reduced CO_2-emission due to reduced cement consumption is one focus area within COIN [Hammer (2011)], it seemed reasonable to replace 20 % of the cement also in mix 11. For sure, to address the difference in behaviour in bending tests to the aggregate size, it would have been better to make the concrete with reduced d_{max} more similar to the 12-mix. Nevertheless, the final composition might have been somewhat different anyway, because replacing the 8-16 mm fraction with the 0-8 mm fraction increases the total content of fines.

8.2 Ductile low tensile strength concrete

As already mentioned, it was decided to start with making a concrete with low compressive strength to reduce the cracking strength, and thereby to reduce the necessary residual flexural tensile strength of the FRC to fulfil the strength criterion. Large aggregate may have aggregate interlocking effects in cracks, which increase the revealed energy when the concrete cracks. To investigate this effect for this FRC, concrete with d_{max} 8 mm and 16 mm named concrete 11 and concrete 12, respectively were made.

Based on the experience from earlier tests on fibre reinforced concrete, Dramix 6560 and Barchip Shogun were used as fibre reinforcement. From the experimental work on, and analyzes of, the results from pull-out behaviour reported in chapter 3 also a combination of these two fibre types was tested. The fibre content in the different mixes is shown in Table 8-2.

Table 8-2 Fibre contents for the ductile low tensile strength concrete

	Synthetic fibre		Metallic fibre			
	Barchip Shogun (S)		Dramix 6560 (M)		Dramix 6535 (M2)	
Concrete mix no	[vol%]	[kg/m^3]	[vol%]	[kg/m^3]	[vol%]	[kg/m^3]
11-ref, 12-ref	-	-	-	-	-	-
11-1, 12-1	0.5	4.6	-	-	-	-
11-2, 12-2	1.0	9.1	-	-	-	-
11-3, 12-3	-	-	0.5	39.0	-	-
11-4, 12-4	-	-	1.0	78.0	-	-
11-5, 12-5	0.5	4.6	0.5	39.0	-	-
11-16[1]	-	-	0.5	39.5	0.5	39.5
11-17[1]	0.5	4.6	-	-	0.5	39.5
[1]These two mixes were made after analyzing the results from the others.						

Because the fresh properties of the concrete are strongly influenced by the volume relation between the particle phase and the matrix phase, it was decided to keep the matrix volume constant. To have sufficient matrix volume with reduced amount of cement and water, the 11-series was made with replacing 20 % of the cement with limestone. From the results in chapter 3 it was found that the fibres' pull-out resistance increases with increasing limestone amount, which also should result in increased residual flexural strength.

The mix designs for the two mixes of *the ductile low tensile strength concrete* are shown in Table 8-3.

Table 8-3 Mix design concrete 11 and concrete 12, the ductile low tensile strength concrete

	Concrete 11-ref	Concrete 12-ref
Compressive strength (f_{ccm}) [MPa]	23	33
w/(c+Σkp)	0.79	0.74
Cement type	CEM I 42.5 R	CEM I 42.5 R
Super plasticizer[1]	1.3	1.3
Stabilizer[1]	1.4	1.33
Matrix volume[2]	**393**	**393**
Paste volume[2]	346	339
v/p[3]	0.47	0.51
d_{max} [mm]	8	16
Cement [kg/m^3]	286.8	318.8
Limestone [kg/m^3]	71.7	0
Aggregate 0-2mm [kg/m^3]	254.4	480.4
Aggregate 0-8mm [kg/m^3]	1441.6	600.5
Aggregate 8-16mm [kg/m^3]	0	633.5

[1] % of cement content
[2] Litre/m^3 concrete
[3] water/powder. Powder = particles with d_{max} <125μm

As seen from Table 8-3, the mix design of 11-ref and 12-ref deviates not only by the maximum aggregate size, which makes it somewhat difficult to claim that the difference in hardening properties is only due to the aggregate size. As concrete 12 had higher compressive strength and higher cement content, it is expected that this mix should have larger bond to the fibres. On the other hand, the v/p-ratio was somewhat larger and the paste volume was somewhat less, which may lead to the opposite behaviour with respect to the concrete vs. fibre bond.

8.2.1 Results ductile low tensile strength concrete

8.2.1.1 Fresh properties and compressive strength

The slump, slump flow, air content and density were measured for all mixes, and the results are shown graphically in Figure 8-1. The compressive strengths, measured on 100×100×100 mm cubes after 28 days of curing in 20º C water, are summarized together with the fresh concrete properties in Table 8-4.

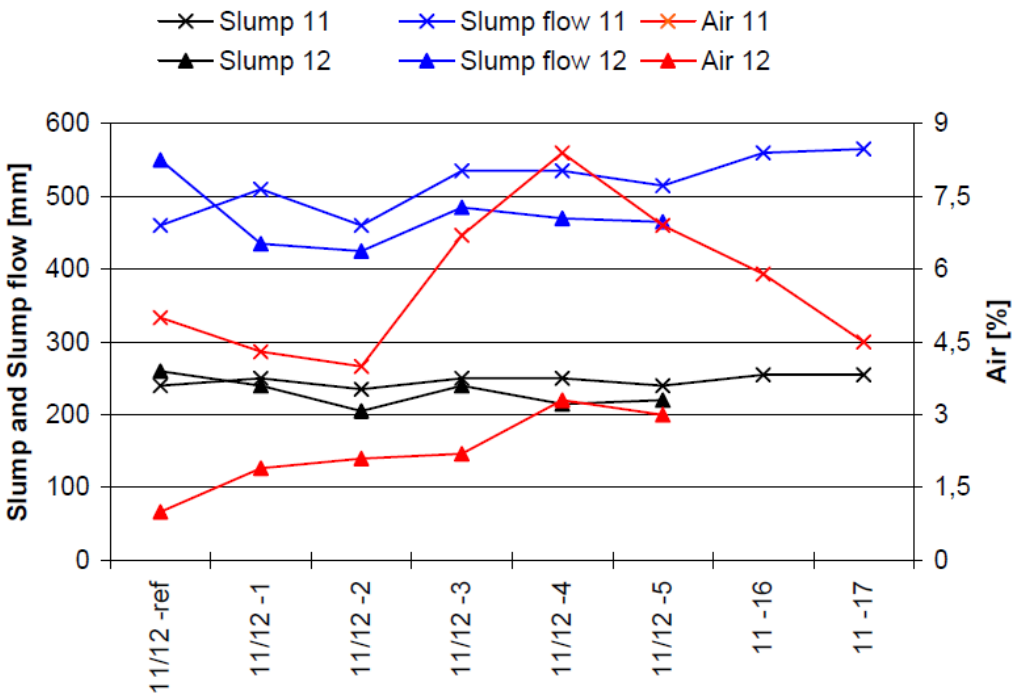

Figure 8-1 Slump, slump flow and air content for the ductile low tensile strength concrete

One interesting observation is that for the 11-series, the slump value was more or less constant even though the fibre content varied. The slump flow was actually larger with fibres than without, except the 11-2 mix where the slump flow was equal to the reference mix. The 12-series had more expected behaviour; both the slump and the slump flow decreased when fibres were added to the concrete.

Table 8-4 Fresh concrete properties and compressive strength for the ductile low tensile strength concrete

Mix no.	Slump (mm)	Slump flow (mm)	Air (%)	Density (kg/m^3)	f_{ccm} [MPa]	Strength relative to ref mix [%]
11-ref	240	460	5.0	2225	23	**ref**
11-1	250	510	4.3	2225	29	126
11-2	235	460	4.0	2215	27	117
11-3	250	535	6.7	2205	25	109
11-4	250	535	8.4	2195	25	109
11-5	240	515	6.9	2195	25	109
11-16	255	560	5.9	2260	27	117
11-17	255	565	4.5	2255	29	126
12-ref	260	550	1.0	2330	33	**ref**
12-1	240	435	1.9	2305	33	100
12-2	205	425	2.1	2290	32	97
12-3	240	485	2.2	2315	33	100
12-4	215	470	3.3	2300	30	91
12-5	220	465	3.0	2300	31	94

As seen from Table 8-4, the compressive strength in the 11-series increased by adding fibres, while the compressive strength in the 12-series was slightly reduced. One possible explanation of this suggested by [Vikan et al. (2011)] is that 11-mix without fibre addition was unstable and had tendency of segregation. Addition of fibre might have increased the stability of the mixture. Increased stability combined with thorough mixing might have ensured that homogenous samples of mixture 11-1 to 11-5 were cast. Increased compressive strength with the addition of fibre might thus be an effect of improved stability by fibre addition.

Regarding the practical concrete criterion, all mixes were considered to have good enough workability and stability for use in real concrete structures.

8.2.1.2 Flexural bending strength

Reference mix without fibres

The *flexural tensile stress vs. CMOD* curve for the reference beams are shown in Figure 8-2.

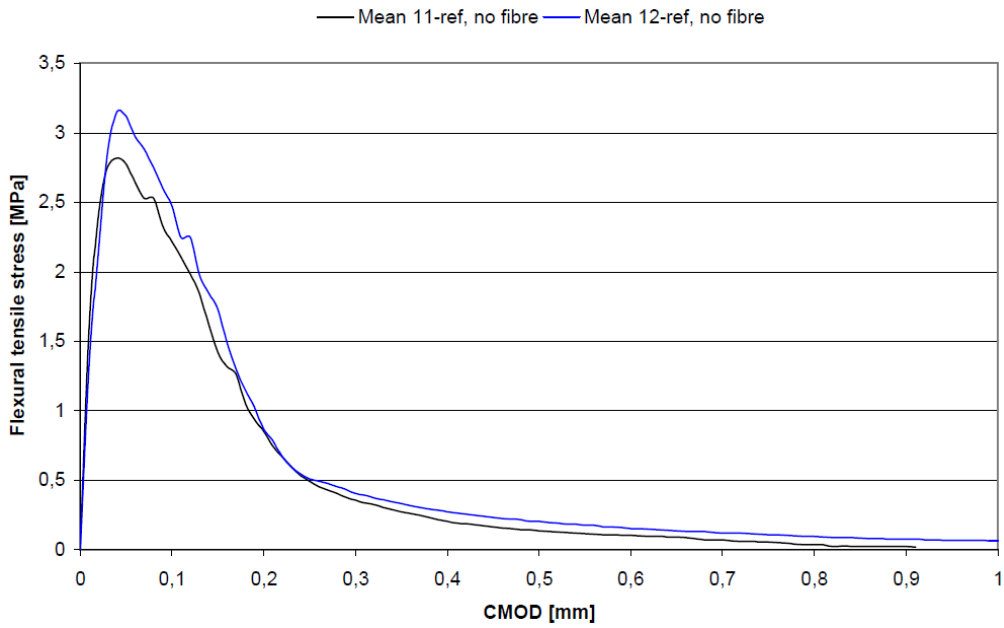

Figure 8-2 Mix 11 and 12, without fibres

The concrete made of mix 12 had higher compressive strength and cracking stress, which is not surprising due to the lower v/b-ratio. The calculated flexural tensile strength according to equation 3.23 in [EC 2] is 2.9 MPa and 3.3 MPa for the 11-ref and 12-ref respectively (if the average strengths in Table 8-4 are considered to be f_{cm}), which is quite close to the measured flexural tensile strength (2.8 and 3.2 MPa).

To show the effect of adding fibres to the concrete, the reference curve is shown together with the flexural tensile stress vs. CMOD curve for the beams with various fibre additions. For simplicity reasons only the *mean 11-ref* curve is shown.

Mix 11 and 12 with various fibre amounts

The *flexural tensile stress vs. CMOD curve* for the different beams made of Mix 11 and Mix 12 are shown in Figure 8-3.

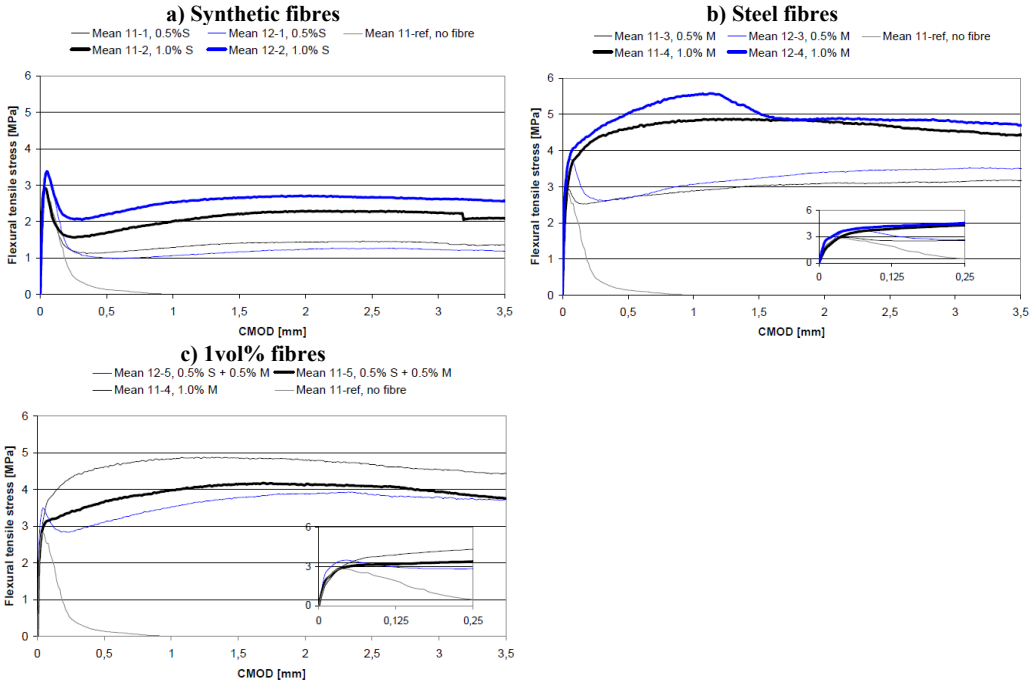

Figure 8-3 Effect of d_{max} and fibre type/dosage on the flexural stress vs. CMOD relation

In general, the 11-series had lower cracking stress than the 12-series, which is expected from the tests on the reference beams. The stress vs. CMOD curve for all beams follows the corresponding curve for the reference beams up to the point of cracking, while the beams reinforced with synthetic fibres also follow the curve for the reference beams beyond the cracking point. The reason for the former is most likely that fibres do not significantly contribute to the pre-cracking behaviour unless the fibre dosage is larger than about 1.0 vol%, while the latter can be explained by the need of relatively large crack widths to activate the synthetic fibres, a matter that is discussed in detail in chapter 3.

With regard to the strength criterion, none of the beams reinforced with only synthetic fibres had larger capacity in the post-cracking stage than at cracking, as shown in Figure 8-3a), which means that they failed this criterion. For the beams reinforced with only steel fibres shown in Figure 8-3b), both mixes with 0.5 vol% steel fibre had their maximum capacity at CMOD larger than 3.5 mm. However, these two mixes had a pronounced drop in capacity immediately after cracking, which may lead to crack localization in larger structures, and are therefore considered not to fulfil the ductility criterion. The 12-4 mix, containing 1 vol% steel fibre, had a pronounced drop in capacity at CMOD around 1.2 mm, which is considered unfavourable. This means that the 11-4 mix is considered to have the best behaviour of the mixes with only steel fibres.

Figure 8-3c) shows the flexural tensile stress vs. CMOD curve for the beams reinforced with a combination of steel and synthetic fibres, together with the 11-4 curve (1 vol% steel fibre).

The 12-5 mix containing 0.5 vol% of both fibre types had a drop in capacity, which is considered disadvantageous, and is therefore considered not to fulfil the ductility criterion. The 11-5 mix containing 0.5 vol% of both fibre types had less maximum capacity than the 11-4 mix, but the maximum capacity occurred at a larger CMOD. Even though the 11-4 mix fulfilled both the strength- and ductility criterion and had higher maximum capacity than the 11-5 mix, the 11-5 mix was considered to have the most promising behaviour due to the larger CMOD at maximum capacity.

The pull-out tests on Dramix 6535 fibres, reported in chapter 3 indicates that Dramix 6535 might improve the residual tensile strength at small deformations. Beam tests on concrete 11-5, which had a combination of 0.5 vol% Dramix 6560 and 0.5 vol% Barchip Shogun, showed that the residual tensile strength was slightly increasing from concrete cracking to a CMOD of 1.75 mm. To see if Dramix 6535 was able to increase the residual tensile strength at CMOD less than 1.75 without reducing the ductility, it was decided to cast and test beams where the Dramix 6560 fibres were replaced with Dramix 6535 fibres. In addition, beams reinforced with a combination of Dramix 6560 and Dramix 6535 were cast and tested. By performing these two combinations, it is also possible to figure out if the predictions from pull tests are correct. The compressive strength of the two mixes with shorter steel fibres (mix 11-16 and 11-17) was somewhat larger than the compressive strength of the other two mixes with steel fibres.

The results from the beam tests on mix 11-16 and 11-17 are shown in Figure 8-4.

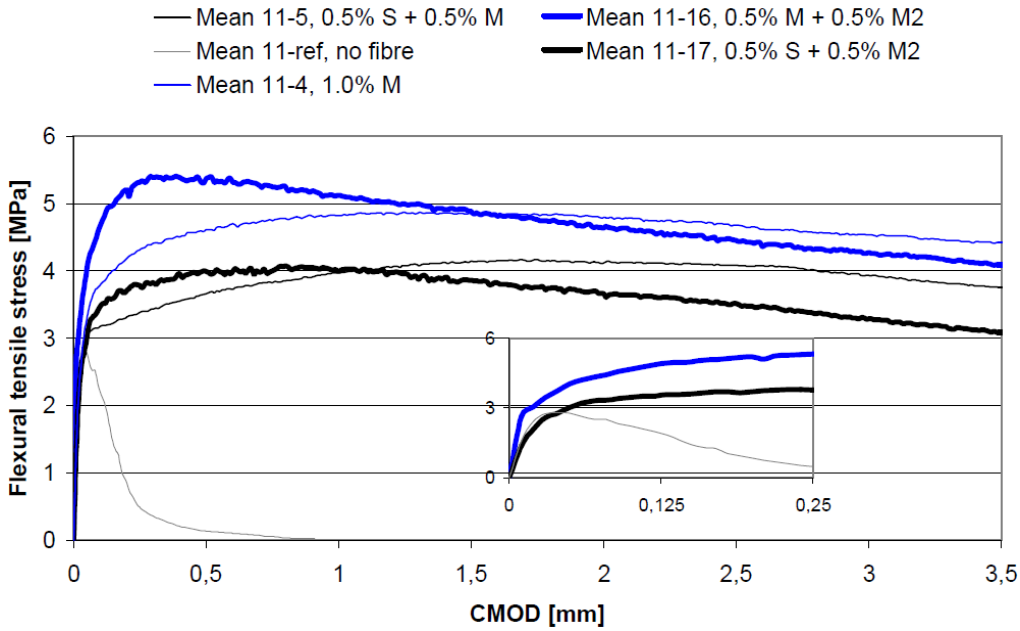

Figure 8-4 Dramix 6535 in combination with Dramix 6560 and Barchip Shogun

By replacing the synthetic fibres with short steel fibres (mix 11-16) it seems like also the pre-cracked behaviour is somewhat affected by adding fibres, and the maximum capacity was increased to around 5.5 MPa. When comparing the two blue curves, which means that the longer Dramix fibres are partly replaced by the shorter Dramix fibres, it is clear that the shorter Dramix fibres contributed to an increase in the capacity at small CMODs, and that the

capacity at larger deformations were reduced. When comparing the two black curves, which means that the longer Dramix fibres are replaced with the shorter ones when the concrete in addition contains synthetic fibres, the maximum capacity was almost not changed, but the maximum capacity occurred at less CMOD. It seems quite clear that the ductility is reduced when the longer Dramix fibres are replaced with the shorter one.

The total impression is that the shorter Dramix fibres are able to increase the flexural tensile strength at small CMODs, but at the same time, the ductility is reduced.

8.3 Ductile medium tensile strength concrete

Based on the results with the ductile low tensile strength concrete, it was decided to proceed with the concrete with reduced d_{max}, and combination of steel and synthetic fibres. Experience at NTNU shows that a maximum fibre content exist at which a further increase in fibre content does not result in increased flexural bending strength [Lauvålien and Sandbakk (2007)]. The reason for this is not fully understood, but one suggestion is that when the fibre content is sufficiently large, the average distance between the fibres, represented by Δc_f in chapter 3.8, is small enough for the fibres to create a collective cone shaped concrete failure.

The following approach can be used if the models and corresponding assumptions from chapter 3.7 to chapter 3.9 are correct.

It was shown in chapter 3.7.1 that if the Dramix 6560 fibres have an embedment length less than 5.8 mm, a cone shaped concrete failure is expected to take place in concrete with tensile strength equal to 3 MPa. From the calculation model in Figure 3-11 this means that the minimum radius of the cone also is 5.8 mm, resulting in a minimum distance between neighbouring fibres to avoid a collective cone shaped concrete failure of about 11.6 mm. For a steel fibre content of 2.0 vol% the average distance between the fibres according to equation 3-15 in chapter 3.8 is about 12 mm. The minimum embedment length to avoid a cone shaped concrete failure according to equation 3-12 is 6.5 mm for a fibre with $\sigma_{f,0}$ = 520 MPa and f_{ct} = 2.2 MPa, resulting in a minimum distance between the fibres of 13 mm.

$\sigma_{f,0}$ = 520 MPa is chosen from pull-out tests on Dramix 6560 fibres embedded in concrete A as reported in chapter 3.2.1 and f_{ct} = 2.2 MPa is chosen from EC 2, table 3-1, (f_{ctm} for a concrete in class C 20/25). These values are considered relatively correct for the *ductile low tensile strength concrete*.

If the average distance between neighbouring fibres are less than the minimum cone diameter necessary to avoid a cone shaped concrete failure, it seems reasonable that the maximum fibre content is reached. For the low strength ductile concrete the calculations above indicates that adding 2 vol% steel fibres will not increase the flexural tensile strength. The obvious choice is then to increase the concrete's tensile strength, leading to the *ductile medium tensile strength concrete*.

It is shown in chapter 3 that increasing the compressive strength results in larger maximum fibre stress. It is therefore expected that the residual flexural tensile strength will increase when the concrete strength is increased for a given fibre content. This is like balancing on a double-edged sword: if the cracking strength is increased more than the residual flexural strength, the strength criterion will not be fulfilled. Once again, by using equation 3-12 and considering l_b=$r_{cone,min}$, the relative increase in maximum fibre stress, $\sigma_{f,0}$, must be less than

the relative increase in the concrete tensile strength, f_{ct}, to increase the maximum fibre content. The *ductile medium tensile strength concrete* was designed to have a compressive strength of about 45 MPa, resulting in a tensile strength of 3.2 MPa according to EC 2, which result in an increase in tensile strength of about 45 % compared to the *ductile low tensile strength concrete*. From pull-out tests on single fibres, Dramix 6560 fibres embedded in concrete in strength classes up to C70/85 had maximum fibre stress about 700 MPa, which is a relative increase in fibre stress of about 35 %.

Even though the above mentioned approach is based on several simplifications (for instance that all fibres are orientated in one of the three principal directions and never in the intermediate directions, and that the fibre centres are evenly distributed), this model predicts that the maximum fibre content should increase when the compressive strength is increased to 45 MPa. This means that it might be possible to increase the capacity also when adding 2 vol% steel fibres to the medium strength concrete.

The *ductile medium tensile strength concrete* is called concrete 21, because it is based on the mix design of concrete 11. The matrix volume and the ratio limestone/cement were kept constant and the d_{max} was kept at 8 mm. The mix design of concrete 21 is shown in Table 8-5, and the investigated fibre combinations are shown in Table 8-6.

Table 8-5 Mix design concrete 21

	Concrete 21-ref
Compressive strength (f_{ccm}) [MPa]	47
w/(c+Σkp)	0.65
Cement type	CEM I 42.5 R
Super plasticizer[1]	1.3
Stabilizer[1]	0.44
Matrix volume[2]	**393**
Paste volume[2]	334
v/p[3]	0.37
d_{max} [mm]	8
Cement [kg/m^3]	313.7
Limestone [kg/m^3]	78.4
Aggregate 0-2mm [kg/m^3]	259
Aggregate 0-8mm [kg/m^3]	1467.8
[1] % of cement content [2] Litre/m^3 concrete [3] water/powder. Powder = particles with d_{max} <125µm	

Table 8-6 Fibre content, ductile medium tensile strength concrete

Concrete mix no	Plastic fibre		Steel fibre			
	Barchip Shogun		Dramix 65/60		Dramix 65/35	
	Vol%	kg/m^3	Vol%	kg/m^3	Vol%	kg/m^3
21-ref	-	-	-	-	-	-
21-1	0.5	4.6	0.5	39.0	-	-
21-2	1	9.1	1	78.0	-	-
21-3	-	-	2	156.0	-	-

The *ductile low tensile strength concrete* mix with the most promising behaviour was the mix with both steel and synthetic fibres, so it was decided to continue with a combination of these

two fibre types, and in addition to see whether 2 vol% really gave the expected increase in capacity.

8.3.1 Results ductile medium tensile strength concrete

8.3.1.1 Fresh concrete properties and compressive strength

The slump, air content, and density were measured for all mixes, while the slump flow was only measured for the reference concrete and mix 21-1. The fresh concrete properties and the compressive strengths are shown in Table 8-7.

Table 8-7 Fresh concrete properties and compressive strength for the ductile medium tensile strength concrete

Mix no.	Slump (mm)	Slump flow (mm)	Air (%)	Density (kg/m^3)	f_{ccm} [MPa]	Strength relative to ref mix [%]
21-ref	260	625	5.5	2260	47	100
21-1	255	590	3.2	2310	45	96
21-2	215	-[1]	3.5	2335	45	96
21-3	160	-[1]	3.6	2420	49	104
[1]The slump flow was not measured because the concrete cone collapsed due to high amount of fibre						

The slump flow tests on mix 21-2 and 21-3 might have been more successful if the concrete had not been treated as a SCC. Slump flow tests on SCC according to NS-EN 12350-8 shall be performed without tamping the concrete with a tamping bar, in contrast to slump flow tests on ordinary concrete according to NS-EN 12350-5.

The compressive strength for the 21-ref mix was 47 MPa, and the deviation with regard to the various fibre contents was less pronounced than for the 11-mixes. This supports the assumption by [Vikan et al. (2011)] regarding the increased compressive strength with the addition of fibre due to improved stability.

The workability of the 21-1 mix seemed to be quite good. The 21-2 mix had better workability than the slump flow test indicates. When this concrete was slightly vibrated by tamping the surface, it levelled out quite well. While filling the beam moulds, it seemed like the friction between the fibres was easily overcome by the energy that is applied by filling them. With regard to the practical concrete criterion, the 21-1 mix was considered a suitable concrete, while the 21-2 mix was considered somewhat more problematic, but still good enough. The 21-3 concrete on the other hand, was considered to fail the practical concrete criterion.

8.3.1.2 Flexural bending strength

The results from bending test on the ductile medium tensile strength concrete are shown in Figure 8-5.

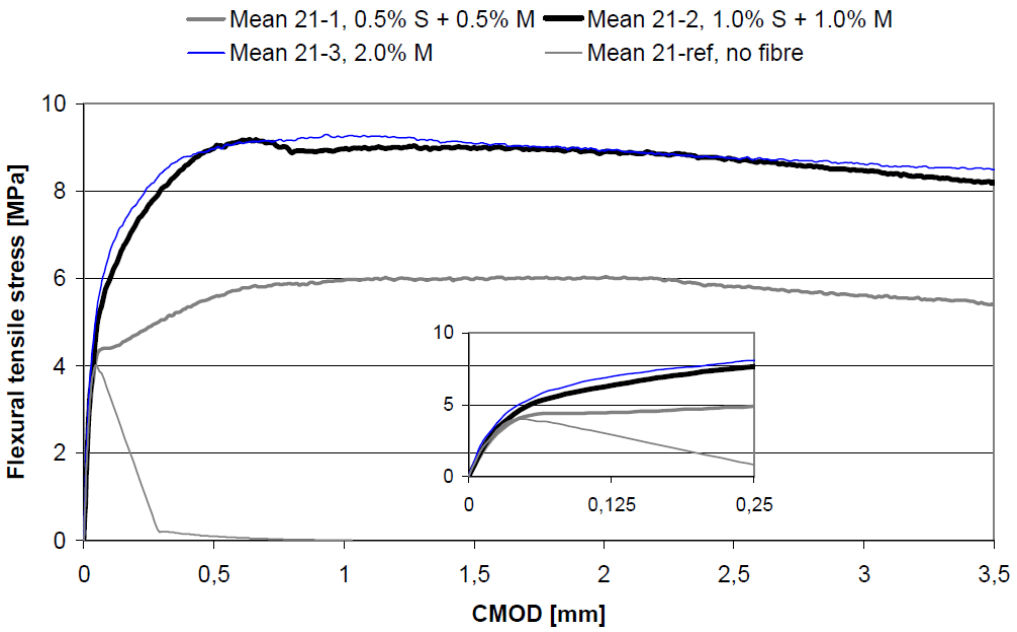

Figure 8-5 Mix 21, ductile medium tensile strength concrete with different fibre alternatives

The flexural bending stress at cracking was about 4 MPa, which again is almost exactly as the flexural bending strength according to EC 2. As for the mixes with the *ductile low tensile strength concrete,* the stress vs. CMOD curve for all beams follows the curve for the reference beams at small CMODs. When the X-axes are scaled to the CMOD range of 0 - 0.25 mm it is possible to see that the 21-1 mix actually follows the reference curve up to cracking, and that also the two other curves have a pronounced change in stiffness at approximately the same CMOD as when the reference beams reached their maximum capacity.

With regard to the strength- and ductility criterions, all mixes fulfilled both criterions. Even though the 21-2 mix had a drop in capacity, which was considered unfavourable when ranging the 12-mixes, this mix is considered to be better than the 21-3 mix, simply because the 21-3 mix had larger scatter and failed the practical concrete criterion. The large scatter in results from beam tests on the 21-3 mix may be due to the workability problems, or it might also be because the maximum fibre content as described in the beginning of chapter 8.3 was reached also for this concrete.

The *low strength ductile concrete* with 0.5 vol% Dramix 6560 and 0.5 vol% Barchip Shogun (Mix 11-5) and the *medium strength ductile concrete* with 1.0 vol% Dramix 6560 and 1.0 % Barchip Shogun (Mix 21-2) were the two most promising mixes. To further investigate if these concretes are capable of carrying loads similar to ordinary bar-reinforced concrete, larger beams and plates were cast and tested. This work have been organized as master theses for three students at NTNU [Nordhus, Steinnes and Simpson (2011)], and will be presented in chapter 8.7.

8.4 Ductile high tensile strength concrete

The for the time being last stage in the *ductile high tensile strength all round concrete* project involves a concrete with even higher compressive strength than the two previous concretes (v/b-ratio 0.45), which may be regarded as the *high strength ductile concrete*. Normally high strength concrete is used for concrete with even higher compressive strength, but the *low*-, *medium*- and *high*- prefixes makes the notation in the present chapter easier.

As for the *ductile medium tensile strength concrete*, mix 11-ref was the basis for the mix design of the *ductile high tensile strength concrete.* At first attempt (31-ref-1), the matrix volume and the ratio limestone/cement were kept constant and the d_{max} was kept at 8 mm, at the same time as the v/b-ratio was reduced from 0.65 to 0.45. To make this mix workable at all, the dosage of super plasticizer had to be approximately 9 % of cement weight, which is far greater than the recommended maximum dosage of 1.2 % [Rescon Mapei]. The measured slump flow of this first attempt was 690 mm (after adding 9 % super plasticizer).

In the second attempt, it was decided not to use limestone powder. The limestone powder was added in the *ductile low tensile strength concrete* to increase the stability by increasing the fines without increasing the compressive strength. In the *ductile high tensile strength concrete,* it was clear that there were no stability problems, and there were neither a need for keeping the strength as low as possible. Instead of limestone powder, silica fume was added to keep the v/p-ratio high enough to have a workable concrete without increasing the matrix volume. A second advantage of using silica fume is the favourable effect on the compressive strength compared to the same amount of cement. The slump flow for this second attempt (mix 31-ref-2) was 710 mm, and a visual evaluation of both the stability and the workability was satisfactory for the purpose of this project.

The mix designs for the two attempts on the *high strength ductile concrete* (Concrete 31-ref-1 and Concrete 31-ref-2) is shown in Table 8-8.

Table 8-8 Mix design concrete 31

	Concrete 31-ref-1	Concrete 31-ref-2
Compressive strength (f_{ccm}) [MPa]	Never tested	Never tested
w/(c+Σkp)	0.45	0.45
Cement type	CEM I 42.5 R	CEM I 42.5 R
Super plasticizer[1]	9	2.7[4]
Stabilizer[1]	-	-
Matrix volume[2]	**393**	**393**
Paste volume[2]	334	337
v/p[3]	0.27	0.36
d_{max} [mm]	8	8
Cement [kg/m^3]	386.2	368.0
Limestone [kg/m^3]	96.5	-
Silica fume [kg/m^3]	-	36.8
Aggregate 0-2mm [kg/m^3]	259	259
Aggregate 0-8mm [kg/m^3]	1467.8	1467.8
Aggregate 8-16mm [kg/m^3]	-	-

[1] % of cement content
[2] Litre/m^3 concrete
[3] water/powder. Powder = particles with d_{max} <125µm
[4] 2.7% is also larger than the recommended maximum dosage, but the risk of segregation was considered to be low

Based on the results from beam tests of the *ductile medium tensile strength concrete*, it was decided to keep the Dramix fibre content at 1 vol% and to increase the Barchip fibre content to 2 vol%.

8.4.1 Results ductile high tensile strength concrete

8.4.1.1 Fresh concrete properties and compressive strength

For the *ductile high tensile strength concrete*, the slump flow was the only fresh concrete property that was measured. Due to time limitations, cubes for strength determination were only cast for the final mix including fibres. The air content, density and slump value were not measured for any of the mixes.

The fresh concrete properties and the compressive strength that were measured are shown in Table 8-9.

Table 8-9 Fresh properties and compressive strength for the ductile high tensile strength concrete

Mix no.	Slump (mm)	Slump flow (mm)	Air (%)	Density (kg/m^3)	f_{ccm} [MPa]	Strength relative to ref mix [%]
31-ref-1	-[1]	690	-[2]	-[2]	-	-
31-ref-2	-[1]	710	-[2]	-[2]	-	-
31-1	-	690	-	-	76	**ref**

[1]The slump was not measured because the slump flow was so large
[2]Not measured

8.4.1.2 Flexural bending strength

The flexural tensile stress vs. CMOD curve for the *ductile high tensile strength concrete* is shown in Figure 8-6.

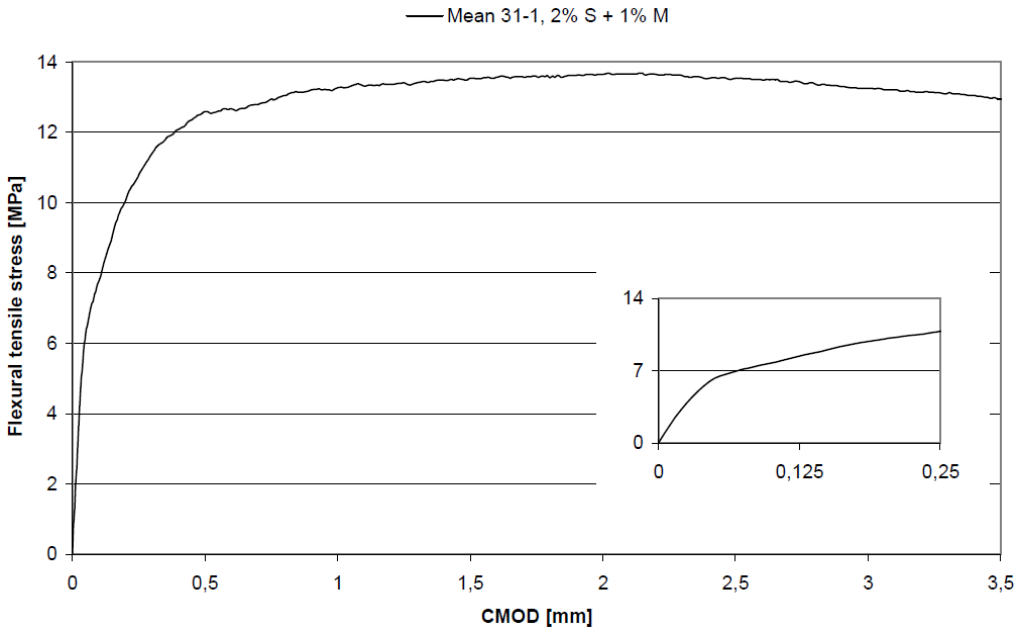

Figure 8-6 Mix 31, High strength ductile concrete

The flexural tensile stress at cracking was of about 6.3 MPa, which is somewhat larger than according to EC 2, and the residual flexural tensile stress increased until a CMOD of about 2 mm.

8.5 General observation from small beam tests

During testing of the beams made of mix 21-2, 21-3 and 31-1, it was not possible to see any crack in the beams even though it was clear from the load vs. deflection curve (which was drawn simultaneously) that the stiffness was changed. The author's opinion on this matter is that the CMOD vs. deflection relationship according to NS-EN 14651 (and all other CMOD vs. deflection relationships based on rigid body movement), must be incorrect for deflection-hardening beams, because even though the deflection increased to about 0.2 mm (which theoretically correspond to a crack opening of about the same), it was impossible to see any cracks. When the reference beams, or the beams made of for instance mix 11-1, were tested, the crack was visible almost at the same time as it was shown on the load vs. deflection curve that cracking had occurred. If a crack at about 0.2 mm is possible to see on some beams, they should clearly be visible on all.

8.6 Effect of concrete strength and fibre volume

Figure 8-7 summarizes the flexural tensile stress vs. CMOD curve for the most promising mixes from the 11, 21 and 31 series.

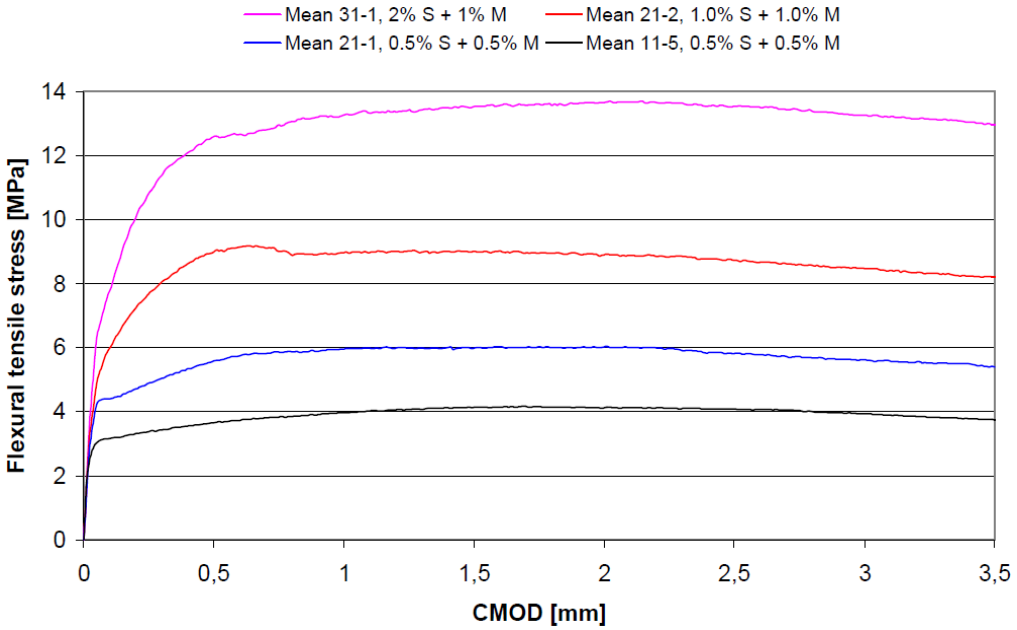

Figure 8-7 The most promising fibre combinations

The 11-5 beams and 21-1 beams were made of concrete with exactly the same fibre addition, namely 0.5 vol% Barchip Shogun and 0.5 vol% Dramix 6560. The increase in residual flexural tensile stress must therefore be due to an increased fibre contribution due to the increased concrete strength. The compressive strength of the 11-5 mix concrete was 25 MPa, while the concrete made of the 21-1 mix had a compressive strength of 45 MPa, which results in an increase in compressive strength of 80 %. The flexural tensile stress at the point where the stress vs. CMOD curves show reduced inclination is considered to be the cracking stress, and this stress was about 3 MPa and 4 MPa for mix 11-5 and 21-1 respectively (shown in Figure 8-3 and Figure 8-5) which results in an increase of 33 %. The maximum residual tensile stress occurred at a CMOD of approximately 1.75 mm for both mixes, and the maximum residual flexural tensile stress was about 4.2 MPa and 6.0 for mix 11-5 and 21-1 respectively, which is an increase of 43 %. The fact that the increase in maximum residual flexural tensile strength is larger than the increase in flexural cracking strength is favourable for the possibility to make a fibre reinforced concrete with higher strength and still showing hardening behaviour in bending.

Figure 8-8 shows the effect of increasing the fibre volume or the concrete strength for directly comparable mixes.

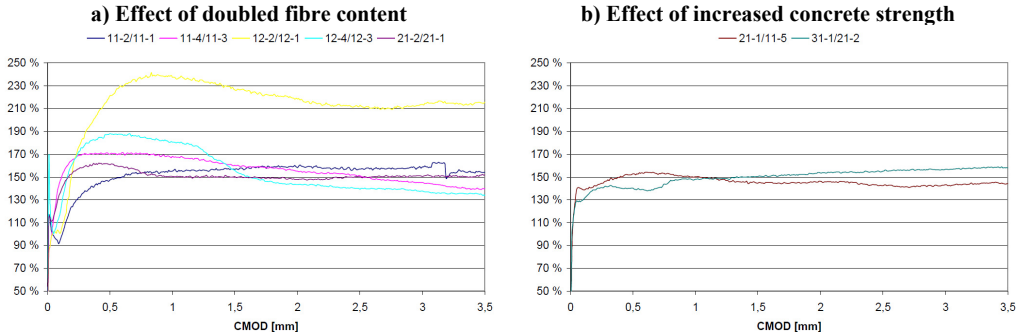

Figure 8-8 Effect of increased fibre volume and concrete strength

Intuitively one might expect the capacity to be doubled when the fibre content is doubled, but as seen in Figure 8-8a) this is in general not the case. The curves in Figure 8-8a) are simply found by calculating the relative effect of the increase in fibre volume. For the 11-2/11-1 curve, for instance, the flexural tensile stress for the 11-2 beams is divided by the flexural tensile stress for the 11-1 beams for every CMOD increments of 0.01 mm. Beside the 12-2/12-1 curve, all other curves stabilize between 140 % and 160 %. The most interesting fact is actually that the increase in compressive strength also leads to an increase of about 50% in flexural tensile stress, as shown in Figure 8-8b). An increase in strength from 25 MPa to 45 MPa is almost a doubling in strength (the 21-1/11-5 curve), so it might be as simple as if the fibre volume or the compressive strength is doubled, then the increase in flexural tensile strength is expected to be about 50 %.

The increase in strength from mix 21-1 to mix 31-1 was about 70 %, and the increase in synthetic fibre content was doubled, while the steel fibre content was equal. The increase in flexural tensile stress was once again about 50%.

The reasons for these effects are not further investigated, but it seems relatively clear that when the fibre volume is larger than 1 vol%, one cannot expect the residual flexural tensile strength to increase proportional to the increase in fibre volume, and further that one might expect the residual flexural tensile to increase when the concrete strength is increased.

8.7 Large beam and panel tests

The test program regarding large beams and panels involves:

- 2 large ductile low tensile strength concrete beams for moment failure; M2-1 and M2-2
- 2 large ductile medium tensile strength concrete beams for moment failure; M1-1 and M1-2
- 2 large ductile low tensile strength concrete beams for shear failure; S1 and S2
- 2 large ductile low tensile strength concrete slabs for moment failure, P1 and P2

In addition to the large beams and slabs, small standard beams according to NS-EN 14651 were also cast and tested. This was done both to control whether it was possible to reproduce the concrete's apparently beneficial behaviour when tested as prescribed in the NS-EN 14651, and to have the results from small beam testing on the exact same batch as the larger specimens to ensure that the small beam results are representative. Finally, one objective by

this test program was to investigate the relevance of the NS-EN 14651 beam test as basis for the residual tensile strength in real structures.

8.7.1 Test setup

The dimensions and the test setup for the large beams tested for moment failure, large slabs tested for moment failure and large beams tested for shear failure were as shown in Figure 8-9, Figure 8-10 and Figure 8-11, respectively. The figures are made by [Nordhus, Steinnes and Simpson (2011)]. The cross sections are shown with the cast surface up.

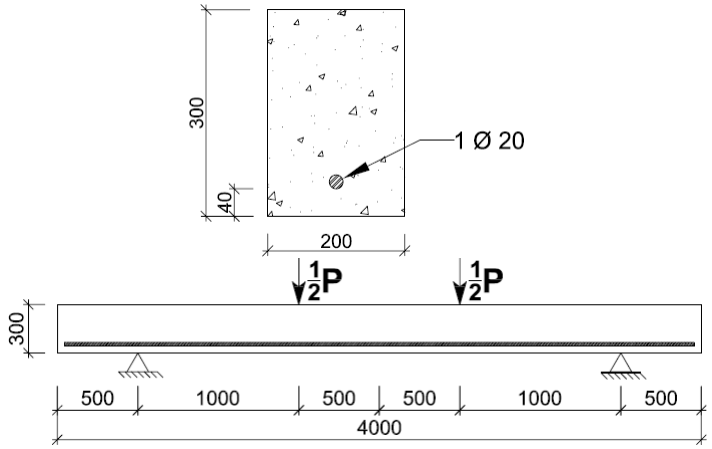

Figure 8-9 Cross section and test setup, large beam tests, moment failure. Dimensions in mm

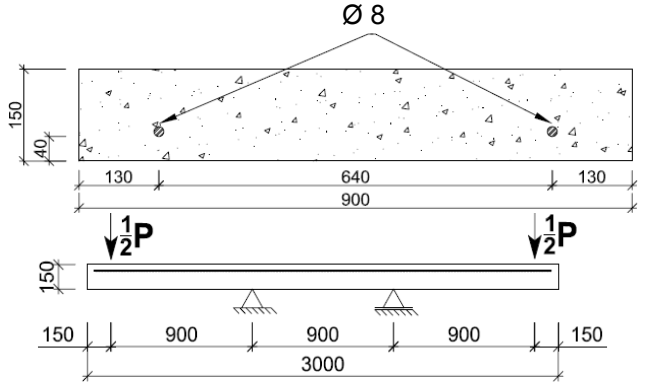

Figure 8-10 Cross section and test setup, large slab testing. Dimensions in mm. The slabs were turn up side down when tested so that it was possible to see the crack development

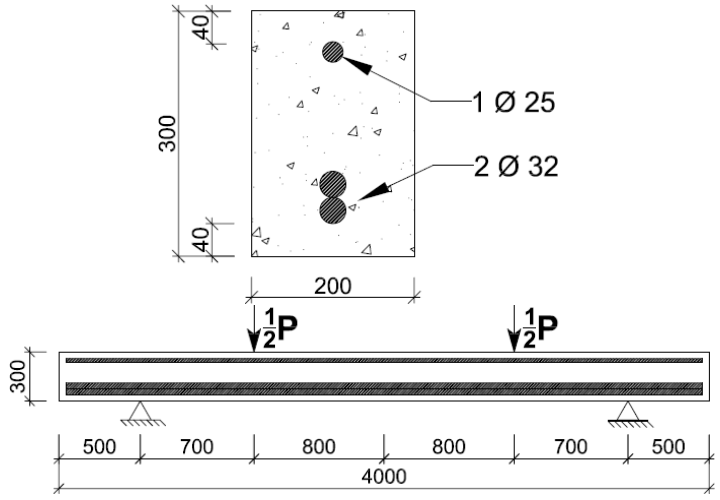

Figure 8-11 Cross section and test setup, large beam tests, shear failure. Dimensions in mm

Due to the relatively large concrete volume necessary to cast these beams and panels (240 litres per beam and 405 litres per slab), and the time consuming testing, reference beams and panels without conventional reinforcement or without fibres were not cast.

8.7.1.1 Control of the test setup

Before the test setup was determined, the estimated moment capacities inclusive the fibre contribution were calculated by use of equilibrium based multi layer model (MLM) and the shear capacities including the fibre contribution were calculated by use of the method proposed in the Norwegian design rule draft (Kanstad et al. (2011)]. The multi layer model is described and used by several authors; see for instance [Døssland (2008)].

The calculated capacities reported in [Nordhus, Steinnes and Simpson (2011)] including the fibre contributions based on NS-EN 14651-beam testing are shown in Table 8-10. It should be noted that the $f_{R,3}$ value for specimen M2, P and S was based on the initial beam tests of the *ductile low tensile strength concrete* reported in chapter 8.2 (mix 11-5), while the $f_{R,3}$ value for the *ductile medium tensile strength concrete*, which was used in the M1-beams, was not known when the test setup was designed. Therefore, the $f_{R,3}$ values for the M1-beams was assumed to be 8.1 MPa, based on experiences from earlier tests program at NTNU.

Table 8-10 Calculated shear and moment capacities inclusive the contribution from the fibres [Nordhus, Steinnes and Simpson (2011)]

	M1	M2	P	S
$f_{R,3}$ [MPa]	8.1	4.5	4.5	4.5
$f_{ft,res2.5}$ [MPa]	3.0	1.67	1.67	1.67
M_{crack} [kNm]	13	10	14	10
M_R [kNm]	59.7	47.8	20.3	131.4
V_E at M_R [kN]	59.7	47.8	22.6	187.7
$V_{R,ct}$ [kN]	43.3	35.6	46.4	48.8
$V_{R,cf}$ [kN]	144.0	79.9	179.8	79.9
$V_{R,c}$ [kN]	187.3	115.5	226.2	128.7
M_E at $V_{R,c}$ [kNm]	187.3	115.5	203.6	90.1
Failure	M	M	M	V

The moment capacities were also calculated by use of the simplified method described in the Norwegian design rule draft [Kanstad et al. (2011)], and both methods give approximately the same results.

Based on the calculated capacities it was expected that the beams and slabs that were designed for moment failure would really break due to moment, and the beams designed for shear failure would really fail due to shear; otherwise the understanding of the behaviour is insufficient.

To evaluate the fibres' contribution to the hardened properties it is assumed that the calculated strength according to EC 2 gives correct values when average strength values are used and all partial factors are set to 1.0.

8.7.2 Casting and fresh properties

The maximum concrete volume possible to mix in one batch at the laboratory at NTNU is 1 m^3, which of course influences the casting plan. The casting plan, including some material properties is shown in Table 8-11.

Table 8-11 Casting plan

	Batch 1[1]	Batch 2	Batch 3	Batch 4	Batch 5
Concrete	Mix 21-2	Mix 11-5	Mix 11-5	Mix 11-5	Mix 11-5
NS-EN beams	- (3)	3	3	3	3
Large moment beams	M1-1 and M1-2	M2-1	M2-2	-	-
Large shear beams	-	-	-	S1	S2
Large slab	-	P1	-	P2	-
Cubes	- (6)	6	6	6	6
Total batch volume [litre]	650	750	310	750	310
Target Slump flow	In the range from 500 mm to 600 mm				
Slump flow without fibre [mm]	-	640	610-650	510	640-650
Slump flow [mm]	700-740	635-650	580-590	560	550-590
Density [kg/m^3]	-	2277	2268	2260	2222
Air [%]	-	1.8	2.3	4.8	6.0
f_{ccm} [MPa]	45.4[2]	33[3]	30[3]	35[4]	27[5]
f_{cm} [MPa][6]	36.3	26.4	24	28	21.6

[1] Batch 1 was somewhat unsuccessful, described later
[2] Tested after 28 days of curing
[3] Tested after 33 days of curing
[4] Tested after 34 days of curing
[5] Tested after 20 days of curing
[6] $f_{cm} = 0.8\, f_{ccm}$ (used as an approximation for strength calculations)

Batch 1: Ductile medium tensile strength concrete
Batch 1 was somewhat unsuccessful due to two operative errors. The first error was due to the fact that the moisture content in the aggregate may vary within one bag. The moisture content was measured before the aggregate was weight out, and after casting it was found that the moisture content was significantly larger in the bottom of the bag, resulting in to much water in the concrete mix. The second error was that too much super plasticizer was used in order to increase the workability. The result of these two errors was that the concrete segregated.

The segregation developed gradually with the time, and during casting, it was observed that the large beams were less influenced than the smaller beams and cubes, and that the large beams could be used for beam testing while the rest of the specimens were discarded.

Batch 2 – 5: Ductile low tensile strength concrete
Based on the experience from the first batch, the aggregate's moisture content was carefully controlled, and the slump flow was measured before adding fibres. When the measured slump flow was within the target range, no more super plasticizer was added. In addition to the slump flow, the behaviour at the table was evaluated, so even though the slump flow before fibre addition in batch 4 was in the lower range of the target it was decided not to add more super plasticizer because the concrete seemed to be applicable.

Pictures of the concrete when measuring the slump flow are shown in Figure 8-12.

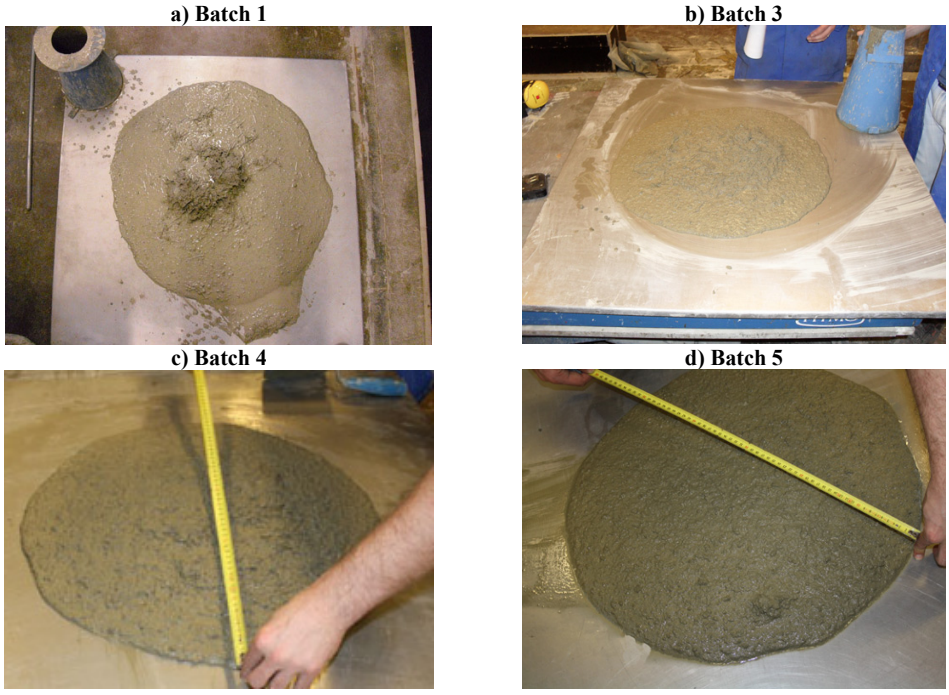

Figure 8-12 Picture from slump flow measurements [Nordhus, Steinnes and Simpson (2011)]

8.7.3 Input from small beam testing

The flexural bending stress for the first 3 beams in the low strength ductile concrete program was about 4 MPa from a CMOD of 1 mm to 3.5 mm, and the intention was to reproduce this results. The average flexural tensile strengths for the beams from batch 2 to batch 5 are shown in Table 8-12, together with the average strengths for the beams from Mix 11-5 and Mix 21-2.

Table 8-12 Results from small beam testing

	Mix 11-5	Batch 2	Batch 3	Batch 4	Batch 5	Mix 21-2[1]
$f_{ct,L}$ [MPa]	3.2	3.5	3.7	3.2	3.1	5.7
$f_{R,1}$ [MPa]	3.6	4.8	5.0	3.5	3.9	8.9
$f_{R,2}$ [MPa]	4.1	5.8	5.8	4.3	4.6	9.0
$f_{R,3}$ [MPa]	4.1	5.2	5.7	4.2	4.5	8.9
$f_{R,4}$ [MPa]	3.9	5.0	5.4	4.0	4.3	9.5
$f_{ft,res2.5}$ [MPa]	1.5	1.9	2.1	1.6	1.7	3.3

[1]Results from the initial beam tests are used because the small beams cast of Batch 1 were discarded

As seen from Table 8-12, there is some variation in the results for the *ductile low tensile strength concrete*. The one-batch variations of $f_{R,1}$ to $f_{R,4}$ are in the range from 7 % to 30 %, which means that the batch-to-batch variations probably are too small to conclude on a statistical basis that the concrete behaviour in fact is different for the different batches.

If all beams made of the ductile low tensile strength concrete, with 0.5 vol% Dramix 6560 and 0.5 vol% Barchip Shogun, are considered to be within the same concrete family, and by

assuming that the test results follow the Gaussian distribution, the average strengths, f_{mean}, and standard deviations, σ, can be calculated for all beams. By calculating a confidence interval according to equation 8-1, the 68.3 % confidence intervals shown in Table 8-13 are found.

$$[f_{mean} - \sigma, f_{mean} + \sigma] \quad (8\text{-}1)$$

Table 8-13 Statistical calculation on the results from small beam testing

	f_{mean}	f_{mean} - σ	f_{mean} + σ
$f_{ct,L}$ [MPa]	3.30	2.96	3.64
$f_{R,1}$ [MPa]	4.11	3.17	5.04
$f_{R,2}$ [MPa]	4.85	3.84	5.87
$f_{R,3}$ [MPa]	4.66	3.84	5.49
$f_{R,4}$ [MPa]	4.46	3.68	5.25
$f_{ft,res2.5}$ [MPa]	1.73	1.42	2.03

A 68.3 % confidence interval simply means that in 68.3 % of the tests, the true expected value, μ, will be within the interval; it is not that the probability for μ being within the interval is 68.3 %. Nevertheless, these values are helpful when the results from the large beam and panel tests are evaluated.

For the ductile medium tensile strength concrete, the only small beam results available are those from the initial test program. These results were shown graphically in chapter 8.3.1, and the residual tensile strength at 2.5 mm crack opening, $f_{ft,res2.5}$, was 3.3 MPa.

8.7.4 Specimens tested for moment

8.7.4.1 Calculation methods to estimate the moment vs. curvature relations

Two calculation methods are used to estimate the moment vs. curvature relations. The three master students preferred the MLM, while the exact solution from EC 2 (ESEC2) described in chapter 4.1.4 is used partly to control the students' calculations but also to examine if the calculation method is suitable also for cross sections that are additionally reinforced with fibres.

Both calculation methods use the material models described in EC 2 for concrete under compression (Figure 3.3 in [EC 2]) and reinforcing steel (Figure 3.8 in [EC 2]). In the MLM calculations the reinforcing steel is assumed to be strain hardening with a factor k = 1.04. When the moment capacities for the beams are calculated, the yield stress is set to 566 MPa, while the yield stress is set to 500 MPa when the moment capacities for the slabs are calculated.

In the ESEC2, the reinforcing steel is assumed to be perfect plastic after yielding, and the yield stress is set to the measured value 566 MPa for both beam and slab calculations.

The contribution from the fibres is calculated as a rectangular stress block with tensile strength capacity equal to $f_{ft,res2.5}$. The height of the rectangular stress block is assumed equal to the height of the tensile zone. These assumptions are equal for both calculation methods.

The expression for the curvature used in both calculation methods is:

$$\kappa = \tan\kappa = \frac{\varepsilon_c}{X} \qquad (8\text{-}2)$$

where

ε_c: is the calculated strain at the compressive surface
X: is the height of the compressive zone [mm]

The moment vs. curvature relations found by use of MLM calculations can be found in [Nordhus, Steinnes and Simpson (2011)], while the results from the ESEC2 calculations are shown in the present thesis. The results from these two calculation methods correspond very well.

8.7.4.2 Results large beams

Figure 8-13 shows the *load vs. deflection* curve for the beams tested for moment failure.

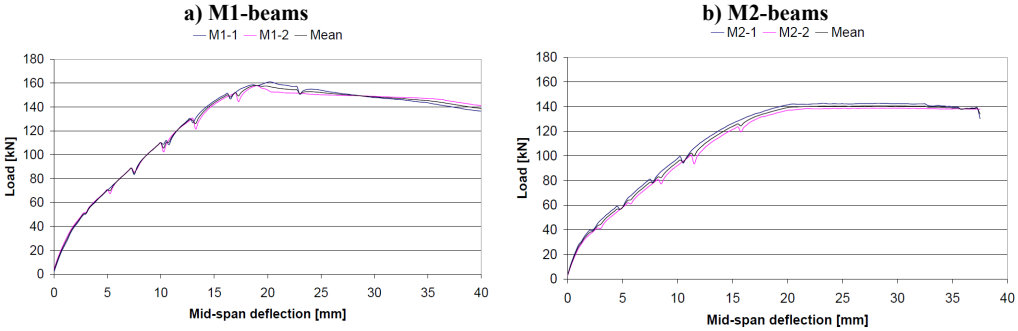

Figure 8-13 Load vs. mid-span deflection M1 and M2

As seen, the two beams within each series had almost identical behaviour, and the mean curves are therefore used when the fibre effect is evaluated.

The experimental and calculated *moment vs. curvature* relationship for the ductile medium tensile strength concrete beams are shown in Figure 8-14.

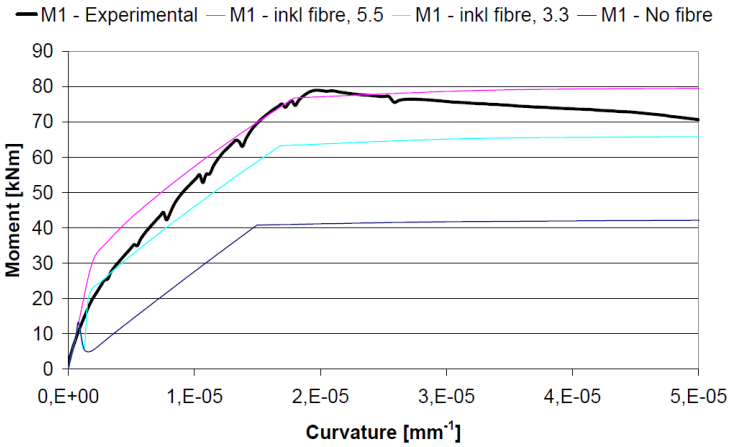

Figure 8-14 Experimental and calculated moment vs. curvature relationship for the medium strength ductile concrete beams

In Figure 8-14 the following abbreviations are used:

- *M1 –No fibre*: The expected curve if no fibres were added
- *M1 –inkl fibre, 5.5*: The calculated curve by use of $f_{ft,res2.5}$ = 5.5 MPa
- *M1 – inkl fibre, 3.3*: The calculated curve by use of $f_{ft,res2.5}$ = 3.3 MPa (determined from small beam testing)

The calculation of the curve with $f_{ft,res2.5}$ = 5.5 MPa is simply performed to find the residual tensile strength that matches the result from testing the large beams most accurately.

The experimental and calculated *moment vs. curvature* relationships for the ductile low tensile strength concrete beams are shown in Figure 8-15, and the same abbreviations are used as for the ductile medium tensile strength concrete.

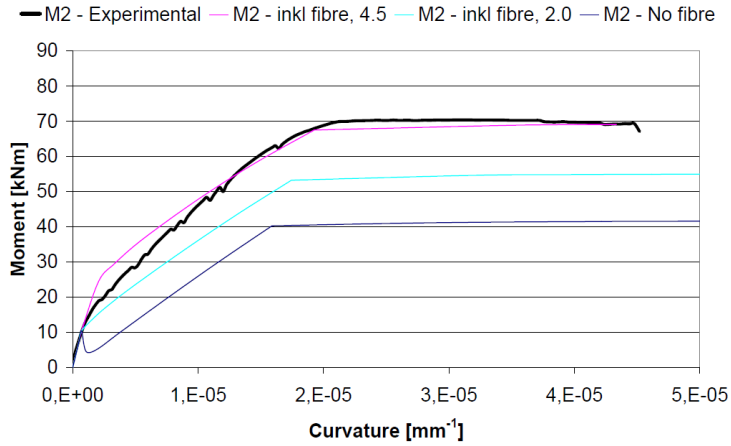

Figure 8-15 Experimental and calculated moment vs. curvature relationship for the low strength ductile concrete beams

As for the medium strength ductile concrete, the *M2- inkl fibre, 4.5* curve is simply curve-fitting. In [Nordhus, Steinnes and Simpson (2011)] the authors preferred to calculate the

capacity for each beam, and because the two beams were cast from different batches, they used the results from the corresponding small beams as input values. In Figure 8-15 the average $f_{ft,res2.5}$ (= 2.0 MPa) from all six small beams from batch 2 and batch 3 is used as input to the calculation.

8.7.4.3 Results large slabs

The experimental *moment vs. curvature* relationship for the ductile low tensile strength concrete slabs are shown in Figure 8-16. The differences between the two slabs were somewhat larger than for the beams, and these curves are therefore shown together with the average curve.

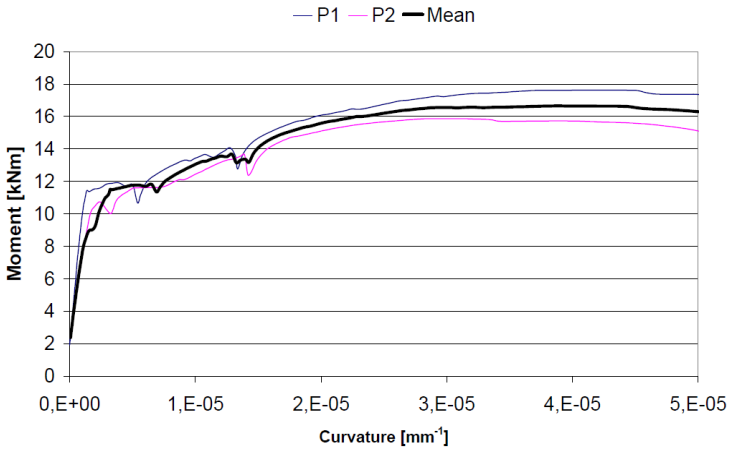

Figure 8-16 Calculated moment vs. curvature relationship for the ductile low tensile strength slabs

The average curve from Figure 8-16 are compared with the calculated moment vs. curvature relationships in Figure 8-17.

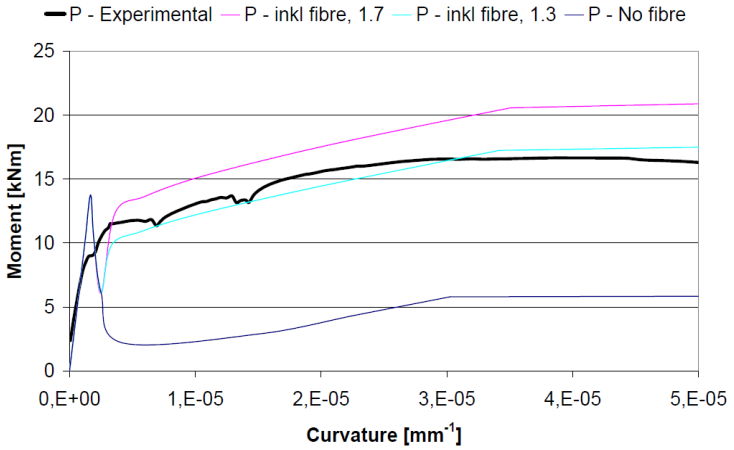

Figure 8-17 Experimental and calculated moment vs. curvature relationship for the ductile low tensile strength slabs

Similar to the beams, the two calculation methods give equal moment vs. curvature relationship also for the slabs. A residual tensile strength of about 1.3 MPa seems to fit the

average curve when the ESEC2 is used. A residual tensile strength of 1.7 MPa is shown because this is the average result from small beam testing of batch 2 and batch 4.

It should be mentioned that when the moment vs. curvature relationships in [Nordhus, Steinnes and Simpson (2011)] were calculated, the yield strength of the re-bars were set to 500 MPa, while the yield strength of the re-bars in Figure 8-17 were set to 566 MPa. This difference does not influence the calculated results in any large extent, because the fibre's contribution to the total capacity is about 72 % when the steel re-bars are yielding. The residual tensile strengths that showed best agreement with the experimental curves in [Nordhus, Steinnes and Simpson (2011)] were 1.2 MPa and 1.5 MPa for P2 and P1 respectively.

8.7.4.4 Evaluation of the fibre effect

The calculated $f_{ft,res2.5}$ results from curve-fitting the large scale tests and corresponding $f_{ft,res2.5}$ results from small beam tests are summarized in Table 8-14.

Table 8-14 Calculated $f_{ft,res2.5}$ from large scale tests and the belonging small beam tests

	$f_{ft,res2.5}$ [MPa]		Ratio large/small
	Large specimens	Corresponding small beams	
M1	5.5	3.3	1.67
M2	4.5	2.0	2.25
P	1.3	1.7	0.76

As seen from Table 8-14 the large beams showed stronger behaviour than expected from the small beams, while the large slab had less capacity than expected. One way of explaining differences like this is to introduce a size-dependent safety factor, for instance as in [RILEM TC 162-TDF (2003)] where the size-dependent factor, κ_h, is defined as:

$$\kappa_h = 1.0 - 0.6\frac{h-125}{475},\ 125 \le h \le 600 \qquad (8\text{-}3)$$

where

h: is the height in mm

The size-dependent factor will be 0.91 for the slabs and 0.78 for the beams, which actually will correct the small beam results in the opposite direction than found from the large scale test.

It is also worth noting that according to the German Rules [DAfStb (2008)], the characteristic value of the tensile strength from the small beams could be used without reduction for the slabs, while it has to be multiplied by a reduction factor for fibre orientation of 0.5 for the beams, and further; the geometry factor is increasing by increasing cross sections. This is in strong contradiction to the present results.

Casting procedure, fibre orientation and segregation

The main explanation to the fact that the large beams had higher capacity, while the large slabs had less capacity than expected, is the possible favourable fibre orientation in the large beams due to wall effects and flow during casting, and the possibility of fibre density variation over the specimen's height caused by fibre segregation due to the difference in density for fibres and concrete. This is only briefly discussed here, and will be followed up more thoroughly in subsequent publications.

Figure 8-18 shows pictures form casting beam M2-2 and slab P1.

a) Casting beam M2-2 **b) Casting slab P1**

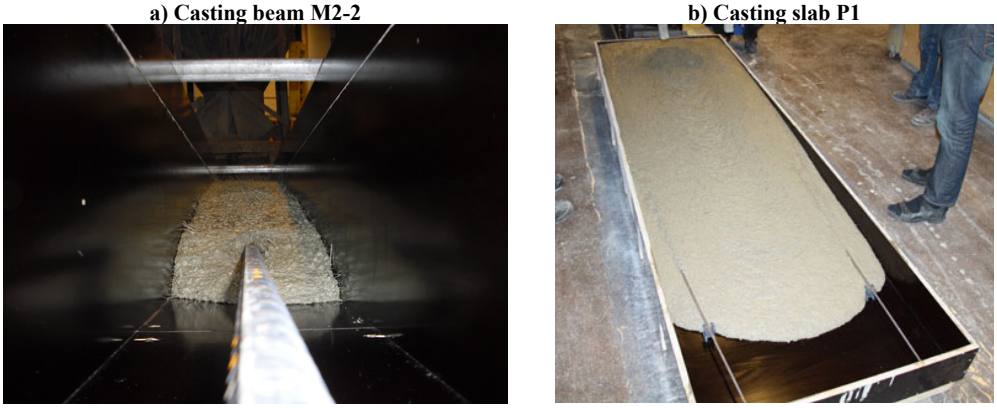

Figure 8-18 Pictures form casting beam M2-2 and slab P1 from [Nordhus, Steinnes and Simpson (2011)]

When casting the beams, the longitudinal reinforcement and the form walls will most likely contribute to longitudinal fibre orientation parallel to reinforcement, resulting in a higher number of fibres crossing a given crack compared to the slabs. When casting the slabs there were no obstacles between the reinforcement, and the distance between the reinforcing steel was, as shown in Figure 8-10, 640 mm. Between the reinforcement in the slabs, the fibres were most likely more plane-orientated than in the beams. The small beams were cast according to the prescription in [NS-EN 14651], and this procedure is schematically shown in Figure 8-19.

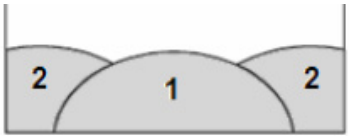

Figure 8-19 Casting procedure [NS-EN 14651]

When casting the small beams, first about 5.5 litres concrete is placed in area 1, and then about 2.25 litres is placed in areas 2, which makes the formwork 90 % filled. The remaining 10 % is used to level out the surface. Before testing a small beam, the beam is rotated 90º around its longitudinal axes and a notch is sawn, and the location of this notch is in the middle of area 1. In contrast to the large beams, the casting procedure will not give a beneficial fibre orientation in the small beams due to the concrete flow. This is actually advantageous from a safety point of view, because otherwise the casting procedure at a building place might have been less beneficial than the casting procedure for the test beams. On the other hand, because the width of the small beams is only 150 mm, an orientation of the fibres due to the wall effect is expected to occur. Another important point with regard to the notch is the possibility for fibres to be embedded outside the height h_{sp}. Fibres oriented as shown in Figure 8-20 would be cut off if the beam were sawn from a larger specimen if the total beam height should be equal to h_{sp}, and it would not be orientated as illustrated if the total beam height of a cast beam had been equal to h_{sp}.

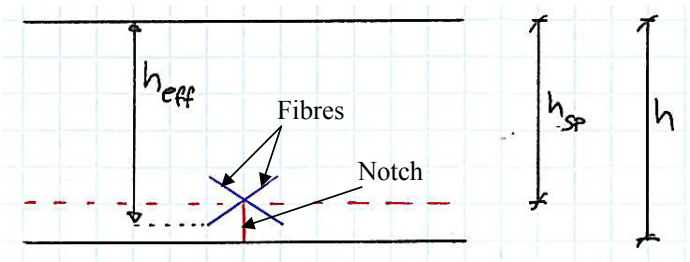

Figure 8-20 Possible fibre orientation near the notch in a NS-EN 14651 beam

As illustrated in Figure 8-20 the effective height of a beam (with regard to the fibre efficiency) tested according to NS-EN 14651 might quite likely be larger than h_{sp}.

To summarize the casting procedure's effect of the fibre orientation, the following assumption may be stated:

- NS-EN 14651 beams may have a larger effective height than h_{sp}, which lead to an overestimation of the residual flexural tensile strength
- Casting slabs might give less beneficial fibre orientation than the small standard beams
- Casting large beams might give more beneficial fibre orientation than the small standard beams

The first two assumptions may explain why $f_{ft,res2.5}$ for the slabs were only 76 % of expected value based on the small beams, while the first and third assumptions only partly may explain the overcapacity for the large beams. These statements will be discussed further in the following.

Thorenfeldt has shown that the residual tensile strength may be calculated as [Thorenfeldt (2003)]:

$$f_{ft,res} = \eta_0 v_f \eta_l \sigma_{f,max} = \eta_0 v_f \sigma_{f,mean} \quad (8\text{-}4)$$

The meaning of η_0, v_f, η_l, $\sigma_{f,max}$ and $\sigma_{f,mean}$ is already described in chapter 6, where this equation also was presented.

If it is assumed that the fibre volume is as prescribed, that the fibres in the large M2 beams are distributed in one direction only, and that the average fibre stress according to equation 8-4 is 450 MPa, the experimental result gives a capacity factor as shown in Table 8-15.

Table 8-15 Possible values of the capacity factor η_0

	$f_{ft,res2.5}$ [MPa]	η_0 [-]
Large moment beams (M2)	4.5	1.00
Corresponding small beams	2.0	0.44
Large slabs (P)	1.3	0.29
Corresponding small beams	1.7	0.38

As shown in Table 8-15 equation 8-4 gives a capacity factor equal to 0.44 (or 0.38) and 0.29 for the small beams and the large slabs, respectively. An average fibre stress of 450 MPa is quite high but with regard to the pull-out tests in chapter 3.2.1 it is reasonable. The Dramix fibre had a maximum fibre stress of 684 MPa and 641 MPa for $l_b = l_f/2$ and $l_b = l_f/6$ respectively, and the Barchip Shogun fibres had a maximum fibre stress of 485 MPa, when

embedded in concrete C (which had comparable strength to the ductile low tensile strength concrete and high amount of fines). For the Barchip Shogun fibres, it seems reasonable to assume that the mean stress in all fibres is 50% of the maximum fibres stress, because in average the fibres should have an embedment length equal to one fourth of the fibre length. If the mean fibre stress for the Dramix fibres is the average of the maximum with half embedding and one sixth embedding, the average fibre stress calculated from the results from the pull-out tests is actually about 450 MPa.

It is possible that all fibres in the large beams really were oriented in a way that the capacity factor can be assumed equal to 1.0, but the probability is not large. However, it is quite likely that the capacity factor for the small beams are about 31 % (0.38/0.29) larger than for the large slab, due to the fibre orientation caused by the casting procedure and the concrete flow. Another point is that according to the statistical calculations shown in Table 8-13, a true $f_{ft,res2.5}$ in the range between 1.4 MPa and 2.0 MPa is not in conflict with the results from the small beam testing. Beside that, if the third assumption cannot fully explain why the large beam showed larger fibre effect than expected from small beam tests, there must be other effects that influence the results because the small beam results might be overvalued.

The overall implication is that the statistical variations and the casting procedure's effect on the capacity factor may explain the *small beams vs. large slab* relation, but not the reason why the large beams had a remarkable higher capacity than expected. The possibility that the fibre contribution to the moment capacity is not fully understood, implicating that the calculation method for fibre reinforced concrete is not absolutely correct, should not be refused, but it is also quite likely that the concrete segregated somewhat, and that this has influenced the large beams in a larger extent than the slabs and the small beams. The Dramix fibres have a density of 7.8 kg/dm^3 compared to the concrete density of about 2.3 kg/dm^3, which means that these fibres may be concentrated in the lower part of the cross section if there is some segregation tendencies. If equation 8-4 is used once again, with an average fibre stress of 450 MPa and a capacity factor equal to 0.9 the fibre volume must be 1.11 % in the tensile zone to reach $f_{ft,res2.5}$ = 4.5 MPa. Whether this variation in fibre concentration is correct or not, is quite easy to investigate by cutting the large beams and investigate the fibre amount with respect to the beam's height.

The same mechanisms are also likely to be valid for the large M1 beams, even though the overcapacity for the large beams where less pronounced for the ductile medium tensile strength concrete. However, fibre counting is so far not performed for these two beams.

Fibre counting

Fibre counting has been performed on all specimens made of the ductile low tensile strength concrete. The cross section of the small NS-EN 14651 beams were divided in three equal parts, and the number of fibres where counted in all three parts. The large panels were sawn at the mid span, and the cross section was divided in six equal parts before fibre counting. For the large beams, the cross section was divided in three equal parts, and while the location of the cross section was in the mid span of the moment beams, the location of the cross section for the shear beams where located 1 meter from the mid span. The locations of the sawn sections are illustrated in Figure 8-21, while the subdivisions of the cross sections are illustrated in Figure 8-22.

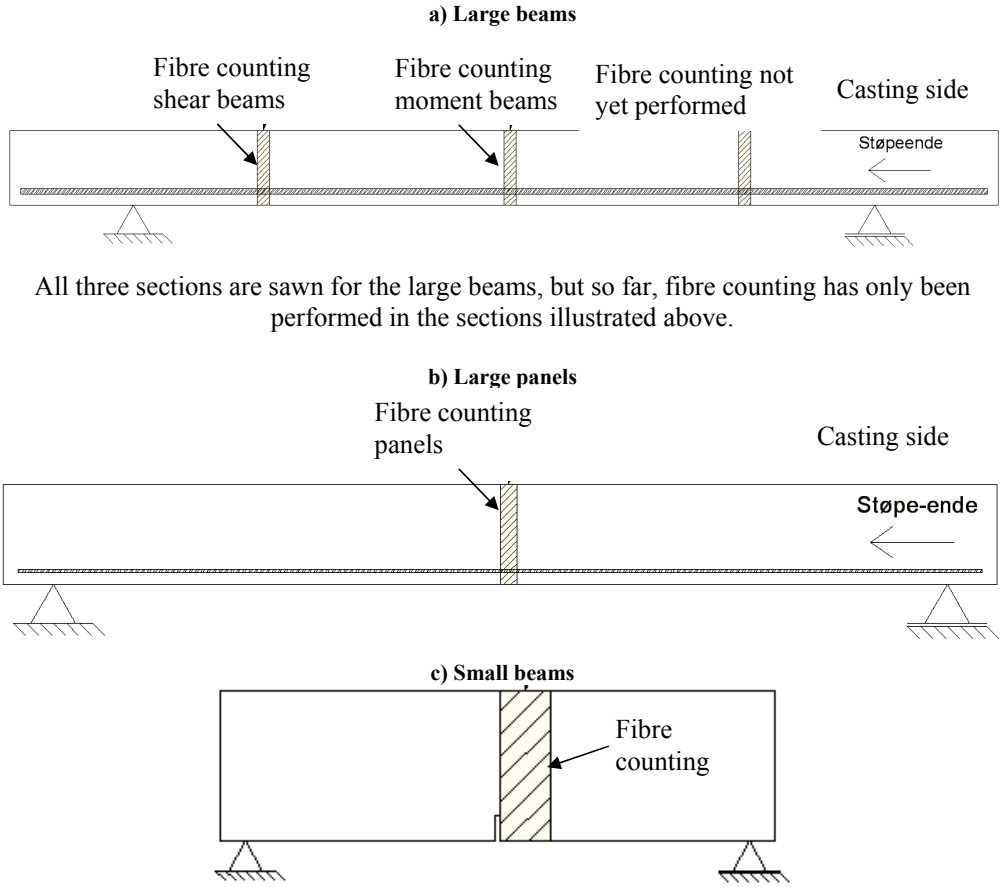

All three sections are sawn for the large beams, but so far, fibre counting has only been performed in the sections illustrated above.

Figure 8-21 Location of the cross sections for fibre counting [Nordhus, Steinnes and Simpson (2011)]

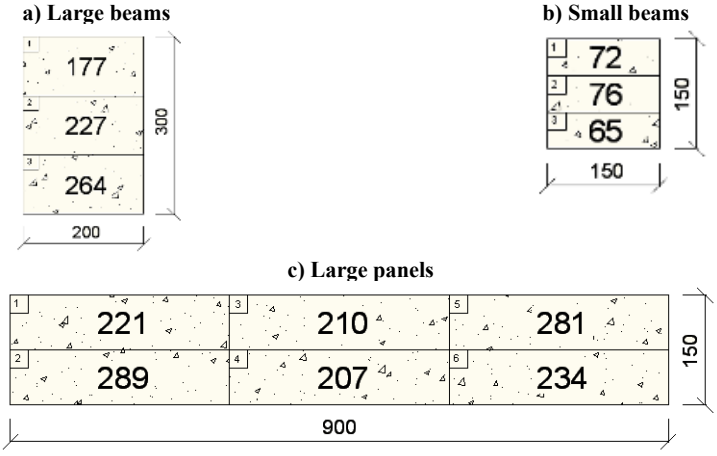

Figure 8-22 Division of the cross sections for fibre counting. The numbers are results from three of the specimens [Nordhus, Steinnes and Simpson (2011)]

By rearranging equation 3-13 to 3-17, the maximum number of fibres crossing the cross section A_c is written as:

$$n_{max} = v_f \frac{A_c}{A_f} \quad (8\text{-}5)$$

where

n_{max}: is the maximum number of fibres
A_f: is the cross section area of one fibre

The number of fibres according to equation 6-2 is written as:

$$n = \alpha \cdot v_f \frac{A_c}{A_f} \quad (8\text{-}6)$$

The maximum number of fibres according to equation 8-6 corresponds to α=1, which means that the orientation factor, α, can be expressed as:

$$\alpha = \frac{n_{counted}}{n_{max}} \quad (8\text{-}7)$$

Finally, the capacity factor can be estimated by use of equation 6-4.

The theoretical maximum number of fibres is calculated with the assumption that all fibres are evenly distributed and oriented parallel to the length of the beam (α=1). If the counted number of fibres is larger than this maximum number of fibres, the total fibre volume at the location of the sawn section must be larger than intended, which means that the fibres are not evenly distributed with respect to the length of the beam. The local fibre volume at the location where the number of fibres was counted is not yet examined. Due to the possibility that the fibre volume varies with respect to the length of the beams, the orientation factor may be somewhat over- or underestimated.

The average number of fibres for the three tested small beams from every batch is summarized in Table 8-16, together with the theoretical maximum number of fibres, the orientation factor, α, and the capacity factor, η_0.

Table 8-16 Fibre counting on the small beams, average of 3 beams

	Batch number: Corresponding large specimen			
	Batch 2: M2-1 and P1	Batch 3: M2-2	Batch 4: S1 and P2	Batch 5: S2
Upper third	90	88[1]	87	95
Intermediate third	106	98[1]	72	83
Lower third	96	87[1]	70	64
Total number of counted fibres	292	273	229	242
Maximum number of fibres according to equation 8-5	354	354	354	354
α	0.83	0.78	0.65	0.69
η_0	0.77	0.70	0.54	0.59
[1]Only two beams were tested				

The number of fibres in the three third parts is relatively equal, which means that the small beam results are representative for the particular fibre distribution. These results cannot be

used to investigate the possibility of segregation tendency simply because the beams were rotated 90 º before sawing the notch.

The number of fibres in the two large slabs is summarized in Table 8-17 and Table 8-18.

Table 8-17 Fibre counting on P1, mid span

	Left third	Intermediate third	Right third	Total
Upper half	221	210	281	712
Lower half	289	207	234	730
Total number of counted fibres				1442
Maximum number of fibres according to equation 8-5				2122
α				0.68
η_0				0.58

Table 8-18 Fibre counting on P2, mid span

	Left third	Intermediate third	Right third	Total
Upper half	215	167	207	589
Lower half	212	133	216	561
Total number of counted fibres				1150
Maximum number of fibres according to equation 3-17				2122
α				0.55
η_0				0.39

For the large panels it seems like fibre segregation did not occur because the number of fibres is quite similar in the upper and the lower half, but the orientation- and capacity factors are less than for the small beams. This means that it is reasonable to assume that the fibre orientation was less favourable for the panels than for the small beams, supporting the second assumption mentioned earlier.

The results from fibre counting on the large beams are summarized in Table 8-19.

Table 8-19 Fibre counting on the large beams.

Large beams	M2-1: Batch 2	M2-2: Batch 3	S1: Batch 4	S2: Batch 5
Upper third	177	184	189	153
Intermediate third	227	267	215	250
Lower third	264	261	183	201
Total number of counted fibres	668	712	587	604
Maximum number of fibres according to equation 8-5	943	943	943	943
α	0.71	0.76	0.62	0.64
η_0	0.62	0.68	0.50	0.53

For the large moment beams, the orientation- and capacity factors are in average considerably larger than for the panels. In addition to this, it seems possible that the fibres are overrepresented in the lower part of the beams which means that fibre segregation may have occurred for the large beams

The results from fibre counting indicate that the fibre orientation was more favourable for the small beams than for the large panels, but also that the fibre orientation was more favourable for the small beams than for the large beams (comparing Batch 2 and Batch 3). By calculating the orientation factor in the lower third, the orientation factor is 0.84 for both beam M2-1 and M2-2, which is just barely larger than for the small beams. The overall impression is that the fibre orientation and possible fibre segregation cannot fully explain the *small beam vs. large beam* inconsistency with the present information from fibre counting.

It is one relatively large simplification in the present fibre counting discussion. When fibres are counted, all fibres crossing the sawn surface are registered, which means that with the present approach all counted fibres are considered to be oriented in the most favourable direction. To find the real fibre orientation the number of fibres in all three principal directions must be counted and the real fibre volume must be determined. This procedure is described in [Døssland (2008)]. As already mentioned, an investigation of the fibre orientation will be followed up in subsequent publications.

If the fibre orientation and possible fibre segregation cannot fully explain the *small beam vs. large specimen* inconsistency, there has to be other effects that influence the behaviour. The strain level in the ordinary steel reinforcement is considerable different for the large panels and the large beams, and this might influence the effect of adding fibres to the concrete.

Strain levels

When the assumption of perfect plastic behaviour of the reinforcing steel is used, there is no need for checking the strain limit [EC 2], which means that the calculated failure will be when the concrete strain at the compressive surface reaches ε_{cu2}. The solutions of this calculation are shown in Table 8-20.

Table 8-20 Calculated moment capacities, no reinforcing steel strain limit

	ε_{cu2} [‰]	ε_s [‰]	M_{cap} [kNm]	κ [10 ⁻6 mm^{-1}]
M1 – No fibre	3.4	25.5	42	115
M1 – incl. fibre, 5.5	3.5	8.5	79.5	48
M2 – No fibre	3.5	17	42	81
M2 – incl. fibre, 4.5	3.3	5.7	69	35
P – No fibre	3.4	127 (!)	6	1233
P – incl. fibre, 1.3	3.4	31	18	326

As seen, the steel strain is quite high before the concrete strain reaches ε_{cu2}. Nevertheless, the moment capacity is not affected very much by the steel strain, and in Table 8-21 the moment capacities are shown when the steel strain is limited to $\varepsilon_s = 2f_{yk}/E_s = 5.66$ ‰.

Table 8-21 Calculated moment capacities, reinforcing steel limited to 5.66 ‰

	ε_s [‰]	ε_c [‰]	M_{cap} [kNm]	κ [10 ⁻6 mm^{-1}]
M1 – No fibre	5.66	1.3	42	28
M1 – incl. fibre, 5.5		2.6	79	33
M2 – No fibre		1.7	41	29
M2 – incl. fibre, 4.5		3.3	69	35
P – No fibre		0.5	6	58
P – incl. fibre, 1.3		1.1	18	64

As seen in Table 8-20 the steel strain must be 5.4 and 3.6 times higher in the slab than in beam M1 and beam M2 respectively, to fully utilize the specimens' compressive capacity. In [RILEM TC 162-TDF (2003)] it is stated that "for steel fibre reinforced concrete which is additionally reinforced with bars, the strain is limited to 25 ‰ at the position of the reinforcement", but as seen in Table 8-21, the strain may be limited to 5.66 ‰ at the position of the reinforcement without affecting the moment capacity.

The "over-capacity" for the M2-beams was found to be 4.5/2 = 2.25, while for the M1-beams the "over-capacity" was about 1.67, and the slabs had an "under-capacity" of 0.76. The corresponding re-bar strains were 5.7 ‰, 8.5 ‰ and 31 ‰ respectively, which show that at least for these specimens, there might be a correlation between the fibre contribution and the strain state of the re-bars.

Another observation is that the calculated cracking moments shown in Table 8-10 were about 25 % of the calculated ultimate capacity for the large beams without the fibre contribution, while for the slabs the calculated cracking moment was about 67 % larger than the calculated post cracking capacity. From these points of view, it seems like the fibres may be more effective if they act together with conventional reinforcement, where the re-bars ensures that the post cracking capacity is larger than the cracking capacity, and even better if the total cross sectional area of the re-bars are sufficient to limit the steel strain necessary to utilize the compressive zone.

8.7.5 Specimens tested for shear

Figure 8-23 shows the *load vs. deflection* curve for the two beams tested for shear failure.

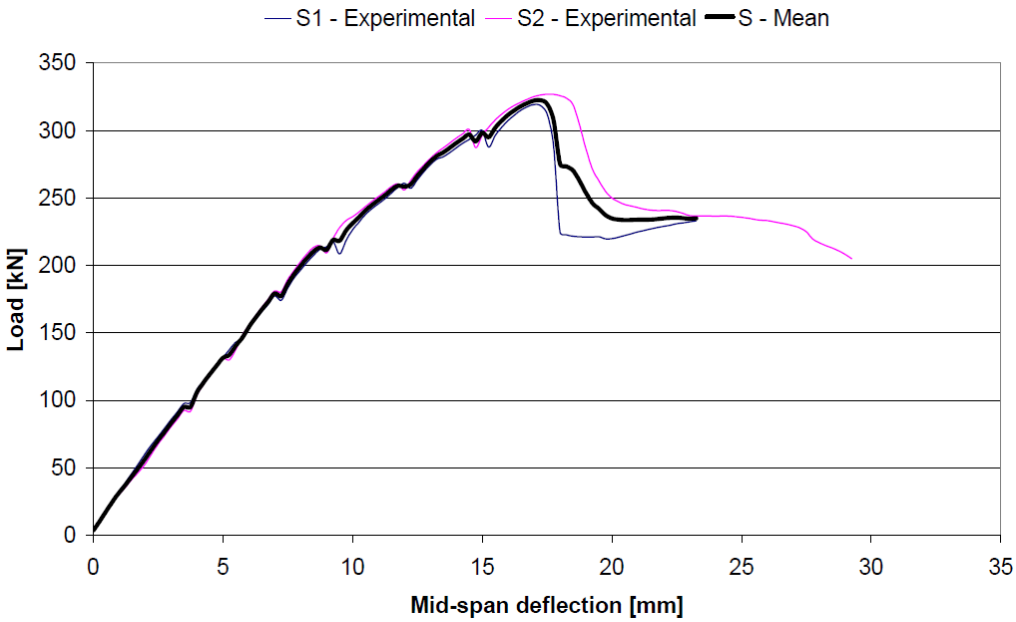

Figure 8-23 Load vs. deflection curve for the two S-beams

The average maximum load for the S-beams was 323 kN, which means that the largest shear force, V_E, was 161.5 kN. The calculated shear capacity without the fibre contribution is 48.8

kN, which means that the fibre contribution to the shear capacity is about 113 kN. If the calculation method in the Norwegian Design rule draft [Kanstad et al. (2011)] is used, the residual tensile strength, $f_{ft,res2.5}$, must have been 3.1 MPa. In Table 8-22 $f_{ft,res2.5}$ calculated from the different tests is summarized. It should be mentioned though, that the shear capacity for plain concrete is much more encumbered with uncertainty than the moment capacity of reinforced concrete, which means that the residual tensile strength calculated from the shear tests is considerably more uncertain than the residual tensile strength calculated from moment tests.

Table 8-22 $f_{ft,res2.5}$, input values from small beams and curve-fitting values from large specimen

	$f_{ft,res2.5}$ [MPa] Small beams	$f_{ft,res2.5}$ [MPa] Large specimen
M2	2.0	4.5
P	1.7	1.3
S	1.6	3.1

It might look like the fibres were more effective as shear reinforcement than as moment reinforcement in the slabs, but less effective than the moment reinforcement in the M2-beams.

Once again, it has to be emphasized that the theoretical calculation of the shear capacity is considerably more uncertain than the theoretical calculation of the moment capacity. Sørensen has compared experimental results from student works at NTNU with the calculated shear capacities according to the Norwegian design rules for concrete structures [NS3473], which was valid in Norway before it was replaced by EC 2. Figure 8-24 shows the result from this comparison.

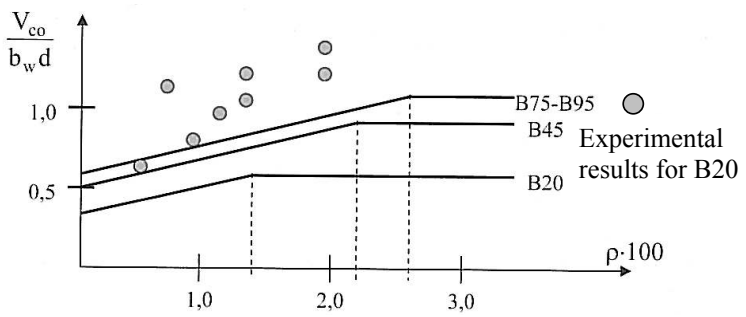

Figure 8-24 Shear strength as function of the reinforcement ratio [Sørensen (2005)]

As shown in Figure 8-24 the calculated shear capacity for beams made of concrete in strength class B20 and B45 were less than the capacities found by testing beams made of concrete in strength class B20 for all reinforcement ratios, ρ, where ρ is expressed as:

$$\rho = \frac{A_s}{b_w d} \tag{8-8}$$

and

A_S: is the cross sectional area of the longitudinal reinforcement

It is therefore important to bear in mind that according to Figure 8-24 it is possible that the concrete's contribution to the shear capacity largely underestimated, which means that the fibre contribution shown in Table 8-22 can be overestimated.

If the fibre contribution to the moment capacity for the S-beams is calculated, some interesting effects are found. First of all, the moment capacity is not affected by the fibres, because the compressive zone is already utilized. Secondly, it is possible that the failures were not only due to shear force, but also due to the fact that the compressive surface of the concrete reached high strains. Figure 8-25 shows the mean *moment vs. curvature* relationship for the S-beams, together with the calculated curves with and without the fibre contribution.

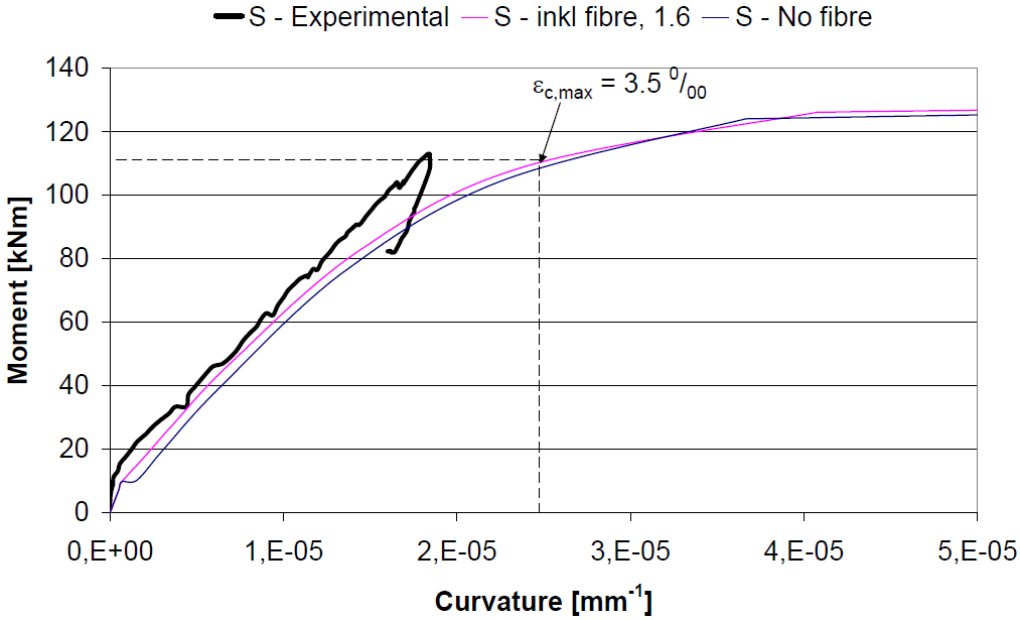

Figure 8-25 Moment vs. curvature, S-beams

The calculated moment capacity is about 128 kNm, if the reinforcement in the compressive- and tensile zone has no strain limit. If the concrete strain in the compressive surface is limited to 3.5 ‰, the reinforcement in the tensile zone can only have a strain about 2.2 ‰ to have force equilibrium, resulting in a moment capacity of 111 kNm, and the beam failure occurred at 112 kNm. It is actually possible that the shear capacity would have been larger if the compressive zone was not fully utilized due to moment.

8.7.6 Large specimens summarized

As already discussed, the residual tensile strength due to the fibre reinforcement varies for the same mix design, and the residual tensile strengths for the large beams are larger than expected from testing the small beams, while it is less than expected for the large slab.

Regardless of this fact, the fibre contribution to both the moment capacity and the shear capacity is quite large. In Figure 8-26, the fibre contribution is shown graphically as the difference between calculated capacities without fibres and the experimental results.

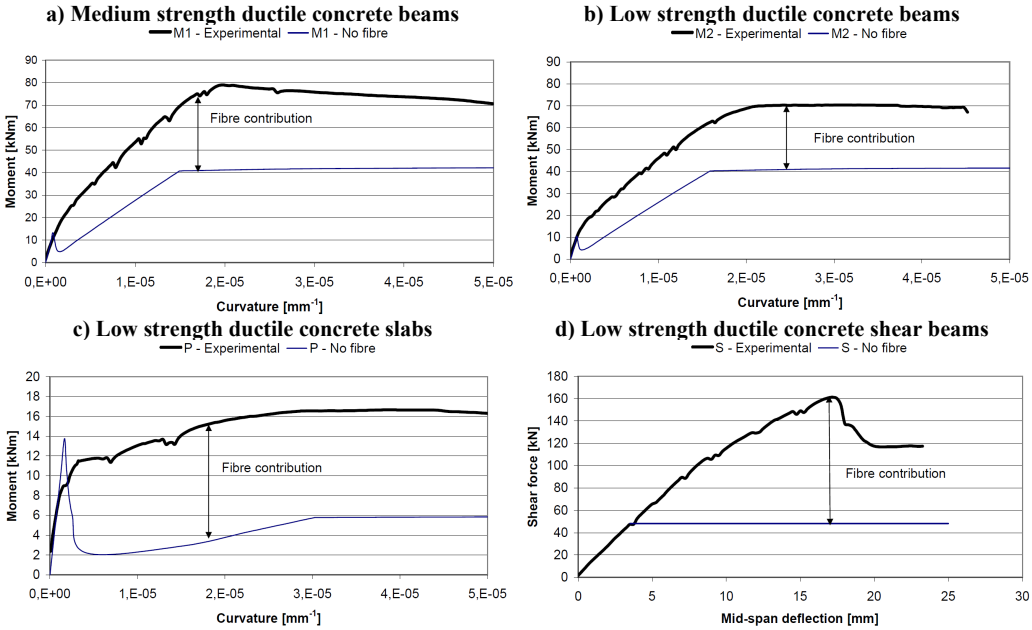

Figure 8-26 Fibre contribution

For the beams tested for moment, the capacities were increased from the estimated 40 kNm to approximately 80 and 70 kNm for the M1-beams and M2-beams respectively, and for the beams tested for shear the capacity was increased from the estimated 49 kN to approximately 162 kN. For the slabs, the situation is somewhat different. A slab that behaves as the "No – fibre" curve does not fulfil the minimum reinforcement requirement according to EC 2, while the fibre reinforced slab does. However, the moment capacity for the slabs was increased from the estimated 6 kNm to approximately 16 kNm.

8.8 Summary of the ductile high tensile strength all round concrete experience

The experience from the present experimental work on the ductile high tensile strength all round concrete indicates that it is easier to make concrete with desired post-cracking behaviour if the maximum particle size is reduced from 16 mm to 8 mm. Even though the initial tests on the ductile medium tensile strength concrete indicated that the mix design was satisfactory, more work need to be done to optimize the mix design with respect to the segregation tendencies. With regard to the ductile high tensile strength concrete only beam test on small beams have been performed. More work remains also for this concrete, but the results from small beam tests are promising.

A combination of steel- and synthetic fibre seems to be favourable with respect to both fresh and hardened properties, and the results indicate that it is actually possible to utilize the steel fibres' advantageous properties at small deformations and at the same time the synthetic fibres' advantageous properties at larger deformations.

With regard to the strength-, ductility- and practical concrete criterions, the following concretes may be considered satisfactory:

- The ductile low tensile strength concrete including
  - 0.5 vol% synthetic fibres and 0.5 vol% steel fibres (Mix 11-5)
  - 1 vol% steel fibres (Mix 11-4)
- The ductile medium tensile strength concrete including
  - 0.5 vol% synthetic fibres and 0.5 vol% steel fibres (Mix 21-1)
  - 1 vol% synthetic fibres and 1 vol% steel fibres (Mix 21-2)

The ductile medium tensile strength concrete had a compressive strength in the range 45-49 MPa, which means that it belongs to strength class C45/35. When comparing the flexural tensile stress vs. CMOD curves for the ductile medium tensile strength concrete with the flexural tensile stress vs. CMOD curves from chapter 4.2.6.1, it may be stated that the ductile medium tensile strength concrete reinforced with 1 vol% synthetic and 1 vol% steel fibres (Mix 21-2) has larger post-cracking capacity than an ordinary C40/50 concrete reinforced with about $2\times A_{s,min}$.

The residual flexural tensile strength determined by testing small standard beams seems to underestimate the moment- and shear capacity for the large beams, while the moment capacity for the large slabs seems to be overestimated. The fibre orientation, due to different wall effects during casting, combined with possible fibre segregation may partly explain the over- and underestimation, but also the different strain levels may play a role. More research is needed to fully understand these effects, and more research on this topic will indeed be performed at NTNU the following years.

Finally, the results from testing the large beams and panels clearly show that fibre reinforcement is able to increase both the moment capacity and the shear capacity.

9 Discussion of paradoxes from the fibre concrete material models

First of all, the present discussion is limited to the material model used in [RILEM 2002)], [RILEM (2003)] and [MC 2010] because these are most often referred to in the literature.

While the RILEM recommendations are limited to steel fibre reinforced concrete, the Model Code is valid for all fibre types, even though it is written in [MC 2010)] that the rules are mostly based on experience with steel fibres. The σ-w design [RILEM (2003)] is in addition limited to fibre reinforced concrete that exhibit softening behaviour in bending, while it seems like the σ-ε design [RILEM (2002)] is valid also for hardening behaviour.

Even though it is not explicitly formulated in [RILEM (2002)] and [RILEM (2003)] (in contrast to [MC 2010]) it seems like these recommendations assume that the concrete's behaviour in compression is unchanged by the fibres.

Figure 9-1a) shows the stress vs. crack opening relationship (σ-w-relationship) shown in [RILEM (2002)], which presumably is found from uni-axial tensile tests according to [RILEM (2001)]. Figure 9-1b) shows the conceptual theoretical modelling of the σ-w-relationship found in [RILEM (2002)], while Figure 9-1c) shows the σ-w-relationship which [RILEM (2002)] refers to.

a) Figure 4a in [RILEM (2002)]

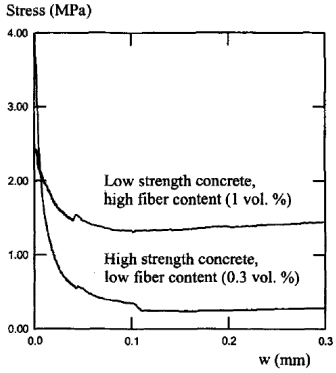

b) Figure 4b in [RILEM (2002)]

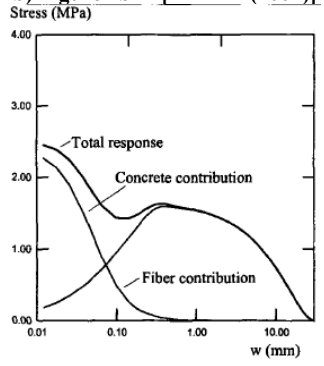

c) Figure 6 in [Li et al (1993)]

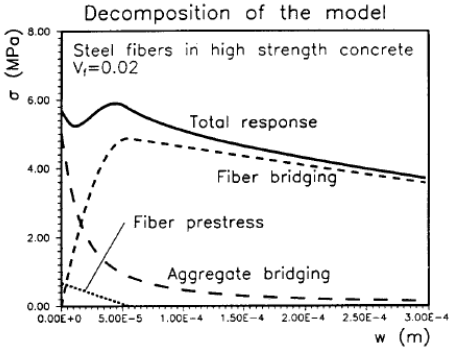

Figure 9-1 σ vs. w-relations

The total response's maximum value in the post-cracking range should be located at the same crack width as the maximum contribution from the fibres. In Figure 9-1c) this corresponds to a crack width of about 0.05 mm, while in Figure 9-1b) this corresponds to a crack width of about 0.33 mm, and in Figure 9-1a) it might correspond to a crack width larger than 0.3 mm, but the X-axis stops at 0.3 mm.

With respect to Figure 9-1a) it should be mentioned that the procedure for uni-axial tension test [RILEM (2001)] will only give correct post-cracking behaviour if all elastic elongation before cracking is located in the notch, regardless of the stiffness of the machine and the logging frequency. In addition, the Model Code recommends beam tests according to NS-EN 14651, and states that uni-axial tensile tests are not advised because they are difficult to perform and interpret. The σ-w-relation in Figure 9-1a) is not in agreement with the conceptual theoretical models in Figure 9-1c) but may be in agreement to Figure 9-1b) if the total response has a maximum around 0.33 mm.

The interesting fact is that even though it is shown in [RILEM (2002)] that the fibre contribution is largest at crack width of about 0.33 mm, this is never accounted for in the illustrations of the stress distribution, neither in [RILEM (2002)], [RILEM (2003)] nor [MC 2010]. Figure 9-2 shows a typical figure for one of the simplified models in [RILEM (2002)], and the model is called "simplified approach by Pedersen".

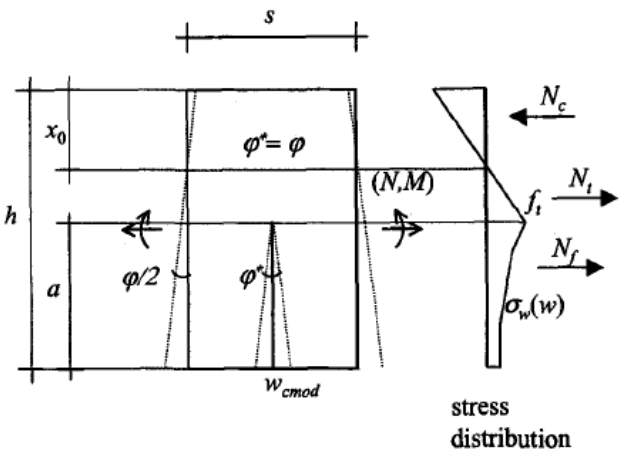

Figure 9-2 Figure 12 in [RILEM (2002)]

In the stress distribution in Figure 9-2 the peak in the tensile zone is due to the concrete's tensile strength, which is in agreement with Figure 9-1, but the maximum fibre contribution is considered to be at a crack opening equal to zero, which is not in agreement to Figure 9-1b) and c), while it is in agreement with Figure 9-1a). More or less the same distribution is used in [MC (2010)] as shown in Figure 9-3.

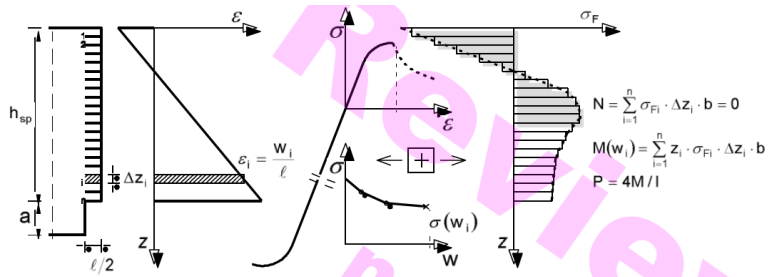

Figure 9-3 Figure 5.6-4 in [MC 2010]

As seen, the σ-w relationship in MC 2010 is also considering the fibre contribution to be largest at zero crack widths.

In contrast to the illustrations of the stress distribution in [RILEM (2002)], [RILEM (2003)] and [MC 2010], Löfgren has illustrated that the fibre contribution first is increasing with increasing crack widths, and thereafter decreasing. The material model from [Löfgren (2005)] is shown in Figure 9-4.

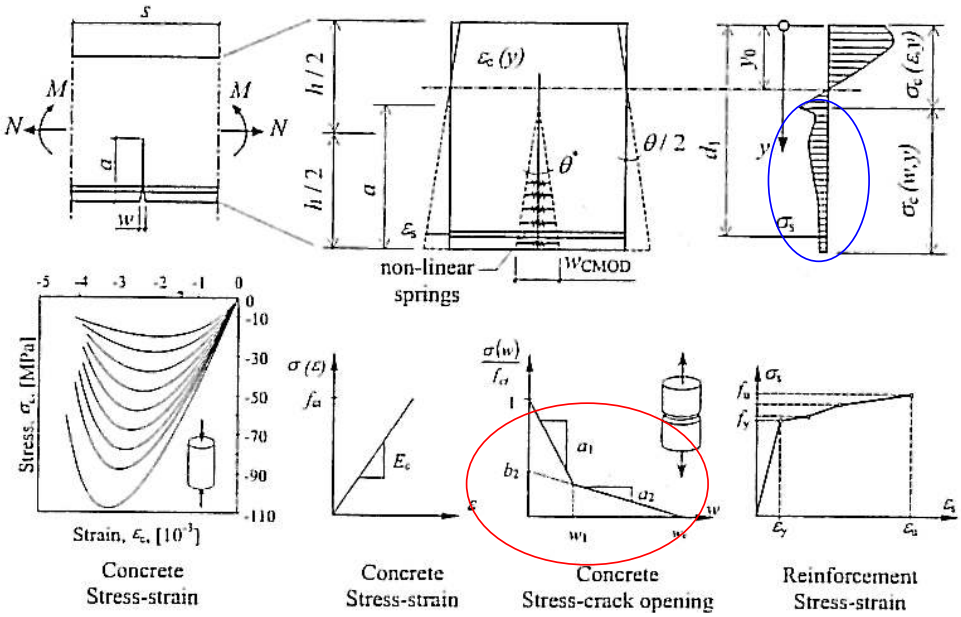

Figure 9-4 Material models from [Löfgren (2005)]

From the illustrations in Figure 9-4 it seems like Löfgren was aware of the fact that fibres are most effective at a certain slip (blue oval), but nevertheless; he chose to use the bi-linear σ-w relationship (red oval) as described in [RILEM (2002)] and shown in Figure 9-5b).

[RILEM (2002)] deals with design principles and applications by use of the σ-w method and four different illustrations of the σ-w relationships are shown. These four illustrations are shown in Figure 9-5 and Figure 9-6.

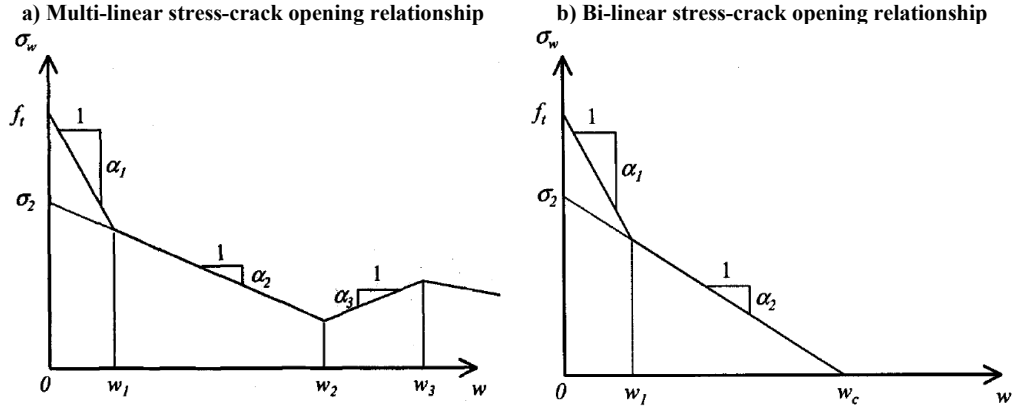

Figure 9-5 Illustration of the multi- and bi-linear relationship [RILEM (2002)]

Even though the multi-linear relationship has a second stress-maximum at w_3, the shape of the stress-crack opening curve is not in accordance with Figure 9-1b) because the X-axes in Figure 9-5 seem to be in linear scale while in Figure 9-1b) and c) the X-axes are in logarithmic scale. It is explained in chapter 3.8 that when uni-axial tensile tests are performed on test specimens where the span is larger than the distance where the elongation is measured, the σ-w relationship is most likely not trustworthy, even though it might have a shape quite similar to Figure 9-5a). For small volumes of fibres without end anchorages it is reasonable to assume that the σ-w relationship may have a shape as illustrated in Figure 9-5b), but then w_c must be quite close to one fourth of the fibre length (or larger), and α_1 must be much larger than then results from uni-axial tests indicate.

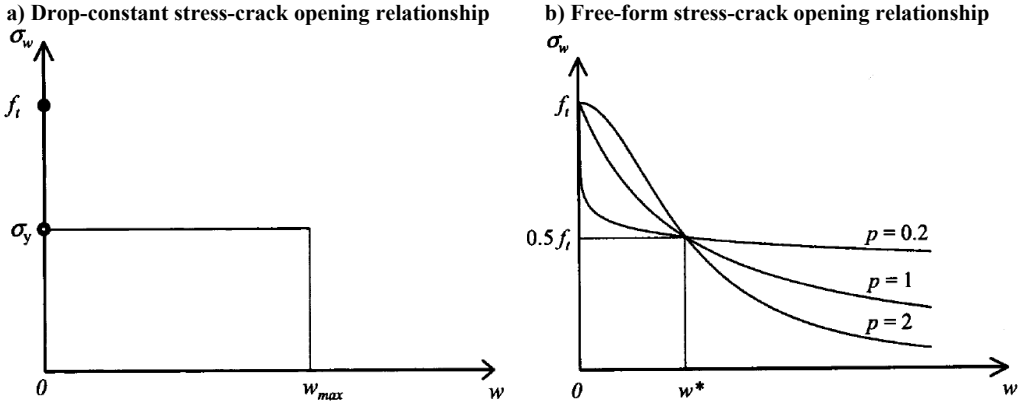

Figure 9-6 Illustration of the drop-constant and free-form relationship [RILEM (2002)]

The drop-constant relationship illustrated in Figure 9-6a) can actually be correct for fibres with an end anchorage, if the end anchorage does not change its geometry when pulled out of the concrete, like the FE-fibres shown in Figure 2-1. Because it is reasonable to assume that the fibres in average have embedment lengths equal to one fourth of the fibre length, w_{max} should be limited to $l_f/4$. The fourth σ-w-relationship illustrated in [RILEM (2002)] is shown in Figure 9-6b), and is called free-form relationship, which reportedly has been used to model a large variety of steel fibre reinforced materials, but it is difficult to relate it to the fibres behaviour when pulled out of the concrete.

It was shown in chapter 3 that the fibres' capacity to obtain loads in pull-out tests on single fibres is largely influenced by the fibre slip, and that the maximum capacity corresponds to a slip of approximately 1 mm for hooked end steel fibres and about 2 mm for the synthetic fibres used in the test program. It was also shown that the apparent softening behaviour immediately after cracking in uni-axial tensile tests might be attributed to the test method, meaning that at least a part of this behaviour is false. The partly stable plateau at larger crack openings on the other hand is real.

The fibre contribution for the beams tested in the *ductile high tensile strength all round concrete* project, reported in chapter 8 can be calculated by subtracting the flexural tensile stress vs. CMOD curve for the unreinforced reference beams from the corresponding curves for beams reinforced with various amount of fibres. These curves are shown in Figure 9-7.

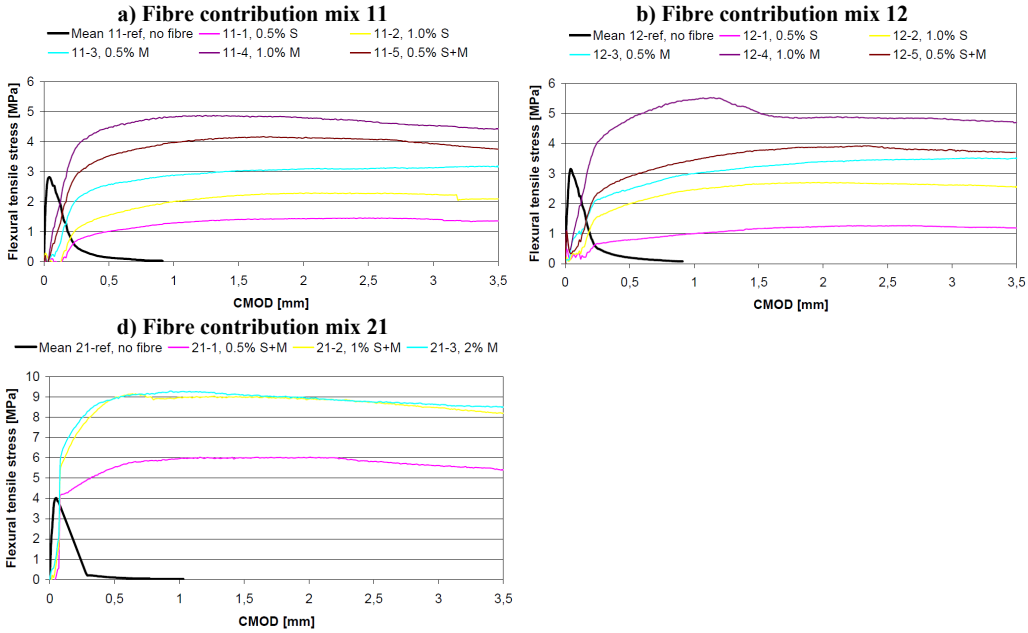

Figure 9-7 Fibre contribution in the beams from chapter 8

There are almost unlimited stress configurations that can be used in inverse analysis to fit the flexural tensile stress vs. CMOD curves in Figure 9-7. The simplest model will be to assume a rectangular stress block in the tensile zone and constant tensile strength. If the height of the compressive zone is considered to be constant with regard to the crack opening, then the capacity in the post-cracking range will also be constant. With regard to the curves in Figure 9-7, these two assumptions are actually reasonably good, because the residual flexural tensile stress vs. CMOD curve for all beams is quite horizontal.

If the height of the compressive zone is decreasing with increasing CMOD, then the fibre stress must vary as a function of the crack width, otherwise the capacity will increase with increasing CMOD. In [RILEM (2003)], the compressive zone is considered to be larger at small CMOD, which means that a constant fibre stress will result in a capacity that is CMOD dependent.

The suggestions by RILEM and MC 2010 imply that both the fibre stress and the height of the compressive zone shall decrease as functions of the crack width for the results in Figure 9-7.

By the linear model in MC 2010, shown in Figure 9-8, the moment capacity can be calculated by the ultimate tensile strength in uni-axial tension, f_{Ftu}, which is determined from bending tests (NS-EN 14651) as:

$$f_{Ftu} = f_{Fts} - \frac{w_u}{CMOD_3}\left(f_{Fts} - 0.5f_{R,3} + 0.2f_{R,1}\right) \quad (9\text{-}1)$$

where

$$f_{Fts} = 0.45f_{R,1} \quad (9\text{-}2)$$

By replacing f_{Fts} with $0.45f_{R,1}$ and $CMOD_3$ with 2.5 mm, f_{Ftu} can be written as:

$$f_{Ftu} = 0.45f_{R,1} - \frac{w_u}{2.5}\left(0.65f_{R,1} - 0.5f_{R,3}\right) \quad (9\text{-}3)$$

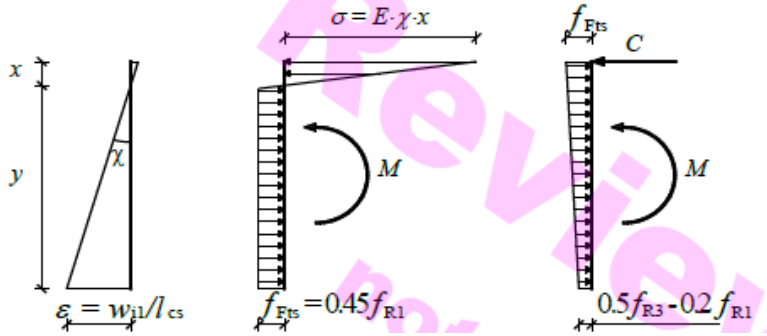

Figure 9-8 Simplified calculation model from MC 2010, figure 5.6-9

If f_{Ftu} shall be independent of the crack width, then $f_{R,3}$ must be equal to $1.3 \times f_{R,1}$, which does not seem logical, because then the tested beams always show hardening behaviour. $f^{f}_{ct,L}$, $f_{R,1}$ and $f_{R,3}$ for the beams in series 11-5, 21-1 and 21-2 from the *ductile high tensile strength all round concrete* project are summarized in Table 9-1.

Table 9-1 Results from beam tests

Series	$f^{f}_{ct,L}$ [MPa]	$f_{R,1}$ [MPa]	$f_{R,3}$ [MPa]	$f_{R,3}/f_{R,1}$
11-5	3.2	3.6	4.1	1.14
21-1	4.4	5.5	6.0	1.09
21-2	5.7	8.9	8.9	1.0

None of these beams will have a moment capacity that is independent of the crack width according to MC 2010 because the ratio $f_{R,3}/f_{R,1}$ is less than 1.3. All beams will therefore have reduced calculated moment capacity with increasing crack widths. However, as seen in Figure 9-7, it is quite clear that the capacity in reality was increasing with increasing CMOD.

With regard to design, it may be reasonable to require $f_{R,3} = 1.3 \times f_{R,1}$ to consider the concrete to have hardening behaviour, but the material model seems to be incorrect. As seen from Figure 9-8, the tensile stress in the material model in MC 2010 varies over the height of the beam and it is largest near the compressive surface. This calculation model is in conflict with the experience from both the pull-out tests on single fibres reported in chapter 3, the fibre contribution from beam tests shown in Figure 9-7 and with the σ-w relations shown in Figure

9-1. The material model should more probably be as shown in Figure 9-9 if the above mentioned effects are taken into consideration.

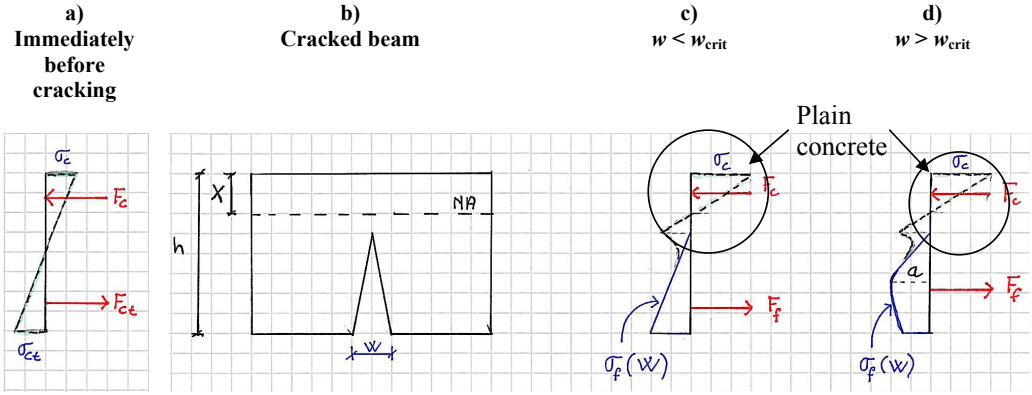

Figure 9-9 Proposed material model

In which way the concrete in compression should be modelled depends on the compressive strain. Normally the compressive strain in fibre reinforced concrete is small enough to justify a triangular stress block, but increased compressive strain due to either large fibre volume or re-bars may result in a more rectangular stress block. In which way the tensile strength of the concrete is utilized has minor influence on the calculated capacity, primarily because the moment arm is very small, and secondly because the contribution to the force equilibrium is small.

The residual tensile strength, $f_{ft,res}$, is due to fibres crossing the crack, and the fibre stress, σ_f, is a function of the crack width, w, and written as $\sigma_f(w)$. Point a in Figure 9-9d) represents $\sigma_f(w=w_{crit})$ meaning that the largest fibre stress is obtained when the crack opening is about 1 mm for steel fibre reinforced concrete and about 2 mm for synthetic fibre reinforced concrete.

As for other material models, the height of the compressive zone, X, can be found by force equilibrium. The stress distribution shown in Figure 9-9 for $w>w_{crit}$ is in reality identical to the stress distribution shown in Figure 9-4 (blue oval), but in Figure 9-9 it is illustrated that $\sigma_f(w)$ can be larger than the tensile strength of the concrete, which is possible if stresses are transferred from one fibre to another.

In Figure 9-4 the concrete stress in the crack is written as a function of both the crack width and the distance from the compressive surface ($\sigma_c(w,y)$), while in Figure 9-9 the fibre stress is written as a function of the crack width ($\sigma_f(w)$). In the latter, the crack width is a function of the distance from the compressive surface, and if the concrete's capacity to transfer stresses across cracks is considered to be zero, the expressions for the capacity in the tensile zone is equal.

The σ-w relationship is mainly of interest as a basic material input for design. By use of some kind of small scale tests (for instance small beam test, uni-axial tensile test, wedge splitting test or other), the σ-w relationship can be determined by curve fitting to the experimental small scale results. With regard to the σ-w relationships shown in Figure 9-5 and Figure 9-6 four different σ-w relationships can be determined, in which all of them may fit the small scale results. When the material properties are defined, the idea is that the behaviour of a

random concrete structure can be calculated by use of the σ-w relationship. Several researchers have found that the bi-linear σ-w relationship provides relatively good agreement with experimental results, but this does not mean that the bi-linear σ-w relationship is a correct material model. In addition, Jansson has found that the multi-linear σ-w relationship describes the cracking procedure better than the bi-linear σ-w relationship [Jansson (2008)]. Further, Jansson has also compared the bi-linear and the multi-linear σ-w relationship with experimental results from third point bending tests on larger beams [Jansson et al. (2010)]. The beams were 2 m long, the free span was 1.8 m, and the cross section was 150×225 mm. These beams were in addition reinforced with re-bars, either 3×Ø8 mm or 3×Ø6 mm. The experience from this comparison was that the bi-linear and the multi-linear σ-w relationship gave equally good agreement with the experimental behaviour.

The σ-w relationships from [Jansson et. al (2010)] and the σ-w relationship that corresponds to the uni-axial tensile test shown in Figure 3-21 is shown in Figure 9-10.

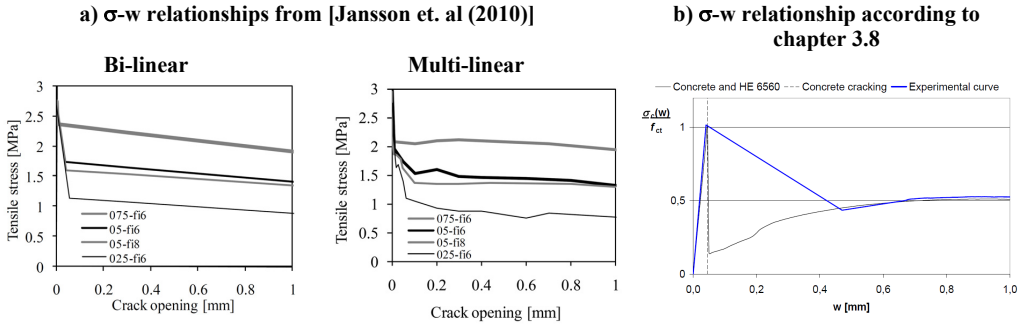

Figure 9-10 Comparison σ-w relationships

In Jansson's studies 35 mm long HE steel fibres were used, while 60 mm long HE steel fibres were used in the studies described in chapter 3.8, which means that Figure 9-10a) and b) are not directly comparable. Even so, results from the present pull-out tests seem to contradict the σ-w relationships from [Jansson et. al (2010)] shown in Figure 9-10a) and b). If the moment capacity at relatively large crack openings is calculated according to the model shown in Figure 9-4, the difference in capacity by using the σ-w relationship in Figure 9-10a) and c) to describe the tensile zone (blue oval in Figure 9-4) should not be that large because the force resultant from Figure 9-10c) would be less than the force resultant from Figure 9-10a, while the internal moment arm would be larger.

10 Overall conclusions and suggestions for further work

10.1 Overall conclusions

The results from pull-out tests on single fibres show that it is a large difference in the necessary fibre slip to fully utilize different types of fibres. While the hooked end steel fibres reached their maximum capacity at a slip equal to about 0.7-1 mm, the flat end steel fibres reached their maximum at approximately 1.5 mm, the synthetic fibres reached their maximum at about 1.8-2.5 mm and finally the sinus waved steel fibres reached their maximum at about 3 mm. The fact that different fibre types reach their maximum capacity at significantly different slip should influence the behaviour in real structures, and a method to use the results from pull-out tests to predict the behaviour in bending and tension is proposed. When this method is compared to results from uni-axial tensile tests and bending tests, the results correspond well.

It is shown in chapter 3 that if a beam made of concrete in strength class C 40/50 is reinforced with the minimum reinforcement ratio according to EC 2, and tested according to the European Standard for beam tests of metallic fibre concrete (NS-EN 14651), the expected value of the residual flexural tensile strength is about 3.5 MPa, and the corresponding stress at cracking is expected to be about 5 MPa. A fibre reinforced beam in the same strength class is therefore expected to show larger capacity than a minimum reinforced beam if the residual flexural tensile strength determined from NS-EN 14651 tests is larger than 3.5 MPa for all crack openings. This requirement is of course much easier to fulfil than the requirement of hardening behaviour in bending. It is also shown that 0.7 vol% Dramix 6560 fibres may be sufficient to show hardening behaviour bending when tested according to NS-EN 14651, while 1 vol% Barchip Shogun fibres may be sufficient to have a residual flexural tensile strength larger than 3.5 MPa. The implication of this is that fibres actually can replace conventional reinforcement in structures reinforced with the minimum reinforcement ratio.

Different codes for determining the energy absorption capacity prescribes different panel dimensions. If the deflection limit is corrected in such a way that the maximum crack opening is equal for all panel dimensions, the capacity to absorb energy will not be dependent of the panel dimension. However, the measured energy must also be corrected for deviating heights.

If results from both beam- and panel tests are expressed as residual flexural tensile stress vs. crack opening, it is possible to compare the results directly, and it is shown in chapter 6 that results from beam and panel tests correspond well. The implication of this is that both beam and panel tests are basically measuring the same material property, namely the residual flexural tensile strength. The main difference is that the panel tests in general measures the behaviour to larger crack openings than beam tests.

A theoretical investigation shows that the relation between results from panels tested according to the Norwegian Concrete Association Publication nr 7 (NB 7) and the American Standard test method for flexural toughness of fibre reinforced concrete panels (ASTM C 1550) is in the range 2.03-2.91, depending on the number of cracks in the NB 7-panels and the contribution due to friction in both test methods. It is also shown that the circular panels prescribed in NB 7 and the quadratic panels prescribed in the European Standard for determination of energy absorption capacity (NS-EN 14488-5) theoretically should give quite similar results. The empirical relation between ASTM-panels and panels tested according to

NS-EN 14488-5 is in other investigations found to be about 2.5, which corresponds well to the theoretical relation obtained in the present work.

From the experimental work related to the ductile high tensile strength all round concrete project, it was found that it was easier to control the post-cracking behaviour if the maximum aggregate size was limited to 8 mm. When steel fibres and synthetic fibres were combined, it seemed like the steel fibres contributed to necessary strength while the synthetic fibres contributed to necessary ductility. The fibres' contribution to the shear- and moment capacity was significant, and can be summarized as:

- The increase in moment capacity due to fibres was about:
  - 100 % for the ductile medium tensile strength concrete beams (1 vol% Dramix 6560 + 1vol% Barchip Shogun)
  - 75 % for the ductile low tensile strength concrete beams (0.5 vol% Dramix 6560 + 0.5 vol% Barchip Shogun)
- The increase in shear capacity due to fibres is more difficult to quantify. If the shear capacity for structures without shear reinforcement calculated according to EC 2 is correct, the increase in capacity due to fibres was about 235 % for the ductile low strength concrete beams (0.5 vol% Dramix 6560 + 0.5 vol% Barchip Shogun). However, based on the experience from shear tests at NTNU the calculated shear capacity of structures without shear reinforcement may be only 50 % of the experimental determined shear capacity, leading to an increase due to fibres of about 68 %.
- The increase in moment capacity for the large slabs made of the ductile low tensile strength concrete (0.5 vol% Dramix 6560 + 0.5 vol% Barchip Shogun) was about 167 %.

Another interesting observation from the large scale vs. small beam tests is that the residual tensile strength, $f_{ft,res}$, seems to be underestimated for the large beams tested for moment failure, while it is overestimated for the large panels tested for moment failure. This is in strong contradiction to German Rules for design of fibre reinforced concrete.

The ductile high tensile strength concrete showed very promising behaviour in bending, and the residual flexural tensile strength determined from beam tests according to NS-EN 14651 was larger than 13 MPa for a crack width from about 0.75-3.5 mm, and the maximum strength was almost 14 MPa, and occurred at a crack width about 2 mm.

From a scientific point of view, the main conclusion is that it seems like it is possible to relate the fibres contribution to the hardened concrete properties by the crack opening, and that material models which take into consideration the different fibre types need of crack width to be fully utilized should be developed.

From a practical point of view, the main conclusion is that fibres can be used both as replacement for conventional reinforcement in minimum reinforced structures, and to strengthen structures which are additionally reinforced with conventional re-bars.

10.2 Suggestions for further work

A relatively large database of results from pull-out tests on single fibres is now available. These results can be used in more sophisticated calculation methods than used in the present thesis. It should be investigated if the results from the pull-out tests, together with the proposed material model can predict the behaviour of a fibre reinforced structure properly by use of more sophisticated calculation methods. Regardless of the calculation method, a material model for fibre reinforced concrete in tension is needed, and the material model shown in the most common recommendations are in conflict with the results from the pull-out tests. To the author's knowledge, there is no proof in the literature, which supports the assumption that fibres are most effective at small fibre slip, a matter that also should be further investigated.

The idea of using sawn concrete specimens from real structures to determine the residual flexural tensile strength is indeed good, but because the European standard for flexural tensile strength determination is based on another beam tests method, the correlation between sawn beams and cast beams should be further investigated. It might also be a good idea to test the sawn beams according to the European standard, which would reduce the difference between these two methods to the casting procedure. If only the casting procedure is different, the relation between the two methods should be easier to quantify.

The calculated relation between results from panel tests according to ASTM C 1550 and NB 7 is in good agreement with the empirical relation found by others. Even so, it should be further investigated whether the relation is correct or not, an investigation that is very easy to conduct: Cast panels and test them according to the two different codes, and compare the results. Be aware of the fact that it is necessary to increase the deflection limit with increasing number of cracks. The relation between the square panels as prescribed in NS-EN 14488-5 and circular panels as prescribed in NB 7 should also be examined further. This investigation is also very easy to perform, and also in this case care must be taken so that the panels are tested to large enough deflection. This investigation should be of interest also for the Norwegian Concrete Association because these two test methods are ranked pari passu in the new revision of the NB 7.

To be able to use fibre reinforced concrete as replacement for conventional re-bars, one has to be sure that the fibres contribution to the strength is in accordance with the strength determined from small scale tests. This is especially important for slabs where it has been shown that the fibre contribution can be less than expected from testing the reference beams.

The goal of COIN's fibre project is quite ambitious. If the ductile high tensile strength concrete project succeeds, it opens for using fibre reinforcement in a large range of concrete structures. Even so, with today's knowledge fibres should have been more used as reinforcement for instance in slabs on ground. The author's conviction after barely one month as a consultant engineer is that the main reason why fibres are not used in such structures is the absence of generally accepted design codes. The contractors within COIN have a lot of knowledge and experience, which should be brought to the consultant engineers. To increase the knowledge of the consultant engineers, one possibility is to work out a publication, which explains how fibres can be used as reinforcement in a particular structure as for instance slabs on ground. Even though the Norwegian design rule draft is already available and valid for all kind of structures, it might be too general for engineers who are not familiar to fibre reinforced concrete.

References

ASTM C 1550 (2008): *Standard Test Method for Flexural Toughness of Fiber Reinforced Concrete (Using Centrally Loaded Round Panel*).ASTM, West Conshohocken

Banholzer, B., Brameshuber, W. and Jung, W (2006): *Analytical evaluation of pull-out tests – The inverse problem*. Cement & Concrete Composites 28 (2006), pp 564-571

Barchip: Data sheet for fibres available at www.elastoplastic.com (June 2011)

Bekaert: Data sheet for fibres available at www.bekaert.com (June 2011)

Bernard, E. S., Tutlu, E. and Diamant1idis, D (2003): *Crack Offset Corrections to Post-crack Performance Parameters Obtained from Third-point Loaded Fiber Reinforced Shotcrete Beams*. Cement, Concrete and Aggregates, Vol. 25, No. 2.

Bernard, E. S. and Xu, G. G. (2010): *Crack widths in ASTM C-1550 panels*. Shotcrete: Elements of a System. ISBN 978-0-415-47589-1

Bernard, E. S.(2005): *The Role of Friction in Post-Crack Energy Absorption of Fiber Reinforced Concrete in the Round Panel Test*. Journal of ASTM International, January 2005, Vol. 2, No. 1

Bernard, E. S. and Pircher, M. (2001): *The Influence of Thickness on Performance of Fiber-Reinforced Concrete in a Round Determinate Panel Test*. Cement, Concrete and Aggregates, Vol. 23, No. 1

Bernard, E. S. (2001): *The Influence of Strain Rate on Performance of Fiber-Reinforced Concrete Loaded in Flexure*. Cement, Concrete, and Aggregates, Vol. 23, No. 1

Bernard, E. S. (2002): *Correlation in the behaviour of fibre reinforced shotcrete beam and panel specimens.* Material and Structures, Vol. 35, pp156-164.

Bjøntegaard, Ø. (2009a): *Energy absorption capacity for fibre reinforced sprayed concrete. Effect of friction in round and square panel tests with continuous support (Series 4)*. Technology report no. 2534, Norwegian Public Roads Administration, Road Directorate. 2009-02-16, ISSN 1504-5005

Bjøntegaard, Ø. (2009b): *Energy absorption capacity for fibre reinforced sprayed concrete. Influence of friction in round panel tests with different support- and bedding conditions (Series 7)*. Technology report no. 2575, Norwegian Public Roads Administration, Road Directorate. 2009-12-08, ISSN 1504-5005

Bjøntegaard, Ø. & Myren, S. A. (2011): *Fibre Reinforced Sprayed Concrete Panel Tests: Main Results from a Methodology Study Performed by the Norwegian Sprayed Concrete Committee*. 6th Int. Symp. on Sprayed Concrete, Tromsø, 12-15 Sept, 2011.

Chanvillard, G. (1999): *Modelling the pullout of wire-drawn steel fibers*. Cement and Concrete Research 29, pp 1027-1037

DAfStb (2008): *DAfStb-Richtlinie Stahlfaserbeton*. Ergänzung zu DIN 1045, Teile 1 bis 4 (08/2008). Deutscher Ausschuss für Stahlbeton, DAfStb, Berlin (in German)

Døssland Å.L. (2008): *Fibre reinforcement in load carrying concrete structures*. PhD-thesis, Department of structural engineering, NTNU, Trondheim, Norway, April 2008

EC 2 (2004): *Design of concrete structures – Part 1-1: General rules and rules for buildings*. (NS-EN 1992-1-1:2004). CEN, European Committee for Standardization

EFNARC (1999*): European specification for sprayed concrete. Guidelines for specifiers and contractors*. Available at www.efnarc.org

Gjestemoen, A. (2005): *Syntetisk fiberarmering i betongkonstruksjoner: Anvendelsesområder og virkemåte etter oppressing*. Master-thesis, NTNU. (In Norwegian)

Gysel, A. van (2000): *Studie van het uttrekgedrag van staalvezels ingebed in een cementgebonden matrix met toepassing op staalvezelbeton onderworpen aan buiging*. PhD-thesis, Laboratorium Magnel voor Betononderzoek, Unversiteit Gent (in Dutch)

Hammer, T. A. (2011): *COIN – Concrete Innovation Centre, Midterm status*. Nordic Concrete Research, Publication No. 43, pp 7-10

Hisdal, J.-M. (2011): *State of the art – Ultra High Performance Fibre Reinforced Concrete (UHPFRC)*. Draft. To be published as COIN Project report

Jansson, A. (2008): *Fibres in reinforced concrete structures – analysis, experiments and design*". Lic. thesis, Chalmers University of Technology

Jansson A., Løfgren I. and Gylltoft K. (2010): *Flexural Behaviour of Members with a Combination of Steel Fibres and Conventional Reinforcement*. Nordic Concrete Research, Publication No. 42, pp. 155-171

Kanstad (2009): *Fibre Reinforced Superlight Concrete. Testing of Materials and Full Scale Beams*. COIN Project report 15, ISBN 978-82-536-1122-8

Kanstad et al. (2011): *Forslag til retningslinjer for dimensjonering, utførelse og kontroll av fiberarmerte betongkonstruksjoner*. COIN Project report 29, ISBN 978-82-536-1223-2 (In Norwegian)

Kennedy, G and Goodchild, C (2003): *Practical yield line design*. British Cement Association Publication 97.375. ISBN 0 07210 1585 9

Laranjeira, F., Aguado, A. and Molins, C. (2010): *Predicting the pullout response of inclined straight steel fibers*, Materials and Structures, Vol 43, No 6, pp 875-895

Lauvålien, K. and Sandbakk, S. (2007): *Fiberarmerte betongkonstruksjoner med stål- og syntetisk fiber*. Master thesis, NTNU. (In Norwegian).

Li, V. and Wu, H.-C. (1992): *Condition for pseudo strain-hardening in fiber reinforced brittle matrix composition.* Micromechanical modelling of quasi-brittle materials behaviour. ASME Book no AMR118, 1992

Li, V., Mishra, D. and Wu, H.-C. (1995*): Matrix design for pseudo-strain-hardening fibre reinforced cementitious composites*. Materials and Structures, Vol 28, No 10, pp 586-595

Li, V. C. and Stang, H. (1997): *Interface property characterization and strengthening mechanisms in fiber reinforced cement based composites*. Advanced Cement Based Materials, Vol 6, pp 1-20

Löfgren, I. (2003): *Analysis of Flexural Behaviour of Reinforced FRC Members*. Design Rules for Steel Fibre Reinforced Concrete Structures, proceedings from Workshop Oslo 6th October 2003, The Nordic Concrete Federation.

Löfgren, I. (2005): *Fibre reinforced concrete for Industrial Construction – a fracture mechanics approach to material testing and structural analysis*. PhD-thesis, Chalmers Göteborg.

Maage, M. (2003): *Betong til ulike formål*. Textbook, Concrete technology 1, UM 1, NTNU. (In Norwegian)

Minelli, F. and Plizzari G. A. (2010): *Fiber Reinforced Concrete Characterization through Round Panel Test – Part II: Analytical and Numerical Study*.

Mørtsell, E. (1996): *Modellering av delmaterialenes betydning for betongens konsistens*. Dr.ing.avhandling (PhD-thesis), NTNU. (In Norwegian)

NB 7 (2003): *Sprøytebetong til bergsikring*, Norsk betongforenings publikasjon nr. 7. (In Norwegian).

NB 7 (2011): *Sprøytebetong til bergsikring*, Norsk betongforenings publikasjon nr. 7. (In Norwegian).

NS3473 (2003): *Prosjektering av betongkonstruksjoner. Beregning og konstruksjonsregler.* Norwegian Standard Institution. (In Norwegian)

NS-EN 12390-5 (2009): *Testing hardened concrete – Part 5: Flexural strength of test specimens*. CEN, European Committee for Standardization

NS-EN 14488-3 (2006): *Testing sprayed concrete – Part 3: Flexural strengths (first peak, ultimate and residual) of fibre reinforced beam specimens*. CEN, European Committee for Standardization

NS-EN 14488-5 (2006): *Testing sprayed concrete – Part 5: Determination of energy absorption capacity of fibre reinforced slab specimens*. CEN, European Committee for Standardization

NS-EN 14651 (2005): *Test method for metallic fibre concrete. Measuring the flexural tensile strength (limit of proportionality (LOP), residual)*. CEN, European Committee for Standardization

NS-EN 206-1 (2000): *Concrete – Part 1: Specification, performance, production and conformity*. CEN, European Committee for Standardization

Nordhus, Steinnes and Simpson (2011): *Fiberarmerte betongkontstruksjoner: Prøving av bjelker og plater av selvkomprimerende duktil fiberbetong*. Master thesis, NTNU (In Norwegian)

Pompo, A., Stupak, P.R., Nikolais, L. and Marchese, B. (1996): *Analysis of Steel Fibre Pull-Out from a Cement Matrix using Video Photography*. Cement and Concrete Composites, Vol 18, pp 3-8

Rescon Mapei: Data sheet for Dynamon SP-130 available at www.mapei.com (June 2011)

RILEM TC 162-TDF (2001): *Test and design methods for steel fibre reinforced concrete. Uni-axial tension test for steel fibre reinforced concrete*. Materials and Structures, Vol 34, pp. 3-6.

RILEM TC 162-TDF (2002): *Test and design methods for steel fibre reinforced concrete. Design of steel fibre reinforced concrete using the σ-w method: principles and applications*. Materials and Structures, Vol 35, pp 262-278

RILEM TC 162-TDF (2003): *Test and design methods for steel fibre reinforced concrete. σ–ε-design method*. Materials and Structures, Vol 36, pp 560-567

Robins, P., Austin, S. and Jones, P (2002): *Pull-out behaviour of hooked steel fibres*. Materials and Structures, Vol 35, pp 434-442

Sandbakk, S., Lauvålien, K. and Stenvaag G. H. (2006): *Fiberarmerte betongkonstruksjoner*. Project work, NTNU. (In Norwegian)

Sandbakk, S., Kanstad, T., Bjøntegaard, Ø., Vandewalle, L. and Parmentier, B. (2010): *International Round Robin Testing of Circular FRC slabs*. COIN Project report 23, ISBN 978-82-536-1172-3

Sørensen, S. I. (2010): *Betongkonstruksjoner*. Design of concrete structures according to NS3473, text book. (In Norwegian)

Sørensen, S. I. (2010): *Betongkonstruksjoner*. Design of concrete structures according to EC 2, text book. (In Norwegian)

Thorenfeldt, E.V. (2003): *Theoretical tensile strength after cracking. Fibre orientation and average stress in fibres*. Design Rules for Steel Fibre Reinforced Concrete Structures, proceedings from Workshop Oslo 6th October 2003, The Nordic Concrete Federation

Thorenfeldt, E.V. et al. (2006): *Stålfiberarmering i betong. Veiledning for prosjektering, utførelse og kontroll*. Draft. (In Norwegian)

Vikan, H., Sandbakk, S. and Kanstad, T. (2011): *Material properties influencing concrete residual bending strength – Experimental study*. COIN Project report 28, ISBN 978-82-536-1222-5

Weiler, B. and Grosse, C. (1996): Pullout Behaviour of Fibres in Steel Fiber Reinforced Concrete. Available at www.mpa.uni-stuttgart.de . German name: Auszieverhalten von Fasern in Stahlfaserbeton

Appendixes

Appendix A: Results from beam tests

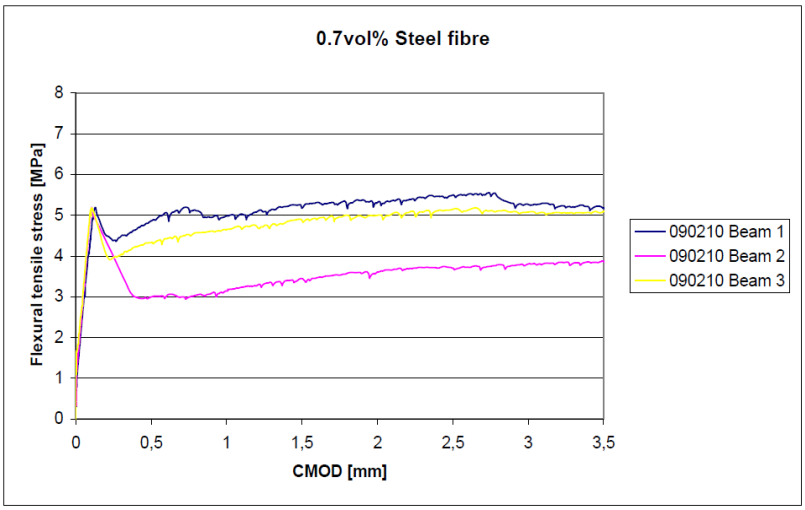

Stress vs CMOD diagram cast beams, 4-point testing (NS-EN 14651, NSBT), steel fibres

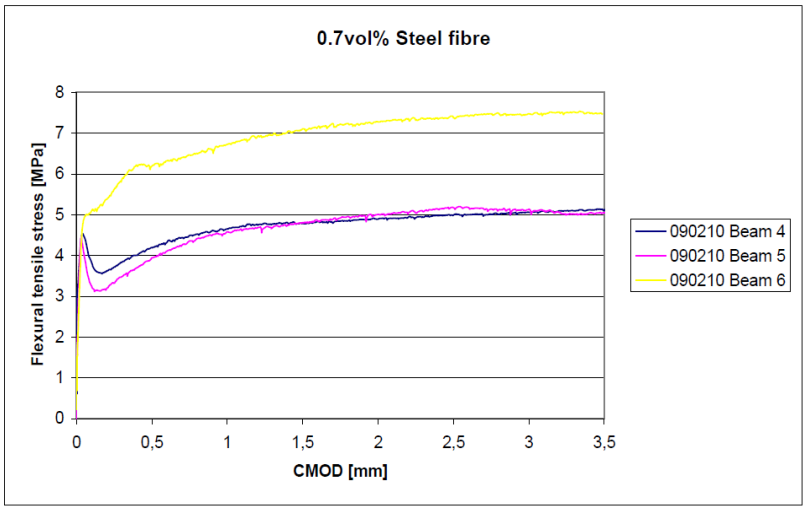

Stress vs CMOD diagram cast beams, 3-point testing (NS-EN 14651, NS-EN 14651), steel fibres

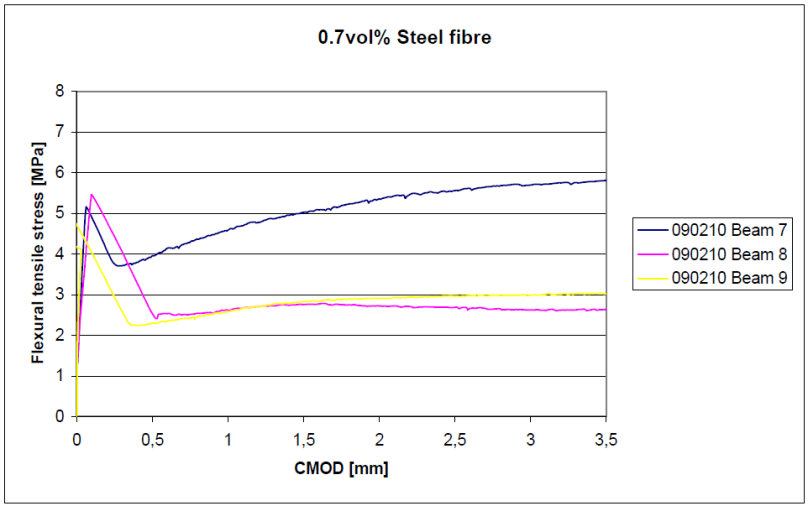

Stress vs CMOD diagram sawn beams, 4-point testing (NSBT, NSBT), steel fibres

Results cast beams, 4-point testing (NS-EN 14651, NSBT), steel fibres

	090210 Beam 1	090210 Beam 2	090210 Beam 3	**Mean value**	Coefficient of variation
b [mm]	151.5	151	150.5	151.00	0.3 %
h_{sp} [mm]	149.5	149	148.5	149.00	0.3 %
l [mm]	450	450	450	450.00	0.0 %
f_{peak} [MPa]	5.19	5.19	5.13	**5.17**	0.7 %
$f_{R.1}$ [MPa]	4.86	2.99	4.33	**4.06**	23.7 %
$f_{R.2}$ [MPa]	5.17	3.45	4.87	**4.50**	20.5 %
$f_{R.3}$ [MPa]	5.49	3.70	5.14	**4.78**	19.8 %
$f_{R.4}$ [MPa]	5.18	3.87	5.08	**4.71**	15.5 %
δ_{peak} [mm]	0.066	0.064	0.062	**0.06**	3.1 %
$CMOD_{peak}$ [mm]	0.130	0.104	0.097	**0.11**	15.8 %

Results cast beams, 3-point testing (NS-EN 14651, NS-EN 14651), steel fibres

	090210 Beam 4	090210 Beam 5	090210 Beam 6	**Mean value**	Coefficient of variation
b [mm]	151	151.5	151	151.17	0.2 %
h_{sp} [mm]	125	125	125	125.00	0.0 %
l [mm]	500	500	500	500.00	0.00 %
f_{peak} [MPa]	4.54	4.46	4.78	**4.59**	3.7 %
$f_{R.1}$ [MPa]	4.19	3.94	6.19	**4.78**	25.8 %
$f_{R.2}$ [MPa]	4.79	4.81	7.10	**5.57**	24.0 %
$f_{R.3}$ [MPa]	4.99	5.17	7.38	**5.85**	22.8 %
$f_{R.4}$ [MPa]	5.12	5.04	7.44	**5.87**	23.3 %
δ_{peak} [mm]	0.040	0.032	0.043	**0.04**	14.8 %
$CMOD_{peak}$ [mm]	0.040	0.032	0.043	**0.04**	14.8 %

Results sawn beams, 4-point testing (NSBT, NSBT), steel fibres

	090210 Beam 7	090210 Beam 8	090210 Beam 9	**Mean value**	Coefficient of variation
b [mm]	150	150.5	151	150.50	0.3 %
h_{sp} [mm]	151	152	153	152.00	0.7 %
l [mm]	450	450	450	450.00	0.0 %
f_{peak} [MPa]	5.16	5.46	4.87	**5.17**	5.7 %
$f_{R.1}$ [MPa]	3.95	2.59	2.25	**2.93**	30.6 %
$f_{R.2}$ [MPa]	5.03	2.76	2.81	**3.53**	36.7 %
$f_{R.3}$ [MPa]	5.56	2.69	2.96	**3.74**	42.3 %
$f_{R.4}$ [MPa]	5.81	2.64	3.02	**3.82**	45.3 %
δ_{peak} [mm]	0.040	0.059	0.025	**0.04**	41.2 %
$CMOD_{peak}$ [mm]	0.063	0.096	0.040	**0.07**	42.4 %

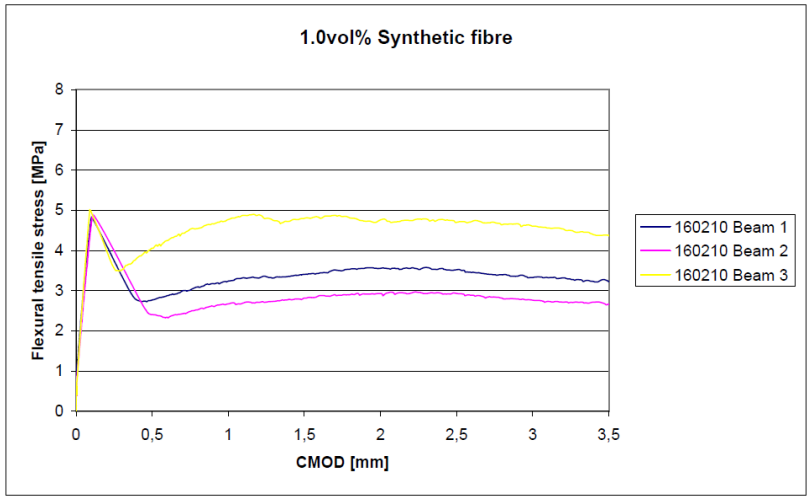

Stress vs CMOD diagram cast beams, 4-point testing (NS-EN 14651, NSBT), synthetic fibres

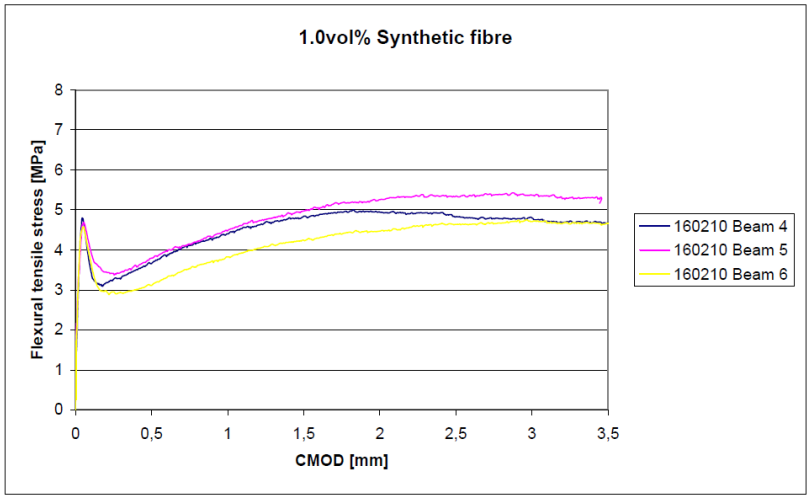

Stress vs CMOD diagram cast beams, 3-point testing (NS-EN 14651, NS-EN 14651), synthetic fibres

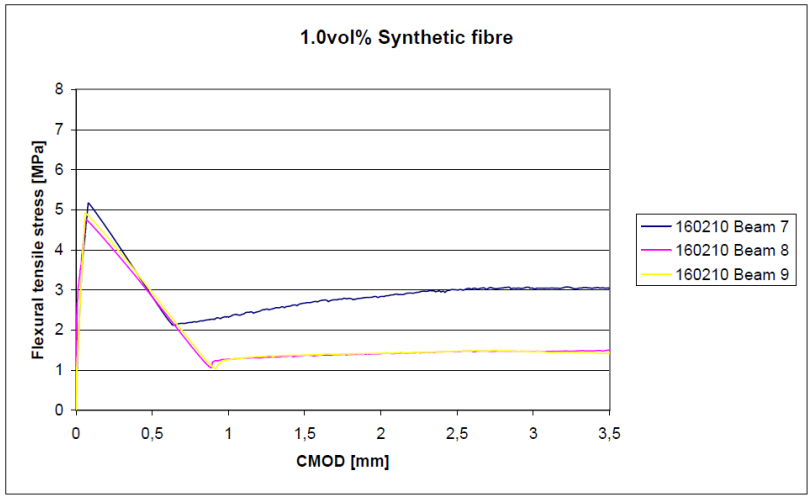

Stress vs CMOD diagram sawn beams, 4-point testing (NSBT, NSBT), synthetic fibres

Results cast beams, 4-point testing (NS-EN 14651, NSBT), synthetic fibres

	160210 Beam 1	160210 Beam 2	160210 Beam 3	**Mean value**	Coefficient of variation
b [mm]	152	153	153.5	152.83	0.5 %
h_{sp} [mm]	150	150	149	149.67	0.4 %
l [mm]	450	450	450	450.00	0.0 %
f_{peak} [MPa]	4.84	4.90	5.02	**4.92**	1.9 %
$f_{R.1}$ [MPa]	2.77	2.40	4.06	**3.08**	28.2 %
$f_{R.2}$ [MPa]	3.41	2.81	4.80	**3.67**	27.7 %
$f_{R.3}$ [MPa]	3.52	2.93	4.70	**3.72**	24.2 %
$f_{R.4}$ [MPa]	3.23	2.66	4.38	**3.42**	25.5 %
δ_{peak} [mm]	0.06	0.06	0.07	**0.06**	9.1 %
$CMOD_{peak}$ [mm]	0.10	0.11	0.09	**0.10**	10.00 %

Results cast beams, 3-point testing (NS-EN 14651, NS-EN 14651), synthetic fibres

	160210 Beam 4	160210 Beam 5	160210 Beam 6	**Mean value**	Coefficient of variation
b [mm]	150.5	151	150.5	150.7	0.2 %
h_{sp} [mm]	125	125.5	125	125.2	0.2 %
l [mm]	500	500	500	500.0	0.0 %
f_{peak} [MPa]	4.80	4.68	4.58	**4.7**	2.3 %
$f_{R.1}$ [MPa]	3.66	3.80	3.11	**3.5**	10.3 %
$f_{R.2}$ [MPa]	4.84	4.98	4.24	**4.7**	8.4 %
$f_{R.3}$ [MPa]	4.83	5.34	4.64	**4.9**	7.4 %
$f_{R.4}$ [MPa]	4.67	5.16	4.67	**4.8**	5.9 %
δ_{peak} [mm]	0.04	0.05	0.05	**0.05**	10.8%
$CMOD_{peak}$ [mm]	0.04	0.05	0.05	**0.05**	10.8

Results sawn beams, 4-point testing (NSBT, NSBT), synthetic fibres

	160210 Beam 7	160210 Beam 8	160210 Beam 9	**Mean value**	Coefficient of variation
b [mm]	150.5	151	151	150.83	0.2 %
h_{sp} [mm]	152.5	153	152	152.50	0.3 %
l [mm]	450	450	450	450.00	0.0 %
f_{peak} [MPa]	5.17	4.76	4.92	**4.95**	4.2 %
$f_{R.1}$ [MPa]	2.88	2.83	2.94	**2.88**	1.9 %
$f_{R.2}$ [MPa]	2.67	1.37	1.38	**1.81**	41.5 %
$f_{R.3}$ [MPa]	3.00	1.46	1.47	**1.98**	44.8 %
$f_{R.4}$ [MPa]	3.04	1.50	1.41	**1.99**	46.2 %
δ_{peak} [mm]	0.05	0.04	0.04	**0.04**	14.1 %
$CMOD_{peak}$ [mm]	0.08	0.07	0.06	**0.07**	14.5 %

Appendix B: Pictures of tested panels

Synthetic fibre reinforced concrete

d600h100 3P

Comments:

- All panels considered to be representative.
- No punching shear cracks.

d600h100 CS

Comment:

- All panels considered to be representative.
- No punching shear cracks.

d600h75 3P

Comment:

- All panels considered to be representative.
- No punching shear cracks.

d600h75 CS

Comment:

- All panels considered to be representative.
- No punching shear cracks.

d800h100 3P

Comment:

- All panels considered to be representative.
- No punching shear cracks.

d800h100 CS

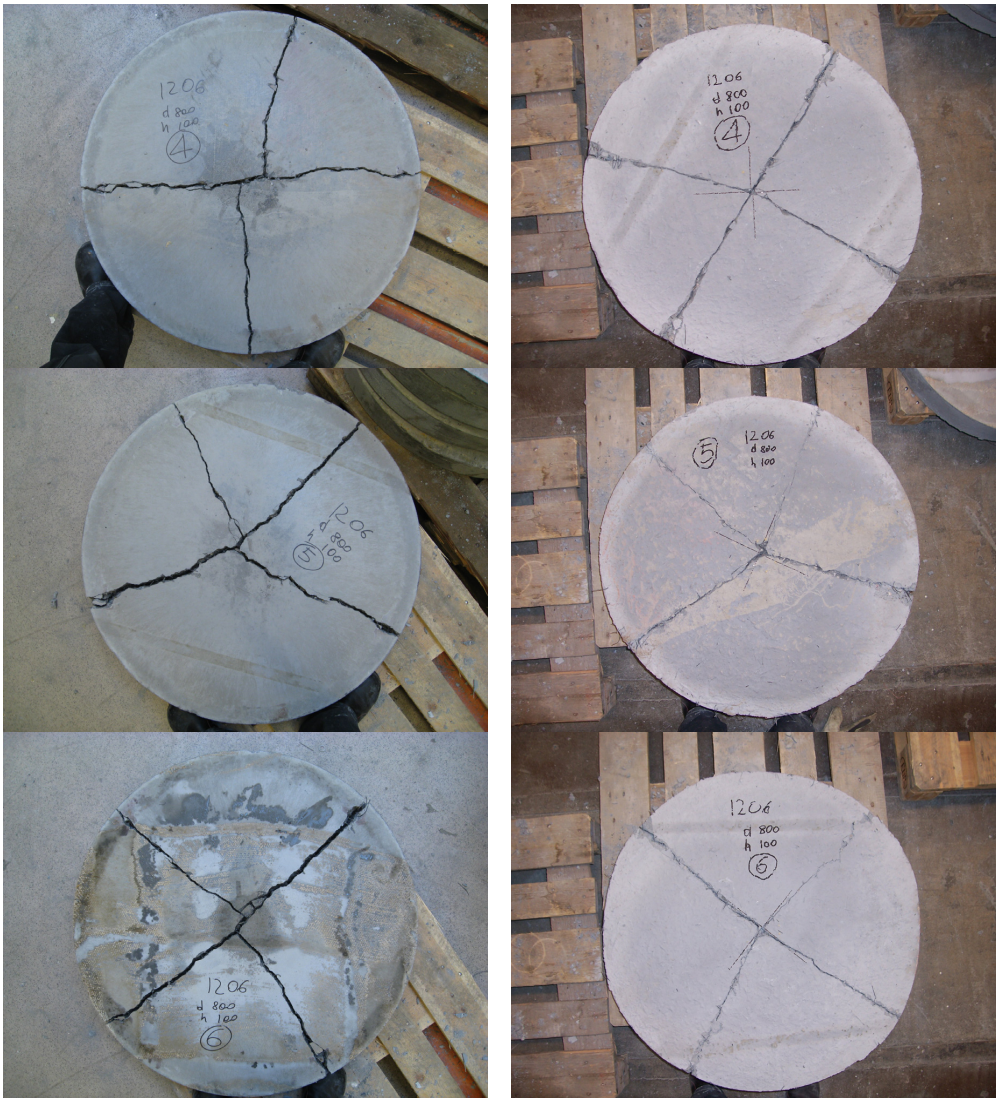

Comment:

- All panels considered to be representative.
- No punching shear cracks.

d800h75 3P

Comment:

- Panel 1 cracked almost in a beam-like mode, and was subjected for load before the deflection was registered. Discarded from the evaluation.
- No punching shear cracks.

d800h75 CS

Comment:

- All panels considered to be representative.
- No punching shear cracks.

Steel fibre reinforced concrete panels

d600h100 3P

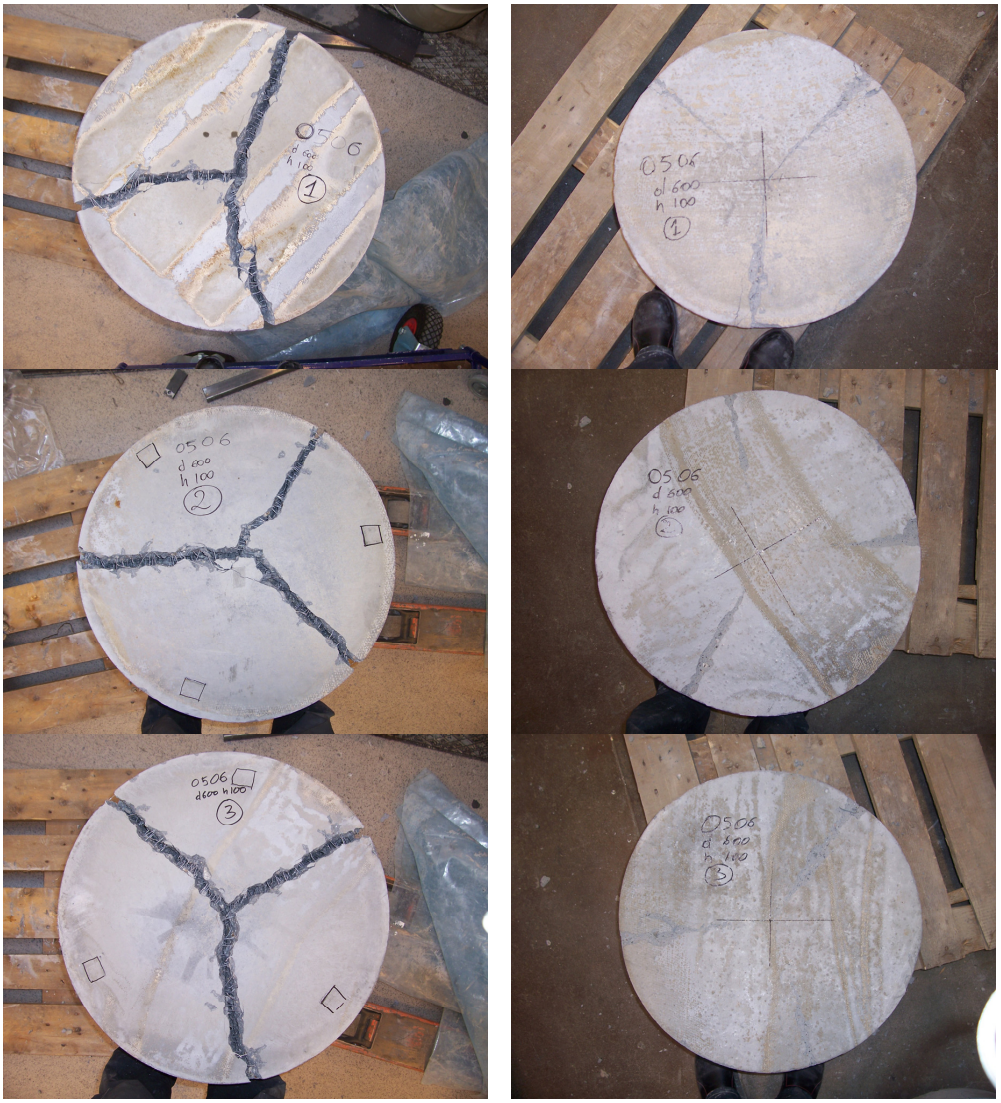

Comment:

- All panels considered to be representative.
- No punching shear cracks.

d600h100 CS

Comment:

- All panels considered to be representative.
- Punching shear cracks in panel 4 and panel 5. These panels had higher capacity than panel 6.

d600h75 3P

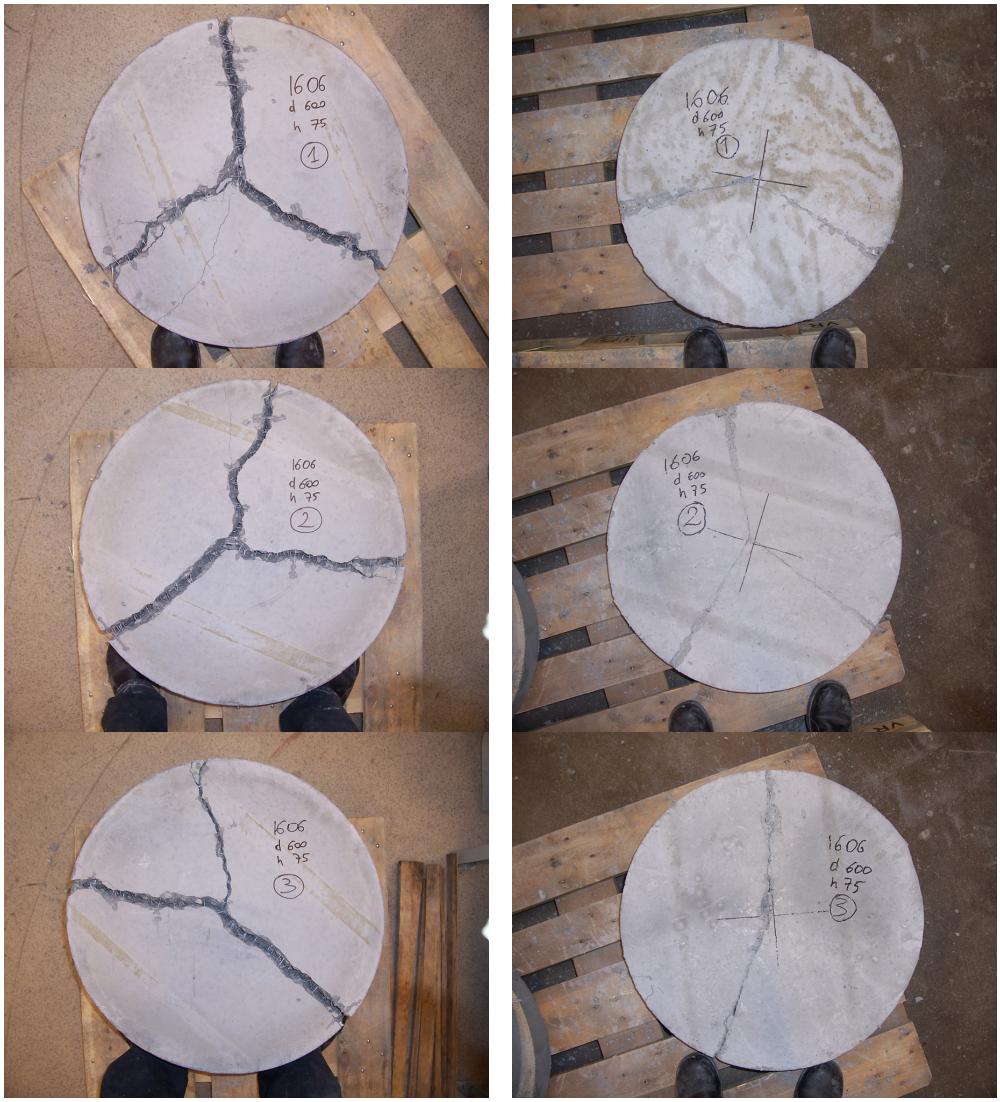

Comment:

- Panel 3 cracked almost in a beam-like mode. Discarded from the evaluation.
- No punching shear cracks.

d600h75 CS

Comment:

- Panel 6 did not crack similar to the other panels.
- Punching shear cracks in panel 4 and panel 5. These panels had considerable higher capacity than panel 6.
- Panel 6 considered to be an underachiever and discarded from the evaluation.

r

d800h100 3P

Comment:

- Panel 3 should have been tested at 3P, but tested at CS because the test on panel 6 was unsuccessful.
- No punching shear cracks.
- None of the panels cracked as expected.
    - Panel 1: Not equally sized segments
    - Panel 2: Almost in a beam-like mode, with two minor cracks where the third major crack should have been.
- Difficult to state the normal results from these two panels.

d800h100 CS








Comment:

- Panel 6 discarded because the load and deflection record was unsuccessful.
- Punching shear cracks in panel 3, panel 5 and panel 6.
- Panel 4 had untypical crack pattern and low capacity, relative to the other panels, and was therefore discarded from the evaluation.

d800h75 3P

Comment:

- Panel 4 and panel 6 cracked in a beam-like mode. Panel 6 and panel 5 had comparable capacity. Even so, panel 4 and panel 6 were discarded from the evaluation.
- Panel 5 had two minor cracks in addition to the three major cracks.
- Untypical crack pattern for all panels; difficult to state the expected result from this test series.
- No punching shear cracks.

d800h75 CS

Comment:

- All panels considered to be representative.
- Punching shear cracks in all panels.

DEPARTMENT OF STRUCTURAL ENGINEERING
NORWEGIAN UNIVERSITY OF SCIENCE AND TECHNOLOGY

N–7491 TRONDHEIM, NORWAY
Telephone: +47 73 59 47 00 Telefax: +47 73 59 47 01

"Reliability Analysis of Structural Systems using Nonlinear Finite Element Methods",
C. A. Holm, 1990:23, ISBN 82-7119-178-0.

"Uniform Stratified Flow Interaction with a Submerged Horizontal Cylinder",
Ø. Arntsen, 1990:32, ISBN 82-7119-188-8.

"Large Displacement Analysis of Flexible and Rigid Systems Considering Displacement-Dependent Loads and Nonlinear Constraints",
K. M. Mathisen, 1990:33, ISBN 82-7119-189-6.

"Solid Mechanics and Material Models including Large Deformations",
E. Levold, 1990:56, ISBN 82-7119-214-0, ISSN 0802-3271.

"Inelastic Deformation Capacity of Flexurally-Loaded Aluminium Alloy Structures",
T. Welo, 1990:62, ISBN 82-7119-220-5, ISSN 0802-3271.

"Visualization of Results from Mechanical Engineering Analysis",
K. Aamnes, 1990:63, ISBN 82-7119-221-3, ISSN 0802-3271.

"Object-Oriented Product Modeling for Structural Design",
S. I. Dale, 1991:6, ISBN 82-7119-258-2, ISSN 0802-3271.

"Parallel Techniques for Solving Finite Element Problems on Transputer Networks",
T. H. Hansen, 1991:19, ISBN 82-7119-273-6, ISSN 0802-3271.

"Statistical Description and Estimation of Ocean Drift Ice Environments",
R. Korsnes, 1991:24, ISBN 82-7119-278-7, ISSN 0802-3271.

“Properties of concrete related to fatigue damage: with emphasis on high strength concrete”,
G. Petkovic, 1991:35, ISBN 82-7119-290-6, ISSN 0802-3271.

"Turbidity Current Modelling",
B. Brørs, 1991:38, ISBN 82-7119-293-0, ISSN 0802-3271.

"Zero-Slump Concrete: Rheology, Degree of Compaction and Strength. Effects of Fillers as Part Cement-Replacement",
C. Sørensen, 1992:8, ISBN 82-7119-357-0, ISSN 0802-3271.

"Nonlinear Analysis of Reinforced Concrete Structures Exposed to Transient Loading",
K. V. Høiseth, 1992:15, ISBN 82-7119-364-3, ISSN 0802-3271.

"Finite Element Formulations and Solution Algorithms for Buckling and Collapse Analysis of Thin Shells",
R. O. Bjærum, 1992:30, ISBN 82-7119-380-5, ISSN 0802-3271.

"Response Statistics of Nonlinear Dynamic Systems",
J. M. Johnsen, 1992:42, ISBN 82-7119-393-7, ISSN 0802-3271.

"Digital Models in Engineering. A Study on why and how engineers build and operate digital models for decisison support",
J. Høyte, 1992:75, ISBN 82-7119-429-1, ISSN 0802-3271.

"Sparse Solution of Finite Element Equations",
A. C. Damhaug, 1992:76, ISBN 82-7119-430-5, ISSN 0802-3271.

"Some Aspects of Floating Ice Related to Sea Surface Operations in the Barents Sea",
S. Løset, 1992:95, ISBN 82-7119-452-6, ISSN 0802-3271.

"Modelling of Cyclic Plasticity with Application to Steel and Aluminium Structures",
O. S. Hopperstad, 1993:7, ISBN 82-7119-461-5, ISSN 0802-3271.

"The Free Formulation: Linear Theory and Extensions with Applications to Tetrahedral Elements with Rotational Freedoms",
G. Skeie, 1993:17, ISBN 82-7119-472-0, ISSN 0802-3271.

"Høyfast betongs motstand mot piggdekkslitasje. Analyse av resultater fra prøving i Veisliter'n",
T. Tveter, 1993:62, ISBN 82-7119-522-0, ISSN 0802-3271.

"A Nonlinear Finite Element Based on Free Formulation Theory for Analysis of Sandwich Structures",
O. Aamlid, 1993:72, ISBN 82-7119-534-4, ISSN 0802-3271.

"The Effect of Curing Temperature and Silica Fume on Chloride Migration and Pore Structure of High Strength Concrete",
C. J. Hauck, 1993:90, ISBN 82-7119-553-0, ISSN 0802-3271.

"Failure of Concrete under Compressive Strain Gradients",
G. Markeset, 1993:110, ISBN 82-7119-575-1, ISSN 0802-3271.

"An experimental study of internal tidal amphidromes in Vestfjorden",
J. H. Nilsen, 1994:39, ISBN 82-7119-640-5, ISSN 0802-3271.

"Structural analysis of oil wells with emphasis on conductor design",
H. Larsen, 1994:46, ISBN 82-7119-648-0, ISSN 0802-3271.

"Adaptive methods for non-linear finite element analysis of shell structures",
K. M. Okstad, 1994:66, ISBN 82-7119-670-7, ISSN 0802-3271.

"On constitutive modelling in nonlinear analysis of concrete structures",
O. Fyrileiv, 1994:115, ISBN 82-7119-725-8, ISSN 0802-3271.

"Fluctuating wind load and response of a line-like engineering structure with emphasis on motion-induced wind forces",
J. Bogunovic Jakobsen, 1995:62, ISBN 82-7119-809-2, ISSN 0802-3271.

"An experimental study of beam-columns subjected to combined torsion, bending and axial actions",
A. Aalberg, 1995:66, ISBN 82-7119-813-0, ISSN 0802-3271.

"Scaling and cracking in unsealed freeze/thaw testing of Portland cement and silica fume concretes",
S. Jacobsen, 1995:101, ISBN 82-7119-851-3, ISSN 0802-3271.

"Damping of water waves by submerged vegetation. A case study of laminaria hyperborea",
A. M. Dubi, 1995:108, ISBN 82-7119-859-9, ISSN 0802-3271.

"The dynamics of a slope current in the Barents Sea",
Sheng Li, 1995:109, ISBN 82-7119-860-2, ISSN 0802-3271.

"Modellering av delmaterialenes betydning for betongens konsistens",
Ernst Mørtsell, 1996:12, ISBN 82-7119-894-7, ISSN 0802-3271.

"Bending of thin-walled aluminium extrusions",
Birgit Søvik Opheim, 1996:60, ISBN 82-7119-947-1, ISSN 0802-3271.

"Material modelling of aluminium for crashworthiness analysis",
Torodd Berstad, 1996:89, ISBN 82-7119-980-3, ISSN 0802-3271.

"Estimation of structural parameters from response measurements on submerged floating tunnels",
Rolf Magne Larssen, 1996:119, ISBN 82-471-0014-2, ISSN 0802-3271.

“Numerical modelling of plain and reinforced concrete by damage mechanics”,
Mario A. Polanco-Loria, 1997:20, ISBN 82-471-0049-5, ISSN 0802-3271.

“Nonlinear random vibrations - numerical analysis by path integration methods”,
Vibeke Moe, 1997:26, ISBN 82-471-0056-8, ISSN 0802-3271.

“Numerical prediction of vortex-induced vibration by the finite element method”,
Joar Martin Dalheim, 1997:63, ISBN 82-471-0096-7, ISSN 0802-3271.

“Time domain calculations of buffeting response for wind sensitive structures”,
Ketil Aas-Jakobsen, 1997:148, ISBN 82-471-0189-0, ISSN 0802-3271.

"A numerical study of flow about fixed and flexibly mounted circular cylinders",
Trond Stokka Meling, 1998:48, ISBN 82-471-0244-7, ISSN 0802-3271.

“Estimation of chloride penetration into concrete bridges in coastal areas”,
Per Egil Steen, 1998:89, ISBN 82-471-0290-0, ISSN 0802-3271.

“Stress-resultant material models for reinforced concrete plates and shells”,
Jan Arve Øverli, 1998:95, ISBN 82-471-0297-8, ISSN 0802-3271.

“Chloride binding in concrete. Effect of surrounding environment and concrete composition”,
Claus Kenneth Larsen, 1998:101, ISBN 82-471-0337-0, ISSN 0802-3271.

“Rotational capacity of aluminium alloy beams”,
Lars A. Moen, 1999:1, ISBN 82-471-0365-6, ISSN 0802-3271.

“Stretch Bending of Aluminium Extrusions”,
Arild H. Clausen, 1999:29, ISBN 82-471-0396-6, ISSN 0802-3271.

“Aluminium and Steel Beams under Concentrated Loading”,
Tore Tryland, 1999:30, ISBN 82-471-0397-4, ISSN 0802-3271.

"Engineering Models of Elastoplasticity and Fracture for Aluminium Alloys",
Odd-Geir Lademo, 1999:39, ISBN 82-471-0406-7, ISSN 0802-3271.

"Kapasitet og duktilitet av dybelforbindelser i trekonstruksjoner",
Jan Siem, 1999:46, ISBN 82-471-0414-8, ISSN 0802-3271.

“Etablering av distribuert ingeniørarbeid; Teknologiske og organisatoriske erfaringer fra en norsk ingeniørbedrift”,
Lars Line, 1999:52, ISBN 82-471-0420-2, ISSN 0802-3271.

“Estimation of Earthquake-Induced Response”,
Símon Ólafsson, 1999:73, ISBN 82-471-0443-1, ISSN 0802-3271.

“Coastal Concrete Bridges: Moisture State, Chloride Permeability and Aging Effects”
Ragnhild Holen Relling, 1999:74, ISBN 82-471-0445-8, ISSN 0802-3271.

”Capacity Assessment of Titanium Pipes Subjected to Bending and External Pressure”,
Arve Bjørset, 1999:100, ISBN 82-471-0473-3, ISSN 0802-3271.

“Validation of Numerical Collapse Behaviour of Thin-Walled Corrugated Panels”,
Håvar Ilstad, 1999:101, ISBN 82-471-0474-1, ISSN 0802-3271.

“Strength and Ductility of Welded Structures in Aluminium Alloys”,
Miroslaw Matusiak, 1999:113, ISBN 82-471-0487-3, ISSN 0802-3271.

“Thermal Dilation and Autogenous Deformation as Driving Forces to Self-Induced Stresses in High Performance Concrete”,
Øyvind Bjøntegaard, 1999:121, ISBN 82-7984-002-8, ISSN 0802-3271.

“Some Aspects of Ski Base Sliding Friction and Ski Base Structure”,
Dag Anders Moldestad, 1999:137, ISBN 82-7984-019-2, ISSN 0802-3271.

"Electrode reactions and corrosion resistance for steel in mortar and concrete",
Roy Antonsen, 2000:10, ISBN 82-7984-030-3, ISSN 0802-3271.

"Hydro-Physical Conditions in Kelp Forests and the Effect on Wave Damping and Dune Erosion. A case study on Laminaria Hyperborea",
Stig Magnar Løvås, 2000:28, ISBN 82-7984-050-8, ISSN 0802-3271.

"Random Vibration and the Path Integral Method",
Christian Skaug, 2000:39, ISBN 82-7984-061-3, ISSN 0802-3271.

"Buckling and geometrical nonlinear beam-type analyses of timber structures",
Trond Even Eggen, 2000:56, ISBN 82-7984-081-8, ISSN 0802-3271.

”Structural Crashworthiness of Aluminium Foam-Based Components”,
Arve Grønsund Hanssen, 2000:76, ISBN 82-7984-102-4, ISSN 0809-103X.

“Measurements and simulations of the consolidation in first-year sea ice ridges, and some aspects of mechanical behaviour”,
Knut V. Høyland, 2000:94, ISBN 82-7984-121-0, ISSN 0809-103X.

”Kinematics in Regular and Irregular Waves based on a Lagrangian Formulation”,
Svein Helge Gjøsund, 2000-86, ISBN 82-7984-112-1, ISSN 0809-103X.

”Self-Induced Cracking Problems in Hardening Concrete Structures”,
Daniela Bosnjak, 2000-121, ISBN 82-7984-151-2, ISSN 0809-103X.

"Ballistic Penetration and Perforation of Steel Plates",
Tore Børvik, 2000:124, ISBN 82-7984-154-7, ISSN 0809-103X.

"Freeze-Thaw resistance of Concrete. Effect of: Curing Conditions, Moisture Exchange and Materials",
Terje Finnerup Rønning, 2001:14, ISBN 82-7984-165-2, ISSN 0809-103X

Structural behaviour of post tensioned concrete structures. Flat slab. Slabs on ground",
Steinar Trygstad, 2001:52, ISBN 82-471-5314-9, ISSN 0809-103X.

"Slipforming of Vertical Concrete Structures. Friction between concrete and slipform panel",
Kjell Tore Fosså, 2001:61, ISBN 82-471-5325-4, ISSN 0809-103X.

"Some numerical methods for the simulation of laminar and turbulent incompressible flows",
Jens Holmen, 2002:6, ISBN 82-471-5396-3, ISSN 0809-103X.

“Improved Fatigue Performance of Threaded Drillstring Connections by Cold Rolling”,
Steinar Kristoffersen, 2002:11, ISBN: 82-421-5402-1, ISSN 0809-103X.

"Deformations in Concrete Cantilever Bridges: Observations and Theoretical Modelling",
Peter F. Takâcs, 2002:23, ISBN 82-471-5415-3, ISSN 0809-103X.

"Stiffened aluminium plates subjected to impact loading",
Hilde Giæver Hildrum, 2002:69, ISBN 82-471-5467-6, ISSN 0809-103X.

"Full- and model scale study of wind effects on a medium-rise building in a built up area",
Jónas Thór Snæbjørnsson, 2002:95, ISBN82-471-5495-1, ISSN 0809-103X.

"Evaluation of Concepts for Loading of Hydrocarbons in Ice-infested water",
Arnor Jensen, 2002:114, ISBN 82-417-5506-0, ISSN 0809-103X.

"Numerical and Physical Modelling of Oil Spreading in Broken Ice",
Janne K. Økland Gjøsteen, 2002:130, ISBN 82-471-5523-0, ISSN 0809-103X.

"Diagnosis and protection of corroding steel in concrete",
Franz Pruckner, 20002:140, ISBN 82-471-5555-4, ISSN 0809-103X.

"Tensile and Compressive Creep of Young Concrete: Testing and Modelling",
Dawood Atrushi, 2003:17, ISBN 82-471-5565-6, ISSN 0809-103X.

"Rheology of Particle Suspensions. Fresh Concrete, Mortar and Cement Paste with Various Types of Lignosulfonates",
Jon Elvar Wallevik, 2003:18, ISBN 82-471-5566-4, ISSN 0809-103X.

"Oblique Loading of Aluminium Crash Components",
Aase Reyes, 2003:15, ISBN 82-471-5562-1, ISSN 0809-103X.

"Utilization of Ethiopian Natural Pozzolans",
Surafel Ketema Desta, 2003:26, ISSN 82-471-5574-5, ISSN:0809-103X.

"Behaviour and strength prediction of reinforced concrete structures with discontinuity regions",
Helge Brå, 2004:11, ISBN 82-471-6222-9, ISSN 1503-8181.

"High-strength steel plates subjected to projectile impact. An experimental and numerical study",
Sumita Dey, 2004:38, ISBN 82-471-6282-2 (printed version), ISBN 82-471-6281-4 (electronic version), ISSN 1503-8181.

"Alkali-reactive and inert fillers in concrete. Rheology of fresh mixtures and expansive reactions."
Bård M. Pedersen, 2004:92, ISBN 82-471-6401-9 (printed version), ISBN 82-471-6400-0 (electronic version), ISSN 1503-8181.

"On the Shear Capacity of Steel Girders with Large Web Openings".
Nils Christian Hagen, 2005:9 ISBN 82-471-6878-2 (printed version), ISBN 82-471-6877-4 (electronic version), ISSN 1503-8181.

”Behaviour of aluminium extrusions subjected to axial loading”.
Østen Jensen, 2005:7, ISBN 82-471-6873-1 (printed version), ISBN 82-471-6872-3 (electronic version), ISSN 1503-8181.

”Thermal Aspects of corrosion of Steel in Concrete”.
Jan-Magnus Østvik, 2005:5, ISBN 82-471-6869-3 (printed version), ISBN 82-471-6868 (electronic version), ISSN 1503-8181.

”Mechanical and adaptive behaviour of bone in relation to hip replacement.” A study of bone remodelling and bone grafting.
Sébastien Muller, 2005:34, ISBN 82-471-6933-9 (printed version), ISBN 82-471-6932-0 (electronic version), ISSN 1503-8181.

“Analysis of geometrical nonlinearities with applications to timber structures”.
Lars Wollebæk, 2005:74, ISBN 82-471-7050-5 (printed version), ISBN 82-471-7019-1 (electronic version), ISSN 1503-8181.

“Pedestrian induced lateral vibrations of slender footbridges”,
Anders Rönnquist, 2005:102, ISBN 82-471-7082-5 (printed version), ISBN 82-471-7081-7 (electronic version), ISSN 1503-8181.

“Initial Strength Development of Fly Ash and Limestone Blended Cements at Various Temperatures Predicted by Ultrasonic Pulse Velocity”,
Tom Ivar Fredvik, 2005:112, ISBN 82-471-7105-8 (printed version), ISBN 82-471-7103-1 (electronic version), ISSN 1503-8181.

“Behaviour and modelling of thin-walled cast components”,
Cato Dørum, 2005:128, ISBN 82-471-7140-6 (printed version), ISBN 82-471-7139-2 (electronic version), ISSN 1503-8181.

“Behaviour and modelling of selfpiercing riveted connections”,
Raffaele Porcaro, 2005:165, ISBN 82-471-7219-4 (printed version), ISBN 82-471-7218-6 (electronic version), ISSN 1503-8181.

”Behaviour and Modelling og Aluminium Plates subjected to Compressive Load”,
Lars Rønning, 2005:154, ISBN 82-471-7169-1 (printed version), ISBN 82-471-7195-3 (electronic version), ISSN 1503-8181.

”Bumper beam-longitudinal system subjected to offset impact loading”,
Satyanarayana Kokkula, 2005:193, ISBN 82-471-7280-1 (printed version), ISBN 82-471-7279-8 (electronic version), ISSN 1503-8181.

“Control of Chloride Penetration into Concrete Structures at Early Age”,
Guofei Liu, 2006:46, ISBN 82-471-7838-9 (printed version), ISBN 82-471-7837-0 (electronic version), ISSN 1503-8181.

“Modelling of Welded Thin-Walled Aluminium Structures”,
Ting Wang, 2006:78, ISBN 82-471-7907-5 (printed version), ISBN 82-471-7906-7 (electronic version), ISSN 1503-8181.

”Time-variant reliability of dynamic systems by importance sampling and probabilistic analysis of ice loads”,
Anna Ivanova Olsen, 2006:139, ISBN 82-471-8041-3 (printed version), ISBN 82-471-8040-5 (electronic version), ISSN 1503-8181.

“Fatigue life prediction of an aluminium alloy automotive component using finite element analysis of surface topography”.
Sigmund Kyrre Ås, 2006:25, ISBN 82-471-7791-9 (printed version), ISBN 82-471-7791-9 (electronic version), ISSN 1503-8181.

”Constitutive models of elastoplasticity and fracture for aluminium alloys under strain path change”,
Dasharatha Achani, 2006:76, ISBN 82-471-7903-2 (printed version), ISBN 82-471-7902-4 (electronic version), ISSN 1503-8181.

“Simulations of 2D dynamic brittle fracture by the Element-free Galerkin method and linear fracture mechanics”,
Tommy Karlsson, 2006:125, ISBN 82-471-8011-1 (printed version), ISBN 82-471-8010-3 (electronic version), ISSN 1503-8181.

“Penetration and Perforation of Granite Targets by Hard Projectiles”,
Chong Chiang Seah, 2006:188, ISBN 82-471-8150-9 (printed version), ISBN 82-471-8149-5 (electronic version), ISSN 1503-8181.

“Deformations, strain capacity and cracking of concrete in plastic and early hardening phases”,
Tor Arne Hammer, 2007:234, ISBN 978-82-471-5191-4 (printed version), ISBN 978-82-471-5207-2 (electronic version), ISSN 1503-8181.

“Crashworthiness of dual-phase high-strength steel: Material and Component behaviour”,
Venkatapathi Tarigopula, 2007:230, ISBN 82-471-5076-4 (printed version), ISBN 82-471-5093-1 (electronic version), ISSN 1503-8181.

“Fibre reinforcement in load carrying concrete structures”,
Åse Lyslo Døssland, 2008:50, ISBN 978-82-471-6910-0 (printed version), ISBN 978-82-471-6924-7 (electronic version), ISSN 1503-8181.

“Low-velocity penetration of aluminium plates”,
Frode Grytten, 2008:46, ISBN 978-82-471-6826-4 (printed version), ISBN 978-82-471-6843-1 (electronic version), ISSN 1503-8181.

“Robustness studies of structures subjected to large deformations”,
Ørjan Fyllingen, 2008:24, ISBN 978-82-471-6339-9 (printed version), ISBN 978-82-471-6342-9 (electronic version), ISSN 1503-8181.

"Constitutive modelling of morsellised bone",
Knut Birger Lunde, 2008:92, ISBN 978-82-471-7829-4 (printed version), ISBN 978-82-471-7832-4 (electronic version), ISSN 1503-8181.

"Experimental Investigations of Wind Loading on a Suspension Bridge Girder",
Bjørn Isaksen, 2008:131, ISBN 978-82-471-8656-5 (printed version), ISBN 978-82-471-8673-2 (electronic version), ISSN 1503-8181.

"Cracking Risk of Concrete Structures in The Hardening Phase",
Guomin Ji, 2008:198, ISBN 978-82-471-1079-9 (printed version), ISBN 978-82-471-1080-5 (electronic version), ISSN 1503-8181.

"Modelling and numerical analysis of the porcine and human mitral apparatus",
Victorien Emile Prot, 2008:249, ISBN 978-82-471-1192-5 (printed version), ISBN 978-82-471-1193-2 (electronic version), ISSN 1503-8181.

"Strength analysis of net structures",
Heidi Moe, 2009:48, ISBN 978-82-471-1468-1 (printed version), ISBN 978-82-471-1469-8 (electronic version), ISSN1503-8181.

"Numerical analysis of ductile fracture in surface cracked shells",
Espen Berg, 2009:80, ISBN 978-82-471-1537-4 (printed version), ISBN 978-82-471-1538-1 (electronic version), ISSN 1503-8181.

"Subject specific finite element analysis of bone – for evaluation of the healing of a leg lengthening and evaluation of femoral stem design",
Sune Hansborg Pettersen, 2009:99, ISBN 978-82-471-1579-4 (printed version), ISBN 978-82-471-1580-0 (electronic version), ISSN 1503-8181.

"Evaluation of fracture parameters for notched multi-layered structures",
Lingyun Shang, 2009:137, ISBN 978-82-471-1662-3 (printed version), ISBN 978-82-471-1663-0 (electronic version), ISSN 1503-8181.

"Modelling of Dynamic Material Behaviour and Fracture of Aluminium Alloys for Structural Applications"
Yan Chen, 2009:69, ISBN 978-82-471-1515-2 (printed version), ISBN 978-82 471-1516-9 (electronic version), ISSN 1503-8181.

"Nanomechanics of polymer and composite particles"
Jianying He 2009:213, ISBN 978-82-471-1828-3 (printed version), ISBN 978-82-471-1829-0 (electronic version), ISSN 1503-8181.

"Mechanical properties of clear wood from Norway spruce"
Kristian Berbom Dahl 2009:250, ISBN 978-82-471-1911-2 (printed version) ISBN 978-82-471-1912-9 (electronic version), ISSN 1503-8181.

"Modeling of the degradation of TiB_2 mechanical properties by residual stresses and liquid Al penetration along grain boundaries"
Micol Pezzotta 2009:254, ISBN 978-82-471-1923-5 (printed version) ISBN 978-82-471-1924-2 (electronic version) ISSN 1503-8181.

"Effect of welding residual stress on fracture"
Xiabo Ren 2010:77, ISBN 978-82-471-2115-3 (printed version) ISBN 978-82-471-2116-0 (electronic version), ISSN 1503-8181.

"Pan-based carbon fiber as anode material in cathodic protection system for concrete structures" Mahdi Chini 2010:122, ISBN 978-82-471-2210-5 (printed version) ISBN 978-82-471-2213-6 (electronic version), ISSN 1503-8181.

"Structural Behaviour of deteriorated and retrofitted concrete structures" Irina Vasililjeva Sæther 2010:171, ISBN 978-82-471-2315-7 (printed version) ISBN 978-82-471-2316-4 (electronic version) ISSN 1503-8181.

"Prediction of local snow loads on roofs" Vivian Meløysund 2010:247, ISBN 978-82-471-2490-1 (printed version) ISBN 978-82-471-2491-8 (electronic version) ISSN 1503-8181.

"Behaviour and modelling of polymers for crash applications" Virgile Delhaye 2010:251, ISBN 978-82-471-2501-4 (printed version) ISBN 978-82-471-2502-1 (electronic version) ISSN 1503-8181.

"Blended cement with reducted CO_2 emission – Utilizing the Fly Ash-Limestone Synergy", Klaartje De Weerdt 2011:32, ISBN 978-82-471-2584-7 (printed version) ISBN 978-82-471-2584-4 (electronic version) ISSN 1503-8181.

"Chloride induced reinforcement corrosion in concrete" Concept of critical chloride content – methods and mechanisms. Ueli Angst 2011:113, ISBN 978-82-471-2769-9 (printed version) ISBN 978-82-471-2763-6 (electronic version) ISSN 1503-8181.

"A thermo-electric-Mechanical study of the carbon anode and contact interface for Energy savings in the production of aluminium". Dag Herman Andersen 2011:157, ISBN 978-82-471-2859-6 (printed version) ISBN 978-82-471-2860-2 (electronic version) ISSN 1503-8181.

"Structural Capacity of Anchorage Ties in Masonry Veneer Walls Subjected toEarthquake". The implications of Eurocode 8 and Eurocode 6 on a typical Norwegain veneer wall. Ahmed Mohamed Yousry Hamed 2011:181, ISBN 978-82-471-2911-1 (printed version) ISBN 978-82-471-2912-8 (electronic ver.) ISSN 1503-8181.

"Work-hardening behaviour in age-hardenable Al-Zn-Mg(-Cu) alloys". Ida Westermann , 2011:247, ISBN 978-82-471-3056-8 (printed ver.) ISBN 978-82-471-3057-5 (electronic ver.) ISSN 1503-8181.